Mechanisms of Transfer Film Formation on Data Recording Heads

Ciprian Nastasa

Doctor of Philosophy

Aston University

March 2006

Acknowledgements

I would like to express my thanks to those people who helped me during the research programme. Professor John Sullivan for permanent guidance and his critical eye. Andy Abbot for his help and advise with the experimental work.

Acknowledgements must also go to dr. Simon Chandler, for his patience during long talks, and for the helpful observations and ideas with a deep understanding of underlying physics of magnetic tapes and recording techniques, and for his support.

I would also like to thank Dr. S.O. Saied for all her help during the XPS and SIMS experiments and for the helpful hints in spectra interpretation.

I am totally in debt to dr. Ioana Rusu for her patience with me, cheering me up during the research when things weren't very rosy, and for useful scientific advises.

My special thanks to Cristina and Sebastian for their helping hand and warmth during these years.

Summary of the thesis

The increasing demand for high capacity data storage requires decreasing the head-to-tape gap and reducing the track width. A problem very often encountered is the development of adhesive debris on the heads at low humidity and high temperatures that can lead to an increase of space between the head and media, and thus a decrease in the playback signal. The influence of stains on the playback signal of reading heads is studied using RAW (Read After Write) tests and their influence on the wear of the heads by using indentation technique. The playback signal has been found to vary and the errors to increase as stains form a patchy pattern and grow in size to form a continuous layer. The indentation technique shows that stains reduce the wear rate of the heads. In addition, the wear tends to be more pronounced at the leading edge of the head compared to the trailing one. Chemical analysis of the stains using ferrite samples in conjunction with MP (metal particulate) tapes shows that stains contain iron particles and polymeric binder transferred from the MP tape. The chemical anchors in the binder used to grip the iron particles now react with the ferrite surface to create strong chemical bonds. At high humidity, a thin layer of iron oxyhydroxide forms on the surface of the ferrite. This soft material increases the wear rate and so reduces the amount of stain present on the heads. The stability of the binder under high humidity and under high temperature as well as the chemical reactions that might occur on the ferrite poles of the heads influences the dynamic behaviour of stains. A model of stain formation taking into account the channels of binder degradation and evolution upon different environmental conditions is proposed.

Keywords: brown stains, magnetic media, adhesive debris, error rate

Table of Contents

List of tables and figures

1 Introduction

The technology of recording signals using the magnetic medium is more than a century old when, in 1898 Paulsen developed the first magnetic tape recorder. Many things have changed since then: the apparition of high definition television or more recently, 3D home television, audio and video recorders, computers and the Internet explosion. These technologies led to an increase of the quality of the image and sound but also required an increase of the amount of information manipulated and stored. These demands put high pressure in the domains of data storage and data transport technologies, which had and still have to cope with this boom.

Tapes and disc drives have increased their capacity for storage along the years. During the last years, the hard discs had an annual growth rate of 130% per year with recording densities demonstrated by Fujitsu in April 2000 of 56Gbits/in^2 and a theoretical limit to 150Gbits/in^2 [1]. The tape industry made great efforts to keep pace with such an explosion, however the track density of the helical-scan tape systems is still 15 times lower than that of disk systems.[2]

The tape industry does not lack strong competition with the apparition of new technologies such as recordable and rewritable CDs (compact disc) and DVDs (digital versatile disc). Despite this, magnetic tapes are still used in various domains such as back-up systems for workstations, digital audio recordings (DAT) and phone answering machines, databases etc where access rates are not so important as transportability. In 2002, new series of recording technologies were launched to the general public. The technology, called Fluorescent Multi-Layer Disc (FMD) [3, 4, 5, 6] or Hyper-CD-ROM [7], as it is called by its Romanian inventor, is based on the phenomenon of controlled extinction fluorescence and its aim is to smash the barriers of existing data formats proposing discs similar in size to a CD or DVD but being able to store theoretically up to 10 TB (more than 16,100 normal CDs or more than 580 double sided DVDs). The technology also allows writing on the discs. The first generation are designed to store up to 100GB of data. [6]

Another field heavily investigated and of great future is the information storage in DNA-like molecular sequences. The first steps have already been made in the early 2000 by Viviana Risca, a 17 year old Romanian teenager who succeeded to encode the sentence: "JUNE6_INVASION: NORMANDY" in a DNA molecule. For her achievement, she received from Intel Corporation the "Junior Nobel Prize". [8, 9]

If both the tape industry and technology are to survive on the market, the storage capacity of the tapes must be increased. In order to achieve high data densities, several methods are employed [10, 11, 12] involving:

- reducing thickness of the flexible substrate (halving tape thickness can, theoretically, double the capacity);
- lowering the tape speed whilst the head tape speed can be maintained high using rotary heads;
- decreasing the bit length;
- reducing the gap between media and head;
- increasing track density;

Each of these techniques has its own disadvantages. Reducing the thickness of the substrate involves the development of new materials with a higher modulus of elasticity and this would increase costs. The mechanisms of the rotary heads are more delicate and in general more complicated than those of linear heads, which leads to increased costs. The reduction of the bit length is slowed down by the demagnetising process generated by magnetic particles shapes and due to the presence of other bits in the vicinity. The effect of the neighbouring bits could be reduced by increasing coercivity and by reducing the magnetic film thickness. But reducing the magnetic film thickness would involve a reduction in playback signal whereas increasing coercivity involves increasing difficulties in write and read data which means that the heads must generate larger fields. The reduction of the playback signal can be avoided by increasing saturation magnetisation, or in another words, using metal particles instead of ferrite particles. Also the signal amplitude can be improved by reducing the space between heads and media. Therefore, any loose or adhesive debris entrapped between head and tape increases the spacing and hence reducing the signal amplitude and generating errors. Adhesive debris also known as stains can be responsible for signal

degradation. Despite the fact that many studies were focused on understanding the adhesive debris, there is been no agreement in terms of their chemical composition and mechanism of formation.

Two main techniques in data storage using tapes have emerged and are being currently in use:

- **helical scan** (DAT - digital audio tape or later on DDS tapes - Digital Data Storage) similar to that used for VHS videos;
- **linear scan** (QTIC - quarter inch cartridge) technique where the data is read and written using multiple heads;

In order to increase data-transfer rate, Sony has proposed recently a multi-track magnetic head for helical scan systems based on ETF (**E**mbedded **T**hin **F**ilm) with a magnetic core much smaller than that of conventional heads. Using computer simulations, they aimed to minimise crosstalk between the heads and to obtain a good head-tape contact [13]. Magneto-resistive elements have also been implemented in helical scan systems. [14]

One of the newest ideas that emerged recently in terms of tape storage is to use a head made from a single pole. In addition to the common carbon black, the tape will have the backside coating made from a ferromagnetic material. When it has to read or to write the energised pole will induce a virtual (image) pole in the ferromagnetic material of the back coat. Thus a classic head will be created and the gap of this type of head will roughly be two times the distance between energised pole and ferromagnetic material.

As it was said before that in order to increase data density the distance between head and media has to be reduced. During normal operation of the drives, debris are generated. These debris, either loose or adhesive may induce further spacing and hence may lead to poor signal and/or errors. Adhesive debris on the heads are in particular important since, despite 30 years of research, opinions about their composition and mechanism of their development is still split in the research community.

The present thesis is proposing to investigate the adhesive debris (stains) generated by the MP tapes (metal particulate) and to propose a mechanism that could explain their formation.

2 Literature survey

2.1 Magnetic approach

A magnetic recorder is a device that provides ways for storage of information and its subsequent reproduction using magnetic fields. A magnetic media represents a continuous strip of magnetic material used to store information. The process of recording the information is achieved by a device called a write head [15].

Basically, a head consists of a magnetic ring core and one or more windings (see Figure 2-1). A small gap exists in the core thus creating two pole pieces. When it has to record, an electrical signal passes through the windings and creates a variable magnetic flux, guided by the magnetic core of the head. The magnetic circuit is closing through the tape or other magnetic support that is passed at steady speed through this field and thus the tape becomes permanently magnetised. Because the gap dimensions are very small, the magnetic field is focused into a very small area and thus, any element of the tape spends a very short time within this field. Since the time in which the tape interacts with the magnetic field is short, it is assumed that the magnetic field remains quasi constant. In order to achieve high and very well spatially resolved magnetic fields, the magnetic support must be in contact or in a very close proximity to the magnetic head.

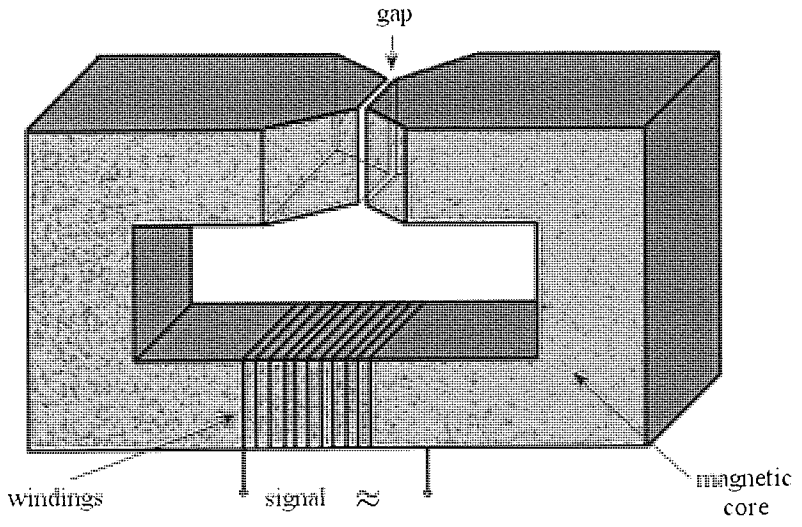

Figure 2-1 Schematic representation of a magnetic head

In order to recreate the original signal, the magnetic medium is drawn past a reproducing head at the same steady speed as at the time the recording was made. The magnetic fields, which surround the medium, create a fluctuating magnetic flux in the head's magnetic core and this will induce an electric current in the windings. The fluctuations of the magnetic flux and of the electric signal correspond to the original signal.

The gap length of the head is dictated by the shortest wavelength to be recorded, the track width by the signal-to-noise ratio azimuth sensitivity and information packing density desired and the gap depth is selected for the minimum value that will yield an acceptable mechanical strength or an acceptable wear life without saturating in the record mode [32].

Apart from inductive head described before other types based on MR (magneto-resistive) or GMR (giant magneto-resistive) elements are used to read the signal. An MR or GMR element is a device that is able to modify its resistance according to the magnetic flux crossing it. Thus the current through such element will vary accordingly and the information stored on tape will be retrieved. GMR are used as reading heads in the hard discs mainly but more recently they have been introduced in the magnetic tape devices as well.

It has been proven that the pulse shape of the current generated by the remanent flux of the media is described by the equation Equation 2-1. The width of the output electrical pulse at half maximum amplitude (PW_{50}), increases if the media is thicker or the distance between head and media is higher leading to a broader pulse and thus to a poorer resolution of two neighbour bits, thus increasing the errors.

$$\mathbf{PW_{50}}=2\sqrt{d(d+\delta)} \qquad \text{Equation 2-1}$$

where: d- head media spacing
δ - media thickness

In addition, the amplitude of the pulse decreases according to Wallace law. As one can see in Equation 2-2, the decrease in amplitude is more exacerbated at shorter wavelengths and thus higher data densities.

For a sine wave recorded signal, the output voltage is given by the equation below [146]:

$$E(x) = -\mu_0 V w M_0 \frac{H_g g}{i} K\delta e^{-Kd}\left(\frac{1-e^{-K\delta}}{K\delta}\cdot\frac{\sin\frac{Kg}{2}}{\frac{Kg}{2}}\right)\cos Kx$$

where:

x - longitudinal position
E (x) - voltage output from longitudinal magnetic recording
μ_0 - magnetic permeability of a vacuum
V - tape to head velocity
w - track width
M_0 - peak value of sine-wave magnetization
H_g - deep gap field
g - gap length
i - current in head coil
K - wavenumber ($K = 2\pi/\lambda$ and λ - wavelength)
δ - thickness of the magnetic medium
d - distance from tape to head

The term e^{-Kd} represents signal attenuation due to distance between the head and the tape. Hence,

Spacing loss (dB) α $e^{-\frac{2\pi d}{\lambda}}$ which is equivalent to

Spacing loss (dB)= $-54.6k(d/\lambda)$ Equation 2-2

Where:
d is head to tape separation
λ is the signal wavelength and
k is a constant related to head's shape

This is why, in order to increase data density, it is necessary to reduce to a minimum the space between head and media and to decrease the thickness of the magnetic layer. In the case of the DDS-2 format where minimum recording length is 0.67μm [16], and considering k=1 in an approximation of a spherical shaped head, the signal loss generated by 20nm stains is:

$$\text{Spacing loss (dB)} = -54.6k\left(\frac{20\cdot10^{-6}\,m}{0.67\cdot10^{-6}\,m}\right) = 1.63\text{dB}$$

As the wavelength of the recorded signal decreases to allow increasing the data density, the spacing loss generated by stains will increase exponentially unless measures to reduce stain thickness and keep it under control are taken. Similarly, head erosion will degrade the signal recorded and will result in data errors unless special steps to prevent them are taken. The strategy in the DDS format is read-after-write technique: compute a frame control number (MD5 sum) of each frame recorded, comparing it with the one stored on the tape and write the frame again if it was found to be corrupted. (see also section 2.3)

If a ferromagnetic material is subjected to a magnetising force that varies in sense as well as magnitude in a cyclic manner, the curve relating B (induction of the magnetic field) and H (the magnetic field) forms a loop called hysteresis loop. Figure below represents a typical hysteresis loop and by studying its shape and its size, one can retrieve considerable information about the magnetic properties of the material.

Remanence is the magnetisation that remains after removal of the magnetic field (B_r). Coercivity is the field that would have to be applied in order to reduce the magnetisation to zero. (H_c)

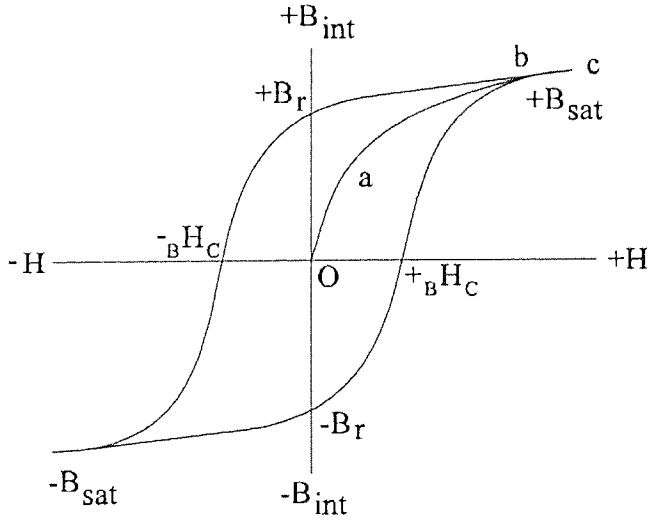

Figure 2-2 A typical hysteresis loop [12]

B_{sat}- saturation level of the magnetic induction

B_r-remanence level of the magnetic induction

H_c-coercive field

The read and write head as well as the magnetic tape must have specific magnetic properties. The magnetic materials used in heads must have low remanence, low coercivity, and high permeability and in the same time must be able to switch magnetisation quickly to follow rapid signal variation. On the other hand, the magnetic media are designed with high coercivity thus minimising self-demagnetisation (allowing the bit of information to be smaller) but not extremely high to enable rewriting capability and also designed with high remanent magnetisation thus enabling a high signal/noise ratio. Taking into account the different properties of the heads and tapes materials, the hysteresis loops will have different shapes accordingly. The figures below represent the hysteresis loops for the tape and head respectively.

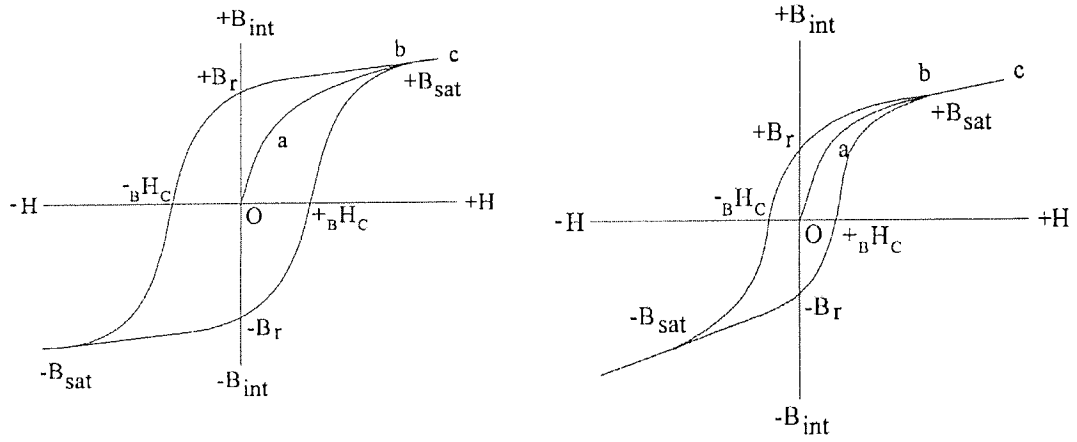

Figure 2-3 Hysteresis loops of magnetic materials used in magnetic tapes (left) and magnetic heads (right) [12]

Some performances of today's tapes are shown in the table below:

	unit	**AMP**	**AME**	**Hi-8 MP**	**DDS-2**
Coercivity	KA/m	189.5	135	146	119 - 167
Saturated magnetic flux density	mT	520	513	350	500
SFDr		0.18	0.96	0.453	0.583
Surface roughness(R_a)	nm	1.8	1.5	3.5	2.7
Magnetic layer thickness	μm	0.1	0.18	0.35	0.5

Table 2-1 Characteristics of the AMP and AME, DDS-2 [16, 33]

AMP- Advanced Metal Particulate tape
AME- Advanced Metal Evaporated tape

Considering the height of the stains is 20nm, the increase of the pulse width due to the increase of the head to tape spacing for a stained head is:

$$\frac{PW_{50}(stained) - PW_{50}(clean)}{PW_{50}(clean)} = \sqrt{1+\frac{\delta}{d}} - 1 = \sqrt{1+\frac{20nm}{500nm}} - 1 = 0.0198 = 1.98\%$$

Given the today's magnetic layer thickness, the pulse width is increasing only by aproximatively 2% due to staining therefore the main concern remains the decrease of the signal amplitude due to spacing loss.

2.2 *Tribology and the general theory of wear*

By definition, tribology is the science of friction. One of the results of friction phenomenon is the wear that represents a progressive removal of material from the sliding surfaces [17]. The tribology of magnetic recording systems is different from the conventional, macroscopic tribology, partially due to the size of the areas in contact. The classical macroscopic friction can be described using two simple laws. The first one states that frictional force is directly proportional with normal load:

$F=\mu W$ Equation 2-3

Where: F is frictional force

W is normal load and

μ is a constant called friction coefficient

The second law of friction says that frictional force is independent of the apparent area of contact. Even though the frictional coefficient has been stated as being a constant, in reality it has been observed that it varies slightly, being smaller for smaller loads and depending also on sliding speed of the surfaces.

Another important law describes the wear rate of a material under a wide variety of conditions and it is known as Archard law: the wear rate of a material varies according to applied load and to the flow pressure.

$\omega=kW/p_m$ Equation 2-4

Where

ω is the wear rate of a given material

W-normal load

p_m- flow pressure or hardness

k-constant (wear coefficient)

As in the case of friction coefficient, it has been found that wear coefficient does not remain constant, though it decreases at very small loads.

Different mechanisms of wear have been described in literature. The following classification is given according to the response of the material to the local stresses [17, 18]:

1. *Adhesive* wear is caused when the shear strength of the interface junction is greater than the shear strength of bulk material;
2. *Fatigue* appears when a material is subjected to repeated loading over a single area due to cyclic stressing;
3. *Abrasive* (2 body and 3 body abrasion) occurs when a hard asperity of a surface protrudes into the softer material; thus, debris from the softer material will be produced and a wear track will arise; if loose debris of a hard material becomes entrapped between two softer surfaces, then third body abrasion will take place; again, a wear track will appear and the loose debris will accumulate at the trailing edge of the head;
4. *Corrosive* wear is caused when surfaces are chemically active; chemical reactions may occur leading to a weaker surface since usually these products are not bonded to the surface very strongly; chemical active atmospheres such as oxygen and water and temperature can lead to this type of wear; for example ceramics wear differentially due to the different chemical reactivities of their components [19]
5. *Erosion* (removal of the material from a surface by impact of solid /liquid particles) takes place when the surface is bombarded with particles; the wear rate depends on the incidence angle and the surface bombarded.

Probably all these types of wear occur at one point when two surfaces are in contact but the most effective depends strongly on the surfaces being in contact and the environmental conditions.

2.2.1 Wear of ceramics

Generally, the ceramic materials are hard brittle materials these are a consequence of the chemical bonds. The energy required to dislodge a covalent or ionic bond within ceramic material is very high. In addition, the covalent bond is strongly

directional, meaning that the atoms within the crystals have very little freedom of movement. The metallic bonds are not directional, the atoms here have a certain degree of movement and as a result, pure metals are soft materials that tend to deform plastically. Ceramics on the contrary, unlike the metals tend to chip and to develop cracks. Fractures occur at the sharp edges or crack tips where the tensile or shear stress is higher than the cohesive force between the atoms. Soft materials like metals do not crack easily because the plastic deformation causes the rounding of the edges therefore reducing the stress. Ceramics are brittle since the development of the cracks and consequently propagation of the stress along the surface cannot be reduced by plastic deformation. [17] Moreover, the interatomic bonds at the fracture site can be weakened by adsorbed molecules such as oxygen or water that may lead to a further decrease of the stress required for crack propagation. The effect is called chemisorpstion embrittlement.

Friction may also change (generally enhance) the rate of chemical reactions of solids. Such modifications of the rate of reactions have been seen for ceramics usually found in the design of the magnetic heads such as alumina (Al_2O_3), silica or glass (SiO_2). There are several causes for this kind of acceleration [17]:

- Removal of the protective layer, exposing a fresh chemically active surface;
- Flash high-temperatures generated by the friction enhance the rate of chemical reactions;
- Destruction and re-creation of new bonds generates highly reactive intermediate products;
- Frictional stresses may cause deformation or micro-fractures in the layer or the solid and produces diffusion paths or high energy sites with increased reactivity;

One kind of ceramic of particular interest is SiO_2 especially because it is the main constituent of the glass used in manufacturing the DDS heads. Studies showed that on immersion in water, silica develops a negative surface charge due to the adsorption of hydroxyl radicals, acting as an Arrhenius acid while the water plays the role of the corresponding Arrhenius base. Also interesting is that acidic complex ions such as PO_4^-, SiO_4^- and derivatives of them tend to adsorb on surfaces. In particular their organofunctional derivatives react strongly with the oxide surfaces through the complex

ion and form strong bonds with the surfaces. Interestingly, some of these complexes are intensively used in the tape binder polymer. (see section 2.5.2) [17]

2.2.2 Wear of polymers

A particular interest for scientist is represented by the wear of polymers since the materials based on polymers are used in large areas of human activity and particularly in the magnetic media.

The term of polymer describes a high-molecular-weight material. However, the difference between a polymer molecule and a simple organic compound is that the polymer has multitudinous repeating chemical units called *mers* and the number of such *mers* exceeds 100. The number of *mers* present in a polymer chain represents the degree of polymerisation.

Apart from the degree of polymerisation, another important parameter of the polymer is the glass transition temperature that is the temperature at which a rubber-like amorphous polymer becomes glass-like and vice versa.

The structure of polymers varies from a linear polymer where the carbon atoms are joined together as a continuous sequence in chain, to branched polymer where the structure of polymer has chemical groups called functional groups that are part of the monomer structure and to network polymers which exhibit crosslinked structures. [20] (see Figure 2-4)

It is easy to predict if a chemical reaction between two reagents could lead to a certain type of polymer. If a molecule has two functional groups (i.e. chemical linkages, atoms, or radicals which undergo reaction) then it can react with another bifunctional molecule to give a linear polymer. A second rule says that if a molecule having two functional groups reacts with a molecule having *at least* three functional groups, then a three-dimensional network polymer will result. These polymers are cross-linked polymers. [21]

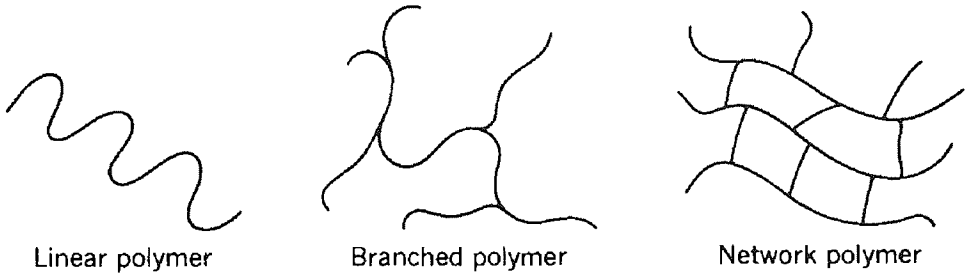

Figure 2-4 Simulated polymer structures [20]

Understanding the polymer tribology is one of the keys in understanding the stain apparition and development on magnetic heads.

For polymers there are two main causes of wear: deformation leading to fatigue and adhesion. One must bear in mind that the contact between two surfaces occurs between the asperity tips and not on the entire macroscopic surface. If two surfaces are put in contact, then the contact will occur on very few asperities. The normal load will then be supported by these asperities leading to very high areas of stress. Consequently, the tips will plastically deform until the increasing contact area will be able to support the load. Given one material, Greenwood and Williamson developed a theory that can predict whether asperities will suffer elastic or plastic deformation in contact with another surface [12]:

$$\Psi = \frac{E_c}{H}\left(\frac{\sigma_p}{R_p}\right)^{1/2} \qquad \text{Equation 2-5}$$

Where E_c is effective elastic modulus of the interacting surfaces
H is the hardness of the softer material
σ_p is the standard deviation of the peak distribution
R_p effective radius of curvature of the contact asperity

If Ψ is greater than 1 then the deformation is elastic, if Ψ is less than 0.6 the deformation is plastic and between these values the deformation is a mixture between elastic and plastic deformations.

However, taking into account the complexity of the polymer mechanics, Bhushan has adapted the model:

$$\Psi_p = \frac{E_c}{Y}\left(\frac{\sigma_p}{R_p}\right)^{1/2} \qquad \text{Equation 2-6}$$

Where E_c has become composite modulus,
Y defines tensile yield strength of the polymer,
and σ_p and R_p having the same meanings as in Equation 2-5

The composite modulus is given by:

$$\frac{1}{E_c} = \frac{(1-\nu_1^2)}{E_1} + \frac{(1-\nu_2^2)}{E_2} \qquad \text{Equation 2-7}$$

With ν_1, ν_2 Poisson's ratios for the interfacing substances
And E_1, E_2 Young's modulus of elasticity respectively

Again, if Ψ_p is higher than 2.6 the surfaces will deform plastically whereas if it is less than 1.8 the deformation will be elastic. The model cannot predict the interaction between polymers when Ψ_p falls between 1.8 and 2.6. Based on this predictive model Bhushan and Doerner have shown that the contact between head and tape is elastic. [12]

Another cause of wear is adhesion. One must take into account that in the case of two bodies in contact, one being a polymer, the normal forces of adhesion operate not only at the points of actual contact but also in adjacent regions. This is due to the distance since there is no contact however molecular forces take place. These forces will develop an extra-contract adhesion and it is believed to take place wherever the distance between the bodies is between 50Å to 100Å.

Another phenomenon that may occur is the accumulation of static charges due to friction that will lead to a double electrical layer build-up. It has been proven that the moment of friction in metal-polymer pairs may be reduced almost ten times by suppressing the tribo-electricity in them. [22]

Under certain conditions, mechano-chemical processes lead to the formation of highly active free radicals, which may undergo chemical reactions: polymer chain scission or growth, the apparition of cross-linkages between chains which will furthermore lead to a reduction in losses due to friction and to an increase in the wear resistance. In such cases, chemical bonding takes place on contact. Ion microscopy and emission spectroscopy have proven the existence of transfer films formed on both metal and polymer when sliding against each other. Moreover, on composite materials based on polymers chemical reactions could be initiated by the filler. Disintegration of the polymer is the result not only of the mechanical degradation but also of thermal degradation due to intense heat liberation on contact. [23, 22, 24]

Many theories try to explain the formation of the adhesion bonds at the interface between two bodies one of which being polymer and unfortunately no one can give a complete picture of the adhesion phenomena. Some of them are summarised below. [22]

The mechanical theory explains the formation of the bonds as due to unilateral or mutual wedging of the material, which penetrates into micro-fissures in the surfaces of the interacting bodies.

Adsorption theory supposes that the molecular bonds are formed between bodies in contact and as a result, the surface is becoming energetically unstable. The forces are either repulsive or attractive depending upon the nature of the interacting elements and the distances between them. Orientation, ionic, induction and hydrogen intermolecular bonds may be involved. Table 2-2 summarises the energy involved in inter molecular bonds.

Bond type	**Energy** (kcal/mol)
Hydrogen	15
Dispersion	10
Orientation	9
Induction	0.5

Table 2-2 Energies in molecule-molecule interactions [after22]

The electrical theory explains the adhesion phenomenon by the means of the electrostatic attraction of charges in a double electric layer that appears at the boundary of two phases due to a phenomenon of contact electrification [22]. The double layer is created by the transition of the electrons and ions from one surface to another. In this case the polymer could be either acceptor or donor of electrons but it has been found that in contact with metals, the polymer is negatively charging. The double electric layer is modulated in the form of the plates of an electric capacitor and the energy of adhesion is equated to the energy in the corresponding capacitor. The theory cannot explain satisfactory the adhesion between polymers themselves and filled polymers which posses electrical conductivity.

An interesting theory called the diffusion theory supposes that adhesion interaction is caused by mutual penetration as a result of diffusion of chain molecules or their segments and the formation as a result of this of a firm bond between polymers. A strong condition for diffusion is the compatibility of the bodies, the mutual dissolution of polymers. Although it can explain very well some phenomena such as the increase in adhesion with the temperature and the relationship between the adhesion effect and the delamination rate, yet it cannot explain the adhesion of the polymers to another substances such as glass or metals.

The experimental works have shown the apparition of chemical bonds in the process of adhesion between polymers and metals and these observations led to the chemical or chemisorption theory. Since the chemical bonds act at a very short range (1-1.5Å) they are therefore much stronger than the intermolecular forces. [22] For comparison, the dissociation energy for covalent bonds is given in the table below. As

one can see from Table 2-2 and Table 2-3, the covalent bonds are much stronger than the inter-molecular forces. The presence of chemical bonds can explain high value for adhesion in polymers when compared with their cohesive strength.

Covalent bond	**Dissociation energy** (kcal/mol)
C-H	98
N-H	93
O-H	111
C-C	83
C-N	70
C-O	84
C-Cl	79
C=C	145
C=O	179
C≡N	213
$-CH_2$	0.68
-O-	1
-COO-	2.90
$-C_6H_4-$	3.90
-CONH	8.50
-OCONH- (urethane)	8.74

Table 2-3 Dissociation energy for some typical covalent bonds [after 20]

The polymer tribology is even more complicated by the presence of fillers such as metals in polymer structure. In such composite materials fillers can undergo chemical changes or they can trigger chemical reactions in polymer structure [24]. It has been shown that the presence of the copper or copper oxide can reduce the friction coefficient. Complex compounds of lead, silver, cadmium, bismuth that are used as fillers are able to dissociate at fixed temperatures isolating the metal in colloidal state. The colloidal metal, which possesses at this moment high chemical activity, reacts with the friction surfaces forming polish films on them. [22]

The chemical changes in the polymer structure can dramatically modify its mechanical properties, particularly strength, rigidity, adhesion etc. Taking into account these facts it is necessary to have a closer look at the chemical reactions that a polymer may undergo, particularly those commonly used in the magnetic media industry. Due to their complexity, there are treated separately in section 2.5.2 and 2.5.3.

2.3 *DDS format and drives*

DDS format (**D**igital **D**ata **S**torage) is a solution that emerged from DAT format (**D**igital **A**udio**T**ape), a technology developed initially for high quality consumer audio recording. The idea was to use the same principle as in videocassette recorders - helical scan - that can provide high relative speed between head and tape and thus an increase of the amount of the information stored. The four heads, two for reading and two for writing are assembled on a drum spinning at high speed. Typical views of a DDS drive and a DDS drum are depicted in Figure 2-5.

Helical scan recorders have a series of advantages compared with linear scan systems. In linear recordings, in order to achieve high transfer rates the tape is moved rapidly across a stationary head. The tape is run back and forth at high speeds in order for the head to reposition itself over a track incresing dramatically the data acces time. Additionally, it induces higher wear of the tape, long start/stop reposition times, and high tension on the tape. In helical scan however, the high data density is achieved through a high *relative velocity* of tape and heads. The heads are moving at high speed whereas the speed of the tape can be decreased to very low values. Faster head-to-tape speeds of helical-scan allow it to record at much higher densities than linear. Additional tracks to help the servo mechanisms to follow precisely the data tracks help increasing the areal density. by 3.6 to 7 times compared with linear systems, allowing more capacity, and smaller tape cartridges [132]. In order to avoid crosstalk, adjacent tracks have different azimuth angles and the gap width of the reading head is smaller compared with the writing head so only the central region of the track is read (see Table 2-4)

The basic organisation of the recorded data in DDS is the same as in DAT for sound recording: blocks of data are organised into tracks and tracks are organised into frames. A pair of adjacent tracks, each with a substantially different azimuth orientation of magnetised stripes, constitutes a frame on DDS tape. Tracks are divided into data areas (which include correction codes) and auxiliary areas that help the drive to follow

tracks and to locate specific data. In addition, three levels of error control have been developed in order to prevent errors and if an error occurs, to correct it.

One of the most important strategy for avoiding errors is the read-after-write technique (RAW) in which each newly written track is read back as soon as possible, usually within a revolution of the drum. In order to achieve this, the DDS drum contains two extra heads whose function is to read data, giving a total of four heads. The other two heads are used to write data. The system reads the error correction codes interspersed with the data and, if it finds the codes incorrect, writes another copy of the data with a primary head and checks it once more with one of the extra heads. Thus, the drive ensures that there is at least one recoverable version of the data on the tape.

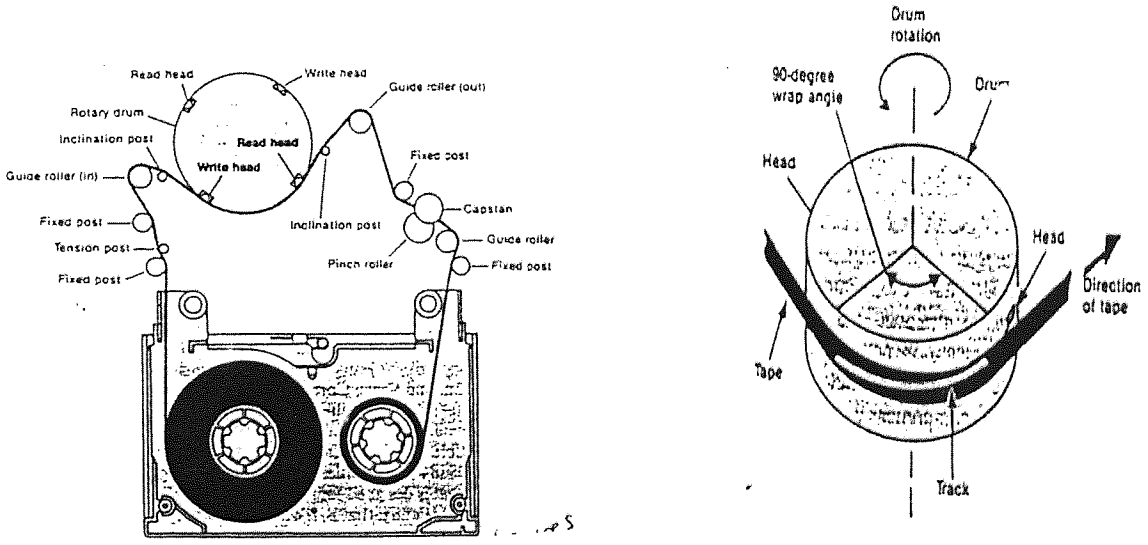

Figure 2-5 A schematic view of a DDS drive and drum [25]

Using the error correction codes a tape can have less than 1 error to 10^{16} bits written which is comparable to that of compact disc memories, and thus making it ideal for back-up storage of information on hard disk [25]. From a physical point of view, the horizontal correctable error width is 0.3mm and the vertical correctable error width is 2.6mm. [26]

The figures below show a comparison between linear and helical scan in terms of how the data is written on the tape.

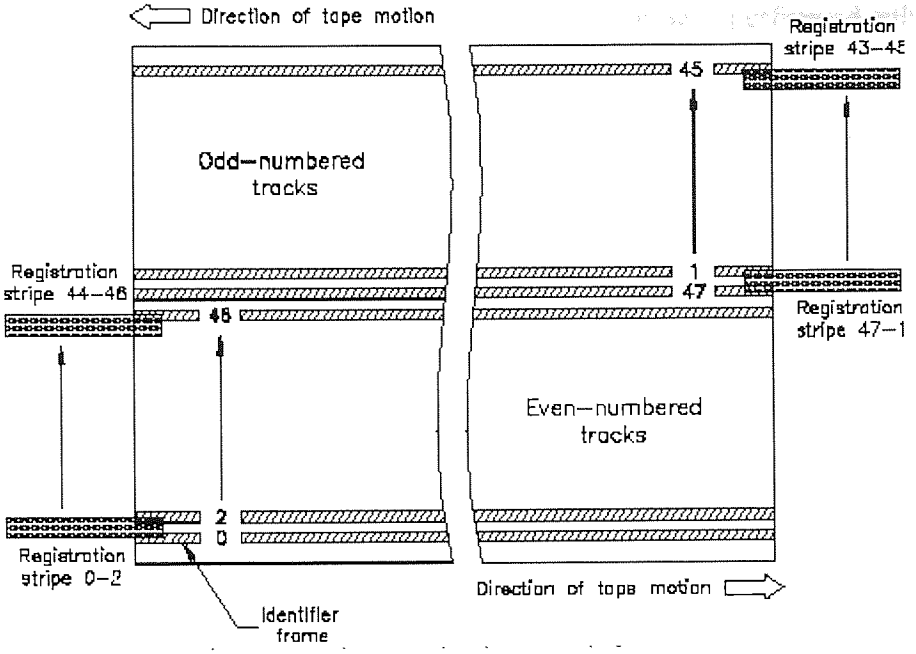

Figure 2-6 Schematic representation of data tracks in linear scan systems [132]

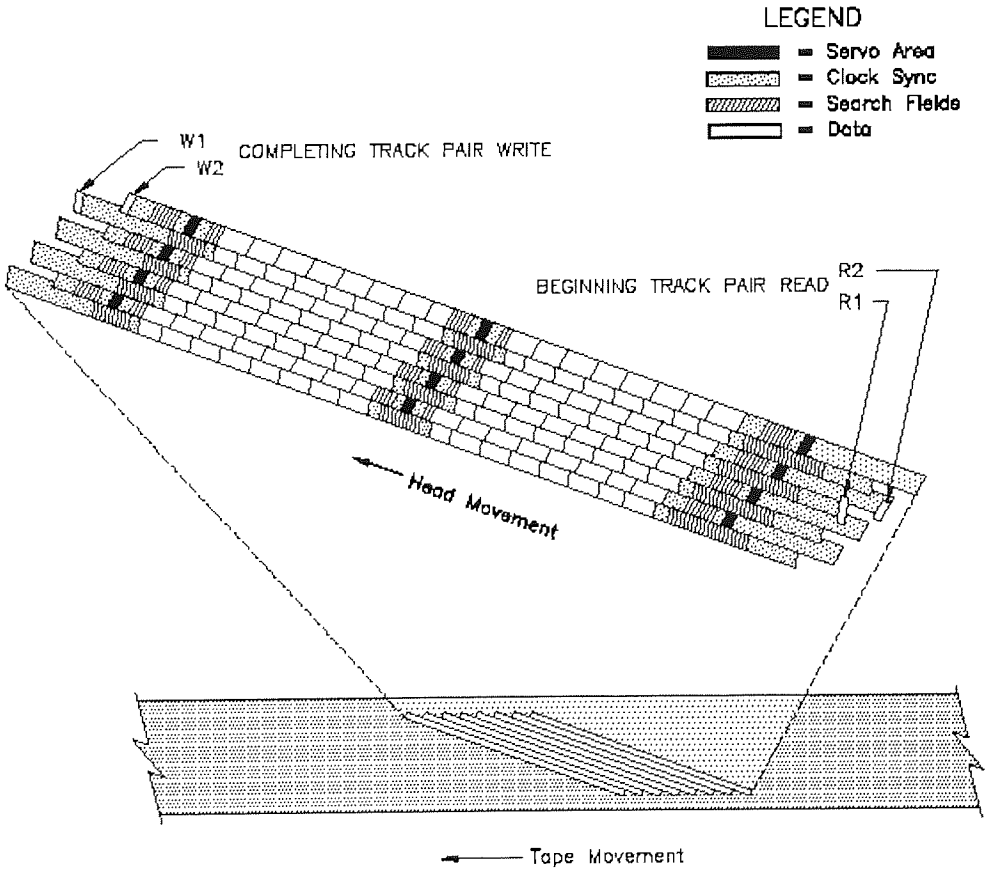

Figure 2-7 Track format in helical (DDS) scan systems [132]

In the linear systems, the control of the head positioning is performed only at the beginning of the track. Hence, in order to insure low level of errors, manufacturers have to insure that any minute changes in tape position does not lead to a loss of the track by the reading head. Therefore, the tracks themselves are designed wider and the read head is very narrow. In helical scan, the length of the tracks being short, the task of the head of following the tracks is alleviated and the tracks can be narrower.

In the case of the DDS format, the information is digitally recorded as a string of ones and zeros the signal is present and above a certain threshold level for a fixed duration of time as it is the case for bit "1" or below the threshold value as it is the case of bit "0".

Some parameters of the DDS4 drives are given in Table 2-4:

Recording frequency (1T)	54MHz
Gap width	310nm write head, 210nm read head
track width	6.8 μm
drum speed	11479.6rpm
tape speed	23.39 mm/s
bit rate	108 Mbit/s
linear data density	122 kb/inch

Table 2-4 Some DDS4 Parameters

Taking into account the data above, one can compute the bit length as:

$$\text{Bit length} = \frac{1inch}{lineardatadensity} = \frac{2.54 \cdot 10^{-2} m}{122 \cdot 10^{3} bit} = 0.208 \mu m$$

2.4 Tribological problems in helical scan systems

In order to increase several approaches are taking into account. However, these approaches introduce tribological problems that need to be solved. For example, decreasing the tape thickness in order to accommodate greater lengths of tape on the same size cartridges will reduce its mechanical strength. With reduced strength, lateral tape damage is likely to occur and since the data tracks are small, this will induce in

turn data errors. The use of the substrates with superior mechanical properties helps alleviate the problem.

As in the case of tapes moving at slower relative speeds, the magnetic head of the DDS drives is in contact with the magnetic head. Several features insure this behaviour: the designed curvature of magnetic head surface, the tape is pulled towards the head with a constant tension by using of the guiding rollers and fixed posts. At higher head-to-tape relative speeds, the air is dragged along between the tape and head interface thus a cushion of air is created and hence the head looses contact with the tape. To alleviate the problem, a series of small longitudinal grooves are present on the rotating part of the drum and the heads are mounted in windows within the drum. In addition, head protrusion, typical around 40nm, is chosen in order to achieve a good contact between head and tape, and to control the normal load force of the tape on the head. [139, 140]

The increase of transfer rate and rotating speed of the drum involves an increase of wear rate of the tape and head. The initial asperities of the tape and head are worn out and the friction coefficient tends to increase due to adhesive forces. The use of diamond-like carbon films (DLC) on tapes in conjunction with lubricant is very effective in preserving the initial height surface asperities hence insuring a constant friction coefficient and wear rate. The DLC asperities height is chosen so the signal spacing loss is smaller than on the tapes without the DLC coatings. If the friction force increases stick-slip phenomenon will occur and may result in an unstable movement of the tape, hence errors. [133]

In order to accommodate more tape in the same case, the tape thickness is reduced. However, more tribological problems occur, especially at the tape guidance posts and roller guides. The purpose of these posts is to guide the tape towards the rotating drum and to regulate the tape tension. These posts are slightly inclined and the tape is driven up or down and the tape edge is pressed on the flange of the roller guides by static friction force as seen in figure below. If the mechanical properties of the tape degrade with the decrease of the tape thickness, edge damage of the tape is likely to occur. The damage will reflect in errors of the signal recorded on tracks. Additionally, wear debris is likely to occur, hence more errors. Therefore improvement of the mechanical properties of the tape and a decrease of the static friction coefficient is needed. Currently for DDS drives the posts are made of stainless steel with 0.8%S, and

2% Mn with a roughness of 0.2μm. [133]. The use of polymer based posts is not recommended for posts since it is proven that the static friction coefficient between them and the tape is dramatically increasing with time leading to stick-slip phenomenon and unstable movement of the tape. [40] Reducing the friction coefficient and wear is beneficial for the magnetic heads as well. However, this may lead in thicker transfer film on the magnetic heads, which causes spacing loss. In order to prevent the production of wear debris from the head surface, the tape should be covered by a thicker layer of lubricant and moreover the lubricant should adhere strongly on the surface of the tape.

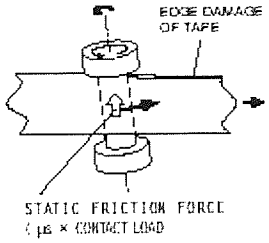

Figure 2-8 Edge damage of the tape due to excessive friction coefficient [133]

For the same purpose of reduction of static friction coefficient and wear resistance, the drums are made of silicon modified aluminium alloy. [29]

Considering the head, several authors [27, 10, 19, 28] have identified gap erosion, pole or MIG material recession, spacing loss caused by loose or adhesive debris, macroscopic changes of the head profile or changes in microstructure of the head material due to an increase in contact temperature between head and tape, as sources of errors.

All of the above mentioned processes introduce spacing between head and media and according to Wallace law (Equation 2-2) a decrease in signal playback. The decrease in signal playback means that the signal output corresponding to bit "1" decreases, ultimately will be below the threshold value and will be read by the head as bit "0" hence an error.

2.4.1 Head Materials

Generally, the demands on the materials used on heads are very high: these materials should have a high elastic modulus, high fracture strength high mechanical and thermal stability. The interfacial adhesion and the shear strength must be low compared with the bulk cohesive forces in order to prevent adhesive transfer from media to tape [10]. The materials should also have suitable magnetic properties: low remanence, low coercivity, high permeability in order to guide the magnetic flux with minimum loses (see also Figure 2-3)[12].

After Mizoh [29], the helical scan heads could be classified as follow:

1. bulk ferrite head
2. metal in gap head (MIG head)
3. laminated head

DDS drives used during the experiments are from the third generation (DDS3). The schematic representations for both types of heads (read and write) are in Figure 2-9 and Figure 2-10. The gap of the magnetic head is tilted in order to prevent cross-talk between adjacent tracks (see also Figure 2-7). For the same purpose, the gap width of the reading head is narrower compared with the gap of the write head (Table 2-4). Hence, the tracks are written with different azimuth angles and the reading head is reading only the central part of the track thus preventing interferences from the neighbouring tracks. In terms of the materials used, there are differences between heads according to their function: the read head is a bulk ferrite head and the write head is a MIG type (**M**etal **i**n **G**ap) head.

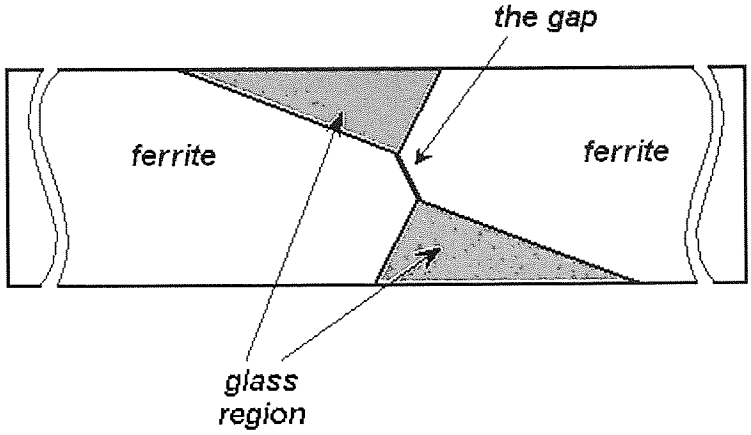

Figure 2-9 A schematic representation (top view) of the read head on DDS3 drives

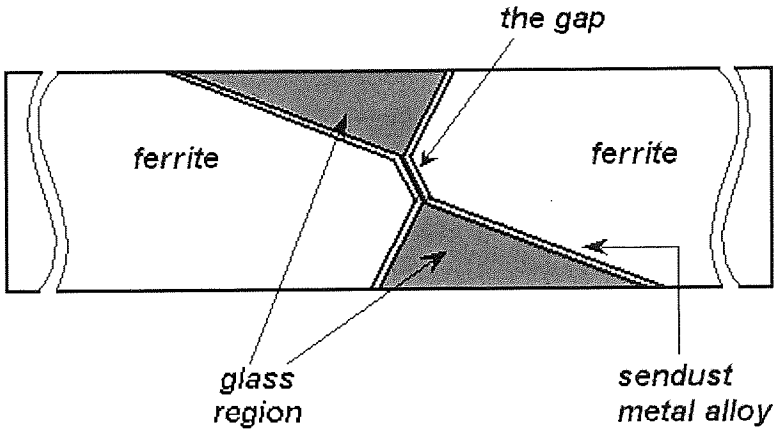

Figure 2-10 A schematic representation (top view) of the write head on DDS3 drives

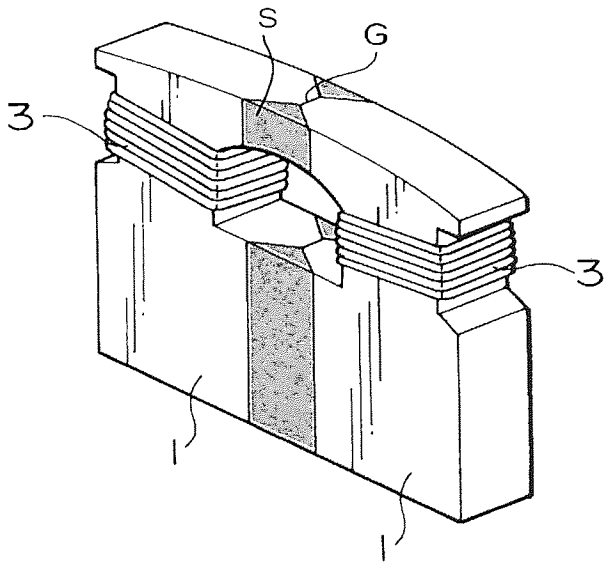

Figure 2-11 DDS head profile; Legend: G – gap, 3 – windings, I – ferrite, S – adhesive glass [after 30]

Most usual ferrites employed in head design are Mn-Zn or Ni-Zn ferrites. They have been chosen due to their good mechanical and magnetic properties since it was proved that they have a low wear rate [29, 31]. Both types of ferrites are commonly used as single-crystals or as hot-pressed ferrites. In the seventies and eighties, the Mn-Zn ferrites were used only for low frequency applications where their high permeability was required. A careful control of the ingredients had allowed a nearly zero magnetostriction constant as well as zero crystal anisotropy. Despite these facts, resistivities on the order of $1\Omega\cdot$cm for bulk materials prevented their use at frequencies higher than 0.1MHz. The trend towards shorter wavelengths in recording systems has dictated the improvement of electrical characteristics of Mn-Zn ferrites by controlling the grain size and porosity. Basically, the increased resistivity has been obtained by additives which diffuse to the grain boundary under sintering and form a highly insulating layer thus increasing the resistivity up to three orders of magnitude and making this particular ferrite even better for applications up to 20MHz than the Ni-Zn ferrites [32]. The grain boundaries must be carefully controlled because if they are too thick, they tend to allow the grains to demagnetise themselves and thus induces a loss of permeability or can lead to crystal pull out and a general weakening of the ferrite [32].

There are two ways of producing the ferrites. The first one is used in the case of hot pressed ferrites and it is called sinterisation. These kinds of ferrites are prepared by blending a stoichiometric ratio of Fe_2O_3, MnO and Zn in a typical molar ratio of 52:26:22 respectively and then the material is prefired in a controlled oxygen atmosphere. The prefired material is milled and densified by isostatic pressing which will reduce its porosity down to about 5%. The material is then sintered in vacuum under very high pressure with oxygen bled in as a function of temperature to maintain a proper oxygen balance [32]. Top temperatures employed during sinterisation process are about 1600K [33]. The oxygen pressure during sintering is critical in order to produce a ferrite with good mechanical properties. The quality of Fe_2O_3 is also essential since it has been found that oxides such as P_2O_5 can reduce dramatically the resistivity of the ferrite and thus increase power loss [34]. The control of the stoichiometry between reagents during manufacturing must be very strict as well: if the Fe^{2+} concentration becomes too high, the ZnO will be reduced and some of the Zn atoms will

be lost at grains boundaries. [35, 32, 33] This will produce a highly internally strained ferrite that will readily chip at machining and with high crystal anisotropy and magnetostriction. Stoichiometry differs from manufacturer to manufacturer but it has been proven that the higher Zn content on the ferrite, the lower Curie temperature will be [32]. Also, recent studies revealed that electrochemical corrosion of the ferrite depends on the MnO/ZnO ratio. [36]

The single crystals of ferrite are produced using the Bridgman method or by flame fusion. The difficulty consists in the fact that during the growth, a general segregation of the Mn and Fe^{2+} occurs with the Mn concentration being higher at the bottom of the crystal and the iron's being higher at the top. Again, in order to prevent Zn loss a proper oxygen atmosphere must be maintained. Studies made by Koinkar et Bhushan show that single phase materials like single crystals ferrite exhibit better microtribological behaviour than multiphase materials such as hot pressed ferrites and that any surface defect affects the wear resistance of the material [37].

Another problem of the single crystal ferrite consists in its mechanical and magnetic anisotropy. Experiments revealed that the wear rate of the heads depends on the orientation of single crystal ferrite and it is lower on single ferrite crystal than on polycrystalline ferrite [29, 38]. Wear rate was also found to increase towards lower temperatures as the elastic modulus of the tape increases thus increasing the tape load [38]. Generally, the <110> crystallographic plane is most commonly used due to its higher hardness and electrical resistance [32, 39] despite the fact that wear rate is higher compared with <100> crystallographic plane [40]. In such crystals, the bending energy is low and it is easy to induce cleavage along the crystallographic plane.

The most exposed region of the head is the gap, where glass bonding could cause considerable strain in the structure. Matching the anisotropic thermal coefficient of expansion of the single crystal ferrite with that of the glass is quite a challenge and mismatches will inherently occur. The tension could generate micro-cleavage of the ferrite, generating a high level of noise due to magnetostriction [32].

One of the common phenomena encountered with the iron oxides is that in presence of moisture they tend to develop on the surface a thin layer of oxyhydroxide

(FeOOH) [41]. Under normal conditions, the iron oxyhydroxide is amorphous, resistant to prolonged exposure to vacuum and decomposes at 136°C [42, 43, 44, 45]. Studies made using XPS and infrared techniques showed that the amount of oxyhydroxide increases in time at constant humidity due probably to its porous characteristic and with the increase in humidity [46]. The oxyhydroxide or other hydrated by-products that result during a tribochemical reaction may also act as a solid lubricant, reducing friction coefficient [47, 48]. Although no studies of the oxyhydroxide have been made on ferrite, since the ferrite is composed mainly from Fe_2O_3, it is probably correct to assume that it will undergo a similar process.

As for non-magnetic material, the glass with additives such as B, Pb, Al or K is used extensively along with other ceramics such as MnNiO, CaO-TiO_2-NiO, $CaTiO_3$, AlTiC or SiC. In DDS heads glass with additives such as boron and lead has proven to be reliable from the point of view of stability for non-contact operations or resistance in contact operation. The bonds between glass and ferrite are created through the wetting of the ferrite by low-temperature lead borate glasses, which react with the surface of the ferrite. The improper control of the glass and head temperature can lead to an uncontrolled diffusion of the glass inside the ferrite, which can furthermore produce unwanted elongation of the magnetic gap. The phenomenon is more frequently encountered on heads made from Ni-Zn ferrites rather than those made from Mn-Zn ferrites due probably to the fact that Mn-Zn ferrites are less porous. [32]

In the MIG heads, a layer of metal is interposed between the ferrite and the glass and one of the most frequently used is an alloy of iron, aluminium and silicon known as *sendust* (85%Fe, 9%Si and 6%Al). Due to the sendust alloy, the head has a higher saturation magnetisation and this property makes it ideal to use with high coercivity media and, at the same time, its reproducing efficiency remains comparable with the bulk ferrite heads [19]. The sendust alloy is not the only magnetic alloy used to improve the heads performances; permalloy (80%Ni, 20%Fe), FeN or Co-Nb-Zr are also used [29].

In order to manufacture the head, the ferrite material is cut and polished, the gap is deposited by sputtering, and the two halves of the head are then bonded and shaped. The

curvatures of the head depend on the protrusion of the head above the drum surface, the tape tension and the stiffness of the tape [49] The head may also be coated with a thin film of DLC or CrN in order to improve its wear resistance [50]

2.5 *General view of MP tapes*

The technology of magnetic particulate (MP) tapes has improved continuously in the last 60 years since its introduction. First MP tape was made by Germans by coating the magnetic paint on top of a paper substrate. It was not a very reliable tape due to the fact that paper tends to rip. A big step forward was made after the huge advances in polymer science during and after the Second World War. At this point, tape started to become a very reliable storage media and since then, the way of making these MP tapes hasn't changed too much. In this chapter a brief description of magnetic tapes is given with emphasis on metal particulate tapes.

Basically, an MP tape consists of a polymer substrate of 5-10μm in thickness coated with a very thin magnetic layer. On the backside of the tapes, a layer of about 1 μm of carbon black is applied in order to improve tape's friction properties and to prevent build up of static charge. A cross section view of a typical MP tape is in figure below.

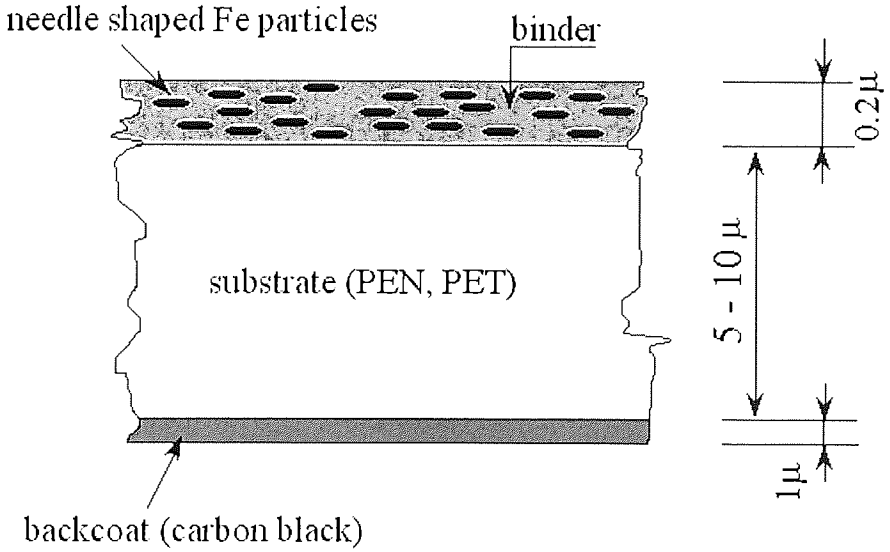

Figure 2-12 Cross section through a single layer metal particle tape (not at scale)

The magnetic pigment is a mixture of magnetic particles (γ-Fe_2O_3, magnetite, cobalt-modified iron oxide, chromium dioxide, barium ferrite or ceramic-coated iron), and abrasive particles (Al_2O_3, CrO_2 or α-Fe_2O_3) finely dispersed in a polymer binder and lubricant. The substrate material could be PET (polyethylene terephtalate) or PEN (polyethylene naphtalene) but efforts have been made to introduce new materials with better physical and chemical properties such as ARAMID and PBO, which have higher elastic modulus and better dimensional stability [51].

The magnetic paint has a thickness between 0.1-0.2μm. If the thickness of the magnetic layer exceeds 0.2μm, it makes the diffusion of the binder insufficient, reducing the durability of the surface of the magnetic layer. On the other hand, if the thickness of the magnetic layer falls below 0.07μm, the resulting output is reduced [52, 53]. Indeed, according to Equation 2-1, decreasing the magnetic thickness of the magnetic layer leads to an increase in the number of bits but this affects the output signal. Hence more sensitive read sensors are required.

More recently, a new technology called AMP (Advanced Metal Particulate) using an additional layer in between the magnetic layer and the substrate made from a non-magnetic material (as α-hematite) has emerged [52, 33, 54, 55, 56]. The advantage is that double coating technique can produce ultra-smooth coatings thus reducing spacing loss, demagnetisation fields and isolated pulse width [52, 54].

The magnetic materials used nowadays in high-density MP, BaFe and ME (Metal Evaporated) tapes have a higher coercivity than conventional metal oxide particles. The magnetic layer is designed with lower surface roughness than conventional MP tapes to increase the output signal by reducing the flying heights of the tape [55]

One disadvantage of the MP tapes is that DC erase noise of MP media is relative higher than other types of media (such as metal evaporated tapes) because of its inhomogeneity [57].

2.5.1 Tape Ingredients

2.5.1.1 Magnetic Particles

The magnetic particles are the "core" of an MP tape. The magnetic, chemical and mechanical properties of them are very important since they are responsible for storing the information on the tape.

There is a large number of materials used as magnetic particles such as: γ-Fe_2O_3 (γ-hematite), CrO_2, Co-modified iron oxide, barium ferrite, ceramic coated iron, passivated iron [29, 52]. The shape of the particles varies from acicular or rice grain for γ-Fe_2O_3 to hexagonal for barium ferrite [55] and the standard size of the particles is about 0.05 to 0.5μm, thickness about 0.03μm and the aspect ratio (length/width) is situated between 10:1 to 10:5[55, 57]. Nagai and Inoue have proven using a dark-field microscope that larger particles tend to have a multi-domain structure whilst most of the smaller particles have one single magnetic domain [57].

Another important way of quantifying the amount of the magnetic particles within the magnetic paint is the so-called packing-ratio and it represents the volume fraction of magnetic material in total material on the magnetic layer of the tape. Usually, the packing ratio is controlled by adding non-magnetic particles such as α-Fe_2O_3, TiO_2, $BaSO_4$, ZnO or Al_2O_3 and by controlling it, one can vary various parameters of the tape such as coercivity and roughness [52, 57]. In order to achieve the highest possible signal the magnetic pigment loading should be as high as possible. However, mechanical properties of a filled polymer degrade if the particle loading is too high therefore a careful choice must be made. Modern MP tapes have packing ratio between 20%-50% [57]

Since 1948 when the first ferric acicular particles were produced, the technology has continuously advanced and nowadays smaller and smaller metal particles are produced.

In the beginning, in the early stages of the tape manufacturing, the magnetic particles used were γ-Fe_2O_3 but they had a low coercivity. The increased demands for higher data storage densities and the reduction of the track width have lead the industry towards magnetic particles with higher magnetic saturation fluxes. Thus, the industry focused on metal iron particles that, in addition, are less abrasive than the iron oxide particles and allow, for the same thickness, a higher output signal and a higher resolution. [58]

The technology of producing these particles is quite complicated since they must be produced at the right size and with the appropriate anisotropy. There are three main stages that involve:

1) producing the non-magnetic acicular particles,
2) treating these particles in order to become ferromagnetic and then,
3) passivating them;

In order to generate the acicular shaped particles, different methods are employed:

a) reduction of the goethite (FeOOH) using hydrogen or an organic compound (oxalate);
b) pyrolysis of a metallic carbonyl compound;
c) adding a reducing agent to an aqueous solution of a ferromagnetic metal;
d) evaporation of a metal in an inert gas under reduced pressure to obtain a finely divided powder;

In the first step, a chemical reaction between an aqueous solution of ferrous iron with an alkali hydroxide or carbonate is produced leading to the formation of a colloid suspension of iron hydroxide or carbonate. By blowing the suspension with oxygen containing gas at pH bigger than 11 and temperature lower than 80°C, the hydroxide or carbonate undergoes an oxidation reaction leading to a particular acicular goethite (FeOOH). Then the newly produced goethite is carefully dehydrated at a temperature up

to 500°C followed eventually by a heat treatment for annealing at a temperature up to 800°C in order to obtain a particulate acicular α-Fe_2O_3. [52]

The next step consists of heating the particles in the presence of hydrogen to a temperature of about 400°C and maintained under this condition until all the material has been converted to Fe_3O_4 (magnetite) or γ-Fe fact denoted by the jet black appearance of the powder. The difference between these two species is given by the treatment time. After that, the material is then allowed to cool down to about 100°C. [15]

In order to reduce the corrosive wear of the binder and to support a better cohesion within the magnetic pigment but also to avoid spontaneous combustion, the newly produced γ-Fe particles are treated in order to create an outer shell of oxides [44, 45, 52, 59, 60]. The process is called passivation and there are several ways of doing it:

a) Dipping the metal powder into an organic solvent with an oxygen-containing gas bubbled to form the oxide film and then drying or,
b) Controlling the oxygen content of the atmosphere where these particles are baked; [52].

Unfortunately, passivating the iron particles is also reducing the saturation magnetisation of the pure metal and may induce oxidation along grain boundaries thus accentuating inhomogeneities already present in the unpassivated particle [60, 61]. The coercive force obtained is generally between 1500 to 4000Oe and the saturation magnetisation is from 110 to 190 emu/g. The water content of the particles depends usually on the binder to be used during mixing. Further surface treatment with aluminium, silicon or phosphorus may be applied in order to optimise surface adsorption of specific lubricants and binders.

2.5.2 Binder

The role of the binder system is to hold the metallic particles to the substrate and together with the metallic particles and lubricants it forms the so-called magnetic paint or magnetic layer. The substances chosen to be a binder must have a good physical and chemical stability and must retain their characteristics in various environmental conditions. They also must insure a good dispersability of the acicular magnetic particles since an asperity of one magnetic particle diameter in height may induce a spacing loss of 8dB [60]

The binder consists of a mixture of various cross-linked polymers such as vinyl chloride resin, polyurethane resin, or amine-quinone polyurethane [61]. Generally, the polymeric compounds consist in two phases: a hard glassy phase to give mechanical integrity and a soft, rubbery phase. The glass transition temperature of the hard co-polymer is much higher than that of the soft co-polymer, so the first one acts as the physical cross-link whereas the soft co-polymer retains the rubber elasticity between glass transition temperatures corresponding to soft and hard co-polymers [62]. The degree of cross-linking between these phases must be carefully controlled since a low degree would reduce chemical resistance of the polymer whereas an increase would result in a more resistant to chemical attacks and an increased abrasion resistance but also a tougher, harder and less flexible polymer. It is known that in the case of polyurethanes chemical bonds included in several groups such as allophanate, biuret, urea or urethane groups can break as a result of repeated mechanical stress and the energy required can be as low as 20kcal/mol. [72]

The exact chemical formula used for the binder and the amount of the binder used in the tape formulation depends on each manufacturer but generally the cross-linked binder structure looks like in the figure below:

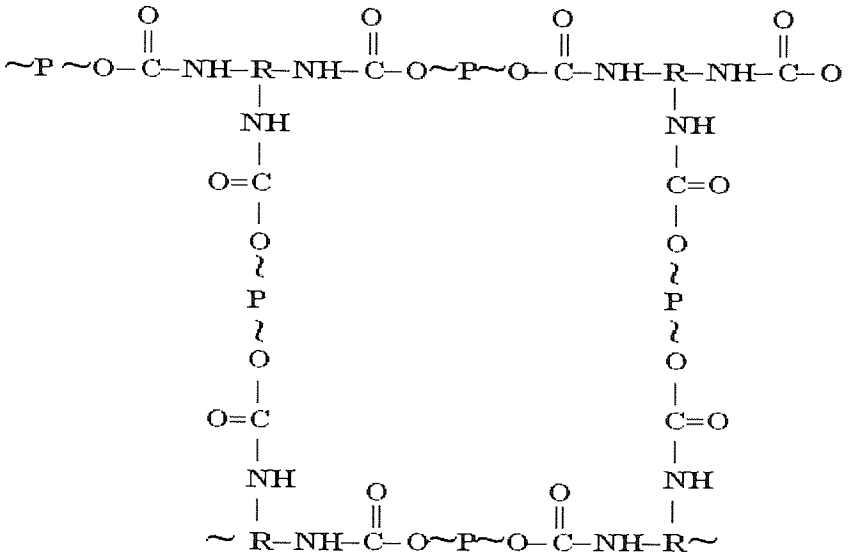

P - polyesther
R - polyurethane

Figure 2-13 Chemical structure of a typical binder [63]

In order to reduce the occurrence of scratches on the surface of the magnetic layer, it is useful to increase the binder amount within the magnetic paint formulation. The polymer has a glass transition temperature situated between 35°C to 90°C in order to reduce the friction coefficient.

The interaction between the binder and the metal particles can be through hydrogen bonding if both polymer and the iron particles have acid sites but it is desirable to have an acid-base interaction since the chemical bonds are much stronger thus improving interparticle adhesion and minimising particle shedding [64, 65]. It has been proven that the surface of the passivated iron particles behaves as a base mainly due to the oxyhydroxide sites on its surface. In this case the binder reacts with oxyhydroxyde on the surface, cleans the surface, and bonds to the surface by primary or secondary valence forces by means of ureas linkages. [66, 72] Additionally, the coupling between the basic sites of the metal particles and acid groups of the binder such as phosphoric acid groups or alcohol groups leads to strong hydrogen bonding between the hydroxyl groups of polymers and particles [59, 67].

The polar groups most frequently used as "anchors" (wetting agents) are: -COOM, $-SO_3M$, $-OSO_3M$, $-P{=}O(OM)_2$, $-O-P{=}(OM)_2$ where M could be a hydrogen

atom or an alkaline metal salt or group [52]. Other studies show that the phosphates groups tend to interact better with the active sites of the metal particles or ferrite, however the amount of the functional groups must be optimised since a higher level of functional groups tends to deteriorate the hydrolitic stability of the polymer. [68] On the other hand, the binders containing aromatic isocyanates groups with hydroxyl groups are found to be more reactive than those containing aliphatic isocyanates. [69]

The amount of binder within the magnetic layer is between 13 to 50% by weight, based on the magnetic powder. Based on the XPS measurements, the Cl/Fe ratio is between 0.3 and 0.6 and N/Fe ratio is 0.03 to 0.12 [16].

Due to its essential role in maintaining the stability of the magnetic properties of the tape, the binder chemistry is particularly of interest and is treated in a special chapter.

By carefully choosing the polyurethane composition and the degree of cross-linking for the binder within the magnetic coating, a relatively stable coating can be achieved having good chemical and mechanical properties.

2.5.3 Substrate

The mechanical properties of the substrate also play an important role in durability of the magnetic tape. During its manufacture, the tape substrate is commonly referred as 'the web'. The thickness of the substrate is nowadays between 4.5 to 8.8 μm and choosing it is of prime importance. A smaller thickness would increase the storage capacity but it would also reduce the stiffness of the tape making it impossible to have a good durability or occasionally making the head-tape interface unstable. On the contrary, if the thickness is too high, the tape may exhibit a high stiffness making impossible a smooth head-tape interface.

According to Hooke's law,

$$\frac{F}{S} = E\frac{\Delta l}{l_0}$$ Equation 2-8

With:

F – force
S – area of the sample
E – elastic modulus
Δl – relative displacement
l_0 – initial

From the manufacturer's data [16], one can compute the elastic modulus:

$2 \cdot F = 40mg \times 10ms^{-2}$

$S = 8 \times 50\ mm^2$

$\Delta l = 5mm$

$$E = \frac{F}{S} \cdot \frac{l_0}{\Delta l} = \frac{20 \cdot 10^{-6} kg \cdot 10m \cdot s^{-2} \cdot 50 \cdot 10^{-3} m}{8 \cdot 50 \cdot 10^{-6} m^2 \cdot 5 \cdot 10^{-3} m} = 5Nm^{-2}$$

The thickness of the tape in this case was 13.5μm that is numerically close to E^3. This rule between tape stiffness and the elastic modulus gives a rough guidance in choosing the right candidate for the substrate.

Polyethylene naphthalate or polyaramide resins are the most common used polymers replacing the older polyethylene terephthalate. The substrate may be subjected to different treatments such as corona discharges, plasma treatments to increase adhesion by generating unsaturated bonds, heat treatments etc. The surface treatment is applied differentially so that the surface on which the back coating is to be applied is rougher than the surface where the magnetic paint is applied. [52] These treatments are performed because research showed that a smaller roughness (a smoother surface) improves the electromagnetic characteristics whilst a rougher surface improves durability.

The current substrates are almost entirely made from tensilised polymers. These polymers are pre-stretched in order to improve their mechanical properties. A tensilised

polymer has a higher tensile strength and a lower break elongation in the longitudinal direction. [58] The substrate is tensilised preferably perpendicular to the direction of motion due to the fact that it exhibits a better head contact [52].

In DDS2 tapes used during experiments, the substrate is made from PET. It is well known that PET film degradation is complex. Both thermal degradation and hydrolysis can occur at the same time. The difficulty arises in identifying which process is the most destructive under a specific environmental condition.

Studies made at the beginning of 90's by Edge and co-workers on PET polymer films under different environmental conditions, particularly at high humidity and high temperatures, revealed that at higher temperatures the effect of thermal degradation appears to be more prominent whereas at lower temperatures hydrolytic degradation dominates. [77] Furthermore, the rate of hydrolysis is increasing as the number of carboxyl-end-group concentration increases. The thermal degradation that occurs at high temperatures seems to be related with the fact that at temperatures above 80°C the glass transition temperature of the polymer is exceeded and atoms of metal impurities are able to migrate more readily into the polymer structure and accentuate the degradation rate. The experiments were done on polymers subjected to natural or ageing tests with the same result.

The authors also confirmed earlier observations which show that accelerated ageing tests performed at 100%RH are giving similar results to those of natural ageing processes.

Since the substrate is covered by the magnetic coat and backcoat, it is unlikely that the substrate will suffer hydrolysis or thermal degradation during the tape lifetime.

2.5.4 Backcoat

Initially, the back coating of the tape was designed with a multiple roles: to inhibit build-up of static charges formed due to friction, to reduce the frictional

coefficient, provide a light screening effect, enhance the film strength and so on. The capacity of dissipating the static electricity of the backcoat was mainly due to the fact that it was intentionally designed to be the most hygroscopic component in the tape formulation. [52, 78] Carbon black is the most commonly used material for back coating. Although carbon black is still used, the newer backcoat has the same mixture of compounds as magnetic coat but with a higher head-cleaning agents loading.

2.5.5 Lubricant

The main role of the lubricant is to reduce friction coefficient and increase the durability of the tape sometimes by three or four orders of magnitude. Media lubricants often consist of fatty acids and fatty esters. Lubricants on the surface of MP tapes are diminished by the operation of the media. The lubrication performance is maintained as a result of migration of the lubricant from the subsurface to the surface [79]. Hence, it is preferred to apply the lubricant internally rather than topically. It is also been shown that the speed of migration toward the surface increases with the decreasing of the viscosity and thus with the chain length. Tests performed by Nishida et al [79] using XPS technique revealed that the time needed for the lubricant to reach the surface is between 50 to 800 seconds. The lubricant of higher migration speed proved to provide a better stability of the friction coefficient. Different lubricants having functional modified polar groups are tested to increase the area coverage and to increase the frictional characteristics. [80]

2.5.6 Head Cleaning Agent (HCA)

Although initially, in the early stages of tape development, the role of the head-cleaning agent was to maintain the head poles and the gap clean from the debris that may results during normal operation, now HCA is been used mainly to give the tape mechanical integrity. Various materials are used but most commonly are Al_2O_3 or SiO_2, Cr_2O_3, artificial diamond, SiN having different shapes (needle, cubes, spheres). Usually, the particle density is chosen to be higher than 50 particles/cm^2. [52] Higher surface asperities improve the tape lifetime and may reduce friction coefficient but on the other hand it may increase the head to tape spacing. [81] In order to improve tribological

properties of the tape, more recently a DLC layer is also applied on the surface of the tape. [82]

2.6 Manufacturing an MP tape

Nowadays, almost all the tapes produced have two layers of coatings. On top of the substrate it is coated a non-magnetic layer with similar formulation as the magnetic pigment except that α-hematite or TiO_2 is used instead of γ-hematite. Then the magnetic paint is applied.

For non-magnetic layer as for magnetic layer, one of these coating methods [15, 52, 58]: are applied

- Blade coating;
- Roll coating;
- Gravure method;
- Extrusion coating;
- Dip coating;
- Spray coating;

The first step in producing the tape consists of mixing the magnetic particles together with the binder and the some additives in order to produce the magnetic paint. The step is accomplished usually in two stages: pre-mixing and dispersion. The particles are added either all at once or they may be premixed with a part of the resin and then added to the whole composition.

Since the magnetic particles have the tendency to agglomerate or to form lumps, in order to obtain a good dispersion, very high shear forces must be developed to separate the iron particles and to allow the solvent to interact with them. The most common technique of dispersion is the ball mill: a jar filled partially with the dispersing medium; as the mill rotates, the dispersing medium is carried up one side of the

container and then falls downwards. The speed of the ball mill is important since at a reduced speed the dispersing medium will lay on the bottom of the jar and at high speed the medium will be carried around the drum by centrifugal force. Other techniques include vibratory ball mills, sand mill or use a very intense mixing in order to achieve high shear. Poor mixing could lead to noise and nonuniformities and, eventually they can cause dropouts. The time required to achieve a good dispersability varies from few hours up to days.

Coating represents the second step and it consists of applying a uniform and very thin film to a web of base film at a reasonable high speed. The speed of the web must be kept constant. The coating must be uniform along and across the web. It should also be very smooth.

The simplest method of coating is called knife or blade coating where the sharp or very blunt blade of a knife forms a dam behind the magnetic paint reservoir. A small gap exists between the knife and the top of the web. The gap size may be kept constant or may be variable. Thickness variation of the substrate film or dirt deposited on the web can cause coating thickness variation. A schematic representation of the device is in Figure 2-14.

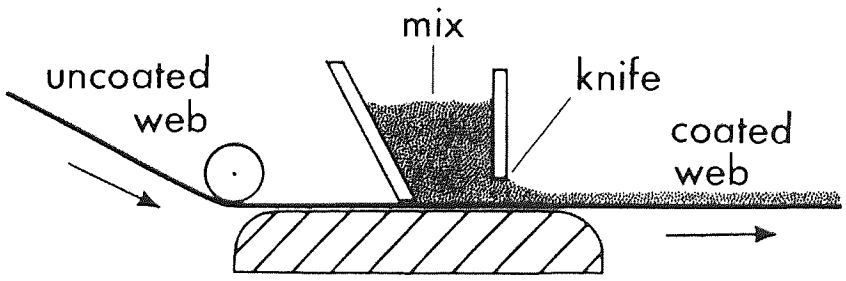

Figure 2-14 A schematic representation of the knife coater [58]

An improved method that eliminates the thickness variation problem is using reverse-roll coating (see Figure 2-15). The magnetic paint is applied in a relatively thick layer to a very accurate, smooth-surfaced roll called applicator roll. The thickness of the layer of magnetic paint carried around the roll is then controlled either by another roll rotating in the same direction or by a blade similar to that used in knife coating. The

mixture is then transferred from the applicator roll to the web the surface of which is sustained on one or more rolls so that the film is moving oppositely to the surface of the applicator roll. Thus, the coating is applied in a wiping action. Unfortunately, the method reduces but does not eliminate thickness variations.

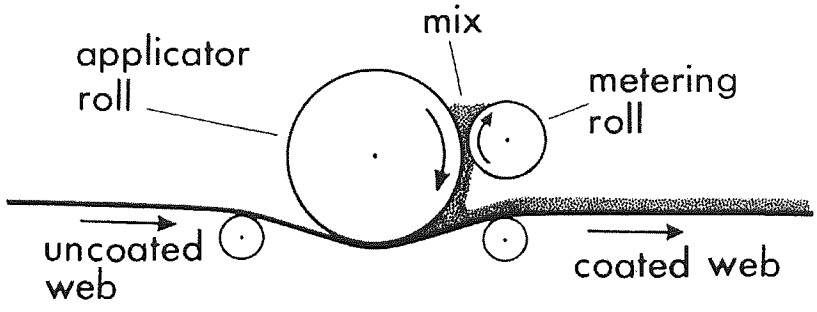

Figure 2-15 Reverse-roll method [58]

The gravure method uses a different concept (Figure 2-16) similar to that used in printing newspapers. The surface of the gravure roll is engraved with a series of fine grooves closely spaced together designed to pick up the magnetic paint. All excess paint is removed by using a blade so that the only material left is that contained in the grooves. Thus, the magnetic paint thickness is depending only by the shape and pitch of the grooves rather than by the spacing between two moving parts. The mixture is transferred to the substrate that is moving in the same direction and at the same speed as the gravure roll. Since the paint is distributed in the form of small ridges distributed diagonally across the substrate, it is smoothed using a roller. Controlling this smoothing is the real major problem of this method.

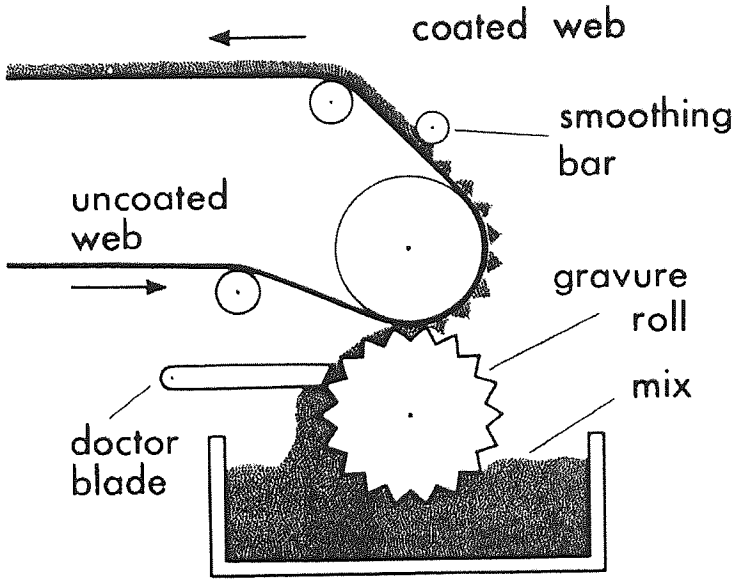

Figure 2-16 Representation of a gravure coater [58]

After coating, while the paint is still wet, a magnetic field is applied in order to enhance the magnetic properties of the tape. Usually, the magnetic field is applied in the direction of tape motion but in the case of tapes used in helical scan, the magnetic field is applied across the tape at a certain angle. The magnetic field must be precisely controlled since a tilt in vertical direction will induce an enhancement in the recording when the tape is played in one direction and a decrease in the output when the tape is played in the opposite direction. Both permanent magnets and electromagnets having the induction up to 2000Gauss are used in order to achieve a higher orientation.

After orienting the magnetic particles inside the tape, the solvents are removed by using heat and by blowing air. Further surface treatments are designed in order to reduce the height of the largest projections on the surface, thereby reducing the head tape gap and thus increasing the output especially at higher frequencies. One of the most used methods called calendering consists in passing the tape through an assembly of two or more highly polished rolls made of metal or polymer. The rolls are subjected to heating up to 120°C. The tape is squeezed between these rolls at a pressure between 200 and 500 kg/cm^2 [52].

The final step involves cutting the web into appropriate widths using circular knives and packing the tape into the cartridges.

2.7 *Stains on magnetic heads*

Today, the tape industry is driven by the necessity of increasing the data density. The first solution involves the reduction of the thickness of the magnetic paint but this will affect the signal playback. In order to increase the signal playback, one must switch to higher coercivity magnetic tapes that will lead to write and erase difficulties. Another solution is to minimise the gap between head and tape and thus, any deposits on the heads must be minimised. Studies [83] show that in the case of MP tapes, in order to achieve higher recording densities, the need to reduce spacing between head and media is more important that the reduction of the acicular particle size.

According to Equation 2-1, decreasing the gap between tape and head will lead to a sharper signal and thus to a higher density of bits per inch. According to Equation 2-2, increasing the number of bits per inch means a shorter wavelength, which furthermore means that the loss of signal will be more dramatic if a gap between head and tape occurs at higher data densities.

Several authors [27, 10, 19, 28] have identified different phenomena as sources of errors such as gap erosion, pole or MIG material recession, spacing loss caused by loose or adhesive debris, macroscopic changes of the head profile or changes in microstructure of the head material due to an increase in contact temperature between head and tape. All of the above-mentioned processes introduce spacing between head and media and according to Wallace law (Equation 2-2) a decrease in signal playback. The decrease in signal playback means that the signal output corresponding to bit "1" decreases, ultimately will be below the threshold value and will be read by the head as bit "0" hence an error.

Chandler et al [27] believe, after experiments made with DDS tapes and drives, that if there is a single cause for spacing loss, it is more likely to be contamination with stain on the ferrite since the brown stain proved to be more continuous and tends to

accumulate at the gap region. Also stain proved to accumulate especially on the trailing edge of the head more than on the leading edge [84]. Stains have been reported in both linear and helical systems [85]

Two types of deposits have been reported on the heads classified as adhesive (adherent) and loose deposits. These deposits could be present as either spotty or as a continuous film [86].

The term of friction polymer appeared for the first time in a paper signed by Hermance and Egan regarding the telephone relays enclosed in plastic containers and their conclusion was that it is mainly composed from degraded polymers [32, 86, 87]. Then, the existence of stains was first reported in a paper on ferrite heads by Lemke in 1971 who launched the hypothesis that stain is a friction polymer continuously being removed and replenished from the binder system within the tape. The thickness of stain was estimated to be less than 100 Å and its presence improved wear resistance of the underlying material by as much as a factor of 100 [32]. The ability of the stain to improve the wear resistance of the heads was also reported in other papers as well. [88]

With the trend towards increasing the data density and the appearance on the market of new types of tapes, the research extended to all kinds of tapes and heads and, surprisingly it was found that the stains formed by an MP or barium ferrite tape are different for those generated using other types of tapes. Its colour is brown but its chemical composition is different.

Apart from its different colour, brown for stain generated by MP tapes and blue or colourless for that generated by other kind of tapes, both types of stain reduce the friction coefficient between head and media and are useful as long as they form a uniform continuous film and their heights do not exceed few nm. A discontinuous thick film would produce high wear and poor signal playback. Another common feature is that they are sticky on the surface of the head and cannot be removed by simply using cotton tipped applicator with a head cleaning solvent, as it is the case of loose debris.

It is generally agreed that stains start as small spots and then grow into bigger patches and then into a continuous film. [86] Another series of visual observations made

on adhesive debris have shown that the film has a preference to form along the edges of the glass and ferrite.

The development of the stain under certain conditions is a dynamic process. While running a tape against the head, new stain is forming continuously and the old one is worn off. The process is balanced by the rates on which the stain is forming and worn away. There are certain factors that can influence this balance:

- Environmental conditions
- Tape tension
- type of the tape (the abrasivity of the tape)
- Certain metals

Most of the authors agree that the adhesive debris tend to develop in atmospheres which involve high temperatures and low humidity [29, 27, 86, 28,]. In the experiments conducted at high humidities (more than 45%RH) the stains were not observed and already present stains on the head were removed. It seems that the key factor is the humidity rather than the temperature.

The tape tension also influences the stain development and evolution. It was pointed out that a low tape tension enhances the development of the brown stain whilst a higher tape tension will slow it down. This is due to the increased tape - head pressure, which leads, according to Archard's law, to a higher wear rate (equation 4). A higher wear rate will involve higher rate of material removal and thus a reduced stain thickness [29, 28, 89].

Another big influencing factor is the abrasivity of the tape but it is directly related to the ability of the materials within the tape, especially head cleaning agents, to wear. Increasing the abrasivity of the tape by increasing the amount of the HCA can reduce staining, however an optimum must be reached since higher abrasivity can exacerbate the wear rate of the magnetic heads [88]. Coating the tapes with a DLC (Diamond-Like Carbon) layer can also reduce staining of the heads [82]. The wear depends also on the number of asperities per unit area. It has been found that CrO_2 tapes

are the most abrasive tapes followed by Co-Fe_2O_3 tapes, MP tapes. The less abrasive tape proved to be ME tape [29, 90].

Certain metals have been found to be catalyst and others to be inhibitors in stain development. Lemke found studying laminated heads that Ni is the poison whereas Cu is the catalyst for stain formation [86]. The results were confirmed by indirect observations made by Bhushan [10] and also in 1995 by experiments of Liew et al [87] who used a block of metal with three parallel surfaces made from copper, aluminium and nickel upstream of the head.

An interesting aspect is to identify the constituent elements of such debris in order to establish a model to explain the generation and evolution of the stain. There has been and still is a large debate whether or not the stain consists of organic materials. An entire arsenal has been used in order to gather the required information. AES (**A**uger **E**lectron **S**pectroscopy), FTIR (**F**ourier **T**ransform **I**nfrared Spectroscopy), EDX (**E**nergy **D**ispersive **X**-ray), ellipsometry, optical profilometry, SIMS (**S**econdary **I**on **M**ass **S**pectrometry), AFM (**A**tomic **F**orce **M**icroscopy), SEM (**S**canning **E**lectron **M**icroscopy), TEM (**T**ransmission **E**lectron **S**pectroscopy) are some of the techniques used. Despite this, the investigation proved to be very difficult due to the size of the area to analyse and to the size of the adhesive deposits themselves.

Initially, it was thought that these stains are frictional polymers, materials of the tape, which were chemically altered during deposition process and compacted unaltered materials (chemically speaking). It was thought that friction is the process that triggers the formations of these kinds of stains and without the frictional heating energy the re-polymerisation reaction would not be possible.

Ota et al [28] reached the same conclusion after studying brown stain on VCR's heads using the Scanning Electron Microscopy (SEM). Haloes observed in the diffraction pattern and also surface charging during SEM investigations led him to the conclusion that brown stain consists of non-conductive substance.

Studies made by Stahle and Lee [84] using AES technique revealed that the brown stain consists of iron particles from the tape that are pressed on the metal region

of the MIG head. They didn't find in Auger spectra any peak coming from the elements of the metal alloy (namely Fe, Si, or Al) or the zinc from the ferrite region and this finding demonstrates that the brown stain is not composed of the sendust alloy or ferrite material.

Using SIMS analysis, Gupta and co-workers [91] found that stain obtained using Metal Particulate (MP) tapes does not contain any organic species from MP tape; when the head was run against MP tape, SIMS analysis revealed high concentration of iron and a low concentration of carbon. The authors also have found low concentration of iron, high concentration of carbon and the presence of chlorine in the top layer of stains on the metal core of the head run against the Co-γFe_2O_3 tape. This fact indicates that stains are organic rich with trace amounts of iron and oxygen [91]. The stains produced by Co-γFe_2O_3 tape were thick and patchy whereas those by MP tape formed a uniform film.

Using AES measurements and sputtering they were able to measure the thickness of the stain: 30-75nm and to compare with the thickness of the stain produced by Co-γFe_2O_3 tape .The last type of stain had more than twice the thickness of the stain formed by MP tape. Biskeborn [86] found, based on the same technique, that deposits extend below the head surface and that they are made of 90% atomic iron and oxygen and do not contain MIG head (sendust alloy) elements such Al or Si and any organic materials.

Until recently, the only solution to remove or to reduce the brown stain width was to lap a relatively high abrasive tape along the head or to use high humidity. [84, 86] The lapping method induces an accelerated wear of the heads therefore it is not desirable. Another solution was proposed by Hirofumi et al and involves coating the magnetic head with a polymer [92, 93]. Kamei et al [94] have found that using a chelating agent they can gradually remove the brown stain formed on the head. They have used various concentrations of 1,10 phenanthroline deposited on the tape using the dip-coating method with toluene used as solvent for dip coating and they have discovered that increasing the concentration of this substance would increase the speed of the removal of the brown stain. Another interesting observation was that 1,10

phenanthroline wasn't able to remove the brown stain when it was applied on the head using cotton-tipped applicator. SIMS analysis performed on the heads revealed metal complexes. They believe that the chelating agent forms metal complexes with the brown stain but there is a threshold energy after which this chemical reaction occurs. The energy is probably given by the frictional heat.

On the other hand, for the chemists the behaviour of phenanthroline as a chelating agent - a ligand capable to attach itself to iron - is known since 1937 [95] and since then it has been used as an indicator of iron presence. The chemical reaction takes place between three molecules of organic compound and one atom of iron according to the following equation [96],

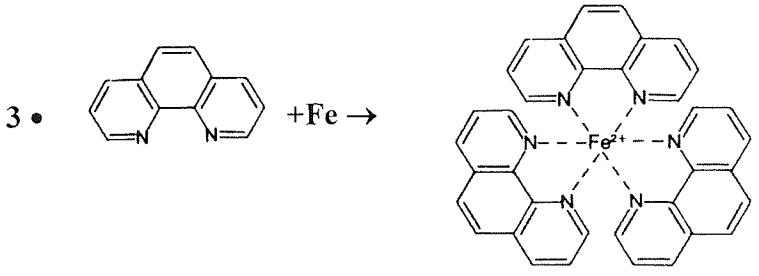

Equation 2-9

and leads to the development of an organo-metallic compound which remains on the tape. The ToF-mass spectroscopy revealed probably the existence of this organic compound on the surface of the tape after running against a stained head. One important thing is that usually these kind of chemical reactions take place mostly in solutions, meaning when the molecules have a high degree of mobility and the fact that the reaction occurs when both reagents are solid could prove that the frictional heat could give additional energy and trigger such events.

Indeed, the real contact area between head and media is much smaller than the visible area and in this contact points the pressure could be very high and thus the temperature. Older studies estimated the local flash temperatures between two asperities up to 900°C [51, 86, 97]. More recently, Ota et al [28] research on copper and iron dummy heads revealed that the temperature at the head tape interface rises up to the dynamic re-crystallisation temperature of the copper but does not exceed that of iron.

They concluded that contact temperature would reach 200-500°C in local and small contact regions. Similar results were found by Sullivan et al. [10]

If the experimentalists agree on the environmental conditions in which the brown stains appear, not the same thing can be told about the phenomena that lead to development of the stains. Several approaches were proposed. Sullivan et al [97] suppose that stains are formed due to particle transfer directly from media to the head produced by adhesive wear and held in place by ion-dipole interactions. The development of the stain is reduced in high humidity atmospheres due to water saturation of the active sites on the head thus reducing the number of adhesive bonds. Another model [84, 86] suggests that the atmosphere moisture provides cooling whereas reduced humidity can lead to higher contact temperatures and thus more energy for more chemical reactions. The third mechanism proposed suggests that the organic materials present in the tape structure may get involved in the early stages of the formation of the deposit with true chemical bonding to the head surface. After that, a phenomenon of building up of oxidised inorganic head and tape materials may follow.

Based on the experimental observations, Sankuer launched an interesting model that has to be mentioned here. He suggested that stains could be a sort of phthalocyanine, an organic or organo-metallic lubricant, derived from head-tape interaction. Some properties of this class of substances are quite interesting:

- Graphite-like structure enabling cleavage and thus low friction coefficients;
- Colourless for metal-free compound, brown-coloured for iron compound, blue for copper ones;
- Stable at high temperatures;
- Resistance to chemical and mechanical removal;
- Electrical semiconductivity.

The mechanism he proposed is that of molecular bonding of a thin layer of metal phthalocyanine followed by additional build up of either metal or metal-free phthalocyanine. Possible sources for this substance would be the binder and the lubricant within the tape formulation, tape substrate and/or the surrounding atmosphere. He went even further including this substance within the tape formulation. The results

showed a reduction in wear, and the XPS and AES analysis gave similar results as for normal stain. [86]

Observations of Talke [31] and then Lee and Talke [110] are very important since some of the previous mentioned models fail to explain the promoting or inhibiting role in stain development played by different metals.

The chemical composition of the adhesive debris is still controversial due to the small amount of material to analyse and although progress has been made, new more sensitive and higher resolution devices will help settle the argument.

To conclude, one must differentiate between debris produced using different sorts of tapes: stains produced by certain tapes (MP, barium ferrite) have been found to be formed mostly from iron and little or no organic material, whereas the debris produced on heads by other types of tapes (γ-iron oxides, CrO_2) are composed mainly from organic materials, degraded polymer. It has also been agreed that stain composition and the amount of adhesive debris generated depend on the type of tape used and on the head materials [85]. The stain growth is accelerated at low humidities and high temperatures whilst at higher humidities stain is removed. Certain metals such as Cu are stain promoters and others like Ni are inhibitors.

3 Experimental procedures and techniques

This chapter describes the principles and techniques as well as the experimental procedures employed during the experimental investigations. Transfer films (stains) on the magnetic heads had to be generated and then analysed. The environmental conditions that lead to the formation of the stains and their physical properties influence on the data reading heads were investigated.

3.1 Apparatus and Techniques

3.1.1 DDS drives

The DDS drives used during the experiments are from the third generation (DDS3). In order to communicate and operate the drive to perform the desired tasks, a UNIX workstation and specific software was used. The sequence of operations the drive has to perform can be customised by writing scripts in a code called mtcl (manufacturing test code language). This feature was used extensively throughout the research programme.

3.1.2 The mtcl scripts

As said before, the DDS drives had to be programmed using the mtcl code. The scripts written in this code offers a large degree of customisation allowing one to perform different tasks with the tape such as moving forward, rewinding, moving the tape at a normal, double or fast speed, writing data, reading the errors occurred in writing the data in a sequence suited for experiments. Once the script was written, it was compiled using a piece of software called xmdb on a UNIX workstation and then the resulting executable uploaded into the drive's EEPROM memory. The advantage of this method is that once the script was uploaded into the memory of the drive, the drive operation itself is not dependent on the UNIX machine. Thus, the drives can be mounted in an environmental chamber and the experiments can be started. The

sequence of actions of the DDS drives as a result of different mtcl codes used are presented in the sections describing each type of experiment.

3.1.3 The magnetic heads of a DDS drive

The schematic representations for both types of heads of a DDS3 drive (read and write heads) are shown in Figure 3-1 and Figure 3-3. As one can see there are differences between heads according to their function: the read head is a bulk ferrite head and the write head is a MIG type (**M**etal **i**n **G**ap) head. To prevent cross-talk between neighbouring tracks, the gap of the magnetic heads is tilted with different angles and the gap of the reading head is narrower compared with that of the writing head.

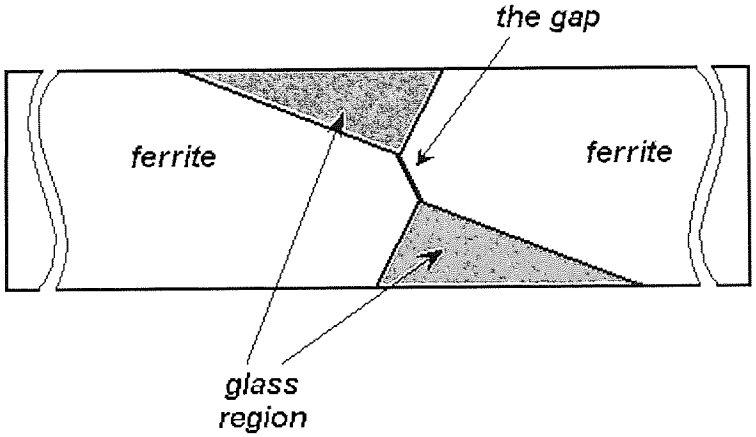

Figure 3-1 A schematic representation (top view) of the read head on DDS3 drives

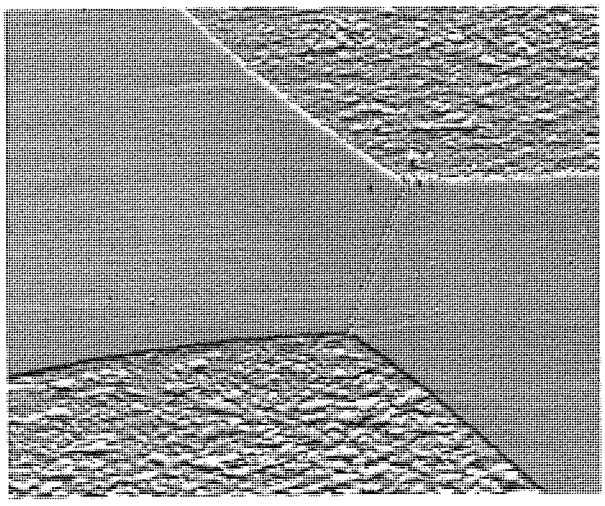

Figure 3-2 AFM scan of a DDS 3 read head

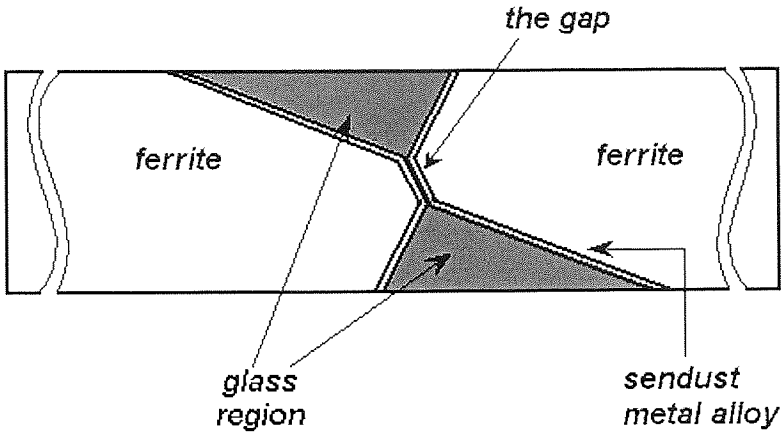

Figure 3-3 A schematic representation (top view) of the write head on DDS3 drives

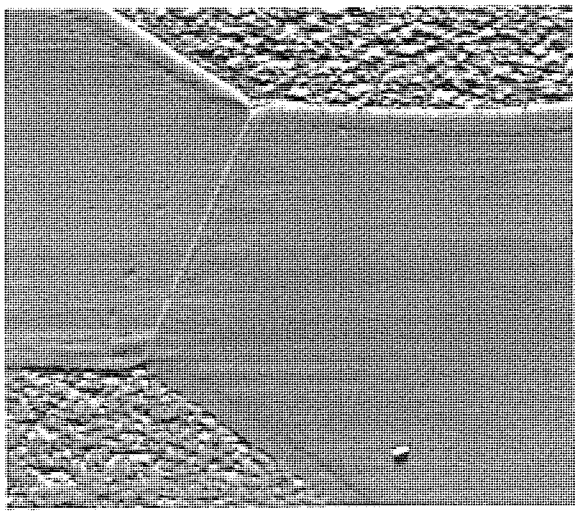

Figure 3-4 AFM scan of a DDS 3 write head

Apart from DDS3 drives, DDS4 drives were used for a study of the wear rate upon the humidity. The reading heads of the DDS4 drives are not bulk ferrite like the previous generation instead they are sandwich heads, built on multiple layers of deposited films. The feature has several advantages: permeability and flux density higher than that of single crystals ferrites, reduced eddy currents, lower magnetostrictive noise, lower wear.

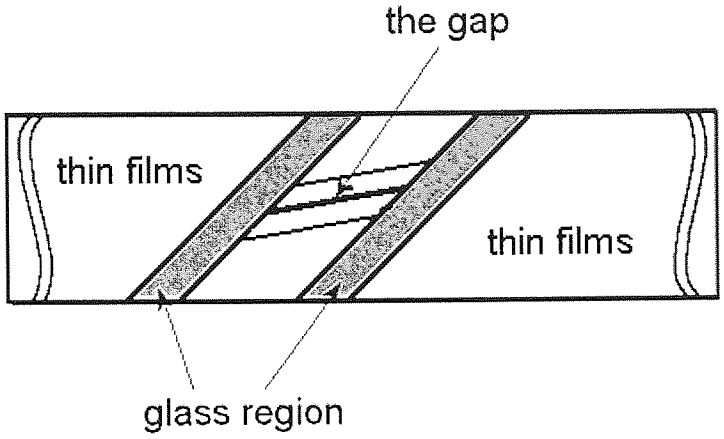

Figure 3-5 A schematic representation of a DDS 4 laminated head

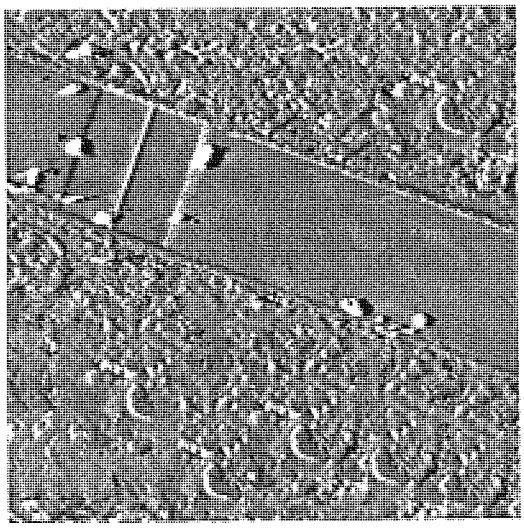

Figure 3-6 AFM scan of a DDS 4 read head

A more detailed description of the DDS drives and heads as well as the technology of recording data on these drives was given in chapter 2.

3.1.4 The tapes

All tapes used during the research were 120m long, metal particulate tapes (MP tapes) from the second generation (DDS2 tapes). In the study concerning the wear of the DDS4 drives, DDS4 tapes were employed instead. The chemical composition of the tapes and the fabrication process is not precisely known but XPS investigation showed the presence of the following elements:

Element	Percentage
Carbon	54.2%
Oxygen	30.6%
Nitrogen	0.9%
Iron	4.0%
Chlorine	4.7%
Aluminium	4.0%
Silicon	1.6%

Table 3-1 XPS quantification table of the tape elements

The presence of carbon and oxygen is due to a variety of components used in the tape formulation. The iron signal is generated by the presence of magnetic particles. The nitrogen and chlorine are good indicators of the binder polymer and finally the aluminium and silicon signals are due to the presence of head cleaning agents [98, 16].

The DDS-4 tape has a different formulation as one can see from the table below:

Element	Percentage
Carbon	48.3%
Oxygen	30.7%
Yttrium	4.1%
Iron	2.3%
Chlorine	1.2%
Aluminium	7.5%
Phosphorus	5.9%

Table 3-2 XPS quantification table of the DDS4 tape

In addition to carbon, oxygen, iron, chlorine and aluminium that have the same role as in DDS2 tape, other elements like yttrium and phosphorus are added to increase the wettability of the iron acicular particles to the binder polymer. [52, 99, 100, 101, 98, 16]

3.1.5 Environmental conditions

The various environmental conditions needed for the experiments were obtained using a Heraeus-Votsch VIK 04/300 environmental chamber. The surface topography and surface chemistry as well as the influence of stains on the error rates and wear rates were studied as a function of moderate temperature and humidity (25°C/35%RH) and extreme temperatures and humidities: 10°C/10%RH, 40°C/80%RH, 5°C/80%RH, 45°C/10%RH. The normal operating conditions for DDS2 and DDS4 tapes are given below: [102]

Env. Condition	DDS2	DDS4
Temperature range (°C)	5 – 45	15 – 55
Humidity range (%RH)	20 – 80	10 – 80

3.1.6 The AFM (Atomic Force Microscope)

The Atomic Force Microscope is a mechano-optical instrument, which detects atomic-level forces (of order of few nN) through optical measurements of movements of a very sensitive cantilever tipped with usually hard, pyramid-shaped crystal moved along surfaces. As it is moved along the surface using a piezo cylinder, the tip is repelled by or attracted to it due to atomic forces between the tip and the atoms composing the surface. The magnitude of the deflection is captured by a laser that reflects at an oblique angle from the very end of the cantilever. The laser deflection is converted into an electrical signal by four photodiodes. Thus, the topography of a surface can be recorded. The figure below is a schematic representation of the microscope. The microscope used for the experiments is a TopoMetrix Explorer scanning probe microscope. Further image processing was performed using Topometrix SPMLab v 3.06 software.

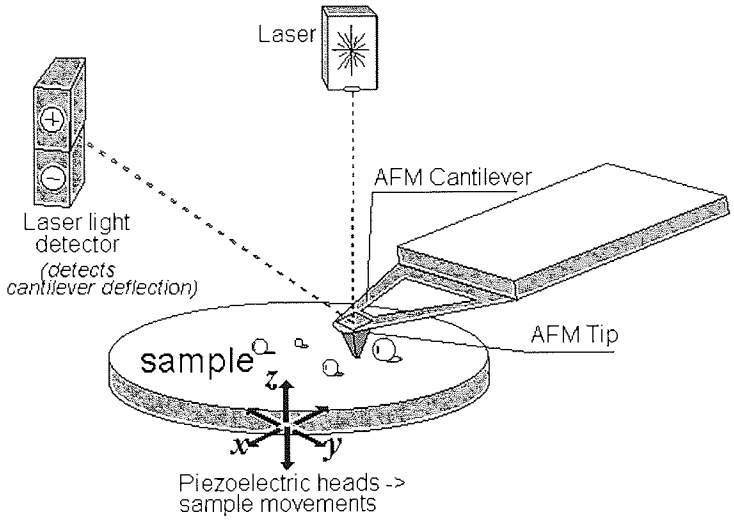

Figure 3-7 Schematic representation of an Atomic Force Microscope

3.1.7 Techniques of chemical analysis

3.1.7.1 X-ray Photon Spectroscopy (XPS)

In order to develop a model of adherent debris formation, information about their chemical composition was needed. Such analyses of the adherent deposits have been made using various techniques such as SIMS, AES (Auger Electron Spectroscopy) and XPS (X-ray Photon Spectroscopy) using VG ESCALAB 200D.

X-Ray Photoelectron Spectroscopy also known as Electron Spectroscopy for Chemical Analysis (ESCA) is a widespread technique for investigating surfaces and surface chemical changes. It consists in irradiating the sample with monoenergetic X-rays and analysing the electrons emitted from the surface. The kinetic energy of the electrons emitted varies according to the formula:

$$KE = h\nu - BE - \phi_s \qquad \text{Equation 3-1}$$

Where

$h\nu$ is the energy of the photon

BE is the binding energy of the atomic orbital from which the electron is emitted and

ϕ_s is the spectrometer work function

The binding energy is the energy required for an electron to be ejected from the electronic shell. Since every electronic orbital has a well-defined energy, the binding energy varies accordingly. Moreover, there are different probabilities of electron emission depending on the chemical element and on the shell from which electron is ejected. The spectrometer function is a constant dependant on the apparatus. If there is more than one atom as it is in the case of surfaces, the energy level of each electronic orbital will depend furthermore on the chemical bonds the atom forms with its neighbours. Therefore, the electron emitted will carry information regarding the chemical structure of the surface from which it generates.

Two elements are widely used as X-ray sources: Mg and Al with X-rays having energies of 1253.6 eV and 1486.6 eV respectively. The penetration power of these radiations limited to 1μm, which encompasses most of the important XPS transitions, made them suitable for surface studies. The electrons excited by the X-ray can escape form depths no more than 1-10nm due to inelastic scattering process. Also the use of Mg and Al sources allows one to separate photoelectron and Auger lines when interferences occur.

The advantage of this method is that it is non-destructive, meaning that the surface will retain its original physical and chemical properties. There are certain limitation though: the method cannot be used on small surfaces and the X-ray beam cannot be precisely focused making difficult to obtain a chemical distribution map of a particular surface. A second disadvantage is that it has to be used in vacuum (pressure below $5 \cdot 10^{-8}$ mbar) in order to allow escaped electrons to be collected. In the case of Fisons Instrument VG ESCALAB 200D, the analysing area is limited down to150 μm.

3.1.7.2 Auger Electron Spectroscopy (AES)

Auger effect takes place virtually in the same time with the photoelectric effect. The time gap between the electron ejected due to photoelectric effect and the

Auger electron is about 10^{-14}s. After an electron from the inner shells has been ejected due to photon absorption, another electron from the outer shell might occupy the vacancy. The energy emitted by the second electron (a virtual photon) is absorbed by a third electron from the outer shell that is being ejected. [103] Thus, the Auger electron will posses a kinetic energy equivalent to the difference between the energy of the initial ion and the double-charged final ion and is independent of the mode of the initial ionisation.

For surface investigations however, the sample to be analysed is bombarded with electrons of known energy and then the energy of the emitted electrons is analysed. A beam of energetic electrons, 3 to 25 keV, is used to eject a core level electron from surface atoms. To release energy, those atoms may emit auger electrons from their induced excited state. The energy of the Auger electron, specific to the atom from which it originated, is measured and the quantity of Auger electrons is proportional to the concentration of the atoms on the surface.

The advantage of the method is given by the fact that the bombarding electrons can be easily focused and then the beam can scan the entire surface and by doing so, a chemical map of the surface can be easily created. However, the method is less sensitive to small amounts of elements. Sensitivity of the method is 1% atomic percentage. Accuracy of qualitative analysis is limited to ± 30% if published sensitivity factors of elements are used. [130, 131] The Auger lines are broader than photoelectric lines hence the chemical shift information cannot be easily obtained. Another drawback especially when using semiconductor or insulator samples is the electrostatic charging in which case the sample should be tilted or its surface bombarded with low energy electrons.

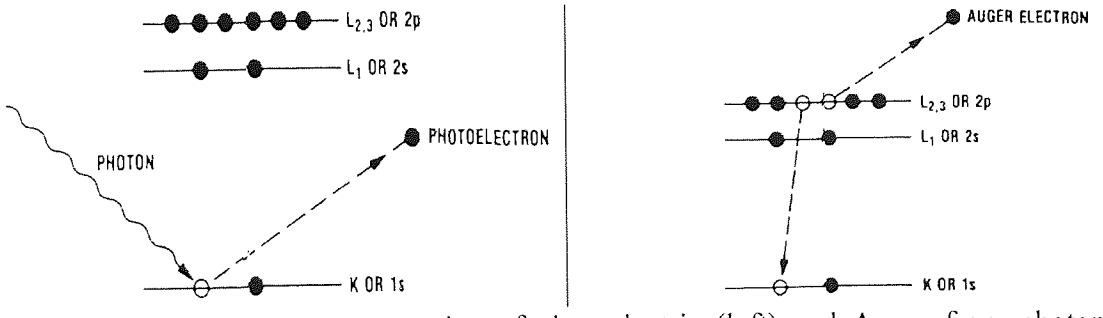

Figure 3-8 Schematic representation of photoelectric (left) and Auger from photon bombardment (right) phenomena [103]

In conclusion, photoionisation usually leads to two emitted electrons, a photoelectron and an Auger electron. The figure below is a schematic representation of both Auger and X-ray electron emission. The figure below shows both photoelectric and Auger phenomena that occur when bombarding a surface with X-rays.

3.1.7.3 SIMS (Secondary Mass Spectroscopy)

The technique is one of the most sensitive methods in surface analysis making possible to identify elements with concentration of I ppm (parts per million). By bombarding the surface with Ar^+ or Ga^+, atomic and molecular particles are emitted and analysed using a mass spectrometer. The emission phenomenon of secondary ions or neutrals from a surface as a result of high-energy particle bombardment is known as sputtering. The sputtered products may be electrically charged or neutrals in which case they need to be post-ionised in order to be analysed. By raster scanning the beam across an area of surface and collecting the secondary ions at each point a chemical map may be generated, technique called imaging SIMS [104].

There are two modes in which the analysis can be performed: dynamic and static. The first one where the flux of the primary ions is large can be thought as a destructive method since it errodes the surface and thus it may be possible to follow the changes in elemental composition with depth. The second, developed late in the 60's by a group of researchers led by Benninghoven, uses a much lower flux, and the surface monolayer removal time is higher compared with the time required for analysis. [104]
Unfortunately, since the sputtering process is not fully understood, it is impossible so far to quantify the amount of elements present on the surface. Therefore SIMS is used as a tool for an early indication of an element presence. Moreover, being so sensitive, it is prone to surface contamination so the results obtained must be confirmed using other analytical methods.

3.2 *Experiment Preparation*

3.2.1 Drive preparation, the reconditioning process

Prior to starting any experiments, the DDS drives were following a procedure called reconditioning in order to remove any stains that might have been generated in the previous experiments. By using an mtcl script, the drives were programmed to pull a new DDS2 tape over its entire length at normal operation speed followed by rewinding at fast speed to the beginning of the media. This process was repeated for 24 times. Each drive that was reconditioned had its own tape. The reconditioning experiment took place with the drives placed in an environmental chamber that was set to 25°C/80%RH. The high humidity and the tape abrasivity were to insure that any adhesive or loose debris were removed from the heads since previous studies have shown that high humidity and a rougher tape can effectively remove any adhesive debris present on the heads. Once the reconditioning process finished, the tapes were removed and never used. The term "0 cycles" that is seen in the AFM scans refers to the heads after the reconditioning process took place.

3.2.2 Tape preparation

The new tapes to be used for experiments were also prepared on a spare drive under pseudo-environmental (laboratory) condition. The procedure was intended to remove high asperities that are usually present on the tapes after fabrication process. The script used in this case was similar to that used to recondition the drives but the number of cycles the tape had to perform was reduced to two. The term pre-cycled tape refers to those tapes that followed this procedure.

3.3 *Experiments*

3.3.1 The Error Rate (ERT) Measurements

The DDS drives are able to measure the errors occurred in writing data on the DDS tapes. The errors are reported as an **E**rror **R**a**T**e (**ERT**), which represents the number of bytes that were erroneous compared to the total number of bytes written on the tape. Thus, an error rate of 10^{-4} means that in 10,000 bytes written on the tape one was found to be erroneous.

The ERT experiments employed three reconditioned DDS3 drives and three pre-cycled DDS2 tapes. The drives were writing 2000 frames of data, which corresponds to about 2.1 metres of tape. The drive is programmed so the tape is written with random generated data at each loop at the beginning of the section cycled, in the middle and at the end thus generating a statistic of error rate per loop. After a specified number of loops, the error rate is stored locally in the drive's EEPROM. Error rates from both positive and negative channels were collected. With this script uploaded, the drives were mounted in the environmental chamber and then the temperature and humidity were set. After 5,000 cycles, the tape is ejected and the error rates can be downloaded and saved a file using the UNIX workstation for further analysis. A *simplified* flow chart of the script is presented in Figure 3-9. The influence of the environmental conditions on the error rate has been studied at 25°C/35%RH, 10°C/10%RH, 40°C/80%RH, 5°C/80%RH and 45°C/10%RH.

Some of the drives failed to perform the designated number of cycles and this occurred more often at high temperature and high humidity. Despite repeating the experiments, the drives failed to complete the experiments in harsh environmental condition. However, the same drives behaved well at moderate environmental conditions suggesting that the fault was not caused by a faulty script but rather by the environmental conditions employed.

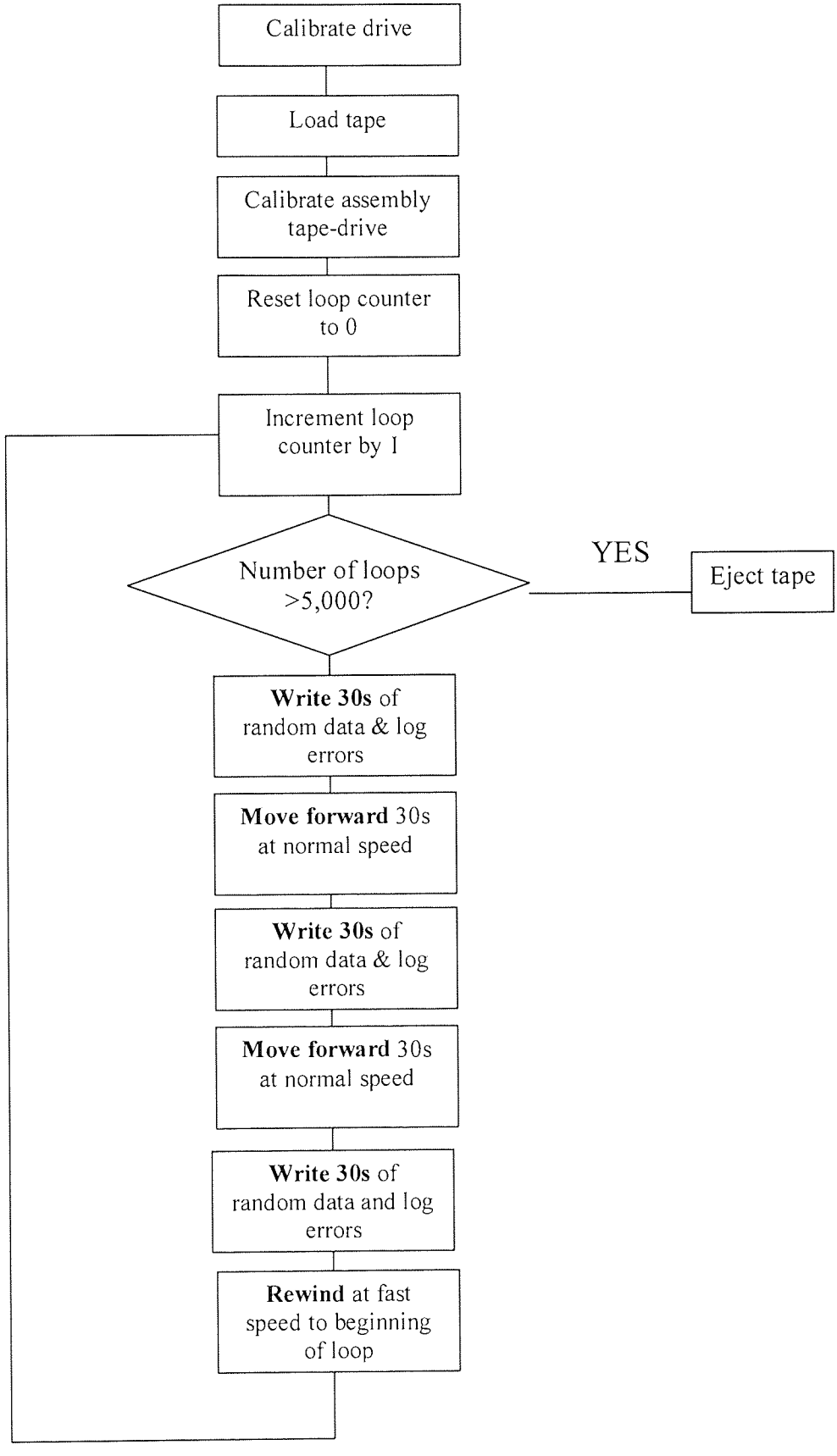

Figure 3-9 Simplified flow chart of the script used for measuring error rate

3.3.2 Wear rate measurements

The script employed for these experiments was similar to that used for measuring the error rate (see Figure 3-9) with the exception that the tape would be ejected after the first 1000 cycles. Three DDS3 drives were used in conjunction with pre-cycled DDS2 tapes. The wear rate variations upon the environmental conditions were studied at 25°C/35%RH, 10°C/10%RH, 40°C/80%RH, 5°C/80%RH and 45°C/10%RH.

The wear rate of the heads was estimated based on the indentation technique which consists of pressing a knoop diamond shaped micro-indent on the head's surface with a constant force and for a fixed period of time (about 10s) and measuring the size of the indent made. The indents were made on the ferrite region of the head at various distances away from the head's gap. There is a direct relationship between the length of the indent and its depth therefore by measuring the indent length at the beginning and at the end of the experiment, one could find the depth change that occurred hence the amount of material that has been removed. After indenting, the drive was mounted in an environmental chamber and was cycling a DDS2 tape under an environmental condition.

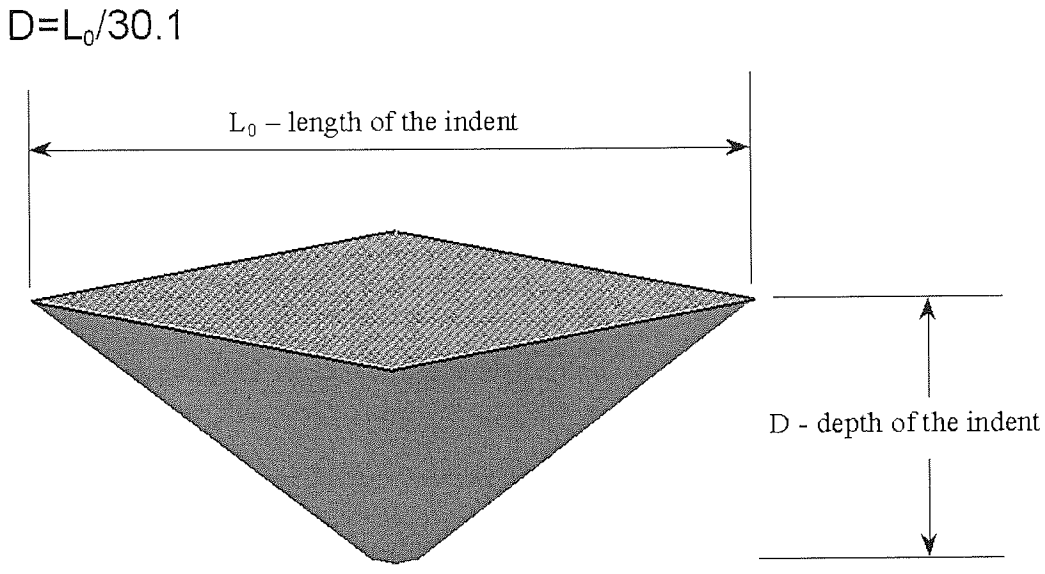

Figure 3-10 A schematic representation of a knoop indent and the relationship between its length and depth

As a convention the distance from the gap was measured using positive and negative numbers, the negative numbers being attributed to the indents made on the leading edge of the heads, whereas the positive numbers were attributed to the indents made on the trailing edge. The indenting force used was 25gf (grams-force) and it was carefully chosen taking into account that a higher force would crack the ferrite poles whilst a smaller one would not make an indent big enough to last for 1000 cycles. After the indenting process took place, the size of each indent was measured for three times either by using an optical microscope or the atomic force microscope. The tape was cycled on these drives at different environmental conditions and then the drums were removed and the size of the indents was measured again for three times. The difference between the length of the indent before the experiment and its length after the experiment is proportional to the wear of the material. Since the depth of the indent is proportional to its length [105], the wear rate of the material can be found. In our research it was calculated using Equation 3-2:

$$\text{Wear rate} = \frac{(L_0 - L_f)}{30.1 \cdot T}$$ Equation 3-2

Where

L_0 – the initial length of the indent

L_f – the final length of the indent

T –length of the tape cycled; in our experiments T≈ 2.1 m

An AFM picture of an indent made on the head is shown in figure below.

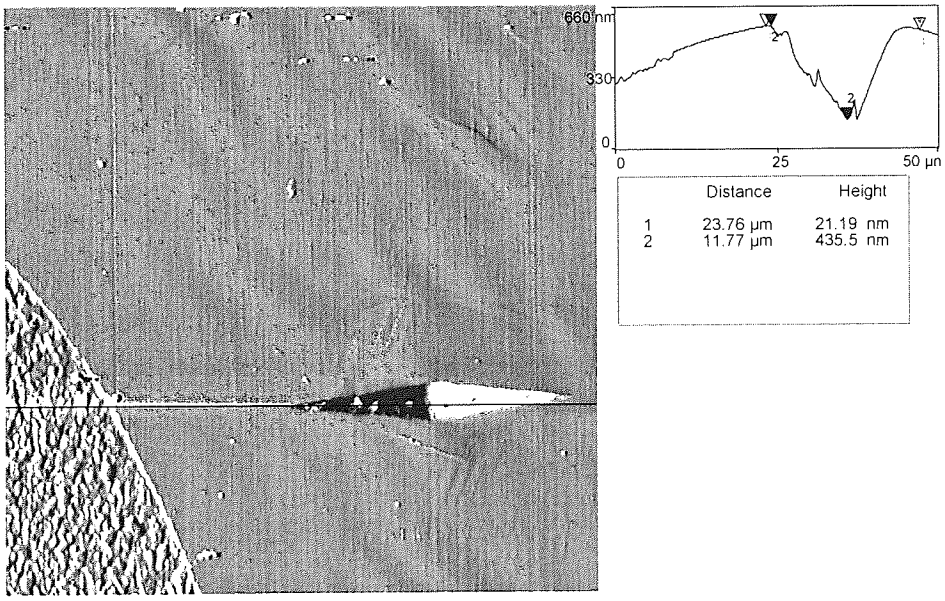

Figure 3-11 Diamond shaped indent made on ferrite poles of a read head

In the early experiments the length of the indents was measured using an optical microscope but it was found to be difficult due to eye tiredness that led to difficulties in appreciating the edge of the indents, therefore prone to generating random errors. Later on, another solution was found, that of using the atomic force microscope to generate the topography of the surface of the heads. Although time consuming it was hoped that the method will reduce the errors of the measurements. Despite reducing the random errors, the AFM seemed to have introduced systematic errors and this could be explained if we consider that sometimes debris may be covering the *real* edges of the indents. It is believed that negative wear rates that can be seen on some of the graphs are the result of the errors occurred during measurements caused by various factors such as debris covering the indents, eye tiredness etc and obviously, they don't have a physical meaning.

Given the Equation 3-2 used for calculating the wear rate of the heads, the error in estimating the wear rate was found to be:

$$\Delta d = \pm \frac{\Delta L_1 + \Delta L_2}{L_1 - L_2}$$ Equation 3-3

Δd is the error estimating the depth;

ΔL_1, ΔL_2 are the errors in reading the indent's length

L_1, L_2 are the length of the indents before and after the experiment respectively

Taking into account the error of reading the indent length is the same then Equation 3-3 becomes:

$$\Delta d = \pm \frac{2\Delta L_1}{L_1 - L_2}$$ Equation 3-4

In the particular case of these experiments, $\Delta L_1 = \Delta L_2 = 0.1\mu m$, and on average $L_1 - L_2 = 2.5\mu m$. Taking into account these values one would get the error in estimating the wear rate of $\Delta d = 8\%$.

However, apart from the error introduced by the instrument and the method of measuring, random errors were also generated by the experimentalist. Generally, these errors were found to be greater, therefore these errors are displayed on the graphs.

3.3.3 AFM measurements

The purpose of the experiment was to assess changes that occur in the topography of the heads at different environmental conditions by means of AFM imaging and to compare with the error rates recorded. Therefore, the three DDS3 drives used were cycling a 2.1m long DDS2 tapes for 5,000 times as in the experiments involving measuring the error rates.

The AFM measurements were focused mainly on positive read head since Chandler et al [27] have found that the errors are caused mainly by the inability of the

heads to read data rather than the failure of the heads to write them on the magnetic tape. The images obtained were compared with the one obtained after reconditioning process. The term '0 cycles' in AFM figures designates a head after reconditioning process. The scan angle of the heads was most of the time set to 270° that is the tip scanning perpendicular to the tape running direction. It has been chosen to use contact mode since comparative scans revealed no difference upon the technique used. Further processing of the newly acquired image included a second order levelling which allows one to fit the scanned image to a plane and then to subtract the plane from the image. In other words, the levelling allowed one to remove the manufactured curvatures of the head and to have a plane image of the heads with their features.

In order to quantify the topography evolution of the head, area RMS was measured. The formula is given by equation below and characterises the height fluctuation from the average height of a particular surface [106, 107]. A smaller number corresponds to a smoother surface whereas a higher number is specific to rougher surfaces.

$$R_{ms} = \sqrt{\frac{1}{N} * \sum_{i=1}^{N} \left\langle Z_i - \overline{Z_i} \right\rangle^2}$$

Equation 3-5

Z – height

N – number of points where Z has been measured

The figure below depicts the way in which the roughness of the surface was measured. The area to be studied was covered by as many rectangles as possible and then area roughness was computed within these rectangles. Although this method is scale and instrument resolution dependent, yet it can give some evidence of the surface changes that occurred. A better method to measure surface roughness requires the use of scale independent fractal parameters that wasn't available to us. [108]

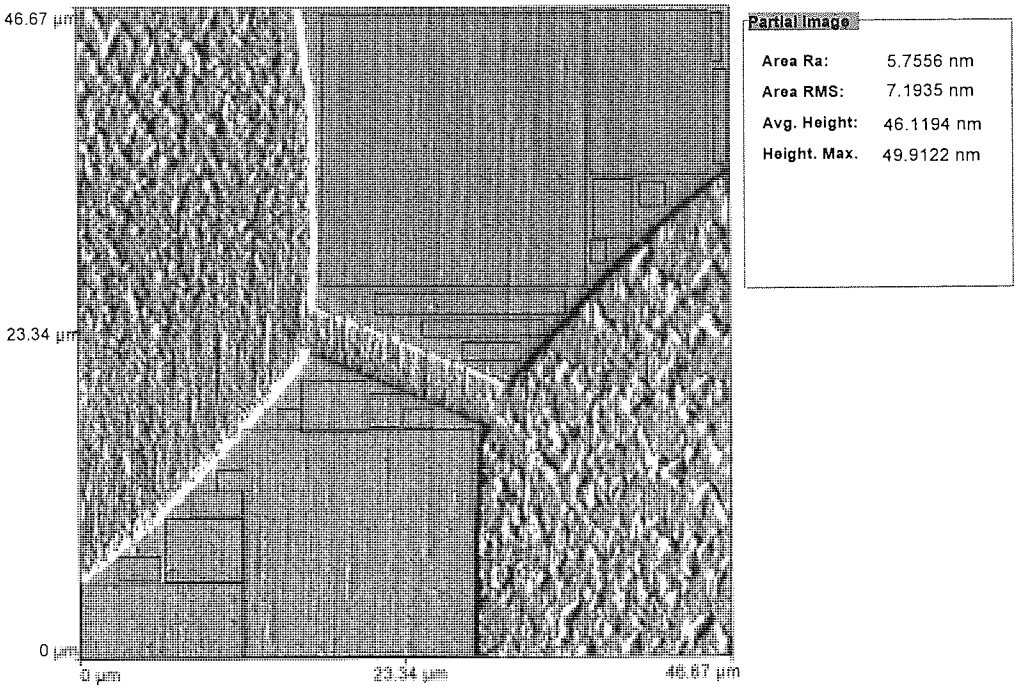

Figure 3-12 The method used to measure area roughness; in this case, the roughness of the ferrite poles is measured

Three DDS3 drives used for these experiments were cycling a 2.1m long DDS2 tapes for 5,000 times as in the experiments involving measuring the error rates. The topography of the heads was analysed before starting the experiment and during the experiment at different stages of tape cycled: 100, 1000 and 5,000 loops. In order to allow topography analysis to be acquired during the experiment, the mtcl script that was used for measuring the error rate was now slightly modified so the drive will eject the tape after a stage of the experiment was completed. The drum of drive was carefully dismantled, the heads cleaned of loose debris using a cotton-tipped applicator and alcohol and AFM scans were performed. After that, the drive was reassembled and put back into the environmental chamber for the next stage of experiment. Same tape was used for the same drive during the experiment on one environmental condition. The environmental conditions used were the same as in the case of error rate experiments.

3.3.4 SIMS analysis of the heads

The technique used gave an early indication of elements present in the adherent deposits. Since the analysis involved removing the heads from the drum, thus destroying the drum, only a limited number of heads were analysed: among them, one head following a reconditioning process showing no visible stains present on it and another being stained. The stained heads were obtained from a drive that has been subjected to 45°C/10%RH and was running a DDS2 tape using the same script as that used in the previous ERT experiments. An AFM scan was taken before SIMS analysis on each of the heads in order to verify the physical presence of the adherent debris.

Both glass and pole regions of the head were investigated. Because of the head sizes, performing SIMS analysis proved to be a trade-off between the intensity of signal and the sputtering rate. Although efforts have been made to reduce the damage induced by bombardment and to perform static SIMS, sometimes unwanted but unavoidable dynamic SIMS conditions were reached, leading to some of the spectra being performed in the dynamic range of SIMS analysis. Due to the rapid depletion of chlorine observed under vacuum conditions by different authors [12, 104], the negative spectra were firstly acquired. The sputtering was performed using Ga in case of heads or Ar in the case of the tape or ferrite samples. The pressure inside the chamber was 10^{-9} mbar, the Ar or Ga current was ranging between 0.7-0.8nA and the beam energy was 5kV.

3.3.5 AES analysis

As in the case of SIMS, only a limited number of heads (2 reconditioned and 3 stained heads) was used for investigation. The head samples were generated using the same script as for measuring the error rates at two different environmental conditions 25°C/80%RH and 40°C/10%RH. When using Auger Electron Spectroscopy, prior to

starting the analysis, the heads were carefully dismantled from the drum and cleaned using cotton tipped applicator and alcohol. Then, while in the main chamber, the sample was etched using a current density of 2μA of Ar^+ for a half a minute in order to remove or at least to reduce surface contaminants. The etch process was not performed on the heads that were operating at high temperature and low humidity due to the fact that the AFM imaging revealed that the adhesive deposits that usually appear under these conditions have 10 – 14 nm thickness. The electron beam current was 0.4 mA and the energy 5kV. Both glass and ferrite regions were investigated and, in order to improve signal to noise ratio, the signal was acquired from the maximum area possible. The samples were tilted in order to reduce to minimum surface charging. The spectra were calibrated based on the assumption that the binding energy of O KL1 peak is 530.1eV.

3.3.6 SIMS and XPS analysis of the tape

SIMS and XPS scans were performed on DDS2 tapes in order to compare these spectra with the spectra obtained from the heads. Pre-cycled DDS2 tapes were used.

In the case of SIMS, an Ar ion beam with the energy of 5kV was used. The beam current was 0.6μA. Both negative and positive spectra were acquired.

The XPS was performed using MgK_α source. The emission current of the filament was 20 mA and the energy of the X-ray photons was 14kV. Several areas of $1mm^2$ were investigated. Spectra were acquired using 0.1 eV step size, and 10ms dwell time. After acquisition, the spectra were smoothed at 15 points and 30 passes and then calibrated assuming the binding energy of the C 1s peak at 284.6 eV. The intensity of the peak was estimated after background subtraction using Shirley algorithm [129].

3.3.7 The stain simulation using the ferrite samples

Both AES and SIMS techniques employed before to analyse chemical composition of the stains on the DDS magnetic heads have their own disadvantages. SIMS, being very sensitive, is prone to record surface contaminants and since there is no known quantification method of the elements present in the spectra, one cannot distinguish between the contaminants and the rest of elements. AES is far less sensitive and is neither able to detect elements present in small amounts nor their chemical state. On the other hand, XPS can quantify the percentage of elements present on the surface and is able to reveal chemical bonds that the atoms are forming with their neighbours but the samples to be used need to be larger compared with the previous two methods. Since the DDS heads were very small, XPS investigation was difficult to use, therefore in order to fully analyse chemical composition of the stains, a way of reproducing them on a bigger scale was required.

To generate stains six ferrite bars were employed, other three being kept for comparison. The samples were 19 x 2.8 x 0.7 mm, having the same chemical composition as the ferrites used in the DDS3 heads and they were polished along <110> crystallographic plane. The six bars were mounted on a loop tester as in Figure 3-13 in an environmental chamber. The conditions inside the chamber were set at 45°C/10%RH, known to promote staining on a DDS3 drive. The set-up employed was an attempt to reproduce the conditions encountered in a DDS drive during operation at high temperature and low humidity. The DDS2 tape used ran at high (>3000 rpm; ~4m/s) and low (<45rpm; ~5mm/s) and the experiments finished when the tape snapped. As a remark, the experiments at high speed took about half an hour whereas that at low speed took two days. The tape tension was set at 39.2mN (4g), similar to that encountered in a DDS3 drive. Due to the fact that the surface of the ferrites was flat, in order to increase the contact area between tape and the ferrite samples, the tape was biased by applying 10V on it. Since the adhesive bonds between of the stains to the surface is very high (up to 10 eV) compared to the energy due to the electrostatic charging [10], it is unlikely that stains generated during this method will differ dramatically from those generated under normal working conditions of a DDS drive. Moreover, electrostatic charging may occur in DDS heads at low humidities taking

into account friction forces between the tape and the head and considering that ferrites are insulators.

Chemical analysis of the surfaces was done using XPS. All ferrite bars were cleaned with a cotton tipped applicator and alcohol prior to analysing. Surface topology of the ferrites was acquired bz using AFM in order to insure that the ferrite surface is stained prior to XPS analysis. Mg K_α X-radiation was employed for the XPS examination, at a source excitation energy of 14 keV and emission current of 20 mA. An analyser pass energy of 20 eV with step size of 0.1 eV and dwell time of 100 ms were used throughout. Calibration of the spectra was done considering C 1s binding energy at 284.6 eV. To avoid any misinterpretation the XPS spectra were saved as they were acquired that is without any smoothing. In order to increase signal-to-noise ratio, the area investigated was $1mm^2$. Several regions along the bars were analysed in order to determine the fluctuation of the concentration of each element thus having an indication whether the element is a contaminant or is present in the stains composition. The pressure inside the main chamber during experiments was below $5x10^{-9}$ mbar.

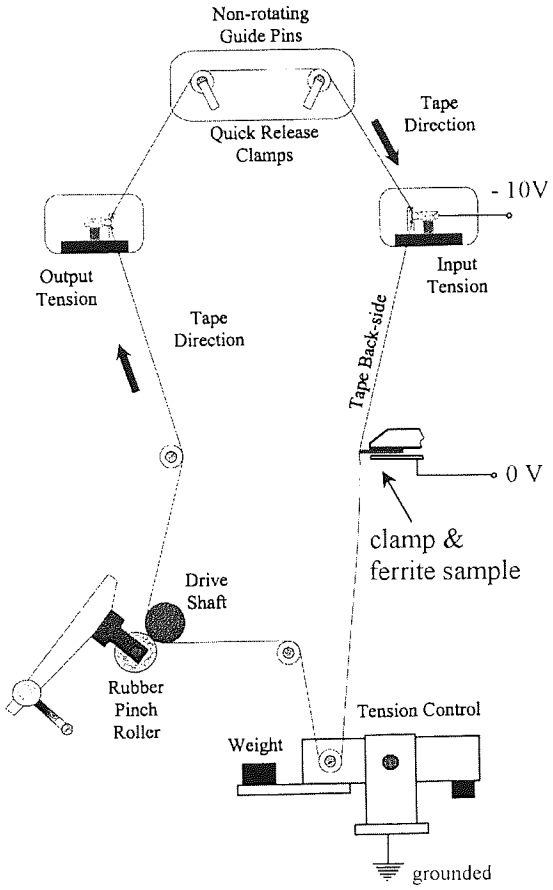

Figure 3-13 The loop tester used for staining the ferrite samples

Another series of experiments were to simulate stains but without biasing the ferrite samples. In order to increase the ferrite-tape contact surface, the surface of the ferrites has been manufactured with a curvature similar to that encountered in real DDS heads. However, the XPS analysis performed prior to the experiments has revealed the presence of chlorine and nitrogen that led to the conclusion that the curvature was made using a lapping techniques, that means a high abrasive tape. The ingredients of this type of tape are similar to that of an ordinary tape, meaning that the binder polymer is present here as in a normal tape. Unfortunately, since no technique that would clean *entirely* the surface to remove any traces of chlorine and nitrogen was found, further experiments involving these ferrites were halted. (see also chapter 4)

3.3.8 The ferrite behaviour at high humidity

The aim of the experiments was to measure the changes that occur on the surface of the ferrites after exposure to high humdities. For all the experiments conducted, three ferrite bars (19 x 2.8 x 0.7 mm) having the same chemical composition as the DDS heads were used. Sample number one was kept under normal laboratory conditions for comparison. The second sample was maintained at 45°C/80%RH for approximately two days using the environmental chamber. Finally, the last sample was boiled in de-ionised water for about two days. Chemical analysis of the surfaces was conducted using XPS (X-ray Photon Spectroscopy) in Fisons Instrument VG ESCALAB 200D using MgK_{α} radiation. A wide energy scan was collected at the beginning of the experiments in order to identify all elements present in the ferrite surface. After smoothing, all the spectra were calibrated assuming C 1s peak at 284.6 eV. After identifying the elements, narrow scans of each element were then collected using a $600\mu m^2$ analysis area. The base pressure inside the chamber during the experiments was below $6x10^{-9}$ mbar.

The time evolution of the peaks upon different conditions was investigated using various other experiments. In one of them the boiled sample was left for about 18 hours at high vacuum conditions (below 10^{-8} mbar) and another scan for the elements was made. Further measurements were done after heating the sample up to 120°C for about two days using a hot plate.

Initially the experiments tried to estimate the changes by measuring the variations occurring in the shape of the Fe 2p/3 peak at 712 eV binding energy but the quantification of the peak proved to be extremely difficult due to the presence in that region of the shake up lines of iron. As a result, the efforts were focused on identifying the chemical changes that might have occurred by using the oxygen O 1s peak. The experimental spectrum of oxygen was modelled as a superposition of three peaks corresponding to oxygen in metal oxygen bonds (M-O), oxygen in hydroxide group (OH) mainly coming from FeOOH formed on the surface and finally, water

(H_2O). The oxygen peak synthesis was carried out assuming the following parameters:

Peak	Binding energy (eV)	FWHM (eV)
M-O	529.5	1.5
OH	531.0	1.6
H_2O	532.4	1.9

We assumed that the water peak is due mainly to chemically bonded water simply because we have not seen a sudden increase in pressure when the sample was exposed to high vacuum prior to experiments. The amount of each component was expressed as relative variation to the total amount of oxygen for easier comparison.

3.3.9 Study of the wear rate at the same water pressure

The study has proposed to give clues about the critical parameter that affects the wear of the heads since it is not yet known whether the relative humidity or the total amount of water influences the wear.

For these experiments, DDS4 drives and DDS4 tapes were used. The mtcl script used was similar to the one used previously but it was slightly modified so the number of cycles performed was 2000. This number was chosen since it has been found that the wear rate in this particular configuration of tape and drive is very low. However, even 2000 cycles were found not being sufficient enough to generate a visible wear, therefore the measurements should be taken with the necessary caution. The low wear rates seen is related probably to an increased hardness of the DDS4 heads compared with DDS3 heads and lower abrasivity of the DDS4 tape compared with DDS2 tape. A further increase in the number of passes would have led to a very large timescale for experiments (more than three weeks).

The environmental conditions were chosen so the water vapour pressure inside the chamber would remain constant and also taking into account the limitations of the environmental chamber.

Experiment. Number	Environmental condition	Water vapour pressure (kPa)
1	10°C/63%RH	0.79
2	24°C/25%RH	
3	41°C/12%RH	

The amount of water present was computed using the following formula [128]:

$$p_a = 6.1365 \cdot 10^{-3} \cdot RH \cdot \exp(\frac{17.502 \cdot T}{240.97 + T}) \qquad \text{Equation 3-6}$$

Where p_a is the actual water vapour pressure in kPa, RH the percentage of relative humidity and T the temperature in degrees Celsius.

3.3.10 Contact angle measurements

The variations of the surface energy upon different environmental conditions were to be studied on both ferrite and tape surface in order to compare the variation of adhesive forces of both surfaces in different conditions. The ferrite samples were square shaped with a large surface, (19.1x19.1x1.7 mm) so that the droplets won't touch the edges. It involved mounting tape and ferrite samples into an environmental chamber and measuring the surface energy of the samples using the sessile drop technique. The measurements took place under pseudo environmental conditions (about 25°C/35%RH) and high temperature and high humidity using a GBX DigiDrop contact angle meter. The contact angle is an average of several measurements that took place in several spots of the surface, insuring that the droplet is placed to a surface not used before. Two liquids were used: diiodomethane (non-polar) and distilled water (polar). The volume of each droplet was 1μl and during the experiments manual and semiautomatic evaluation of the contact angle has been performed. By comparing the adhesion forces of ferrite and tape one could draw some qualitative conclusions about the probability of a loose particle to stick to one surface or to another. If the adhesion forces are higher for ferrites than for tapes surface, then the probability of a particle to stick to ferrite's surface is higher than to tape's surface.

On contrary, if the adhesion force is higher in the case of DDS2 tapes, than a particle will remain stuck to the tape or glue to it in case it is loose.

Unfortunately, due to technical limitations of the devices we were unable to perform a full study. However, from the preliminary results, one can see that there are variations of the surface energy that need to be further investigated.

3.3.10.1 Surface energy evaluation by contact angle technique

Contact angle measurements may offer hints about the interfacial forces between two surfaces. Particularly of interest for our study were the adhesion forces since one mechanism of stain formation emphasises their role [97]. A method very often used is the sessile drop technique, which consists in measuring the contact angle of a liquid with the surface under study. If the surface energy of a surface is less than the surface tension of a given liquid, then the surface will repel the liquid. Therefore if the contact angle is above 90° the surface is said to repel the liquid and if the angle is below 90° then the liquid is said to wet the surface (see Figure 3-14). If the contact angle is acute, the adhesion (polar) forces are stronger the non-polar forces and there are mainly due to hydrogen bonds as stated by Fowkes [109]. The static contact angle is measured by taking the angle between the liquid/solid interface horizontal and a line tangent to the liquid surface at the point where the liquid is in contact with the solid surface. In order to measure both polar and dispersive components of the surface energy two liquids with different tension energy are needed.

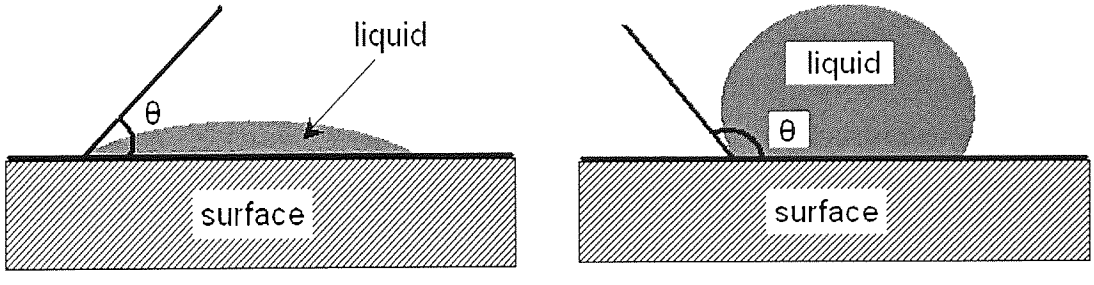

Figure 3-14 Measuring the contact angle: θ<90° and the liquid is wetting the surface (left); θ>90°and the liquid is repelled by the surface (right);

4 Experimental Results

A brief summary of the experiments performed is given in the following tables.

Exp. type/env. condition	25°C/ 35%RH	10°C/ 10%RH	40°C/ 80%RH	5°C/ 80%RH	45°C/ 10%RH
ERT	4	5	3	2	4
Wear rate	4	2	3	2	2
AFM	4	2	2	2	2
AES	2	-	-	-	3
SIMS	2	-	-	-	1

Table 4-1 The number of heads used during various experiments

Limited AES and SIMS experiments involving stained and stain free heads were performed since the analysis involved destroying the drives in order to reach the DDS heads.

Experiment type	Number of ferrite samples used
Ferrite behaviour at high humidity	9
Stain simulation	9
Surface energy evaluation	4

Table 4-2 Number of ferrite samples used in the study of the ferrite behaviour at different environmental conditions and stain simulation

Experiment type/environmental. condition	10°C/ 63%RH	24°C/ 25%RH	41°C/ 12%RH
Wear rate at the same water pressure	4	3	4

Table 4-3 Number of heads used in the study of the wear rate at the same water pressure

4.1 The ERT measurements

Figure 4-1 and Figure 4-2 show the RAW (Read After Write) errors obtained on drive number 2 on positive and negative channels after 10000 passes under 25°/35%RH.

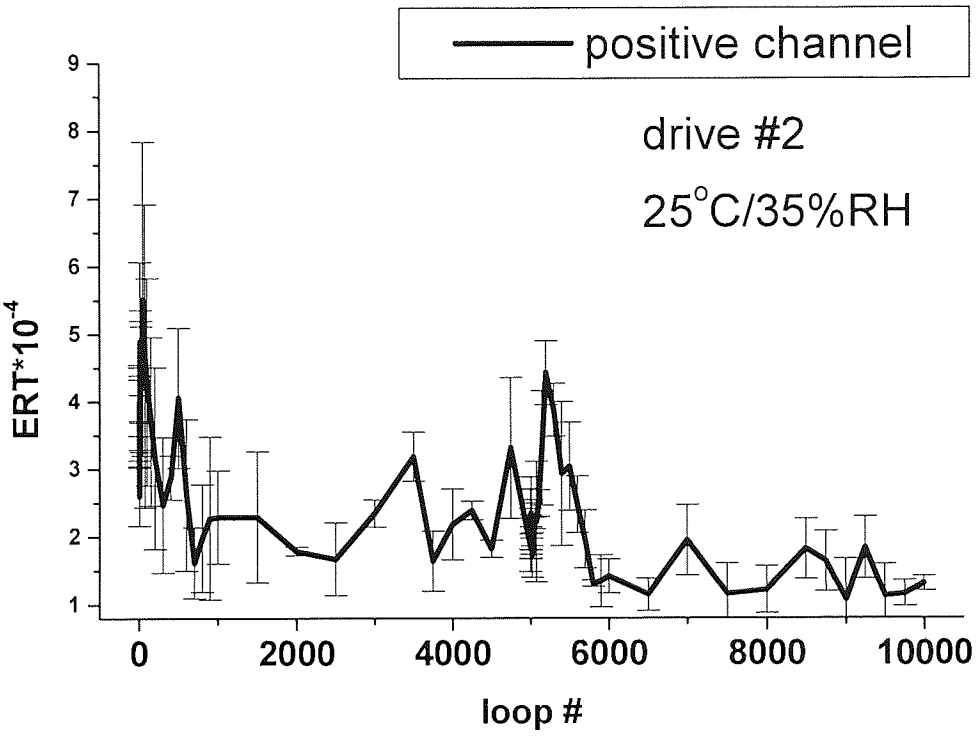

Figure 4-1 RAW errors on positive channel after 10 000 cycles

As one can see, this drive displayed a decrease in error rate with an increase of in number of cycles. Excepting the first 10-15 cycles when the errors were relatively high and fluctuated, the trend was descending. The high error rate from the beginning is due to the reconfiguration of the shape of the head's curvature and reconfiguration of the tape to the head and it commonly occurs in all drives tested. The higher error rate at 5 000 cycles is due to the fact that at that time the tape was ejected from the drive and then put back again and the same process as in the first cycles occurred.

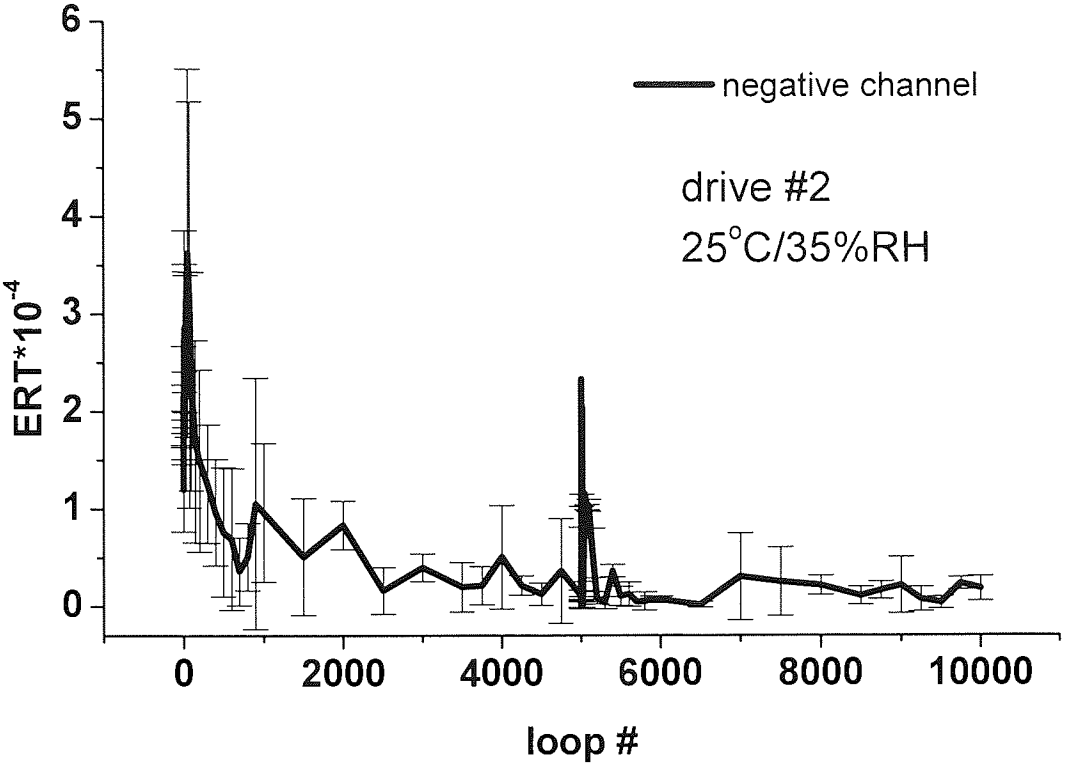

Figure 4-2 RAW errors on negative channel after 10 000 cycles

The second drive tested showed a similar behaviour as one can see from Figure 4-3 and Figure 4-4. However, after the relatively high errors at the beginning the error rate decreased and then at 1000 cycles the errors started to increase again due probably to loose debris becoming entrapped between head and media. Tape failure occurred after 3000 cycles and the drive was unable to finish the experiment. It must be mentioned that despite the slight increase of the error rate, the absolute value remained however very low.

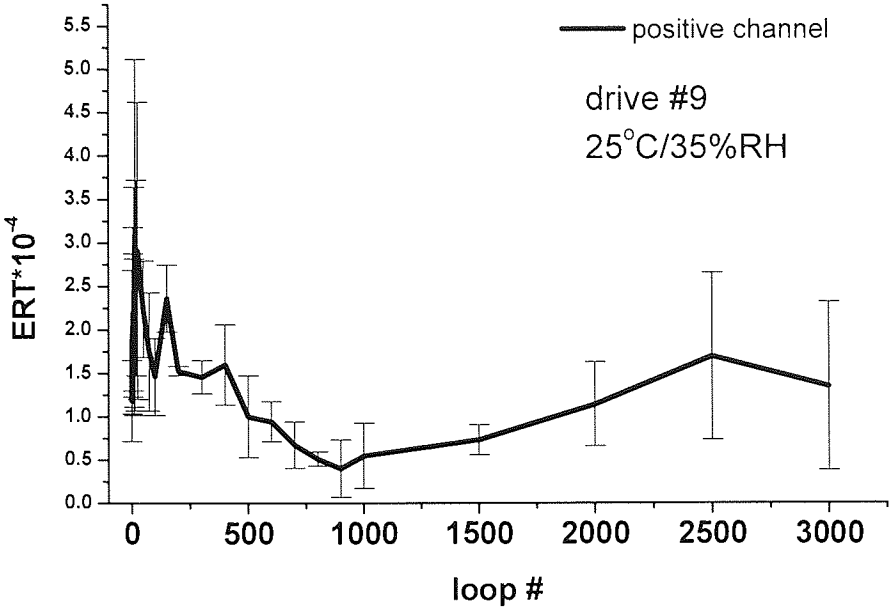

Figure 4-3 RAW errors on positive channel after 3 000 cycles for negative channel

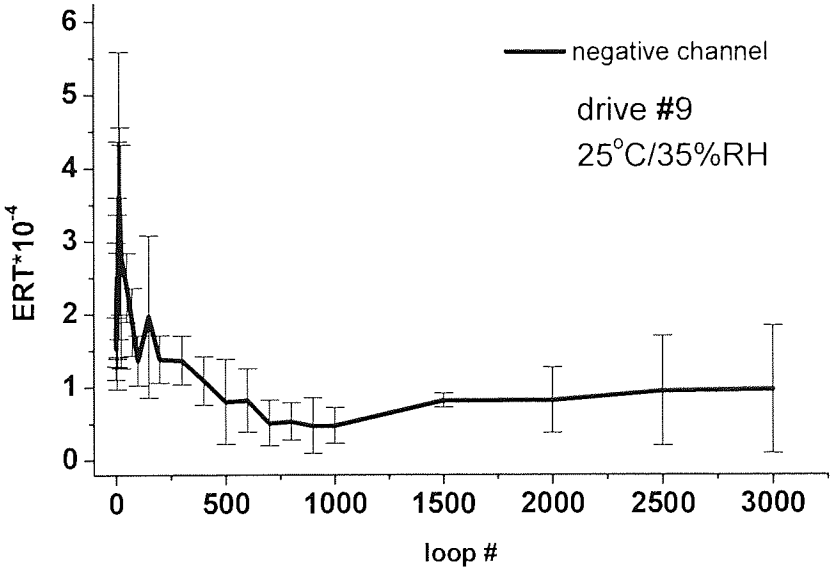

Figure 4-4 RAW errors on negative channel after 5 000 cycles for drive 9

At 45°C/15%RH, the experiments revealed an increase of the error rates as the number of passes increases. The increase was seen on both drives by an order of magnitude from 10^{-4} to 10^{-3}. The process of signal degradation seemed to start after the

first 1000 cycles and continued as the media degraded and the stain became thicker thus increasing the distance between head and media.

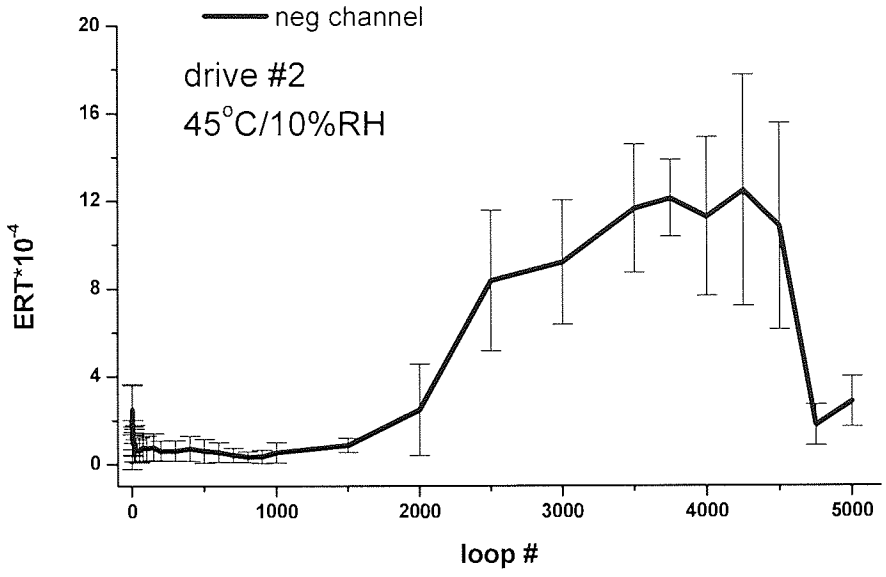

Figure 4-5 RAW errors on negative channel after 5 000 cycles

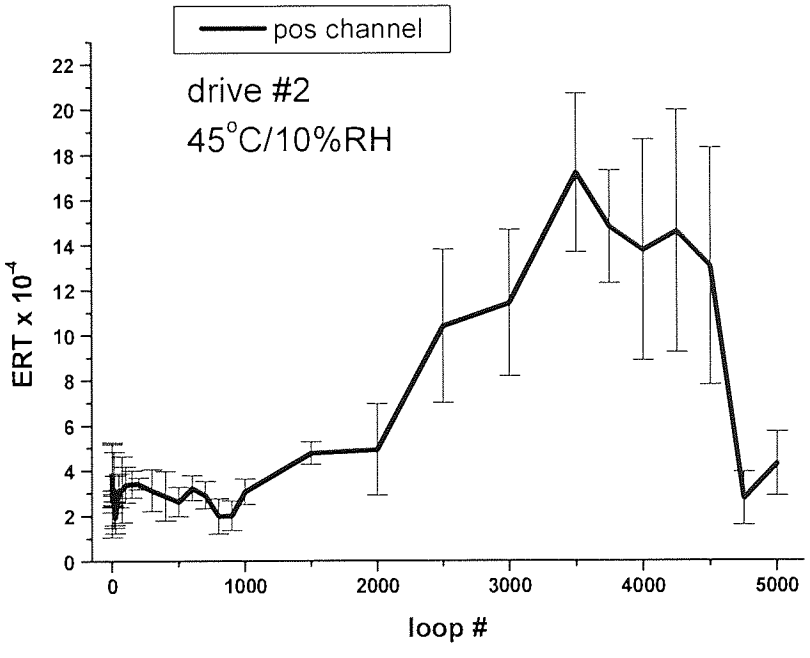

Figure 4-6 RAW errors on positive channel after 5 000 cycles

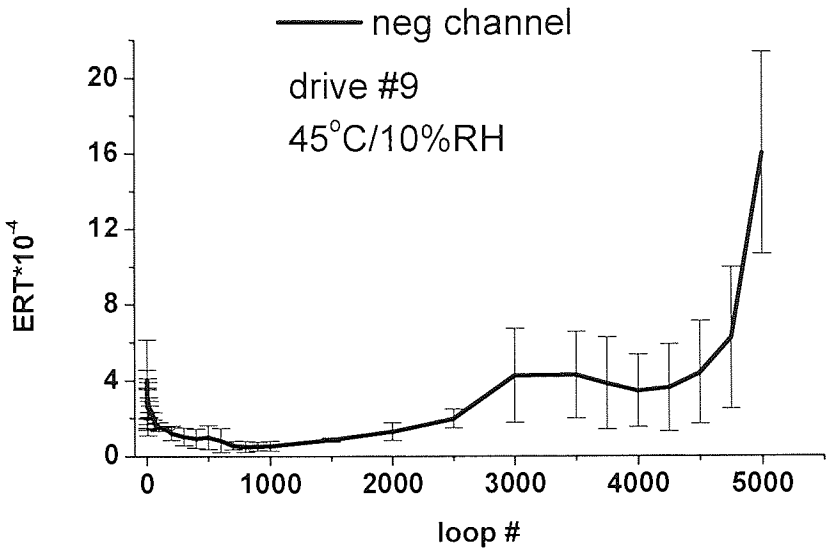

Figure 4-7 RAW errors on negative channel after 5 000 cycles

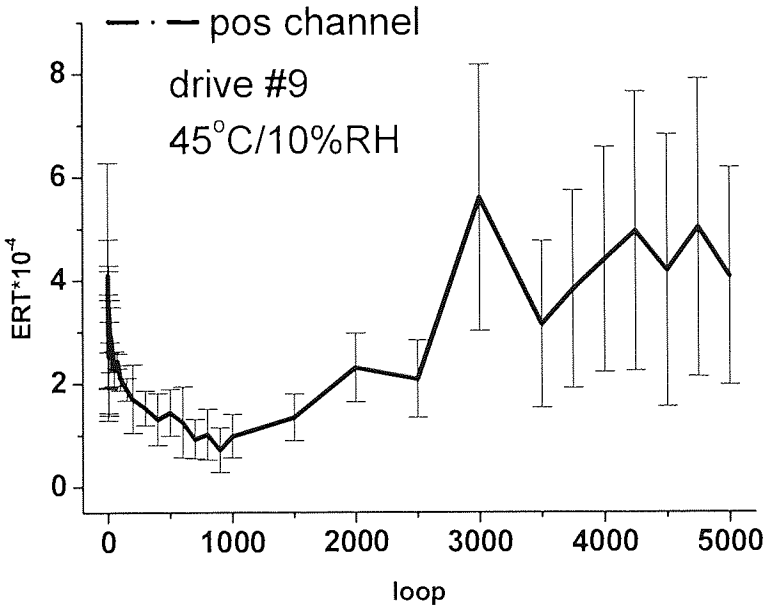

Figure 4-8 RAW errors on positive channel after 5 000 cycles

In the next environmental condition tested, 5°/80%RH, the results obtained show a constant decrease of the errors with the number of passes or maintaining to a low, fairly stable level of them as was the case of drive 2 (Figure 4-11) despite the fact

that both drives did not finish the experiment. It is believed that failure of the drives was caused by the harsh condition employed, at the limit of the manufacturer's recommended temperature and humidity values. The level of errors is comparable with that at 25°C/35%RH and one order of magnitude lower than that at 45°C/10%RH.

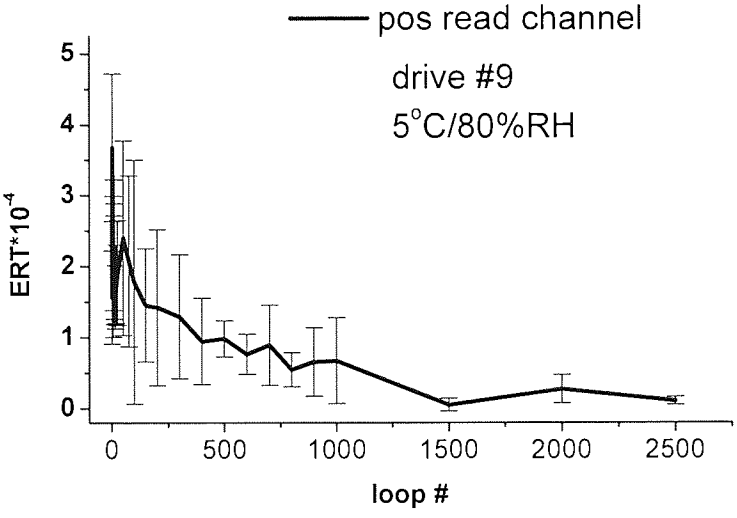

Figure 4-9 RAW errors on positive channel after 2 500 cycles

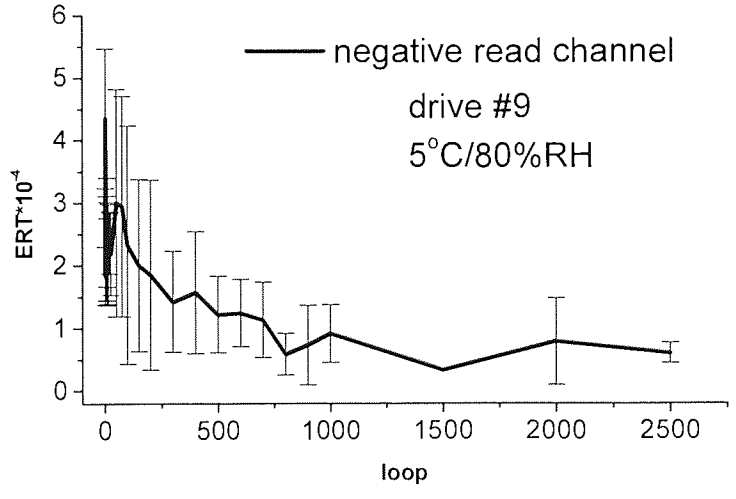

Figure 4-10 RAW errors on positive channel after 2 500 cycles

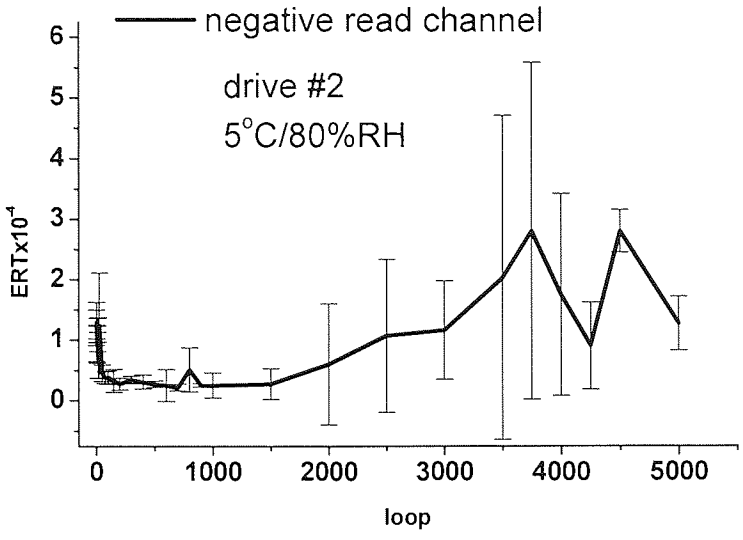

Figure 4-11 RAW errors on positive channel after 5000 cycles

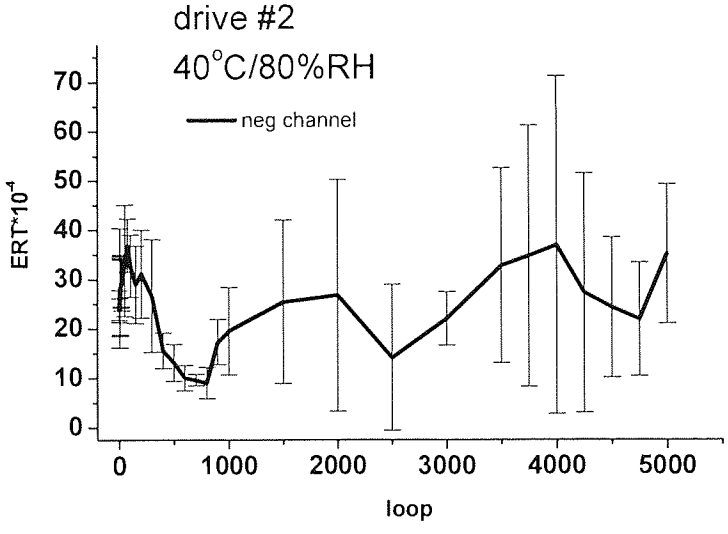

Figure 4-12 RAW ERT of the drive 2 on negative channel after 5000 cycles

At 40°C/80%RH the error rate fluctuated and it was situated at high levels during the experiments for both drives. Errors on both positive and negative channels of the drive 10 had the same trend suggesting that the change must have occurred not on one single head but either on the tape side or on the electronic side of the drive. It also worth noticing the high level of error bars indicates that even during one cycle the errors

fluctuated dramatically, possible due to loose debris or to a very dynamic process of stain building up and removal.

Both drives experienced a worsening of errors, higher fluctuation in the last cycles, fact suggested by the higher error bars towards the end of their tests.

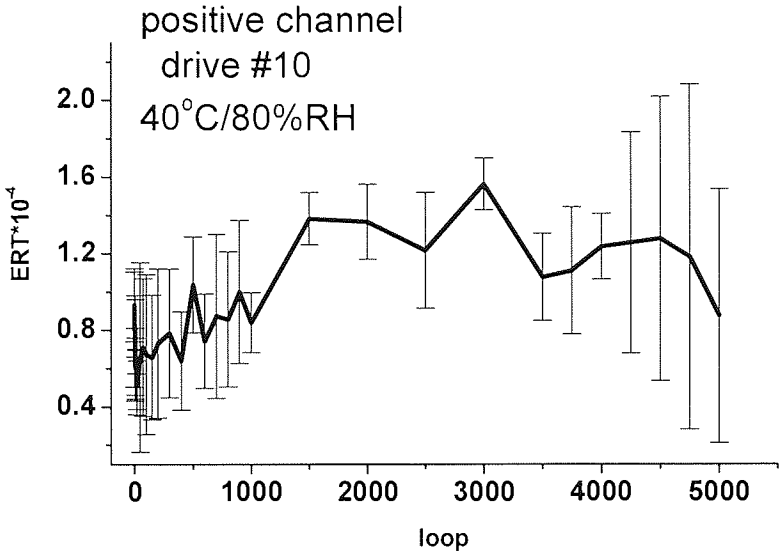

Figure 4-13 RAW ERT of the drive 10 on positive channel after 5000 cycles

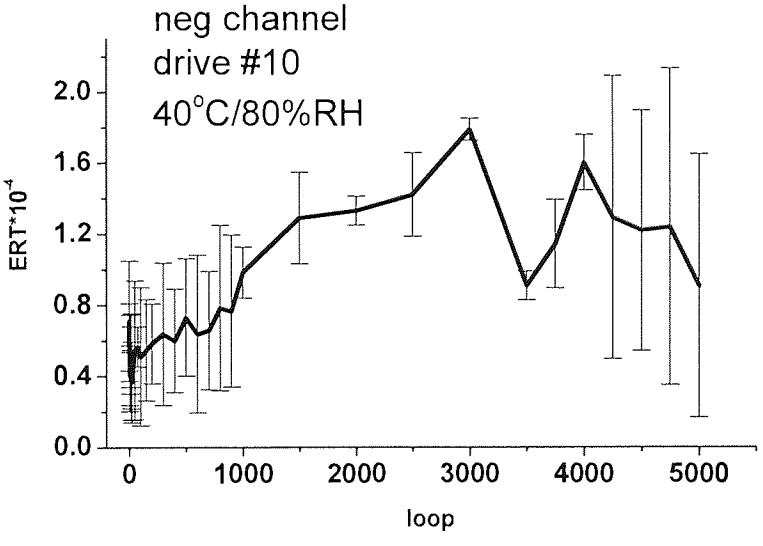

Figure 4-14 RAW ERT of the drive 10 on negative channel after 5000 cycles

At 10°C/10%RH, the drive number 2 had similar behaviour as at 40°C/80%RH, with high fluctuations and error levels measured. In both environmental conditions the drive showed a worsening in level of errors as the experiments progressed.

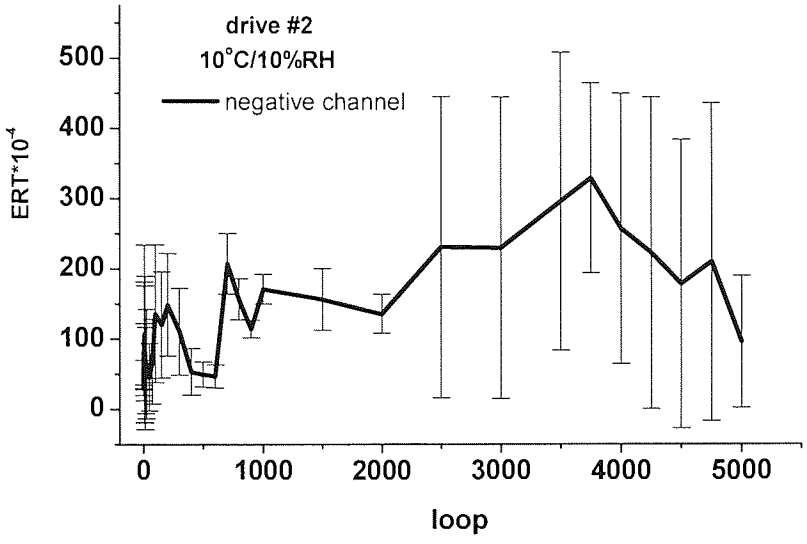

Figure 4-15 RAW ERT of the drive 2 on negative channel after 5000 cycles

On the contrary, on the drive 10 despite the fact they were reduced in absolute value, the error rate showed large fluctuations during the same loop, fact confirmed by the large error bars seen towards the end of the experiment. Drive 9 that failed on previous experiments at 40°C/80%RH, now failed at 2500 cycles. Before failing, it displayed a dramatic increase in errors. Again, the trend was similar to both channels and the errors increase on both channels in the same time. The behaviour may indicate a head failure rather than stains building up on the poles.

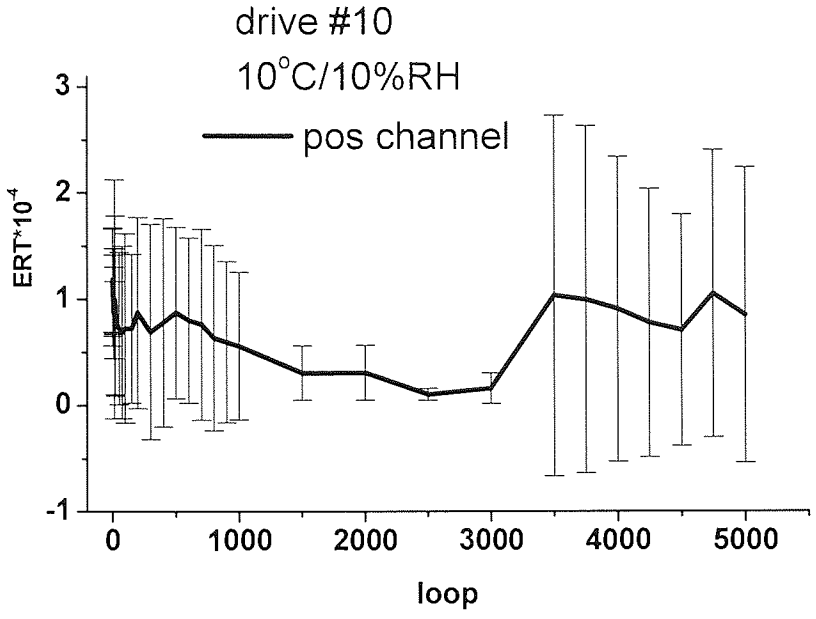

Figure 4-16 RAW ERT of the drive 10 on negative channel after 5000 cycles

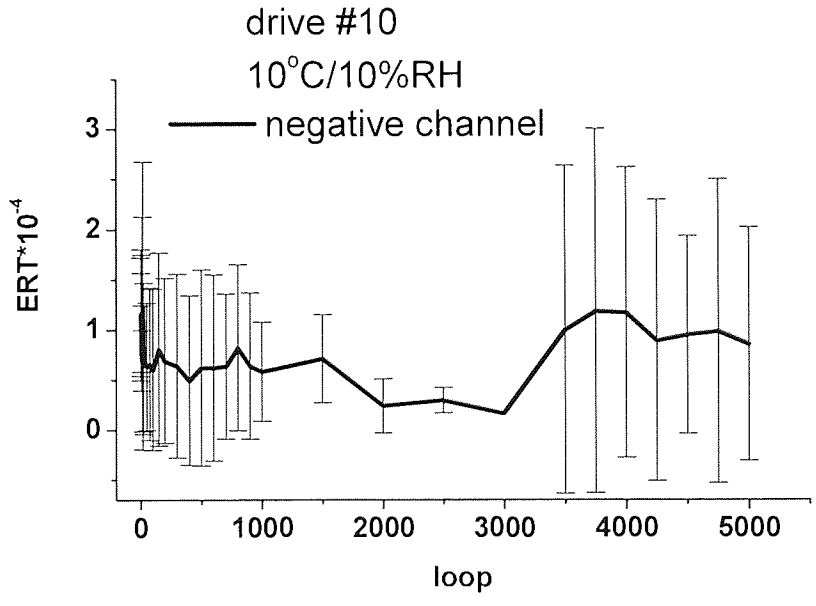

Figure 4-17 RAW ERT of the drive 10 on negative channel after 5000 cycles

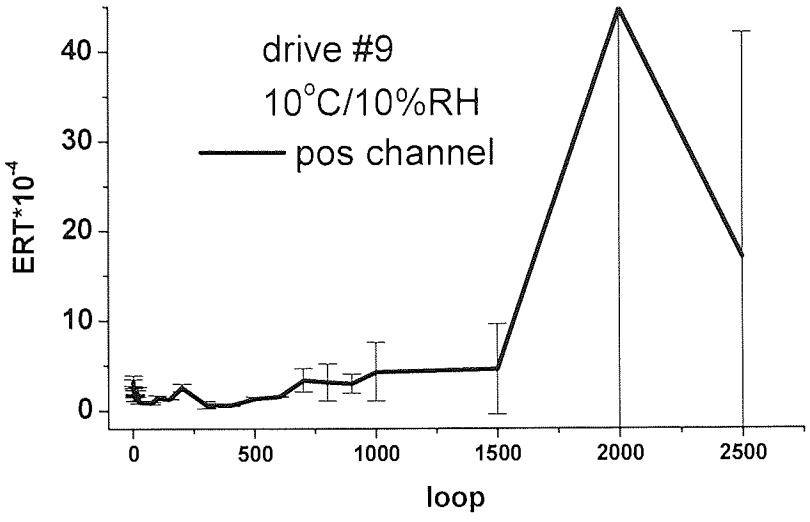

Figure 4-18 RAW ERT of the drive 9 on positive channel after 2500 cycles

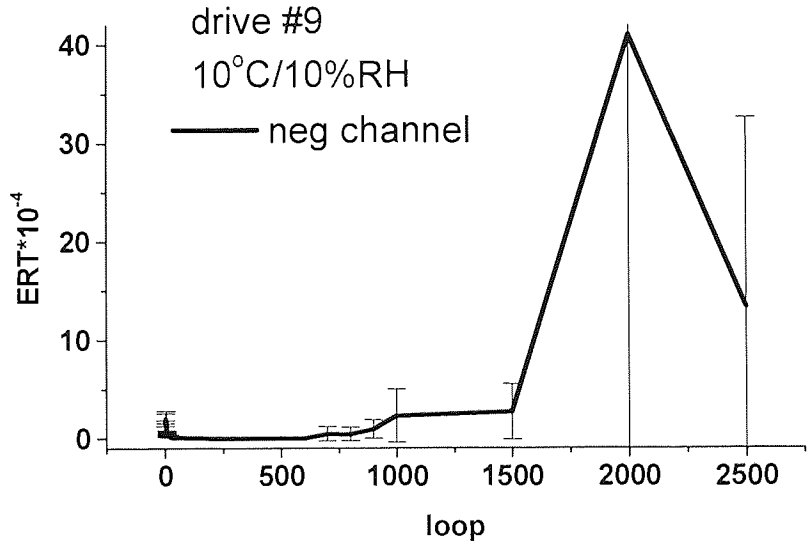

Figure 4-19 RAW ERT of the drive 9 on negative channel after 2500 cycles

4.2 Wear rate measurements

The experiments were focused mainly on the read head from the positive channel. The indents were measured after streaming 2.1 metres of type for 1000 cycles and on one occasion for 5000 cycles. The results obtained for the drives running at 25°C/35%RH confirm that wear tends to be higher in the trailing edge of the head rather than in the leading edge. These results could be explained by taking into account that loose debris tended to accumulate at the trailing edge and to produce three body abrasion which is more significant than the polishing wear process caused by tape. Another explanation would be if one takes into account different orientation of the crystallographic planes in these ferrites used for DDS heads. It has been found that the same crystal wears differently upon crystallographic plane. [29]

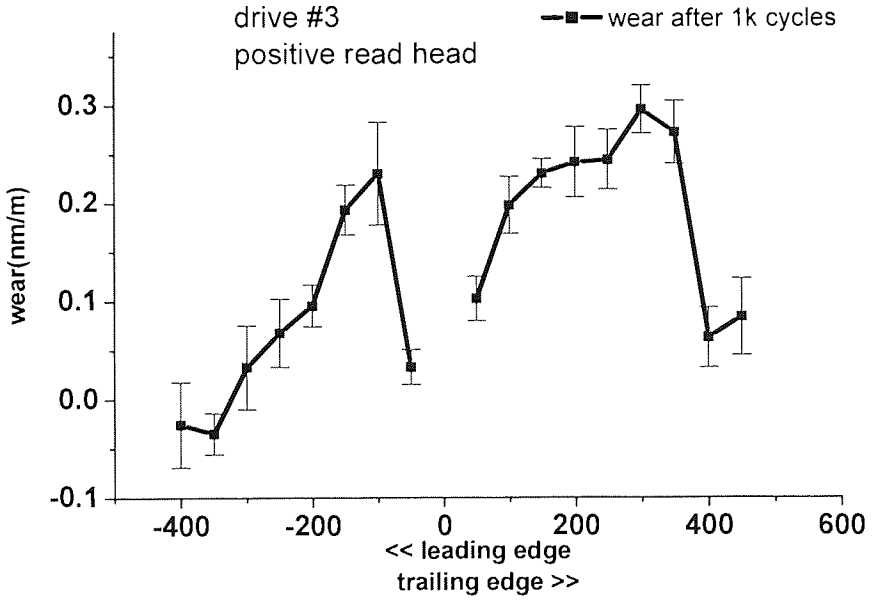

Figure 4-20 Wear rate of the positive read head on drive 3 after 1000 cycles

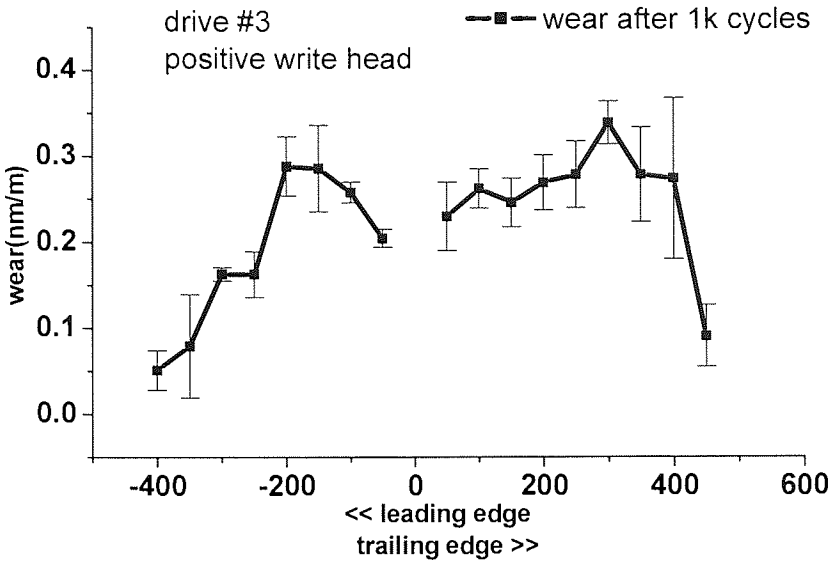

Figure 4-21 Wear rate of the positive write head on drive 3 after 1000 cycles

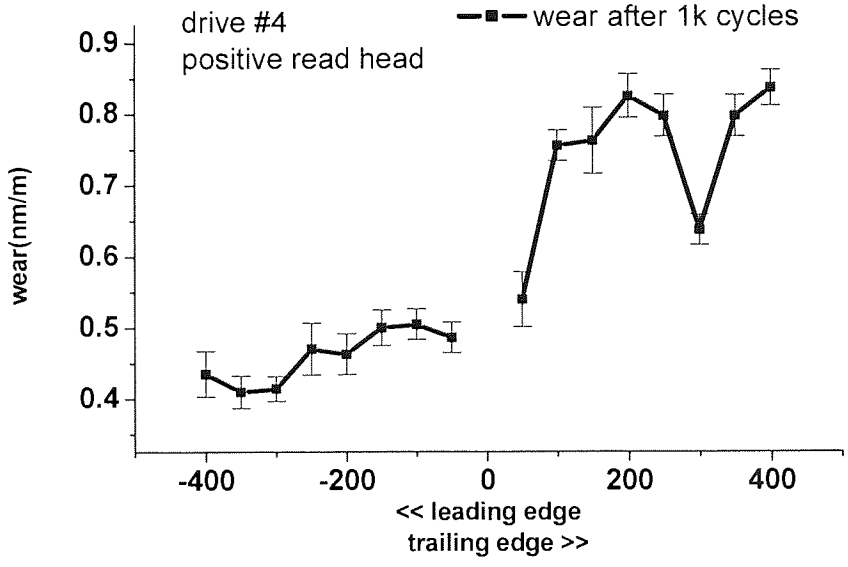

Figure 4-22 Wear rate on drive number 4 positive read head after 1000 cycles

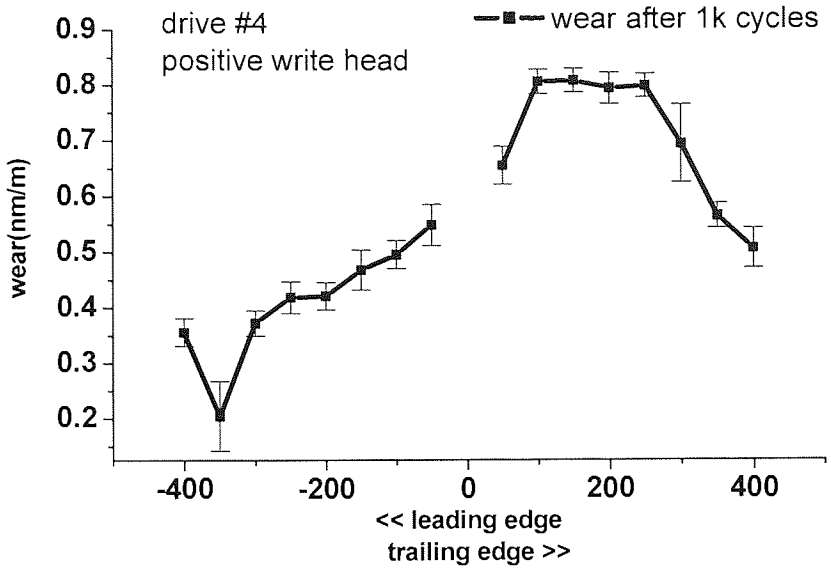

Figure 4-23 Wear rate on drive number 4 positive read head after 1000 cycles

Although it had same behaviour as the previous drive, trailing edge wear rate being higher than that of the leading edge, drive 4 proved to have a very high wear rate overall. Since the reading and writing speed is the same for both drives, the behaviour may be the result either of the different head protrusion in this case compared with the previous drive (a higher protrusion involving a higher wear rate) or a different tape tension [110]. But the fact that both positive read and write heads of the drive number 4 had the same relatively high rate of wear suggests that most plausible hypothesis is that the tape tension was different.

At 45°/10%RH, the characteristic of the heads to wear more at the trailing edge than at the leading edge encountered at moderate humidity has been maintained but in this case, the overall wear rate decreased dramatically. The figures below show the wear profile of the heads. By increasing the number of cycles further to 5000, the trend of the heads seen in the previous environmental conditions to wear more on the trailing edge than on the leading edge tested was maintained.

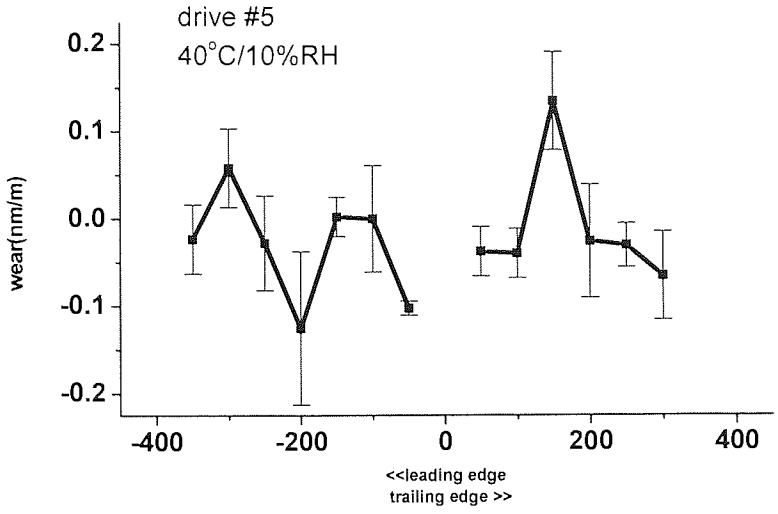

Figure 4-24 Wear rate on drive number 5 positive read head after 1000 cycles

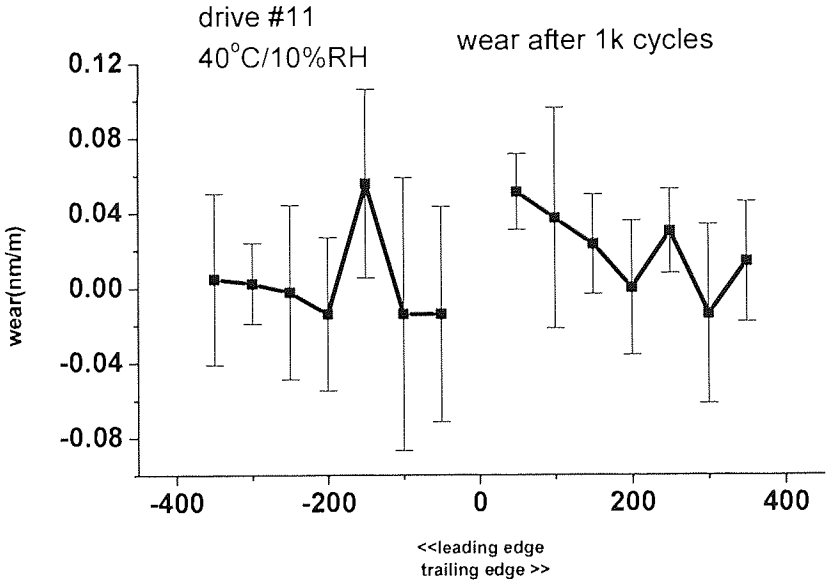

Figure 4-25 Wear rate on drive number 11 positive read head after 1000 cycles

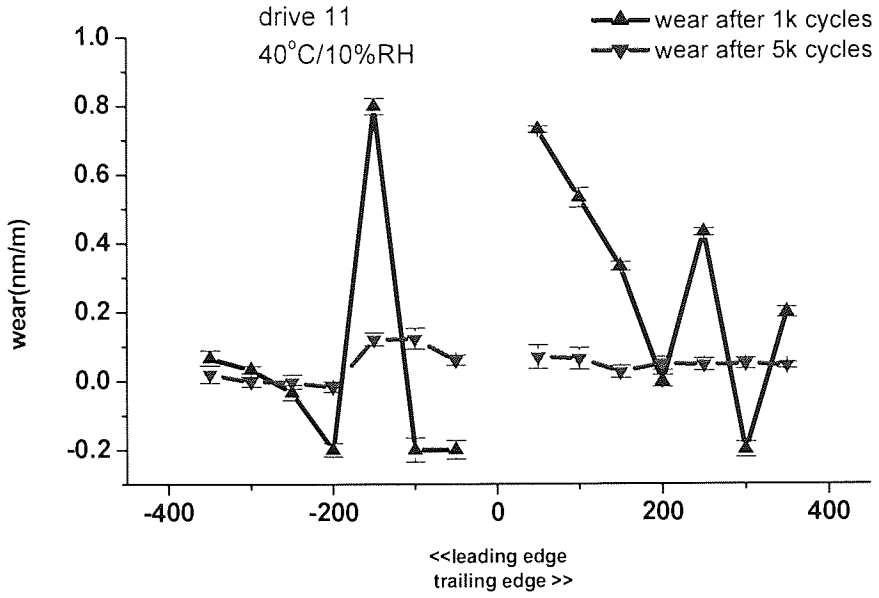

Figure 4-26 Wear after 1000 and 5000 cycles on drive 11

At 5°C/80%RH the overall wear rate proved to be the highest compared with previous environmental conditions. After the first 1000 cycles almost all indents made on the heads had disappeared. Under these circumstances the wear rate was difficult to estimate precisely, however it can be said that the rate was higher than 1.6-1.7 nm/m as shown in Figure 4-27. After further 4000 cycles, all indents had disappeared.

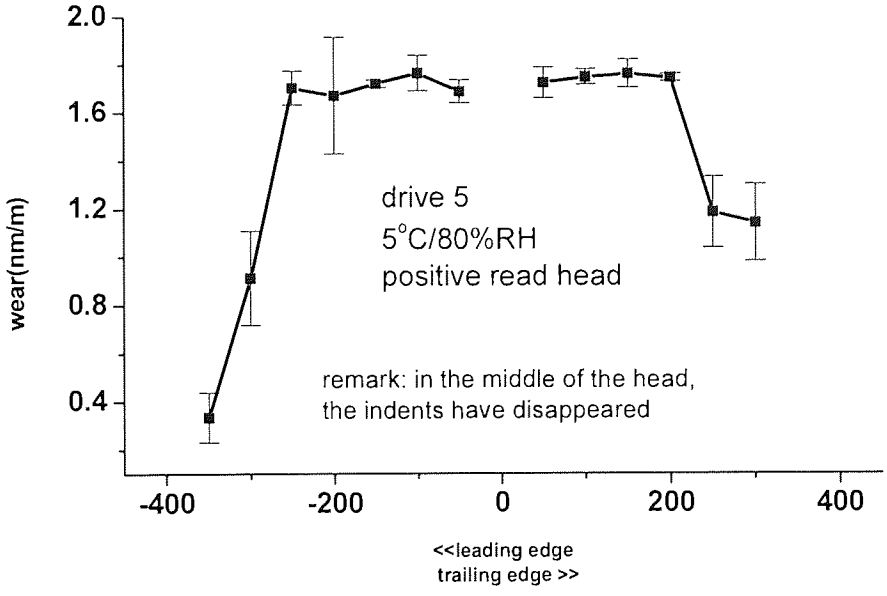

Figure 4-27 Wear of the drive 5 positive read head after 1 000 cycles at 5°C/80%RH

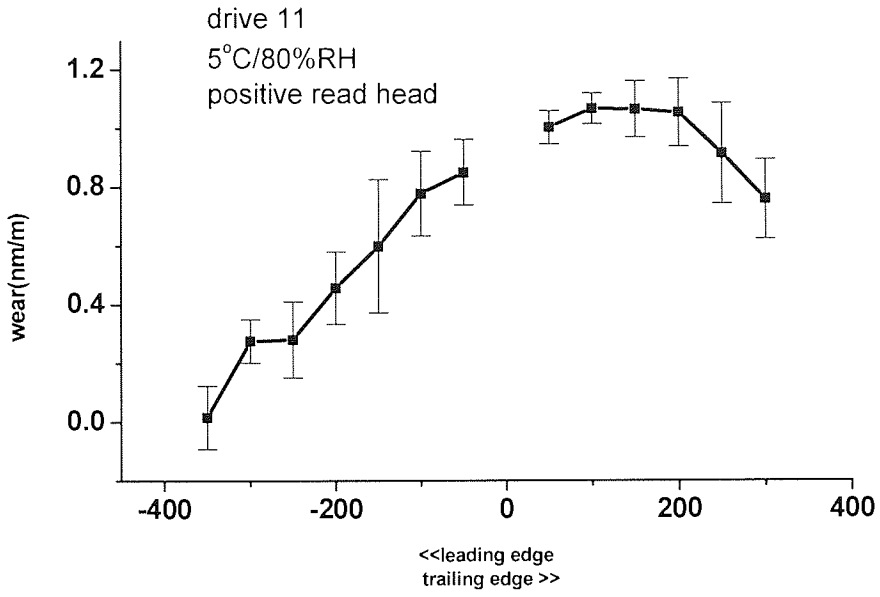

Figure 4-28 Wear of the drives 11 after 1 000 cycles at 5°C/80%RH

The fact cannot be attributed to the amount of water present in the chamber's atmosphere since calculation (Equation 3-6) revealed that at 5°C/80%RH the amount of water is the lowest compared with environmental conditions tested previously (see Table 4-4)

Environmental condition	Water vapour pressure
25°C/35%RH	1.11
45°C/15%RH	1.44
5°C/80%RH	0.70

Table 4-4 Computed values for the water vapour pressure at different environmental conditions

A possible explanation would be if we take into account the glass transition temperature of the polymer within the tape. As the temperature decreases, the polymer is becoming stiffer and thus the polishing process at the interface head-tape is more effective. Probably the highest wear rate encountered at 5°C/80%RH is due to the cumulative effect of the water and the abrasivity effect of the tape. If it were the case of the polymer binder becoming stiffer, the tape contact profile would have been changed

involving tape having more contact with the head in the region of the gap, which means higher wear. Figure 4-28 shows indeed that wear is higher towards the gap region but unfortunately the data cannot be verified using Figure 4-27 since on the positive head of the drive 5 the indents disappeared completely in the middle of the head.

For both drives used for experiments, the wear rate at high humidity was slightly higher towards the trailing edge of the head. This became more evident for the drive 5 that performed 5000 cycles.

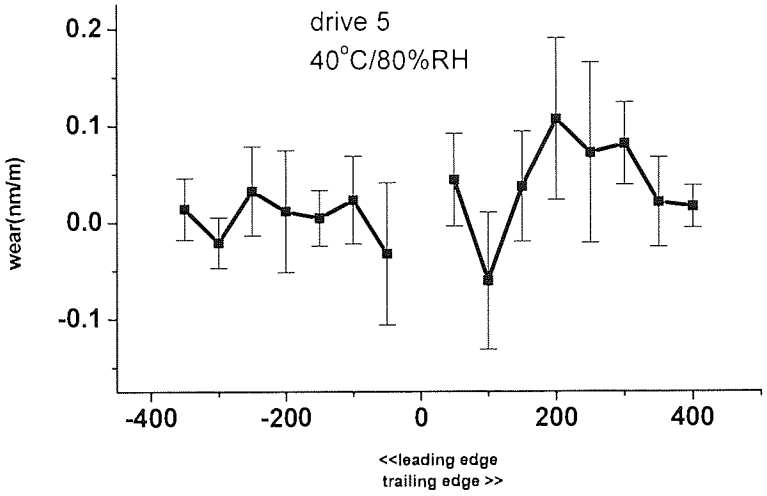

Figure 4-29 Wear rate of the drive 5, positive read head after 1000 cycles

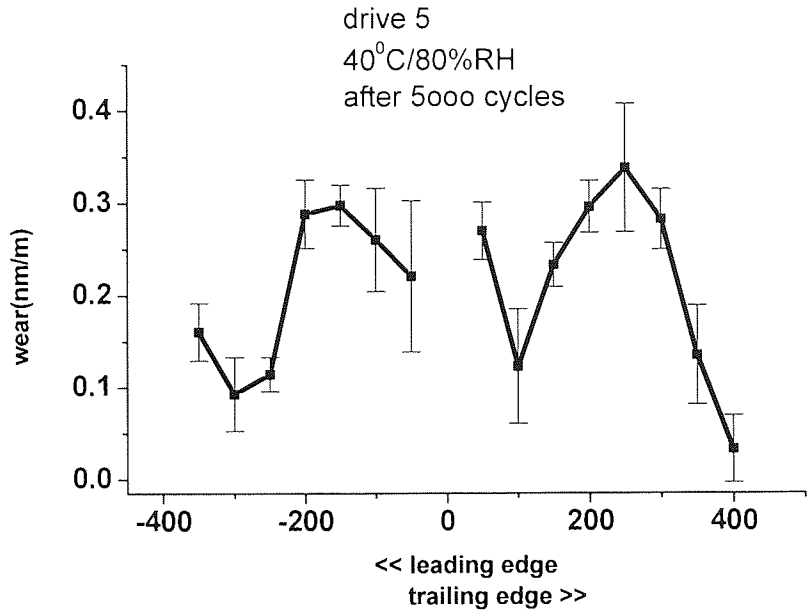

Figure 4-30 Wear rate of the drive 5, positive read head after 5000 cycles

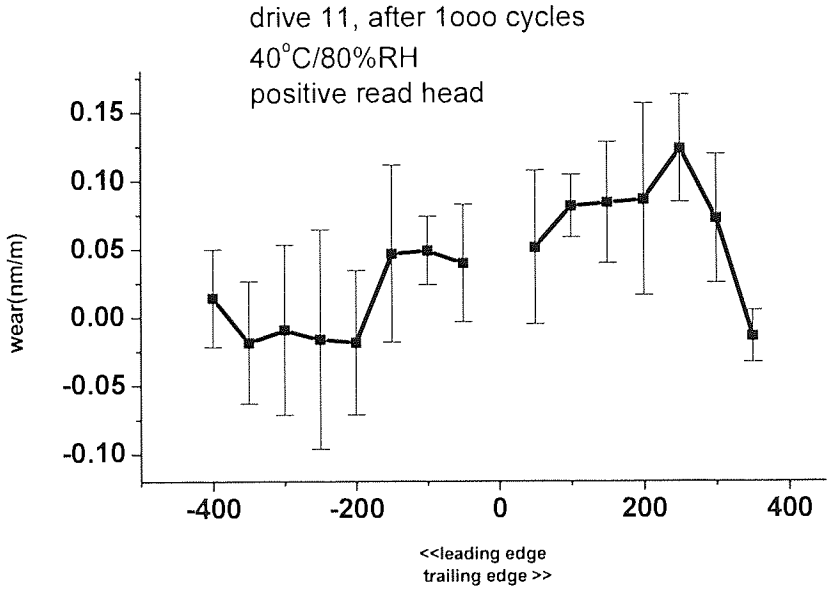

Figure 4-31 Wear rate of the drive 11, positive read head after 1000 cycles

At 10°C/10%RH, the wear rate was found to be small most probably because of the stains forming on the heads (see also next section regarding AFM scans). As a

conclusion, stains have been found to decrease the wear of the heads, its dynamic behaviour preventing large amounts of head material being removed by abrasive wear.

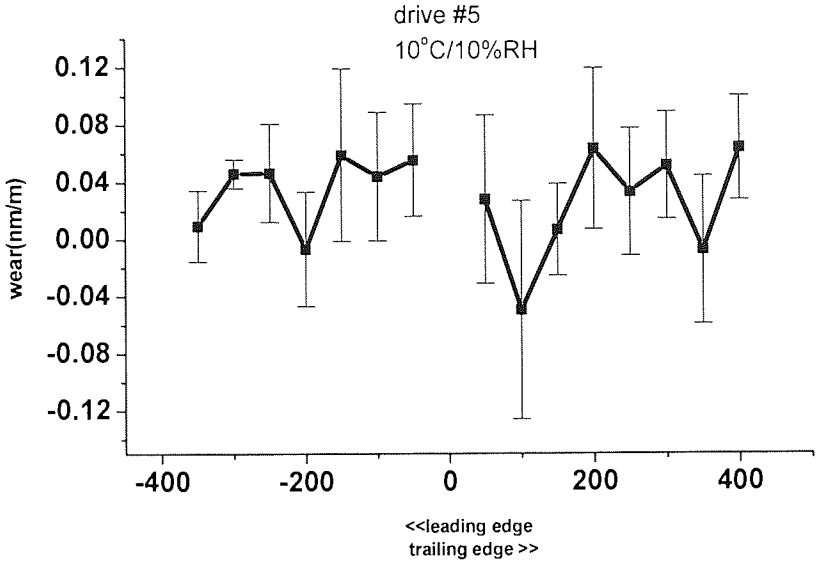

Figure 4-32 Wear rate of the drive 5, positive read head after 1000 cycles

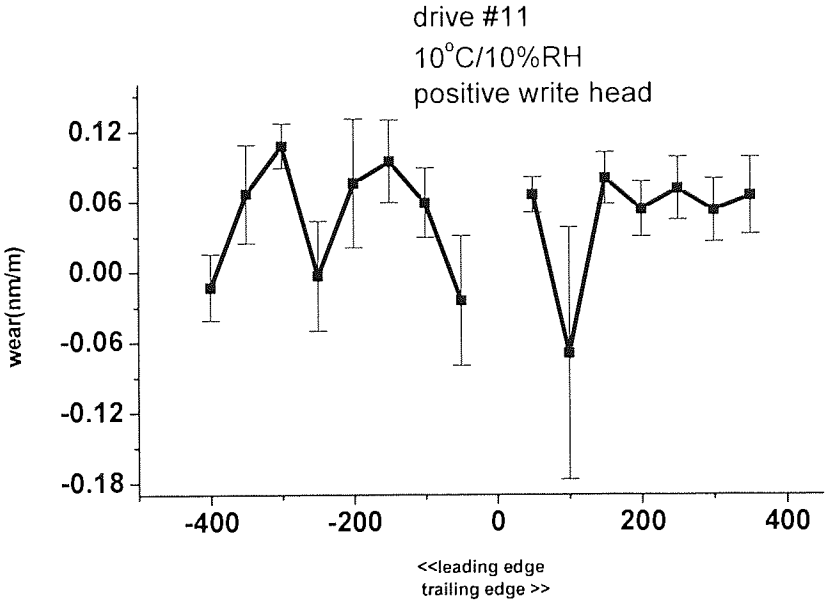

Figure 4-33 Wear rate of the drive 11, positive **write** head after 1000 cycles

4.3 AFM imaging and area roughness results

4.3.1 AFM scans of the tape

AFM scans were taken of DDS2 tapes during the experiments. Generally, the scans reveal small bumps of about 20 nm height that are probably due to polymeric binder. After the first cycles of operation, the top layer of polymer was probably removed revealing other tape constituents as well. After 1000 cycles, crystals of 1μm can be seen on the surface of the tape, probably crystals of SiO_2 and Al_2O_3 that were commonly used in DDS2 tape formulation as head cleaning agents. According to tape manufacturers [16, 99, 100] the head cleaning agents used have a preferably size of 0.2-0.8μm.

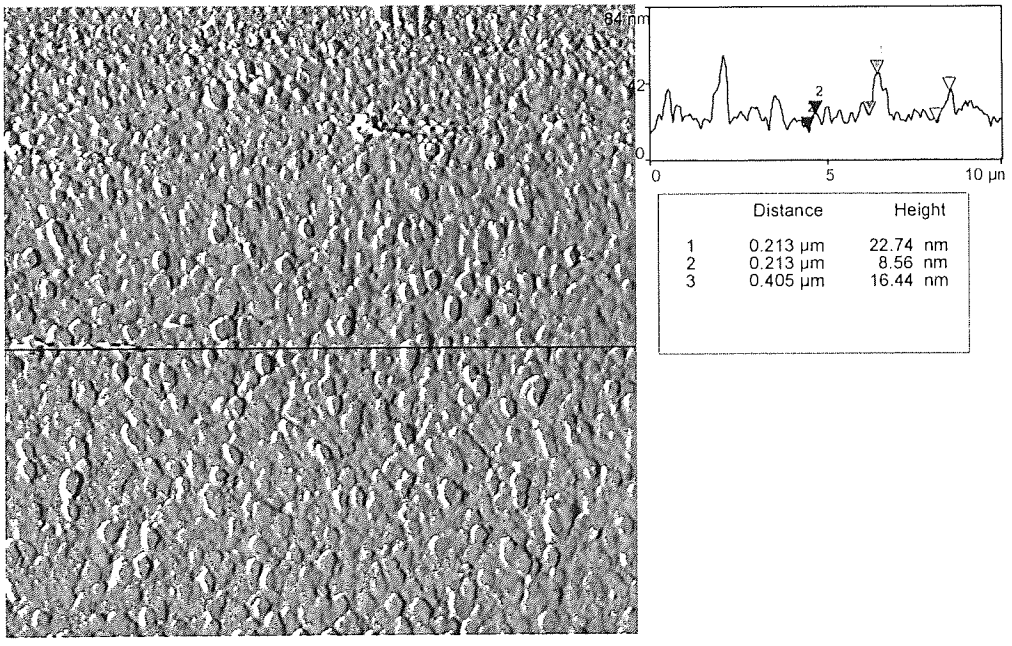

Figure 4-34 AFM scan (10x10 μm) of a virgin tape

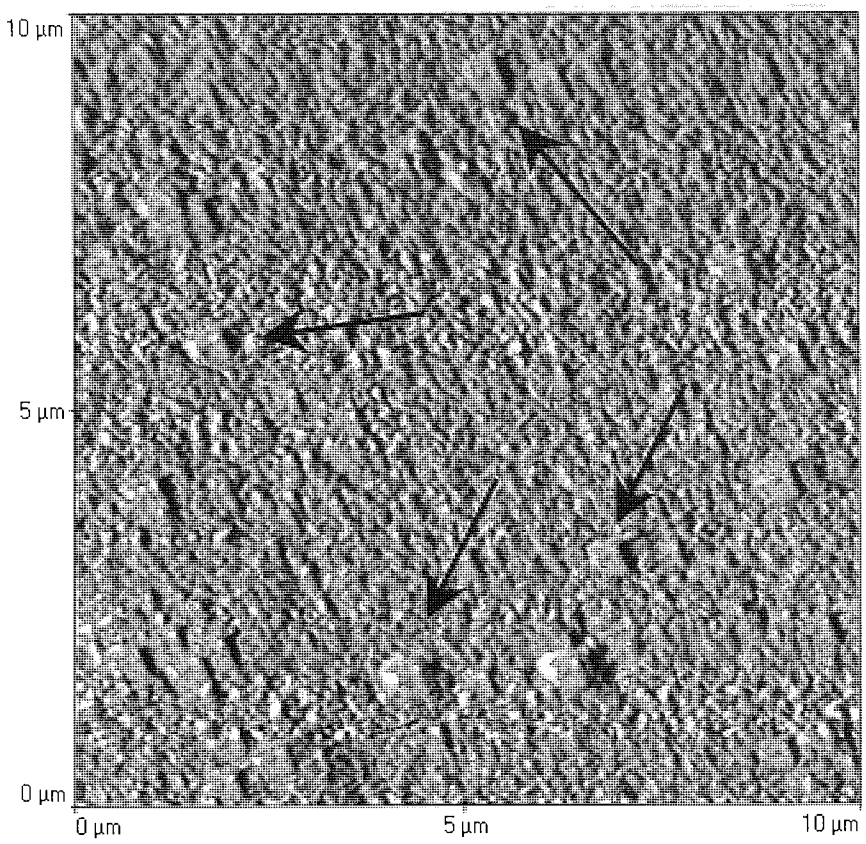

Figure 4-35 AFM scan (10x10 µm) of the tape after 1 000 cycles (the arrows point to HCA particles)

Towards the end of the experiments, the particles have disappeared being removed probably by the intensive wear occurring during normal operation of the tape and a series of pores are uncovered. It is believed that these dips are manufactured in order to allow the lubricant to migrate from the bulk magnetic coating to the surface and replenish the lubricant that is being depleted therefore insuring constant head-to-tape lubrication.

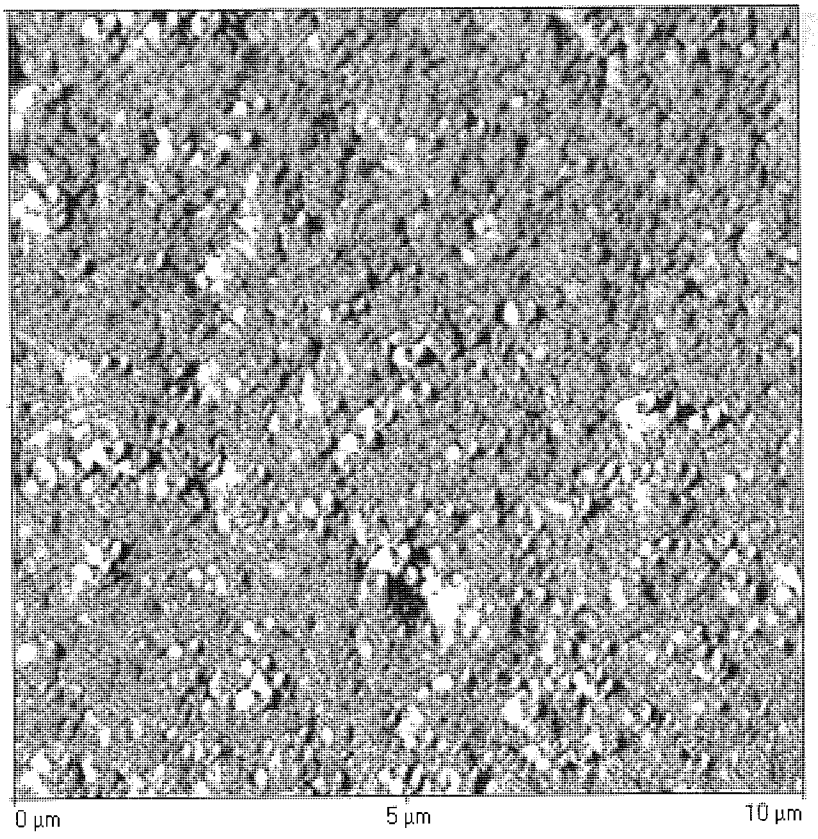

Figure 4-36 AFM scan (10x10 µm) of a tape after 5 000 cycles

4.3.2 AFM scans of the DDS-3 heads

At 25°C/35%RH, as one can see from figures below, the DDS drive shows stain at the upper part of the glass region (left side of the picture) even after the reconditioning process. The stains seem form a continuous layer. There could be two explanations for this feature. First, it could have been the result of the tape tension not being high enough to produce sufficient wear and thus to remove the stain from the previous experiments. Second, if one takes into account the head's curvature the continuous layer of stain could have appeared because the tape did not event make contact on that region of the head. However, in both cases the normal load was lower than in the neighbouring glass regions or ferrite poles.

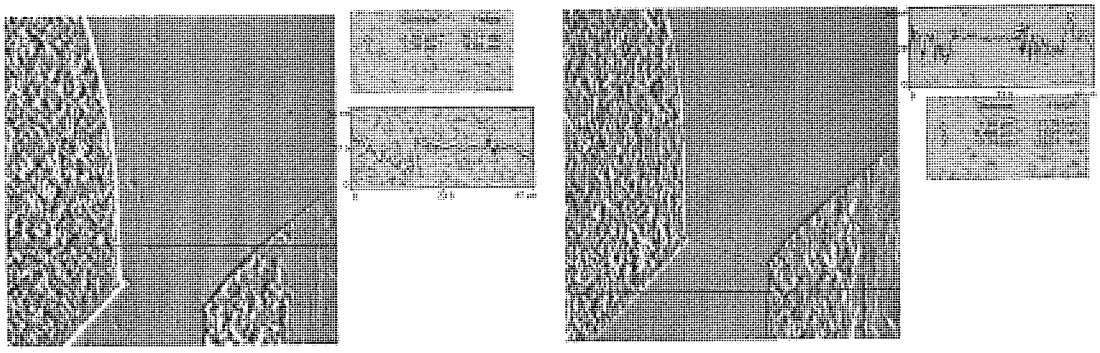

a) b)

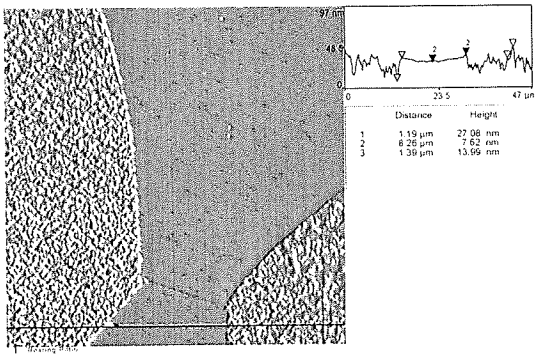

c)

Figure 4-37 Drive 5 after 0 (a), 100 (b) and 1000 (c) cycles

As the number of passes increased, the average height of the glass region increased. Since the wear rate of the ferrite was found to be low, it was supposed that the increase is due to the process of stain building up. The ferrite region of the head seemed to remain clear and few spots of stain or loose debris of 2 to 3 nm height could be seen. The preferential deposition of adhesive debris is probably related to the fact that the glass region is recessed compared with the ferrite region that leads to a lower load force of the tape therefore a lower wear rate.

Patchy areas of stain were present on the glass region of the drive number 6 right from the beginning of the tests. Given the fact that the measured average height is lower than that of the ferrite, it is believed it cannot influence the signal quality. The change in stain areal coverage was visible after the first 1000 cycles. After 5000 cycles, the stain formed a continuous layer all over the glass region but the ferrite poles seemed to remain clear. The stain on the glass increased in areal coverage and height. Abrasion marks were visible along the poles after the first 100 cycles probably due to the tape asperities. Apart from that, a deep abrasion mark present on the glass region after 100

cycles seemed to be totally covered by stain after 5000 cycles. It must be pointed out the big difference between the gaps of the drives. The drives number 6 and 7 had a gap width of about 3μm whereas usually the gap is of order of few hundreds of nanometers. The big gap width is due to the excessive wear encountered by these particular drives during previous experiments.

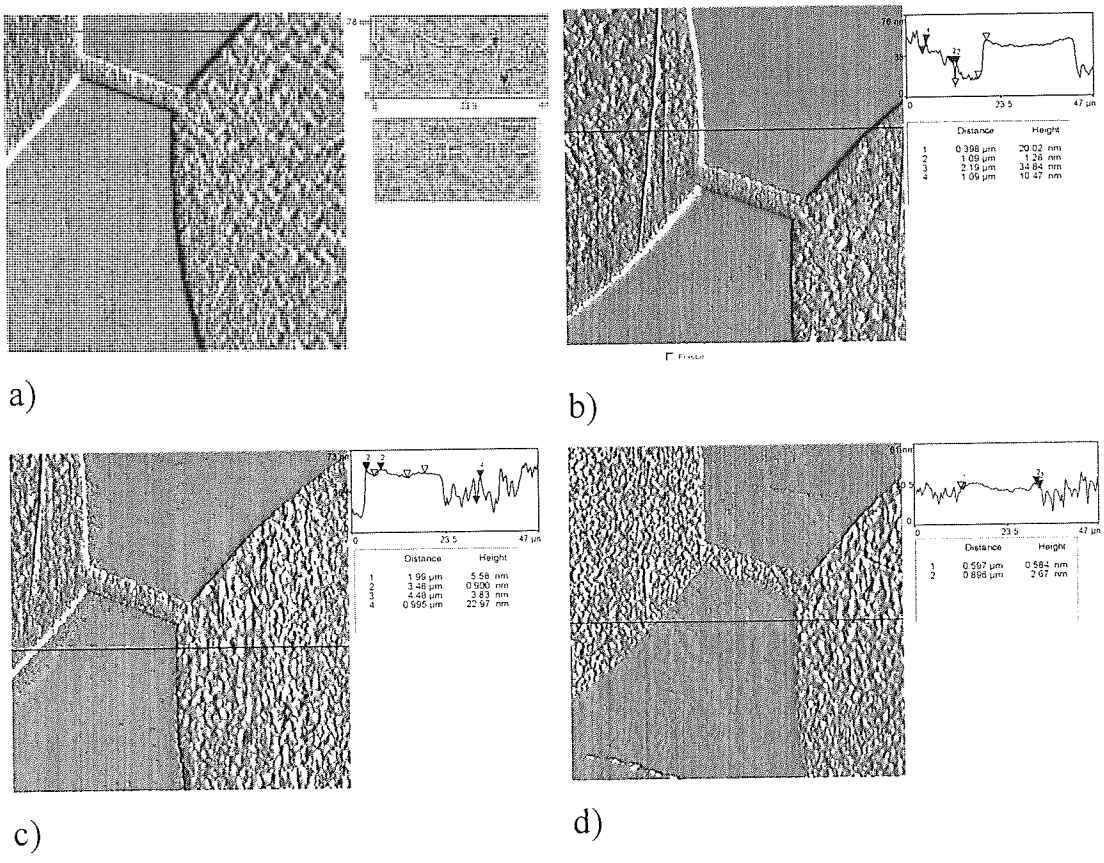

a) b)

c) d)

Figure 4-38 Drive 6 after 0 (a), 100 (b), 1000 (c) and 5000 (d) cycles

The drive 7 has had a similar behaviour as one can see from Figure 4-39. The abrasion marks along the poles, probably caused by the HCA (**H**ead **C**leaning **A**gent) particles, seem to be more pronounced compared with drive 6. A large crack, of about 1mm height, appeared after 1000 cycles and made roughness quantification of the area extremely difficult.

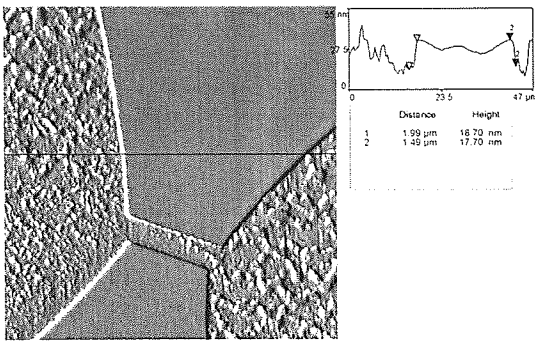

a)

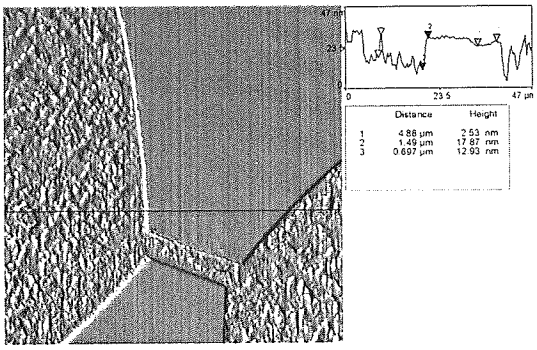

b)

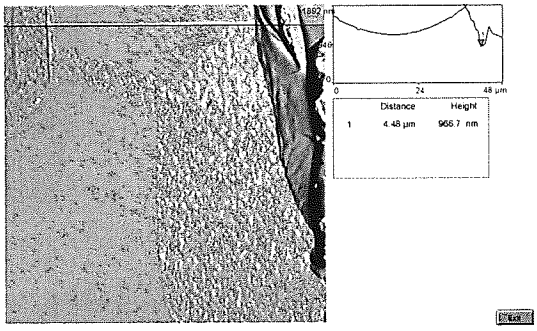

c)

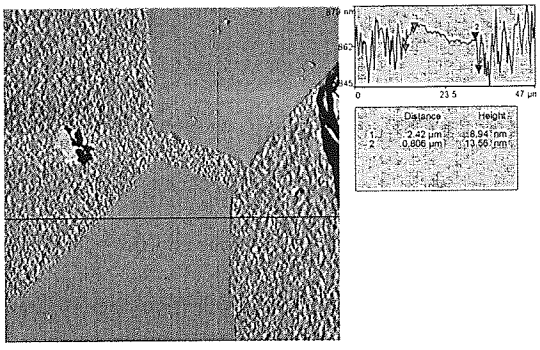

d)

Figure 4-39 Drive 7 after 0 (a), 100 (b), 1000 (c) and 5000 (c) cycles

Similar to drive 5, the drive 8 had its glass protrusions filled with stain in the right side of the head. After 1000 cycles, the stain formed a continuous layer in the glass region. No stains have been identified on the poles.

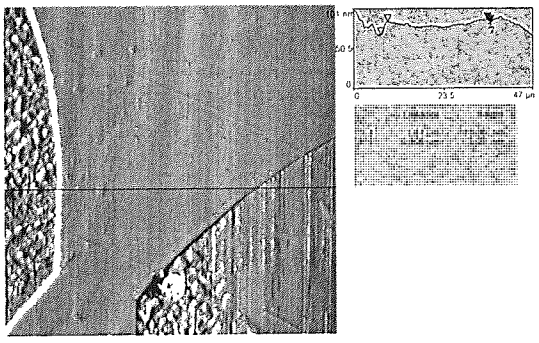

a)

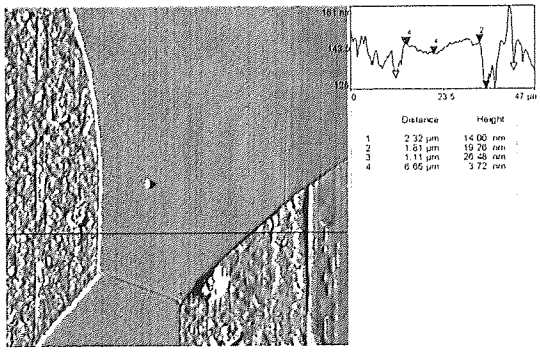

b)

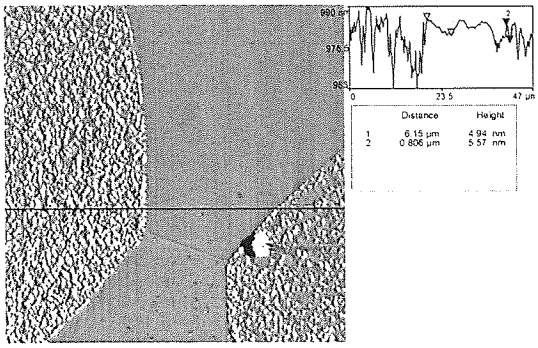

c)

Figure 4-40 drive 8 after 0 (a), 100 (b) and 1000 (c) cycles

At 45°C/15%RH things changed dramatically, as one can see from the pictures below. The reconditioning process was inefficient and thus both poles and glass regions have shown the presence of stain in large amounts. Height measurements on pole areas revealed that stain is about 14-16nm height and it has a smearing feature. As the number of passes increased, the stains covered a larger surface and had the tendency to deposit mostly in the glass region. This is probably due to the fact that glass is rougher and lower than the ferrite and thus the normal load of the tape and thus friction force and wear are lower in these regions compared with the ferrite region. Taking into account the previous images acquired of the same drive at different environmental conditions and the fact that the head was wiped using a cotton applicator and alcohol the conclusion is that at 5000 cycles, the glass region is almost entirely covered by a thick layer of stain. Measurements performed across the gap and in the ferrite and the glass region, supposing that the gap is stain free after reconditioning process, revealed that the thickness of the stain is between 30 to 40nm.

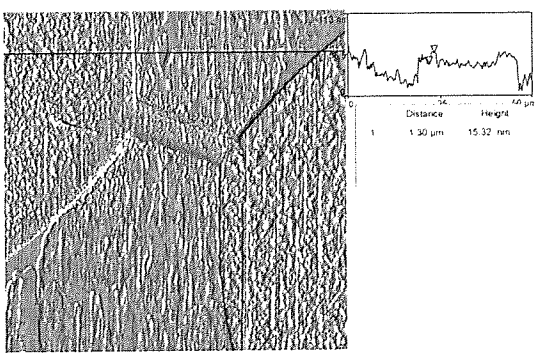

a)

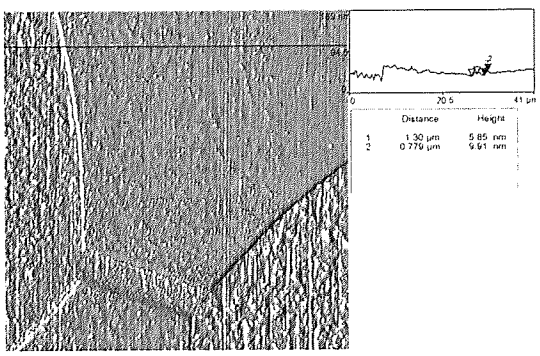

b)

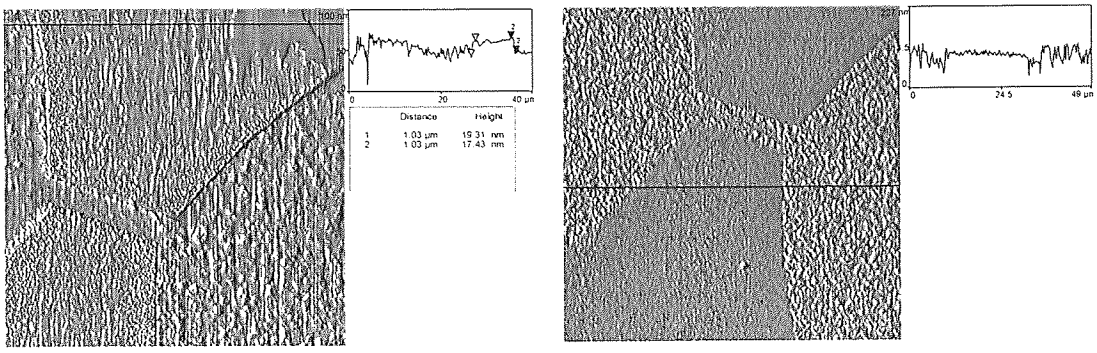

c) d)

Figure 4-41 Drive 6 after 0 (a), 100 (b), 1000 (c) and 5000 (d) cycles respectively

Similar to drive 6, drive 8 showed stain even after reconditioning process as one can see from Figure 4-42. An interesting feature can be seen right after reconditioning process at one of the poles: It could be either caused by crystallographic defects of the ferrite or it may reveal that actually the ferrite poles are covered by an organic/stain layer. After 100 passes these features disappeared, probably being covered by a fresh layer of organic material. At the end, the head is totally covered by a very thick and discontinuous layer of stain. The process could be responsible for the early failures previously seen on other drives when measuring error rate.

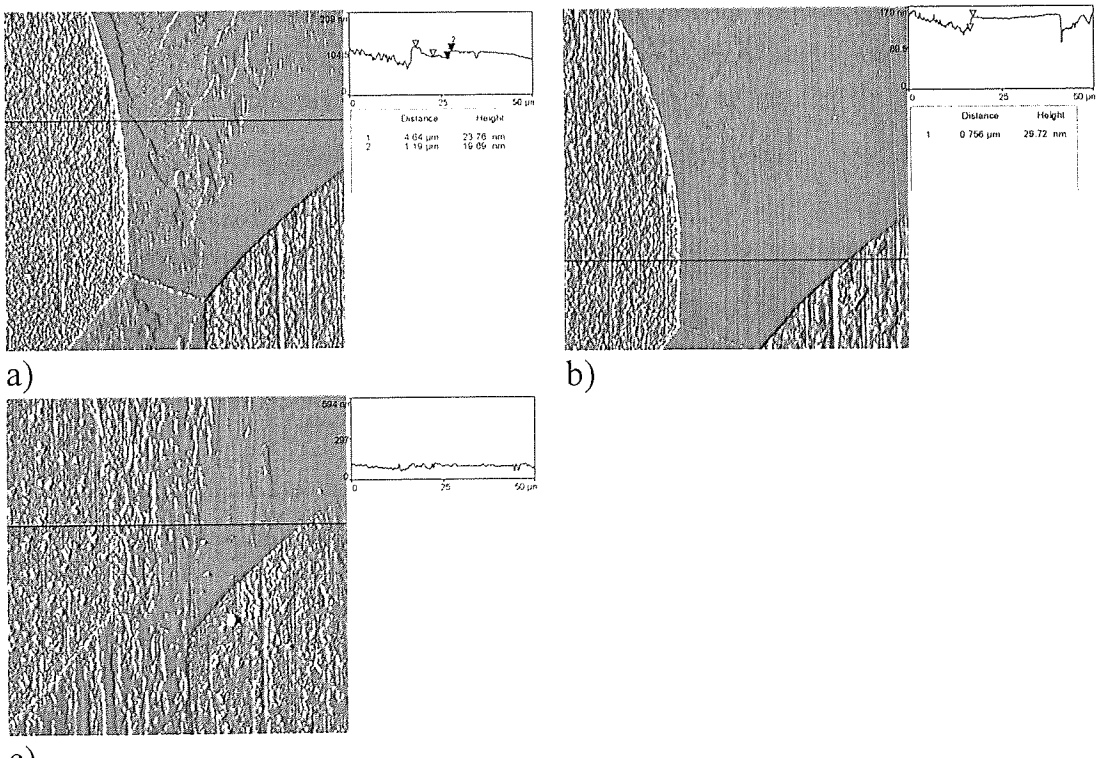

a) b)

c)

Figure 4-42 Drive 8 after 0 (a), 100 (b) and 1000 (c) cycles respectively

The experiments performed at 5°C/80%RH showed very little or no stain on ferrite poles. Although the poles remained clear during the entire length of the experiment, the glass regions displayed patches of stain. Three scratches can be seen on the right side of the glass region of the drive 6 that were probably caused by loose debris becoming third bodies entrapped between head and media. The scratches could have been made in a layer of adhesive deposits or in the glass material. The first hypothesis is supported by the fact that the marks have 14 nm in depth, which is usually the height of the stain formed on ferrite during experiments at low humidity. By the time the drive finished its 5000 cycles, the scars had disappeared.

At the end of its 5 000 cycles, drive 6 had the poles covered in what seemed to be plastic flow of the binder or, more probably, features related to ferrite's crystallography (differential wear) whereas the poles of the drive 8 remained clear. Similar features have been seen and investigated before and, as Chandler [**111**] pointed out, they occur in a particular configuration of drive and tape. If the tape is changed, the phenomenon might not occur. The height of these features was less than 5nm. The plastic flow is usually denoted by the orientation of the deposits perpendicular to the tape motion direction. However, the deposits found here, having less than 5nm in height are not all oriented in this way. Despite changing the scanning angle, the tilt of the tip or modifying the laser beam position on the tip we were unable remove these features and therefore proving that are not artefacts of the AFM microscope.

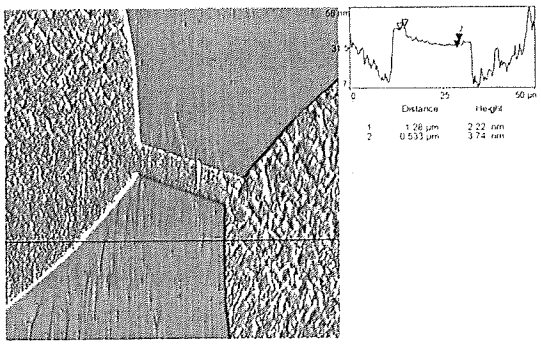

a)

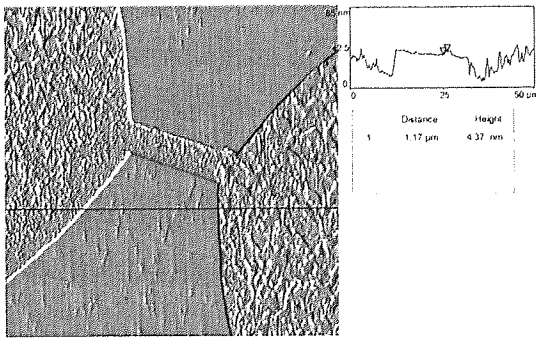

b)

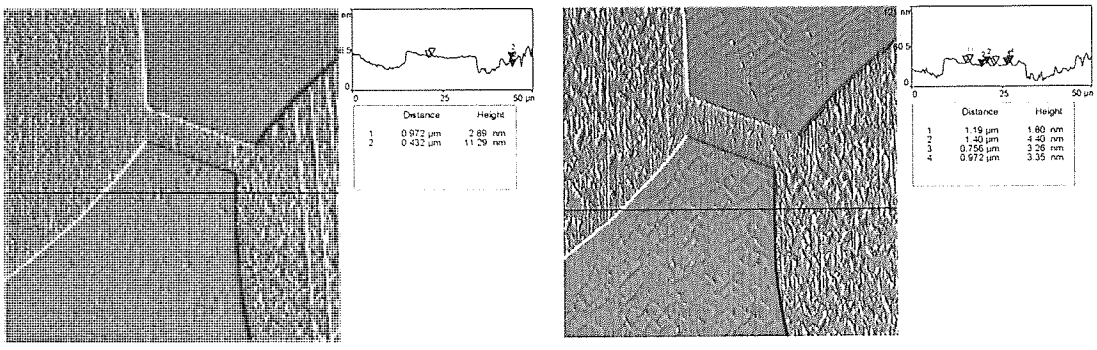

c) d)

Figure 4-43 Drive 6 after 0 (a), 100 (b), 1000 (c) and 5000 (d) passes at 5°C/80%RH

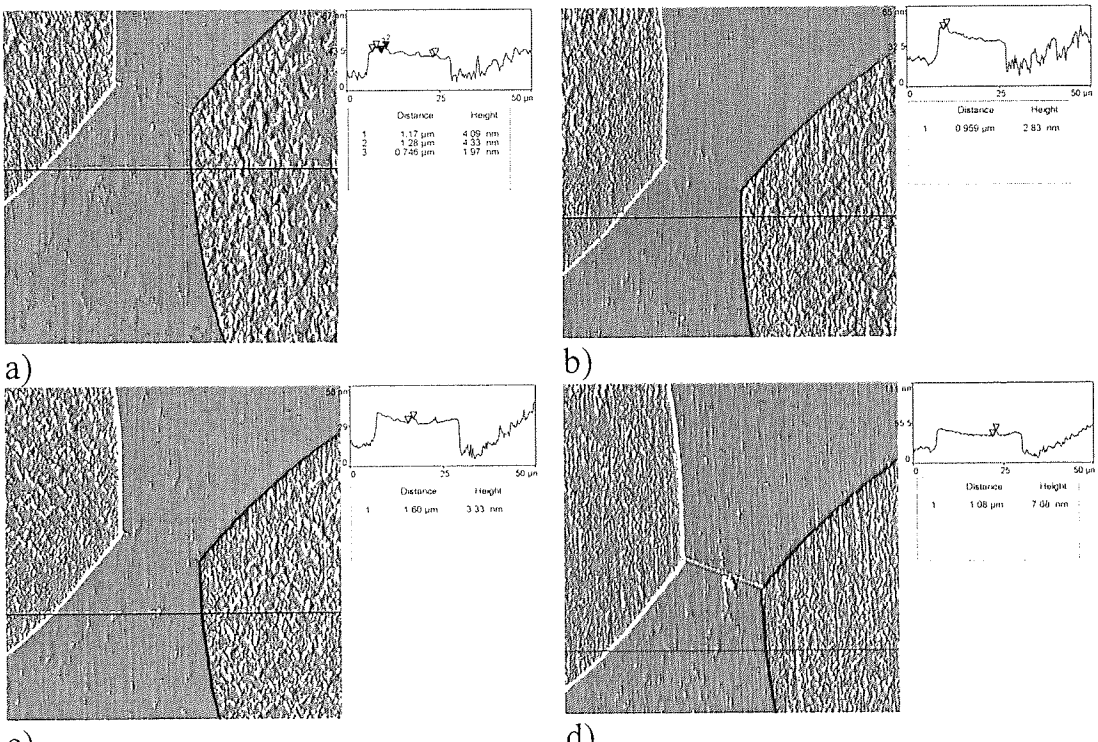

a) b)

c) d)

Figure 4-44 Drive 8 after 0 (a), 100 (b), 1000 (c) and 5000 (d) passes at 5°C/80%RH

At high humidity (40°C/80%RH) no or very few deposits are present on the ferrite poles on both drives tested. The poles remained clear throughout the experiments. The scans of the ferrite poles revealed small deposits of 2-4nm in height, very scattered along the poles. Although deposits seemed to accumulate on the glass region, and the glass seems to become smoother, the heights of the deposits did not increase.

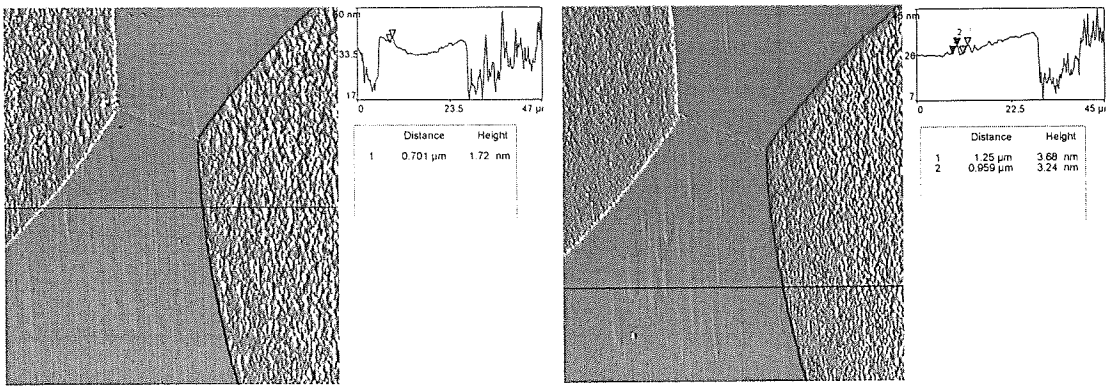

a) b)

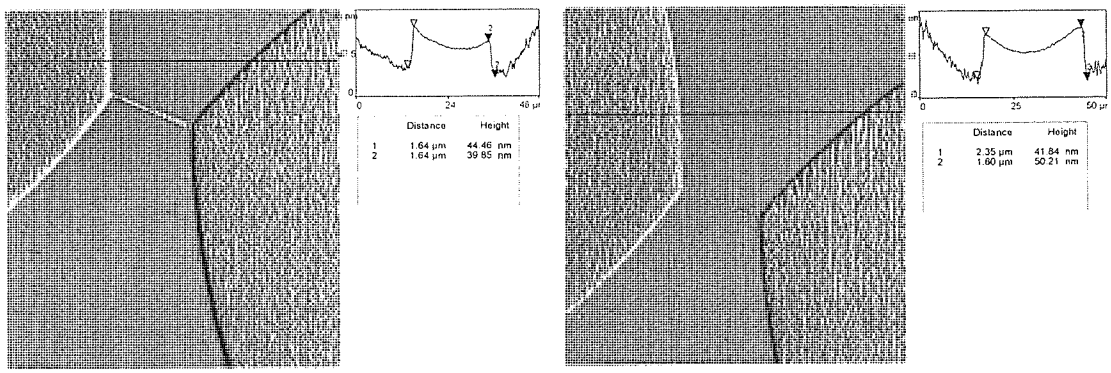

c) d)

Figure 4-45 Drive 12 after 0 (a), 100 (b), 1000 (c) and 5000 (d) passes at 40°C/80%RH

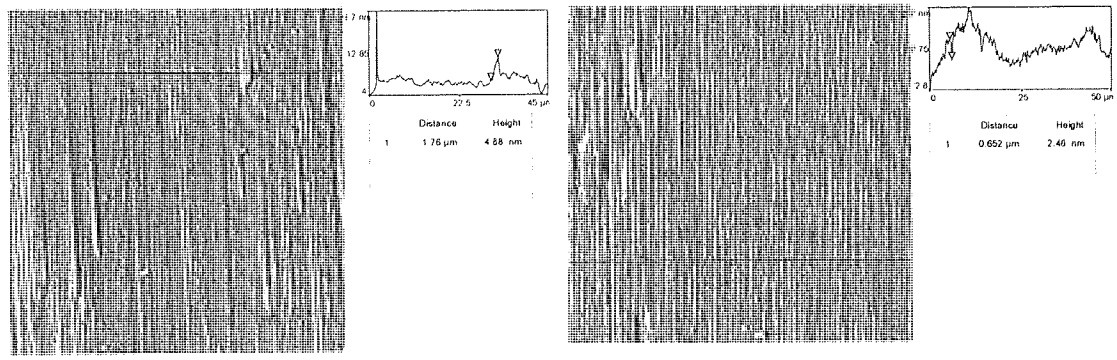

a) b)

Figure 4-46 Drive 12's ferrite poles after 0 (a) and 5000 (b) cycles at 40°C/80%RH

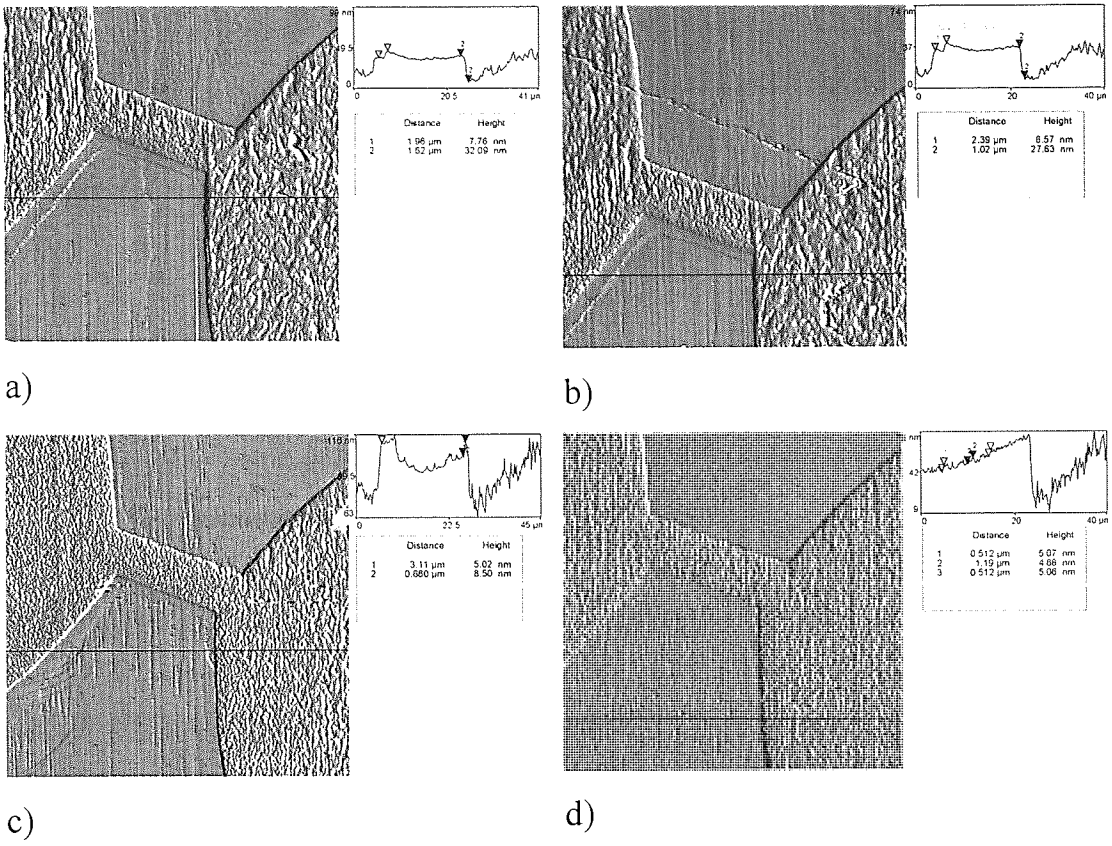

Figure 4-47 Drive 6 after 0 (a), 100 (b), 1000 (c) and 5000 (d) passes at 40°C/80%RH

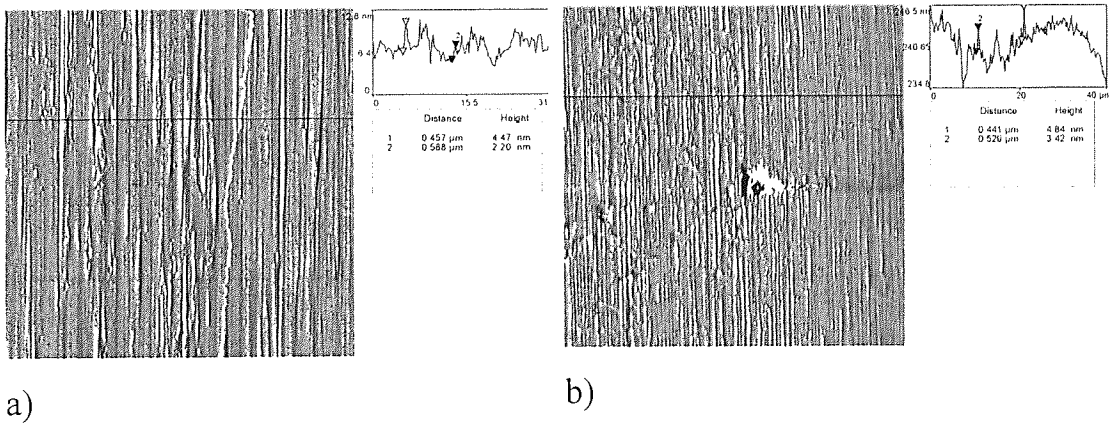

Figure 4-48 Drive 6's ferrite poles after 0 (a) and 5000 (b) cycles at 40°C/80%RH

For the next condition (10°C/10%RH) the drive 6 the presence of small ridges after the reconditioning process was observed. As the number of passes increased, the stain started to accumulate, at the beginning near the edges, and by the end of 100

cycles the stains pattern became evident. Wear tracks were visible on the glass region, but more probably these tracks were on the stained layer covering the glass regions and not on the glass itself. A very interesting feature is present by the end of the experiment. The AFM scan of the top ferrite pole shows a series of depressions. It is believed that these features cannot be pullouts, but there are rather regions were more than one layers of stain has been removed. Measurements show that these depressions are up to 40 nm deep, which leads to the conclusion that occasionally, the deposits grow up to 40 nm thick. It is also worth noting the height of the glass and ferrite regions at the beginning and at the end of the experiment. If at the beginning the glass was recessed by 25-35nm, by the end of the experiments the recession was only 0-5nm. This fact does not mean that the ferrite was heavily worn since the wear rate measured earlier for ferrites was found being low, but rather that the glass region is now covered by a very thick layer of stain. (see also section 4.4 regarding the AES investigation) Certainly, the phenomenon occurred in all the environmental conditions studied but it was more evident at very low humidities due to the large amounts of stain generated. This is further evidence that stain can grow thicker than the usual 14nm.

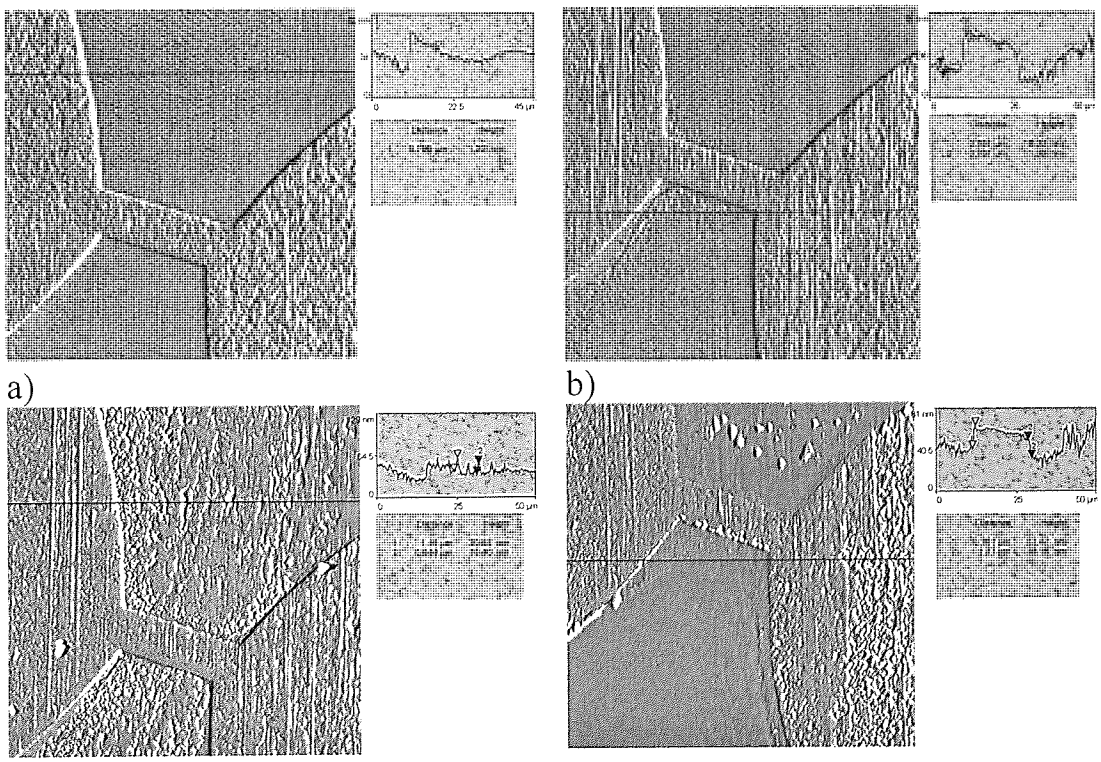

Figure 4-49 Drive 6 after 0 (a), 100 (b), 1000 (c) and 5000 (d) passes at 10°C/10%RH

The ferrite study revealed the evolution of the stain thickness during the experiment. Small ridges of 0.5-2nm in height were found at the beginning of the experiments and, as the experiment progressed, their height increased to 14-20 nm at 1000 cycles and then to 35-40 nm.

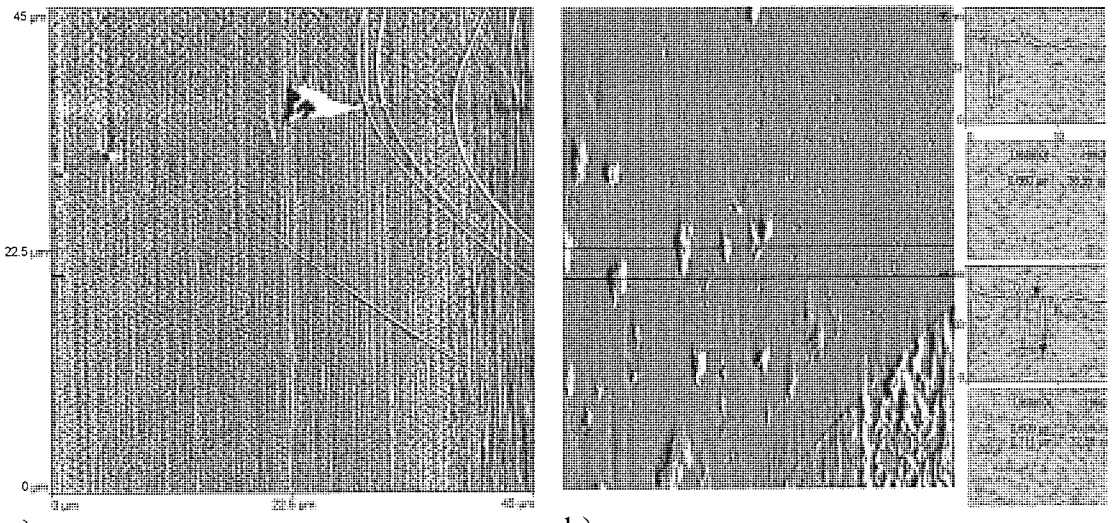

a) b)

Figure 4-50 Drive 6's ferrite poles after 0 (a) and 5000 (b) cycles at 10°C/10%RH

The topography evolution of the drive 12 was found to be similar to that of drive 6, however small differences were noticed. Firstly, after reconditioning the ferrite poles seemed to be clear. Based on the previous experience it is believed that the poles are covered by a very thin and continuous layer of stain (or polymeric binder). Wear tracks were visible on the glass region. At 100 cycles, as a new layer of stains built up, the roughness of the poles appear to increase. The process continued and after further 900 cycles, the new layer is completely formed and covered entirely the poles and even bridged the gap. Ridges of 2-6nm along the tape motion were visible on the ferrite and on the glass region the wear tracks disappeared, probably covered by a fresh layer of stains. At the end of the experiment, the ferrite was continuously covered by a layer of stain and the glass region has changed its topography. The height difference between the poles and the glass region decreased to 3-5 nm.

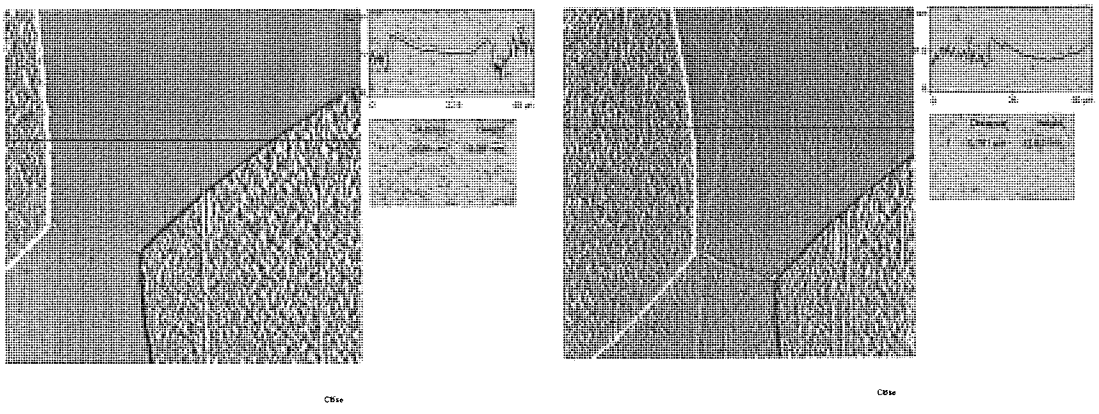

a) b)

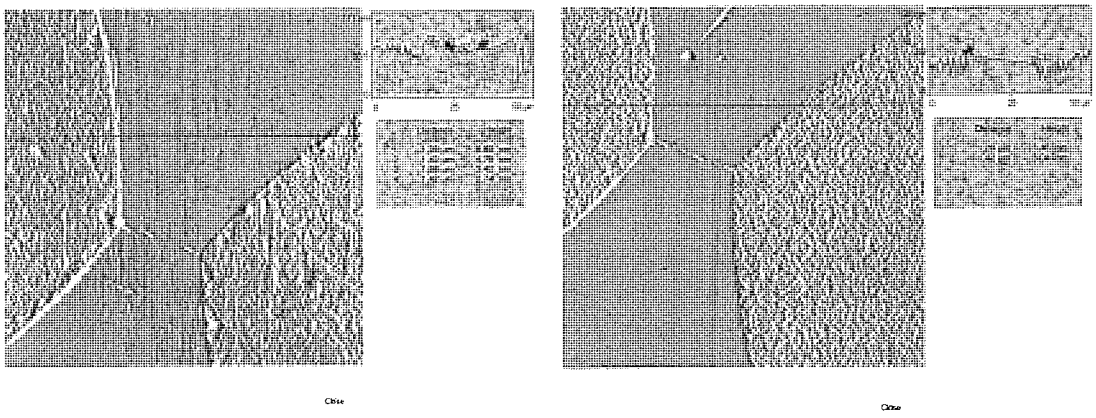

c) d)

Figure 4-51 Drive 12 after 0 (a), 100 (b), 1000 (c) and 5000 (d) passes at 10°C/10%RH

Again, the ferrite study reveals patches of stain present even after reconditioning process. At the end of the experiment, the ferrite was featuring a series of wear tracks made in the layer of stain on top of the ferrite and *not* on the ferrite material itself. It is interesting to compare this final image with the AFM scan obtained from on of the ferrite sample on which chemical analysis was performed. (see Figure 4-52and also Figure 4-91and Figure 4-92)

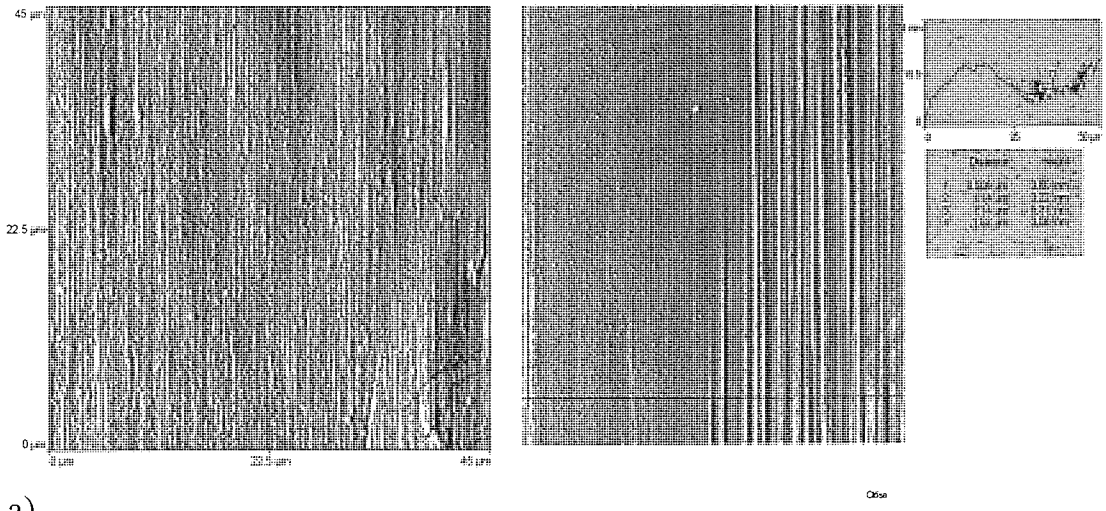

a) b)

Figure 4-52 Drive 12's ferrite poles after 0 (a) and 5000 (b) cycles at 10°C/10%RH

Further investigations were carried out concerning the surface roughness. Three regions were explored: the ferrite region, the left side glass and the right side glass regions. Compared with the glass region, for all the drives investigated, the ferrite region was by far the smoothest region of the head. As one can see from Figure 4-53, at 25°C/35%RH the surface roughness decreases as the number of passes increases. The trend is due probably to the fact that at the beginning the adhesive deposits form mainly patches and cover the dips present on the ferrite and glass surface and then the areal coverage of the deposits increases until they form a continuous layer. The increase in roughness for the drive 7 at 1000 cycles is believed to be caused by the crack appeared at that moment in the glass structure. Even in this case, after 5000 passes, the surface followed the previous drive's trend and became smoother.

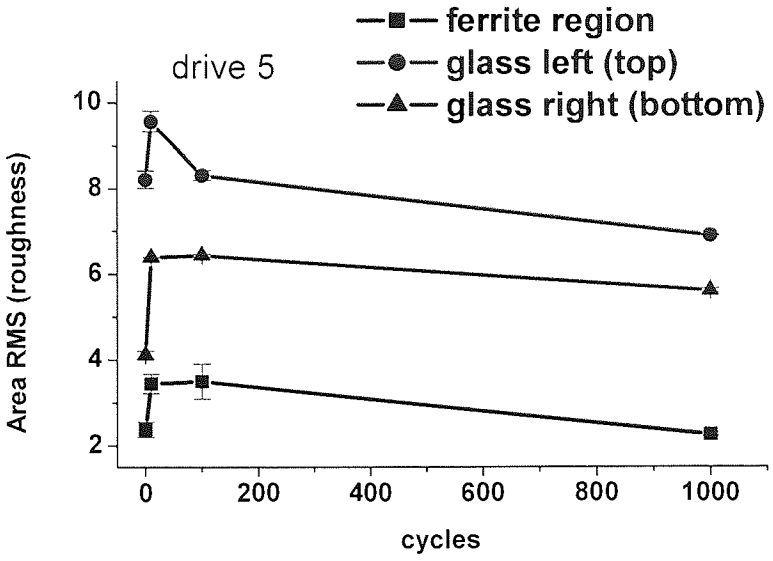
drive 5
ferrite region
glass left (top)
glass right (bottom)
Area RMS (roughness)
10
8
6
4
2
0
200
400
600
800
1000
cycles

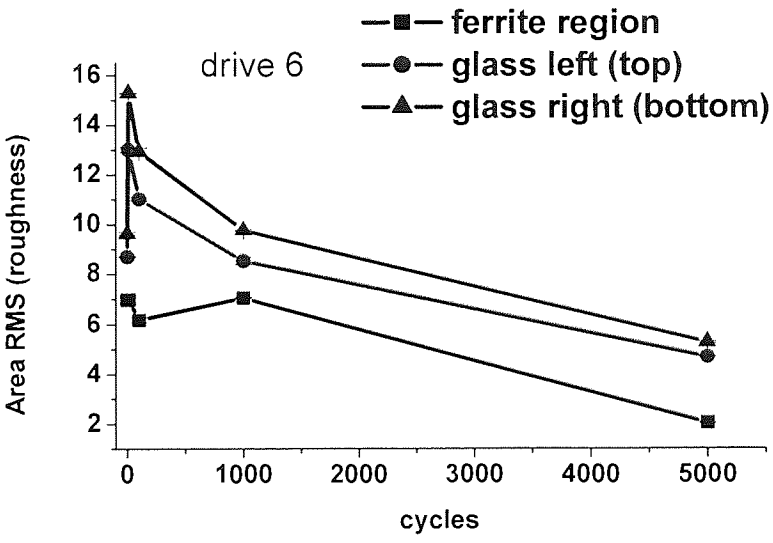
drive 6
ferrite region
glass left (top)
glass right (bottom)
Area RMS (roughness)
16
14
12
10
8
6
4
2
0
1000
2000
3000
4000
5000
cycles

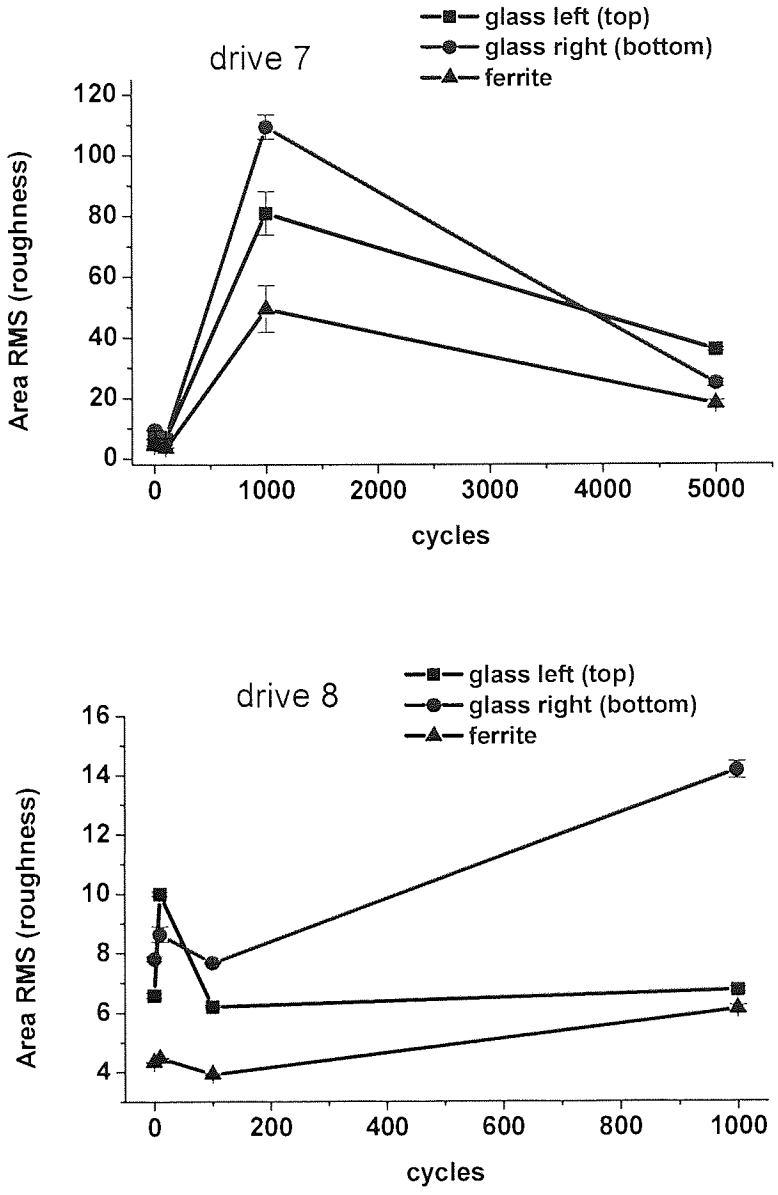

Figure 4-53 Variation of the area roughness of the drives at 25°C/35%RH

At 45°C/15%RH, after the first 1000 cycles when the surface became smoother, a new increase in roughness followed as one can see from figures below. The decrease and then the increase of the roughness could be due to the fact that adhesive debris tends to fill firstly the dips since in these regions there is no contact between tape and head, hence no abrasive wear. Then, as the depressions filled in, the debris started to spread away, and this phenomenon lead to an increase in head roughness.

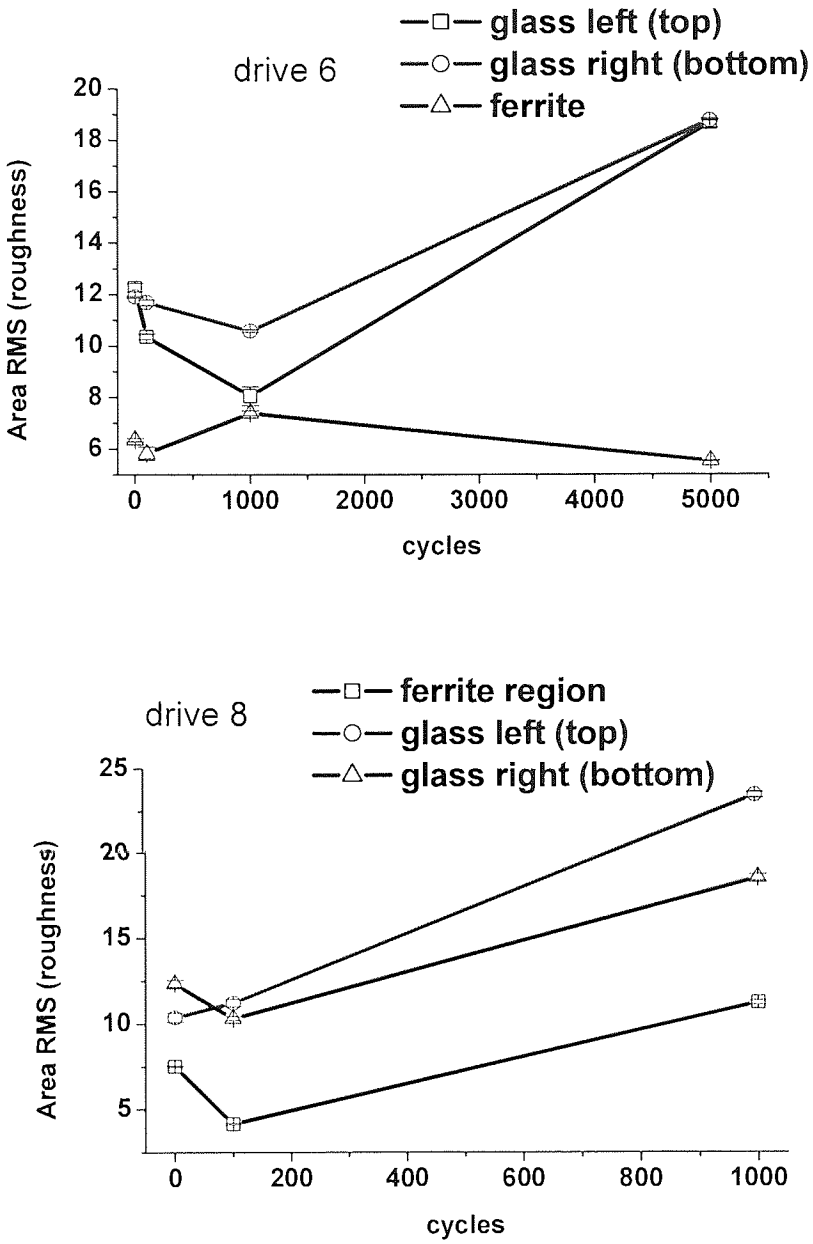

Figure 4-54 Area roughness of the drives 6 and 8 at 45°C/15%RH

At 5°C/80%RH the roughness of the head remained quite constant despite some stain patches appearing toward the end of the experiment. Once again, the ferrite proved to be the smoothest surface.

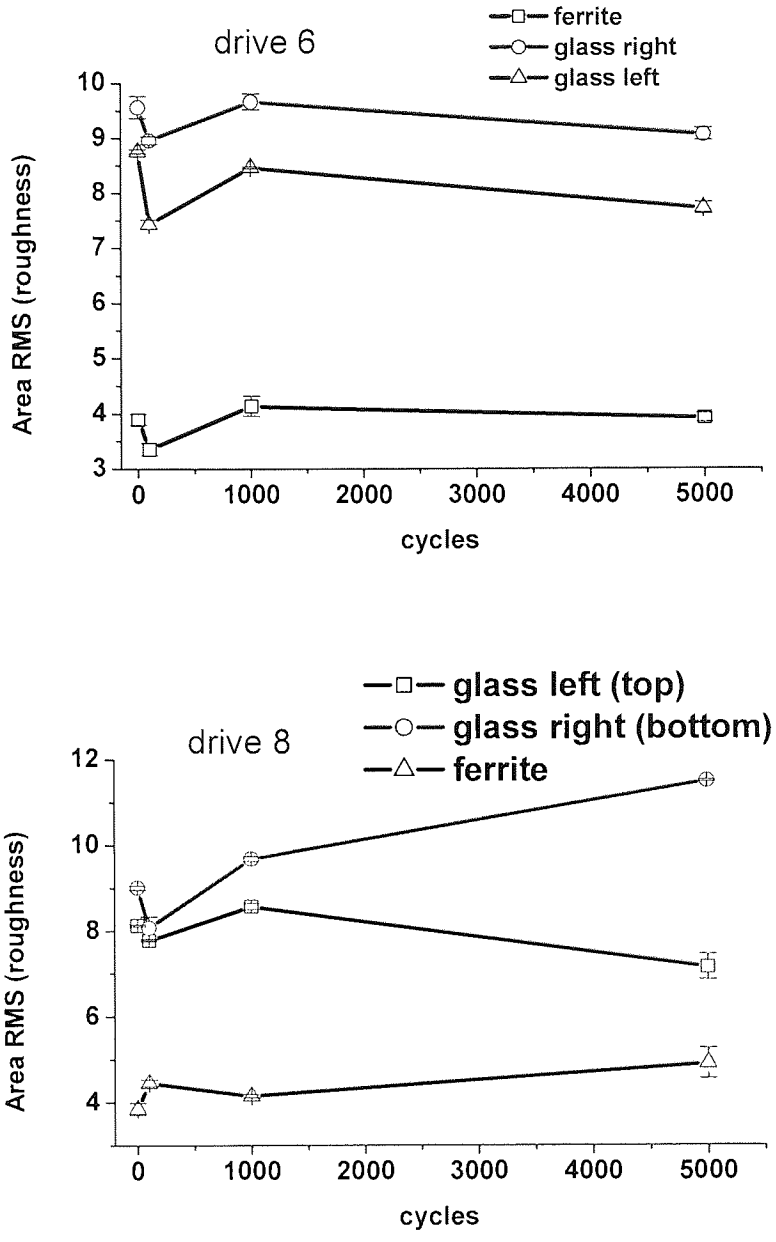

Figure 4-55 Area roughness of the drives 6 and 8 at 5°C/80%RH

The measurements of the roughness of the ferrite poles and the glass region at high humidity show that after an increase in the early stages of the experiment, an equilibrium level was attained.

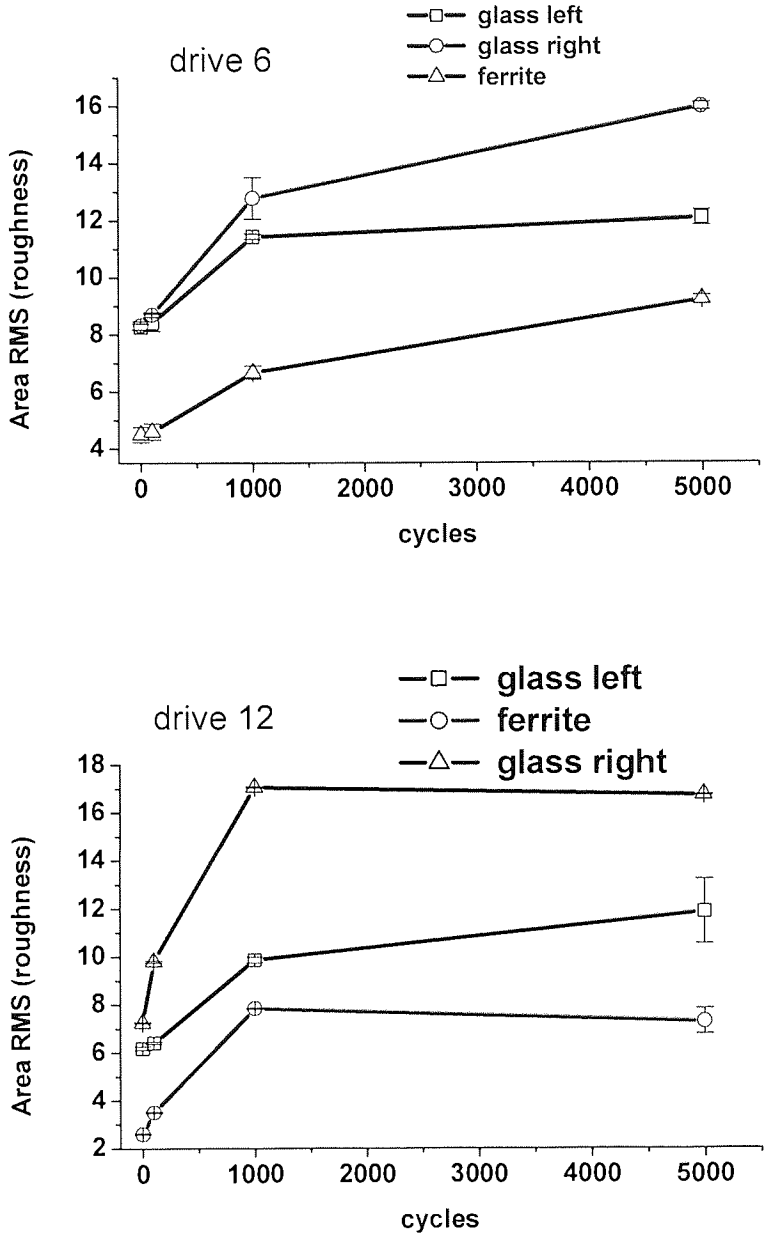

Figure 4-56 Area roughness variation at 40C/80%RH for drive 6 and 12 respectively

The surface roughness graphs show that after an early increase caused by the patchy pattern of the stains, the roughness of the heads remained almost constant. This phenomenon is probably due to the fact that stains tend to cover firstly the depressions where the friction forces are lower and then to develop to a continuous layer. After that, new patches of stain appeared and growed into a new fresh layer on top of the early one.

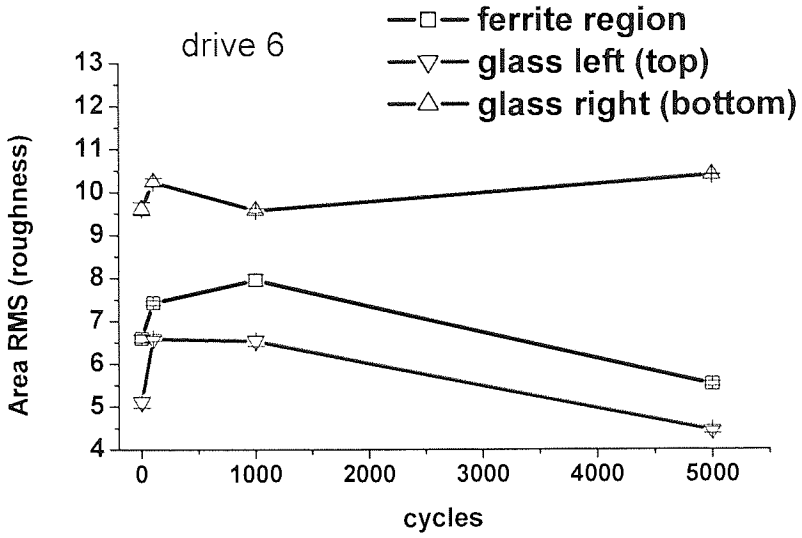

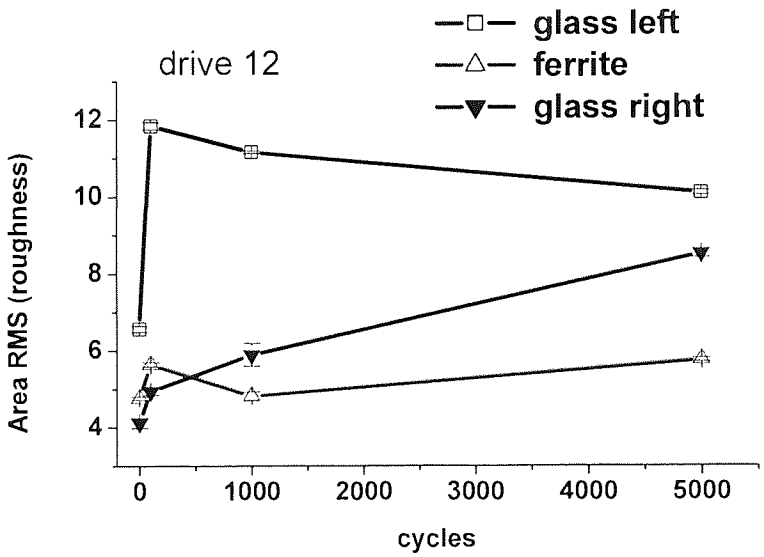

Figure 4-57 Area roughness variation at 10C/10%RH for drive 6 and 12 respectively

4.4 Auger analysis of the DDS-3 heads

Several heads were investigated: two heads that were reconditioned at 25°C/80%RH and three heads stained at 40°C/10%RH. On these heads, the left and right hand side glass regions were scanned as well as the ferrite poles. There is no difference in chemical composition between the two glass regions, the scans were used to compare

the reproducibility of the results obtained. The spectra acquired are shown in figures below.

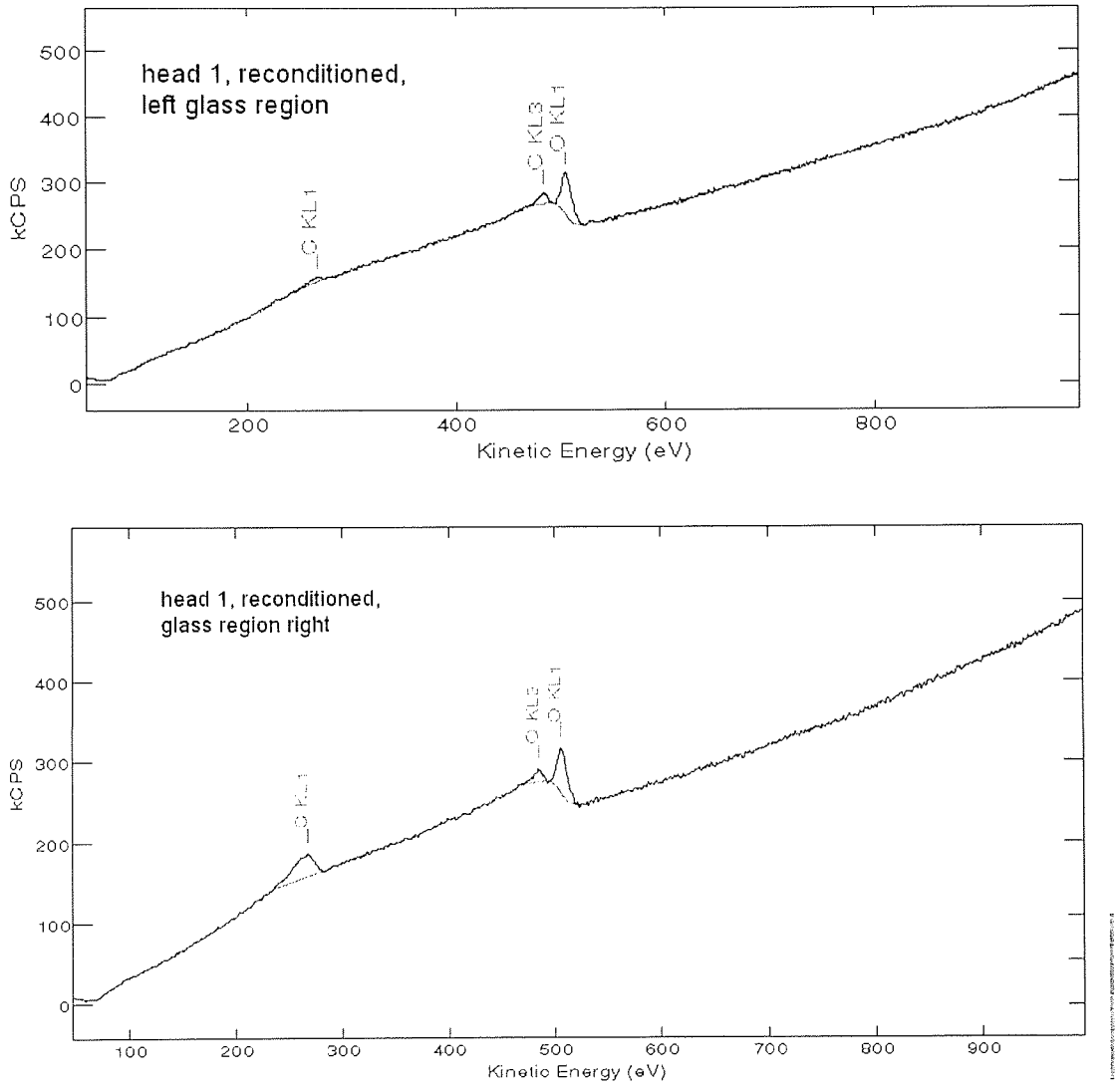

Figure 4-58 AES spectra of the glass regions of the head 1 (reconditioned)

Figure 4-58 shows the Auger spectra of the glass region of the head number 1 after reconditioning at 25°C/80%RH. As one can see, the spectra showed the presence of carbon and oxygen. The carbon is a very common contaminant in all Auger spectra. The oxygen peak is due to the glass composition (mainly SiO_2). Other elements such as silicon that are usually part of the glass' chemical composition did not appear probably due to the lower sensitivity of the method with respect to this element. The carbon peak was higher in the second spectrum since contamination was taking place even during the analysis despite etching the heads at the beginning of the experiment. In order to

have an idea of the rate of the contamination even under high vacuum conditions, it is worth probably saying that both spectra were acquired in less than 15 minutes.

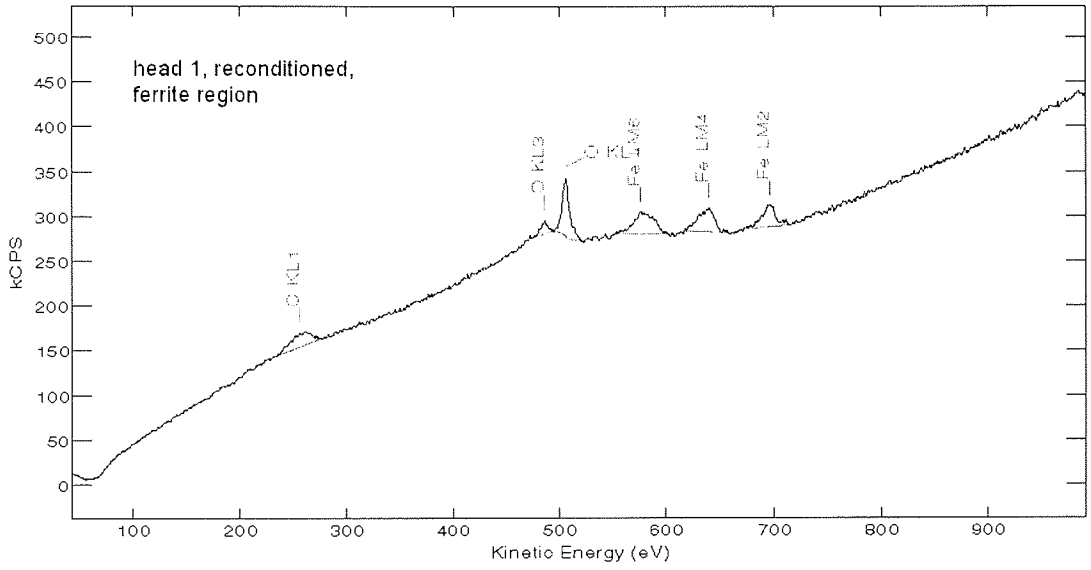

Figure 4-59 AES spectrum of the ferrite region of the head 1(reconditioned)

On the ferrite poles of the head number 1 the spectrum showed the presence of iron in addition to carbon and oxygen. The three peaks near the oxygen peak and towards higher kinetic energies are a very distinctive marker of iron presence. The iron signal was attributed to the iron from the ferrite of the magnetic poles of the head. (Fe_2O_3)

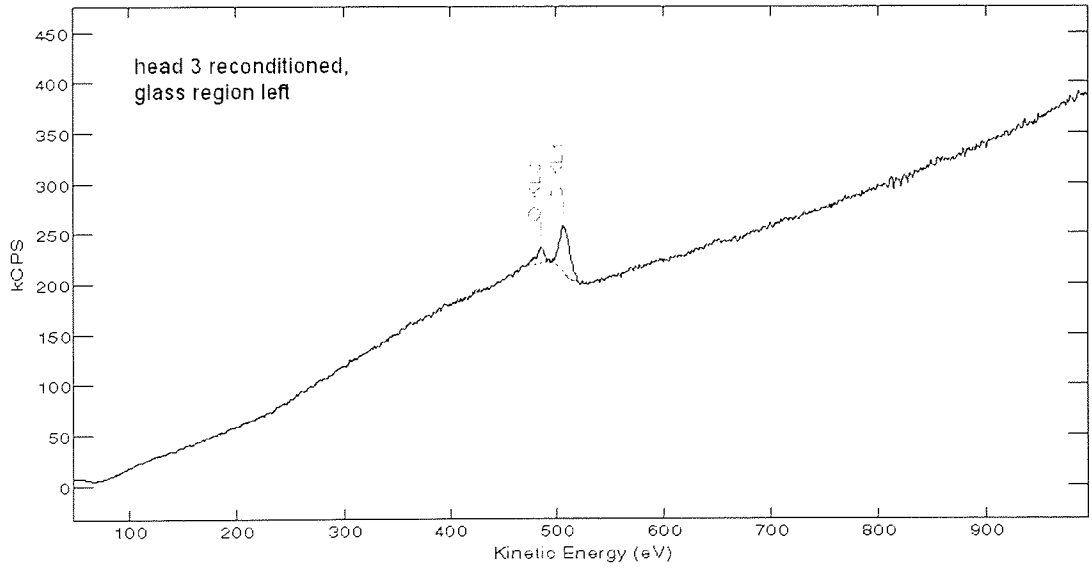

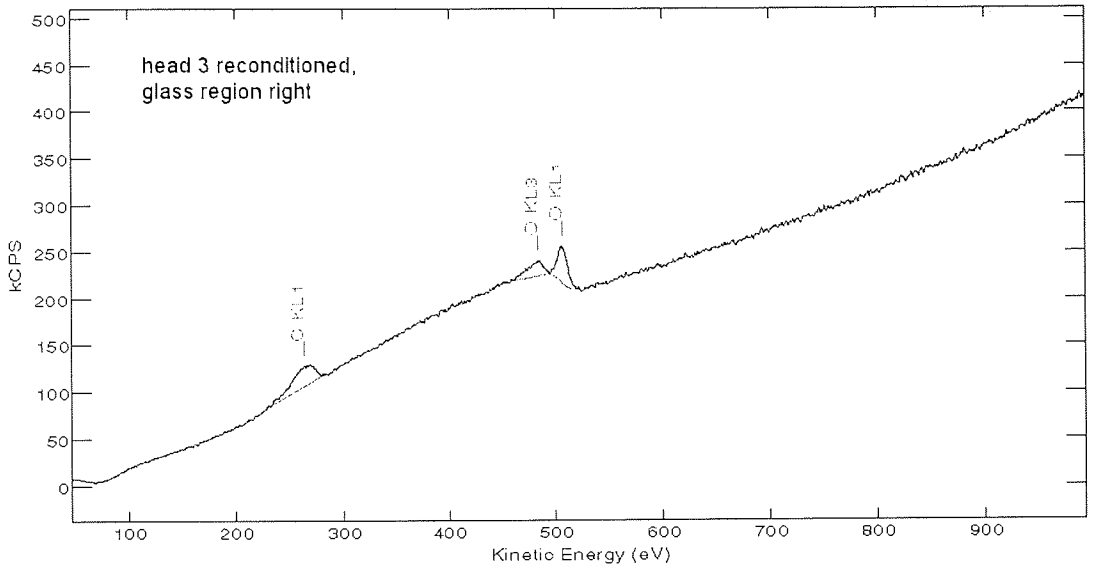

Figure 4-60 AES spectra of the glass regions of the head 3 (reconditioned)

The spectra taken on the glass region of the head number 3 were similar to those of the head number 1. The scan taken right after etching on the left hand side of the glass showed no carbon contamination. Definitely, the etching process had the same effectiveness on the right hand of the glass, but the spectra here was acquired a couple of minutes later. These scans proved once again how fast the surfaces get contaminated even under high vacuum conditions.

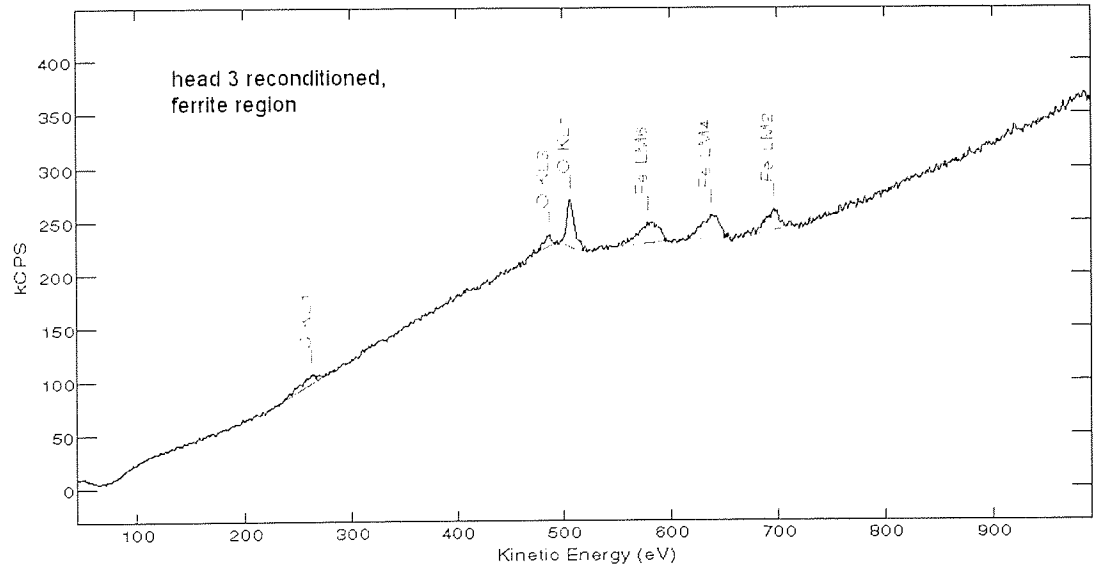

Figure 4-61 Ferrite region of the reconditioned head 3

The ferrite poles (Figure 4-61) showed again iron, oxygen and low amounts of carbon contamination.

The next three heads analysed were stained at high temperature and low humidity (40°C/10%RH). The spectra below show the analysis of the glass and the ferrite regions. The AFM scans performed earlier showed that at high temperatures and low humidity stains were building up on the ferrite poles but also on the glass region as well. (see Figure 4-41, Figure 4-42). The AES spectra taken on the glass region of the stained heads clearly showed the presence of iron in addition to carbon and oxygen seen before. The amount of iron present on the glass region varied but one has to bear in mind that stains have a patchy feature so some regions of the glass might have been stain free.

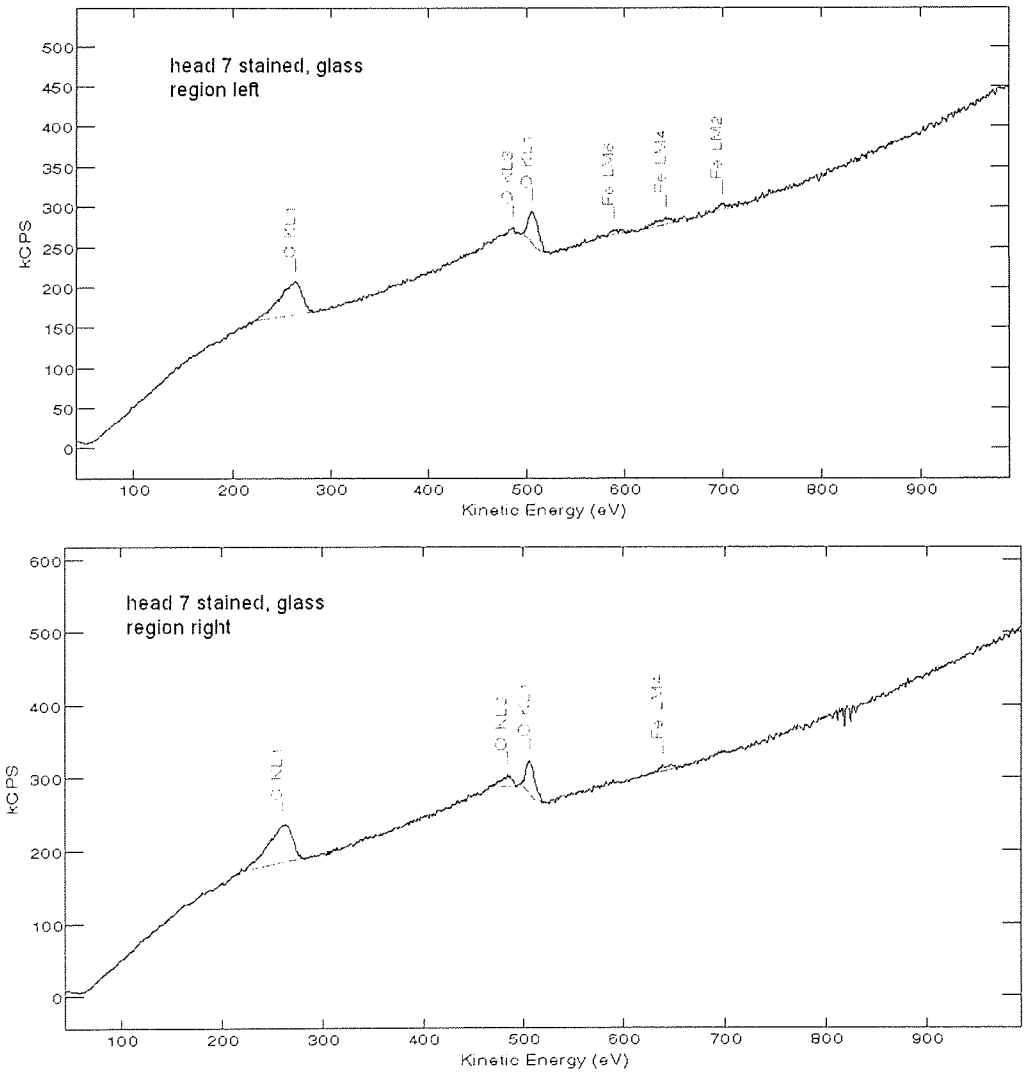

Figure 4-62 AES spectra of the glass regions of stained head 7

The spectra of the ferrite region of the stained heads did not show any other changes despite the efforts of finding other relevant elements such as chlorine.

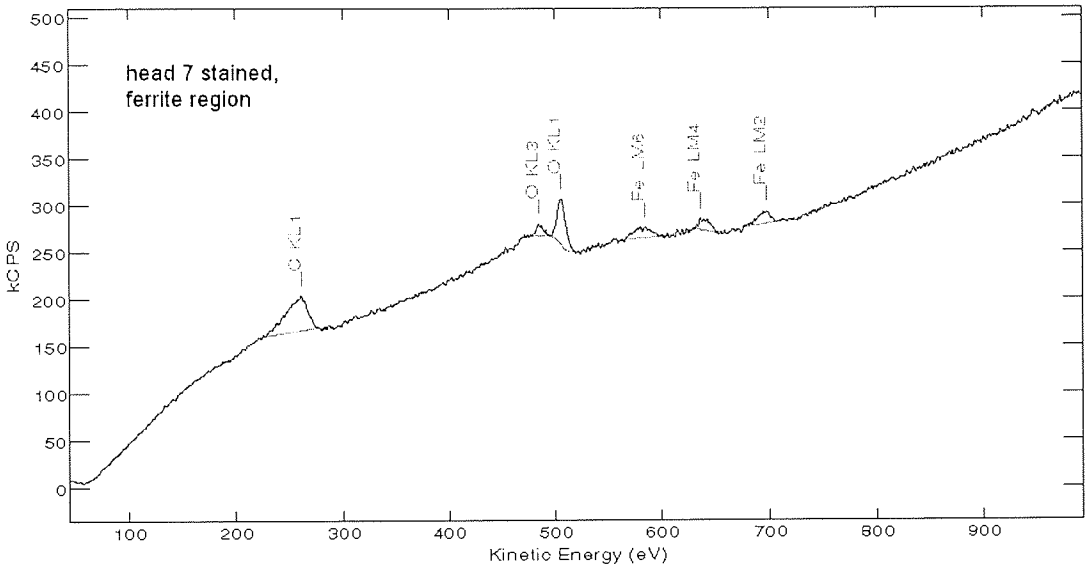

Figure 4-63 AES spectrum of the ferrite region of stained head 7

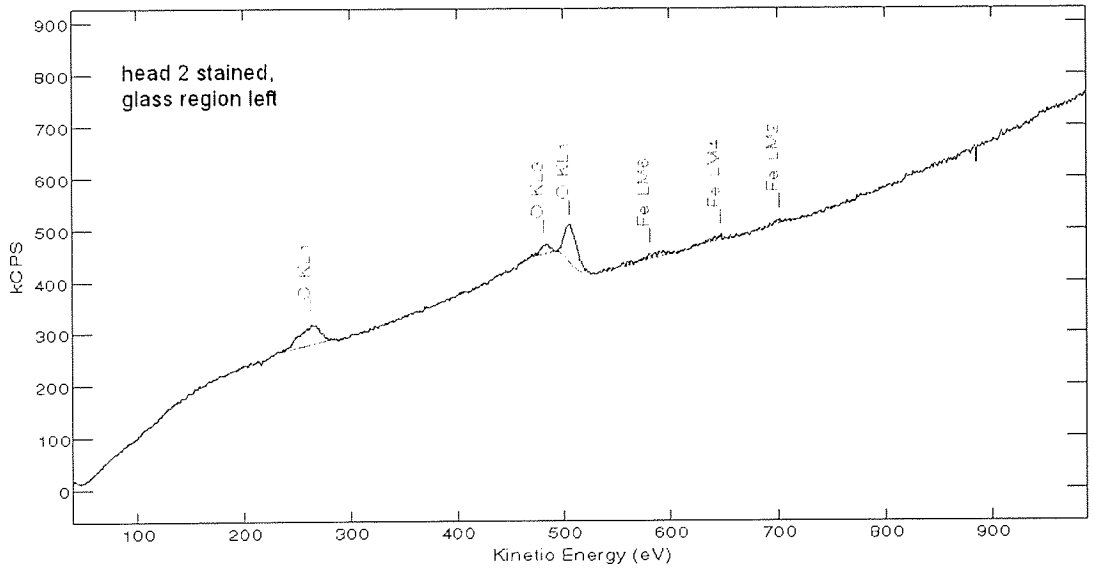

Figure 4-64 AES spectra of the glass region of the stained head 2

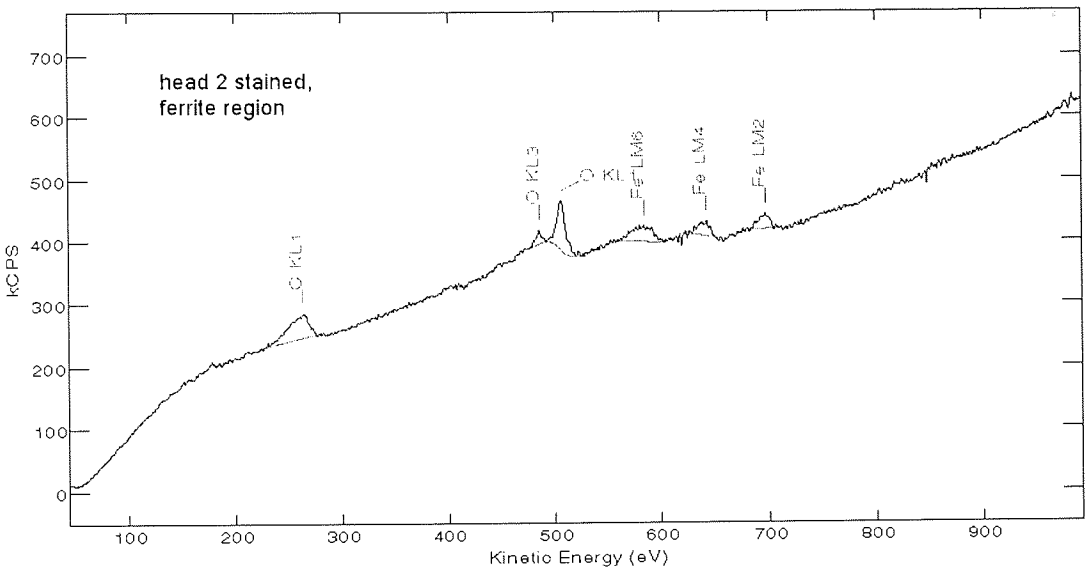

Figure 4-65 AES spectrum of the ferrite region of the stained head 2

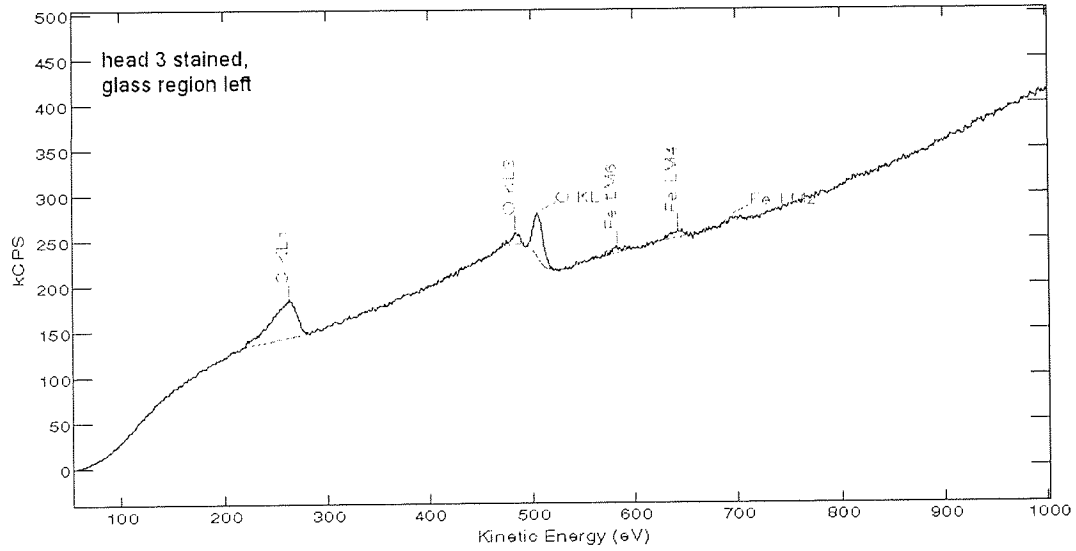

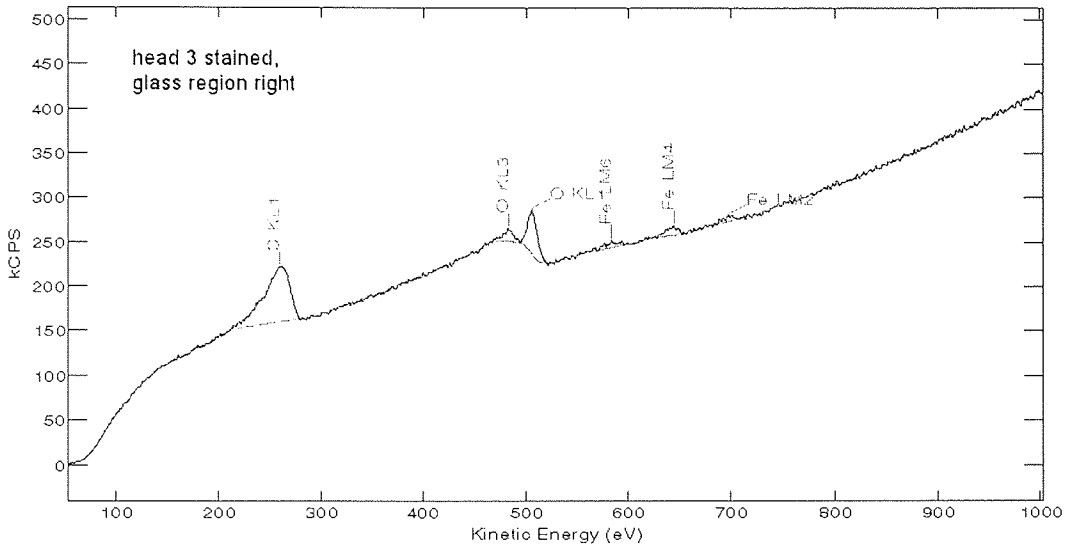

Figure 4-66 AES spectra of the glass region of the stained head 3

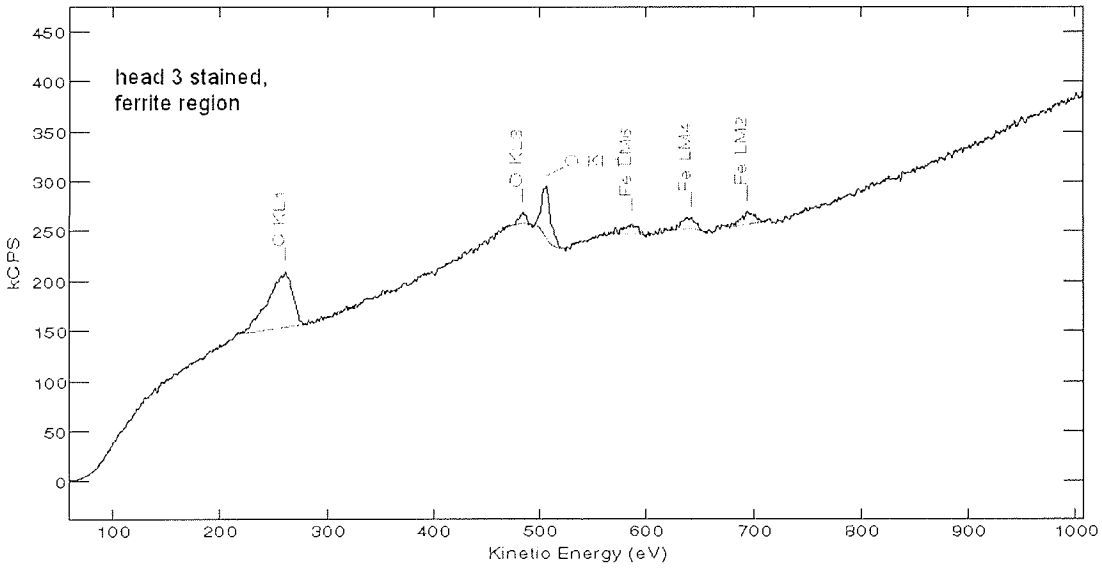

Figure 4-67 AES spectrum of the ferrite region of the stained head 3

As a conclusion, taking into account that AFM imaging revealed topography changes in this area during experiments, and given the spectra acquired on the glass region, it was reasonable to believe that iron is a component of the stains. Despite several other attempts, no other elements have been identified on the heads most probably due probably to the low sensitivity of the AES method.

4.5 XPS analysis of the tape

XPS has been performed on DDS2 tapes in order to identify the elements present in the tape formulation and to compare these results with those obtained by analysing the magnetic heads. The pictures below represent raw data extracted from an acquired spectrum of a DDS2 virgin tape. As one can see, the spectrum indicates the presence of C, O, N, Fe, Cl, Al and Si. The carbon and oxygen peaks are related to a multitude of compounds in tape formulation and by further analysing the carbon peak, more information about the binder and lubricant present in magnetic pigment can be found. The nitrogen and chlorine peaks are attributed to the binder polymers. The presence of magnetic acicular particles is denoted by the iron peak and finally aluminium and silicon are part of the head cleaning agents present in the magnetic coating. A quantification table of these elements is given in Table 4-5:

Element	Atomic Percentage
Carbon	54.2%
Oxygen	30.6%
Nitrogen	0.9%
Iron	4.0%
Chlorine	4.7%
Aluminium	4.0%
Silicon	2.5%

Table 4-5 XPS quantification table of the tape elements

It is interesting to remark, looking and the height of the peaks compared with noise level that the amount of nitrogen is not very high whereas the chlorine peak is very well defined. The quantification table also confirms lower amounts of nitrogen compared with the chlorine. The iron peak is generated by the acicular magnetic particles within the magnetic pigment and the aluminium and silicon peaks are believed to be due to head-cleaning agent, which is probably a mixture of Al_2O_3 and SiO_2.

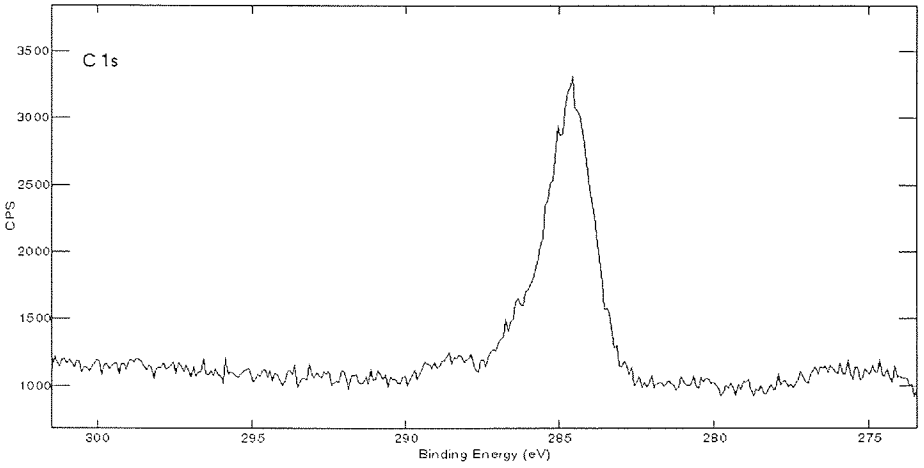
C 1s
CPS
3500
3000
2500
2000
1500
1000
300
295
290
285
280
275
Binding Energy (eV)

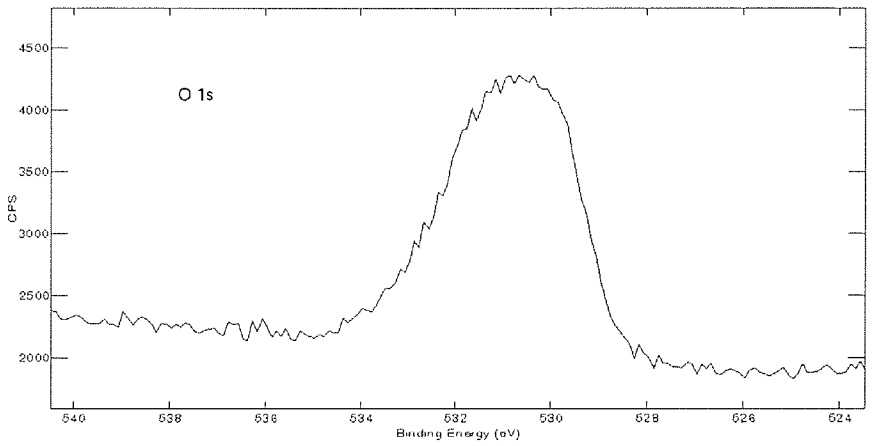
O 1s
CPS
4500
4000
3500
3000
2500
2000
540
538
536
534
532
530
528
526
524
Binding Energy (eV)

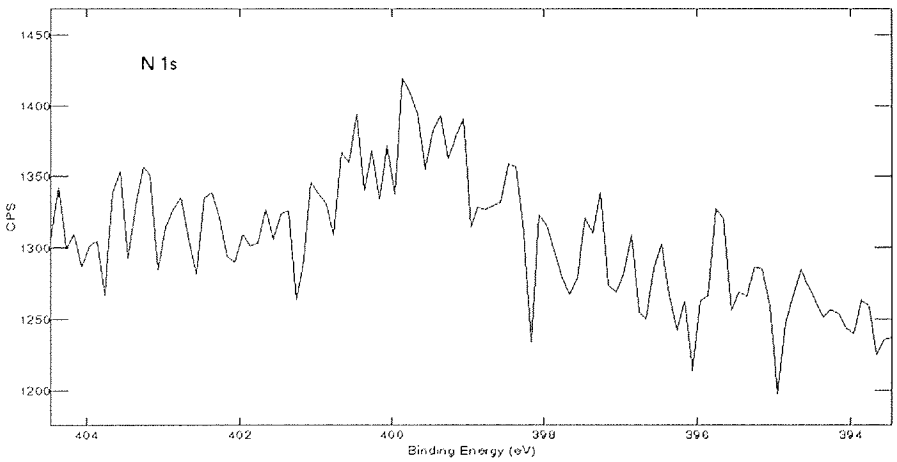
N 1s
CPS
1450
1400
1350
1300
1250
1200
404
402
400
398
396
394
Binding Energy (eV)

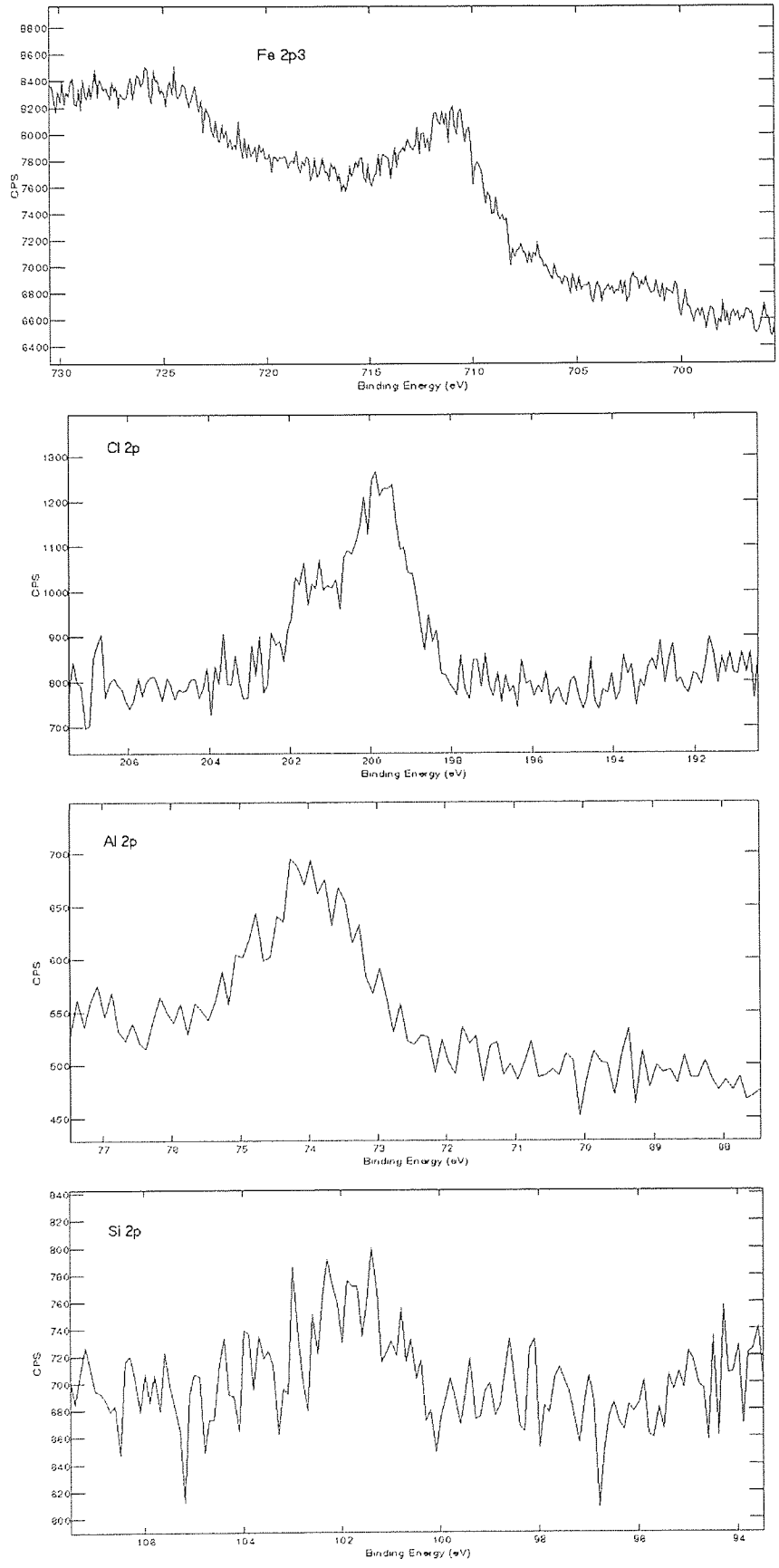

Figure 4-68 XPS spectrum of a DDS2 virgin tape showing the presence of C, O, N, Fe, Cl, Al and Si respectively

4.6 SIMS analysis

4.6.1 The tape

SIMS experiments have been also performed on the heads and for comparison, on pseudo virgin tapes.

For the beginning, spectra of the DDS2 tape together with a zoom on the region towards higher masses is presented. The zoomed area clearly shows, apart from iron presence at 56 and 57amu, the characteristic pattern of organic compounds around 64amu and then around 80amu, 90amu, 100amu corresponding to increased number of carbon atoms within the chain and hydrogen atoms. The pattern is generated by the presence of binder and lubricant within the magnetic coating.

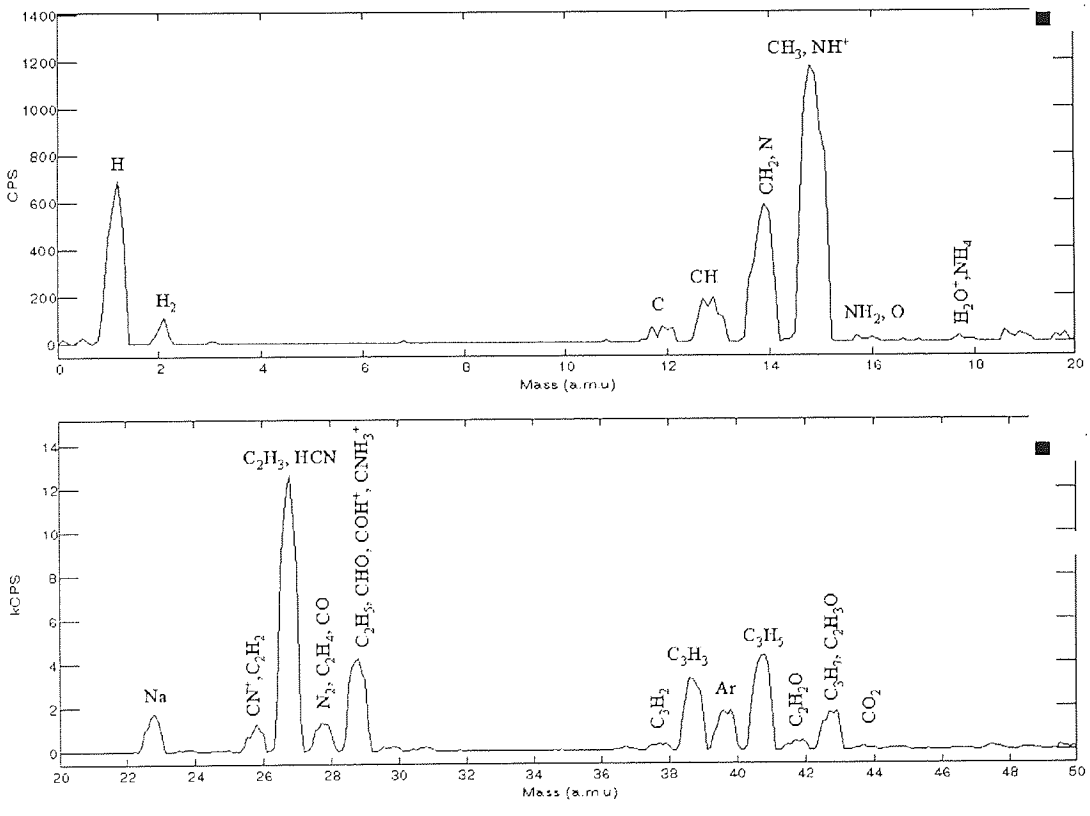

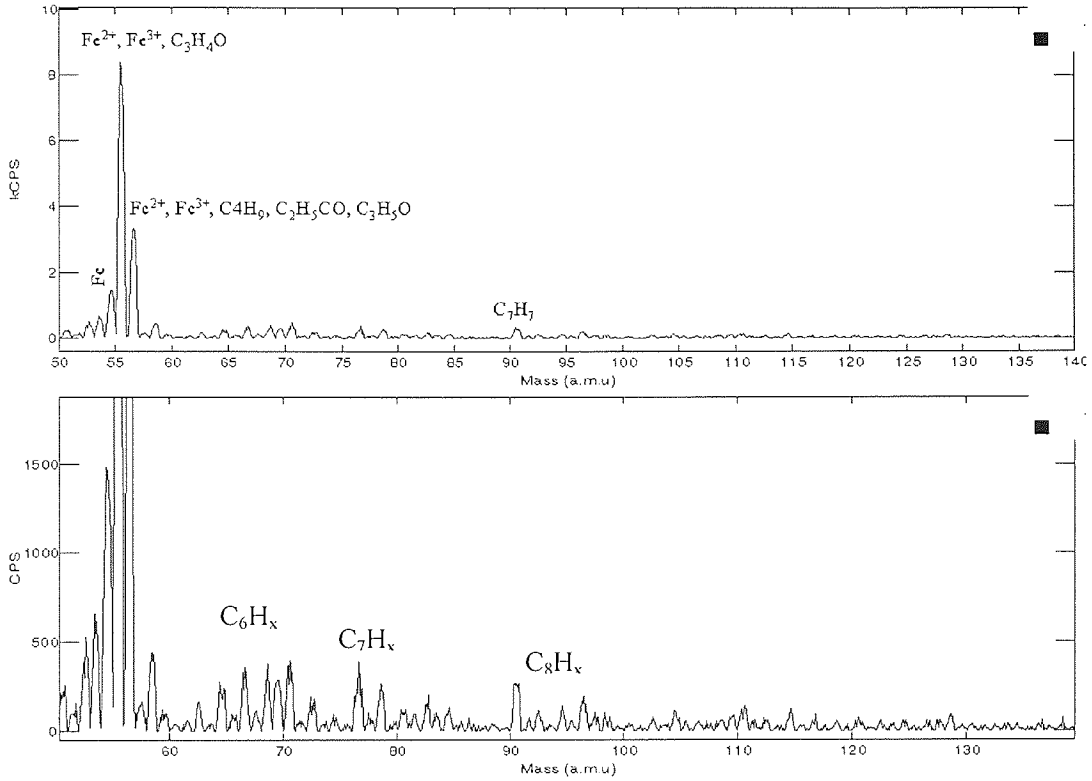

Figure 4-69 SIMS positive spectrum of the tape

On the other hand, the negative spectrum of the tape revealed the presence of chlorine a good indicator of the binder presence.

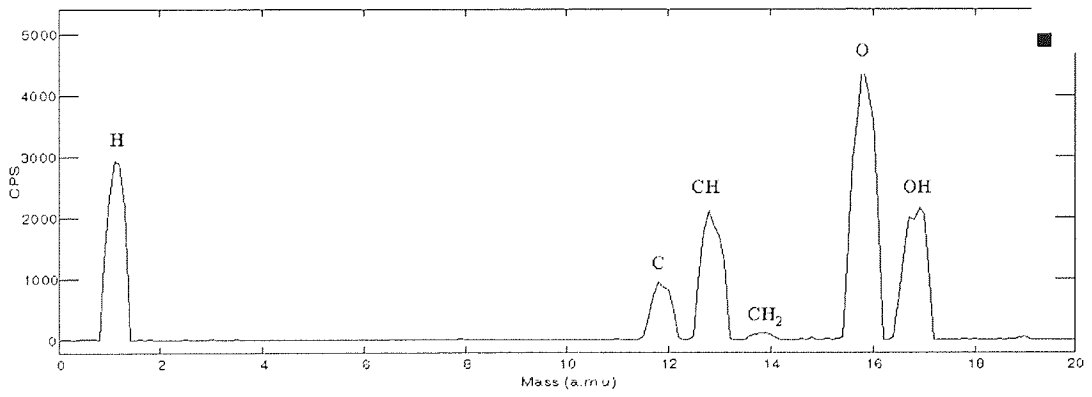

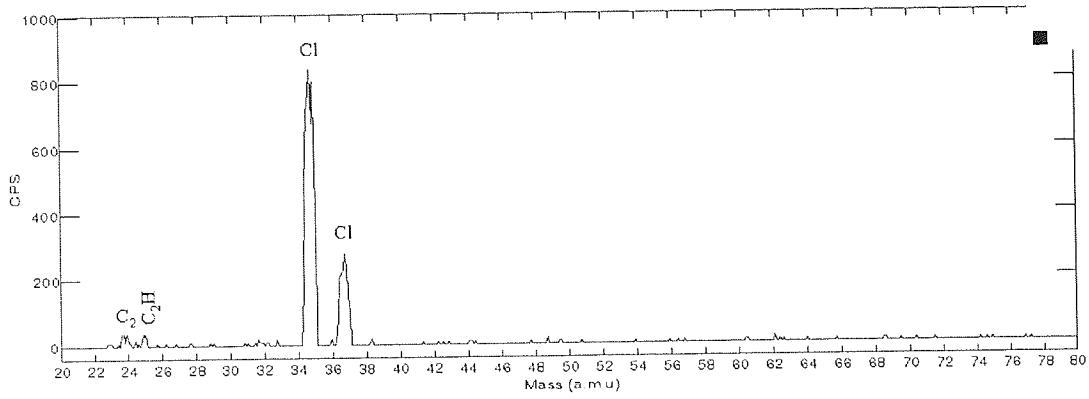

Figure 4-70 The negative spectrum of the tape

4.6.2 The stained heads

SIMS analysis of the stained head in the glass region has given an indication of the presence of binder. Since PVC (polyvinyl chloride) copolymer is very often used in binder formulation, the chlorine is usually a good marker of it. In addition, other organic fragments, in particular those involving CN (cyano) group were discovered. These fragments may indicate the presence of isocyanate, another substance used during the fabrication of the binder for DDS2 tapes. The spectrum did reveal low amounts of iron but signal generated by it level is very low compared with the signal generated by the silicon or gallium.

The results gave good evidence that adhesive debris consists also in polymeric binder.

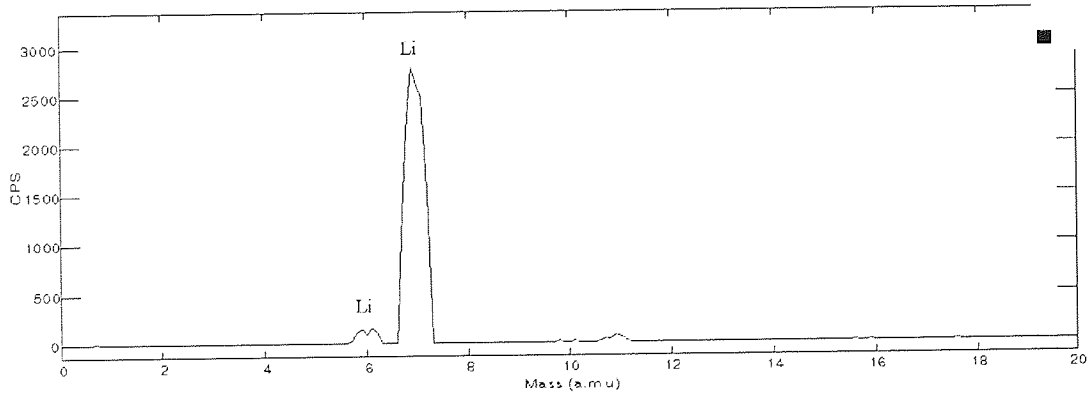

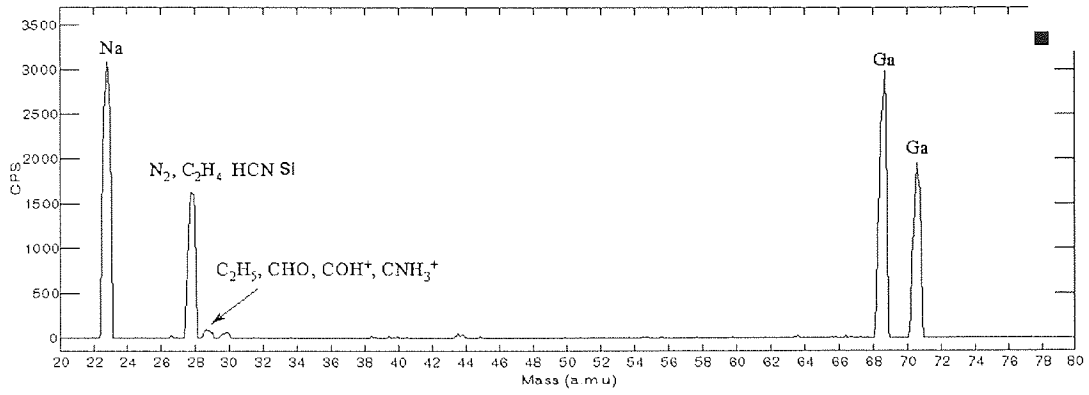

Figure 4-71 SIMS positive spectrum of the head 1 (glass region)

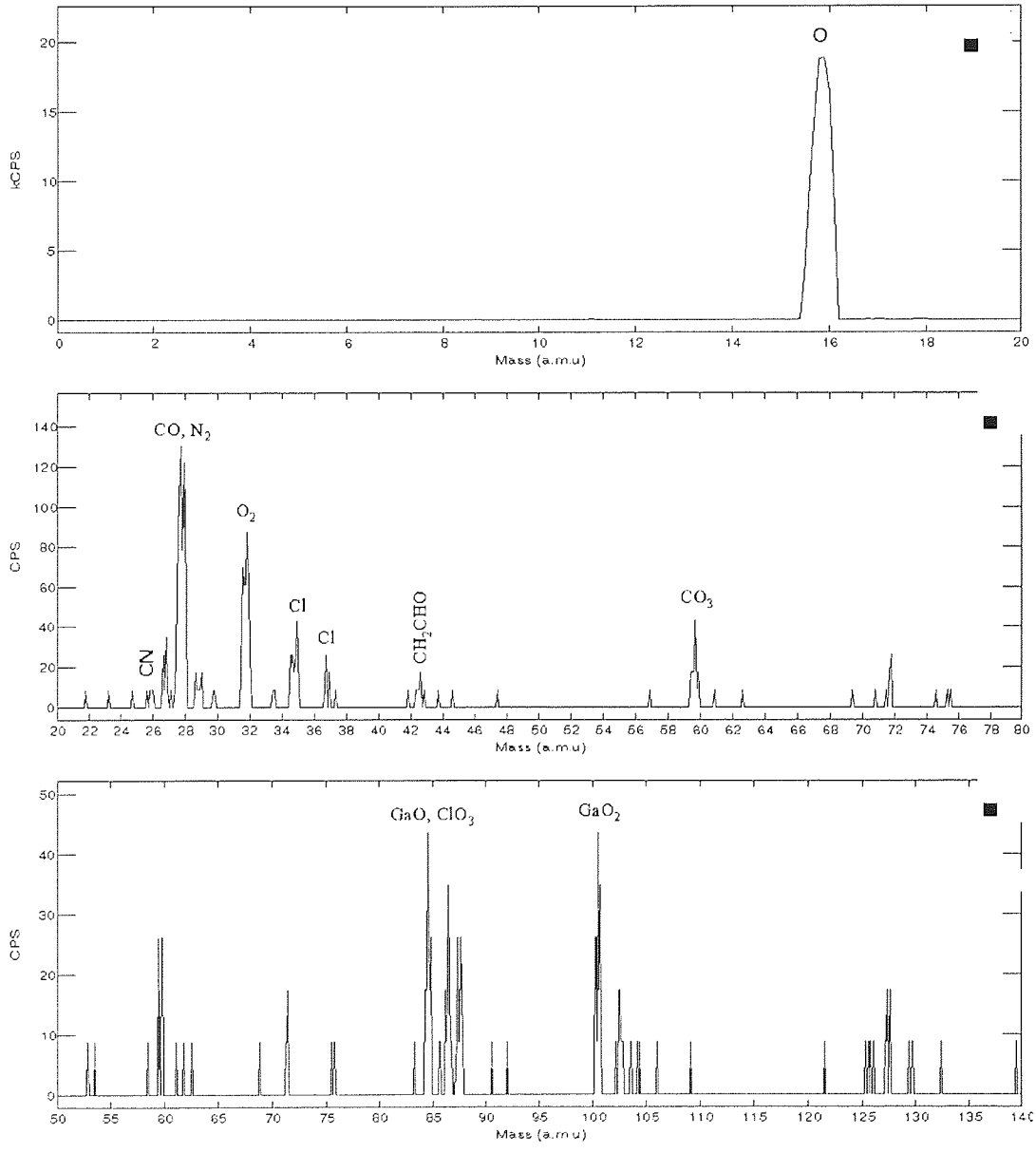

Figure 4-72 SIMS negative spectrum of the head 1 (glass region)

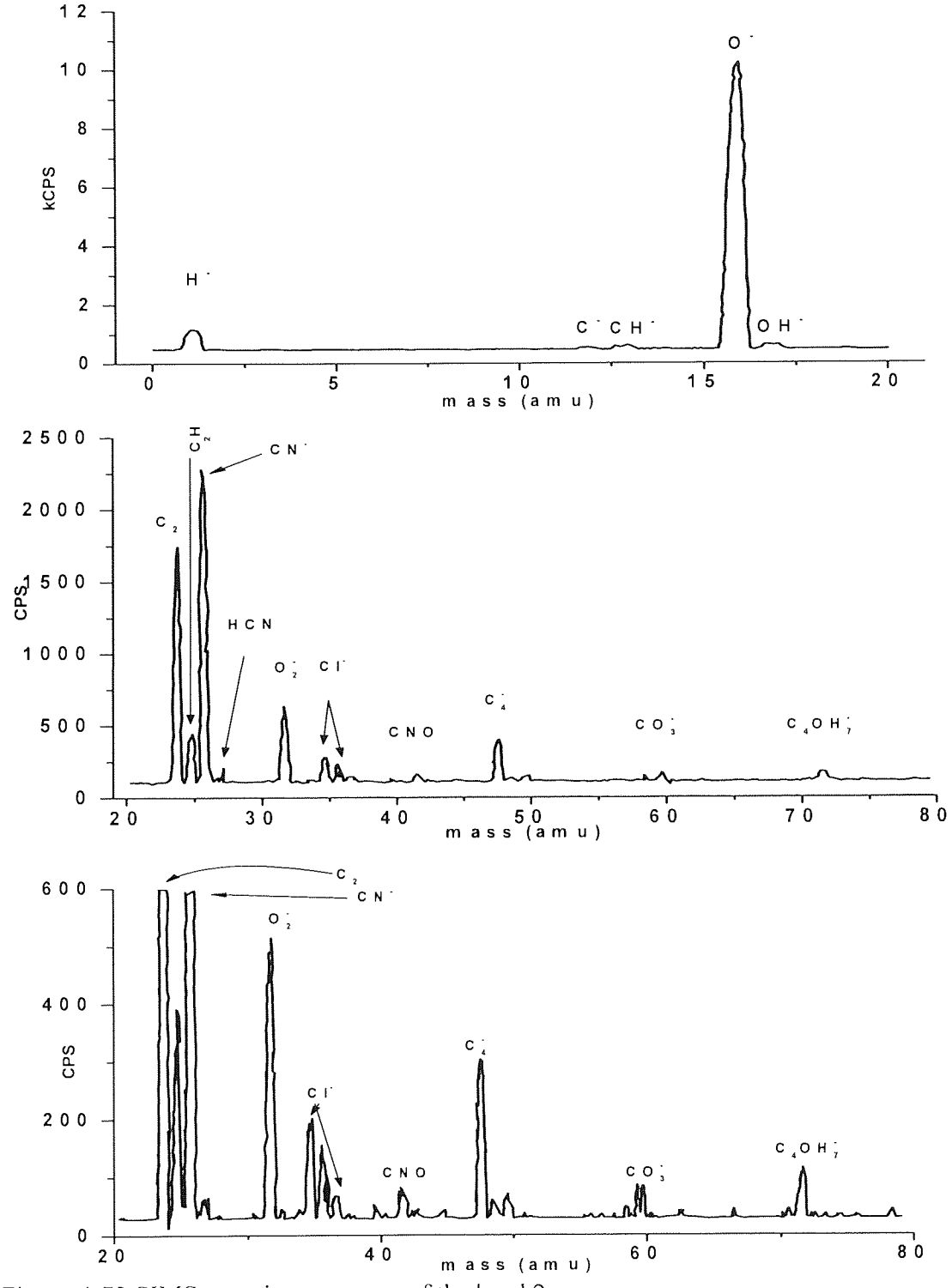

Figure 4-73 SIMS negative spectrum of the head 2

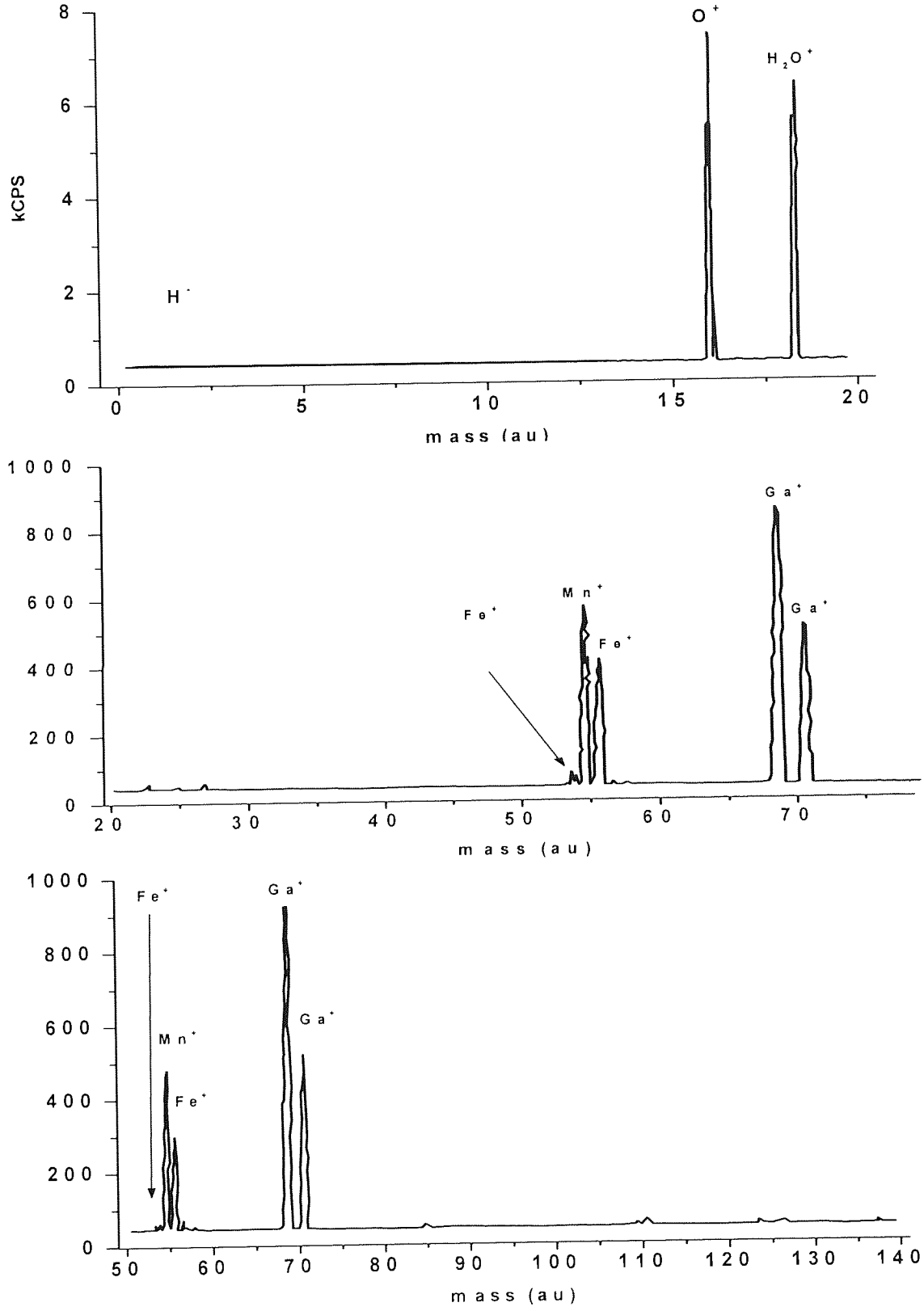

Figure 4-74 SIMS positive spectrum of the head 2

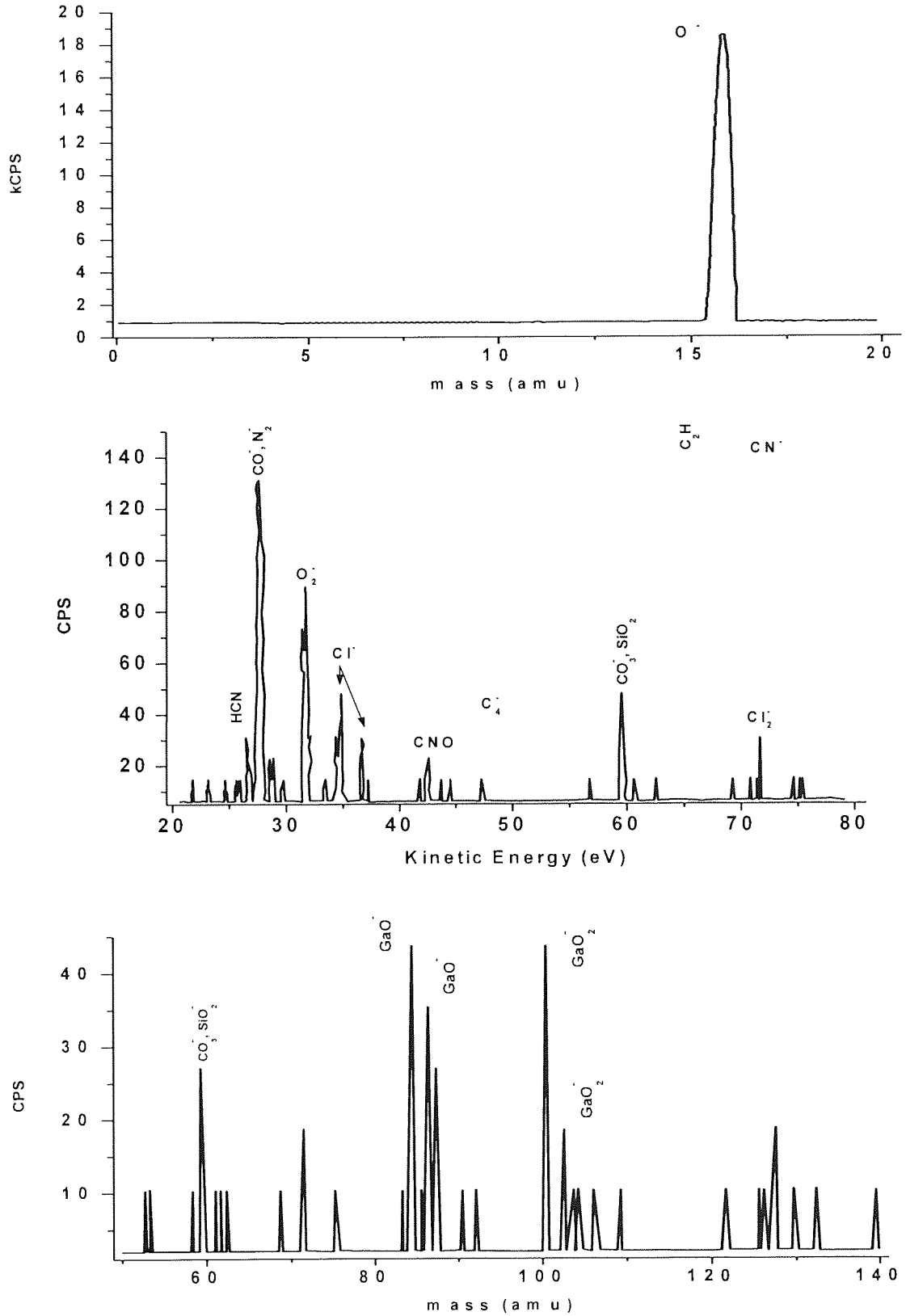

Figure 4-75 SIMS negative spectrum of the head 3

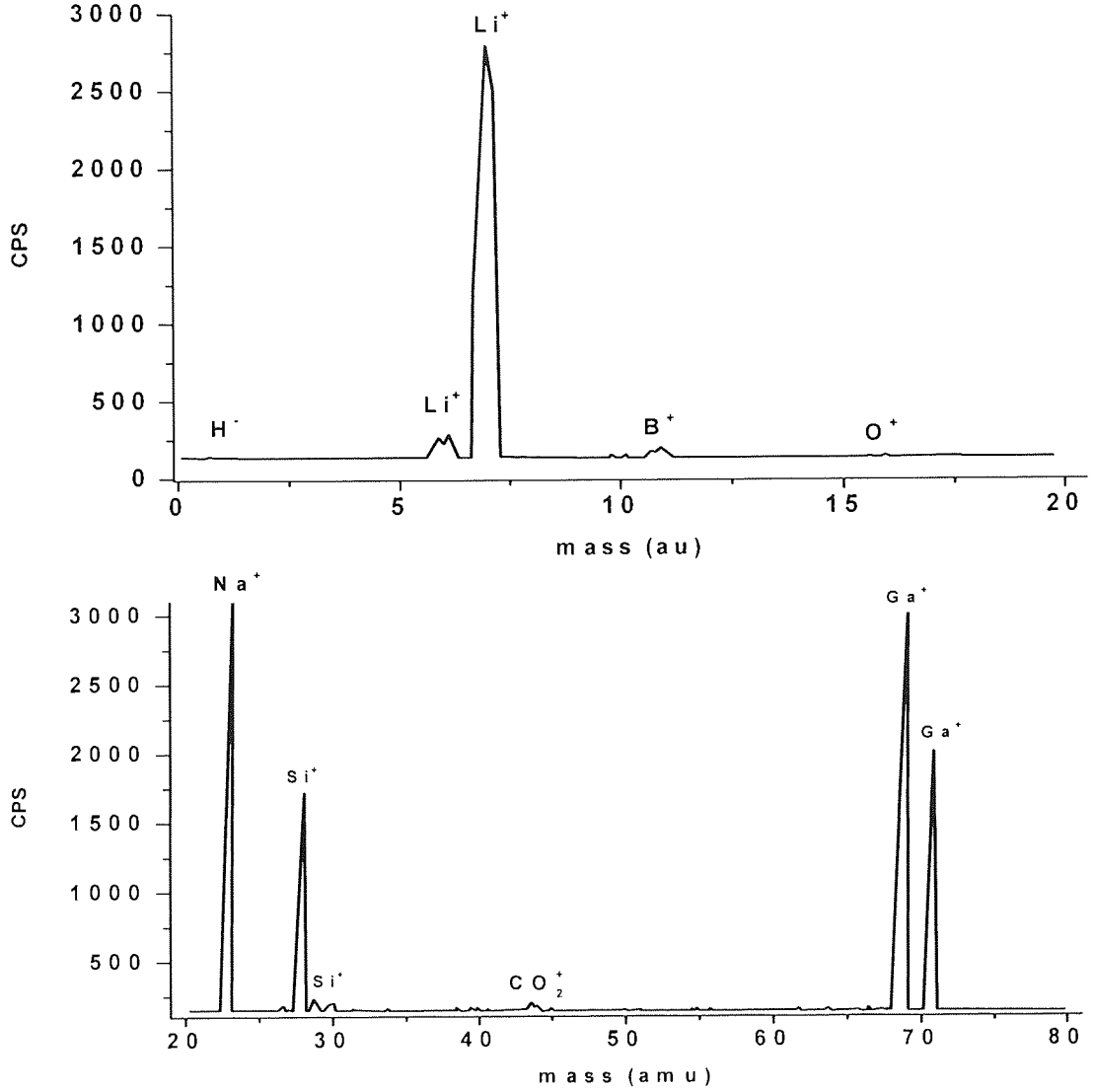

Figure 4-76 SIMS positive spectrum of the head 3

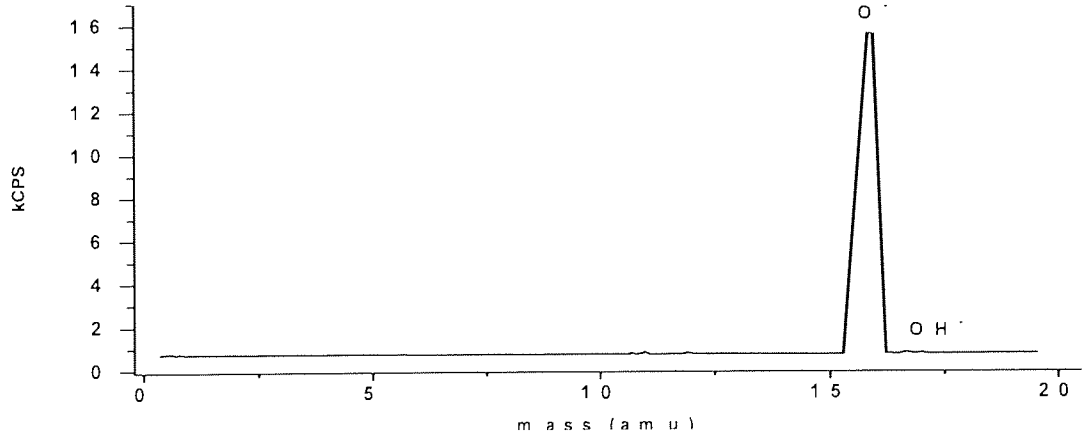

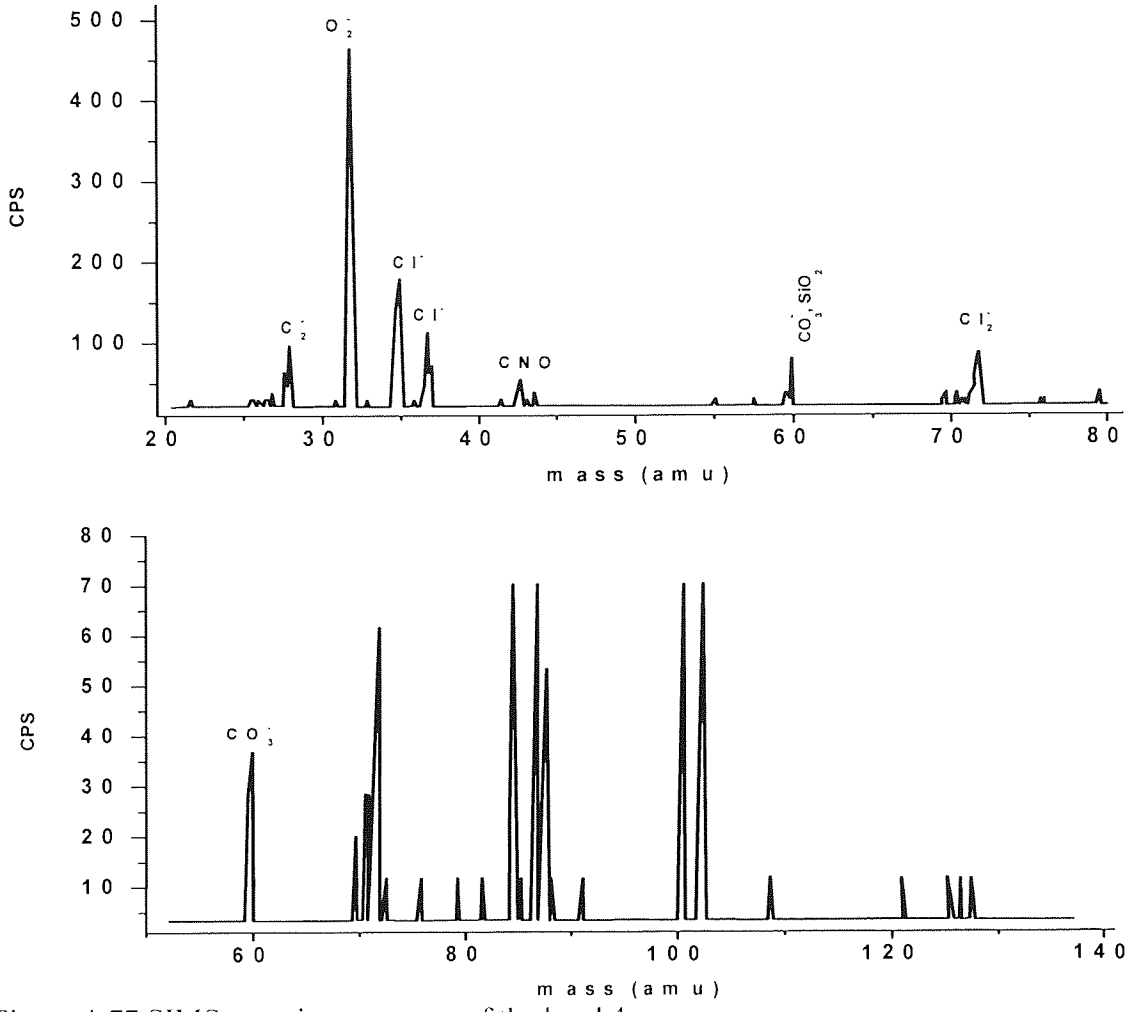

Figure 4-77 SIMS negative spectrum of the head 4

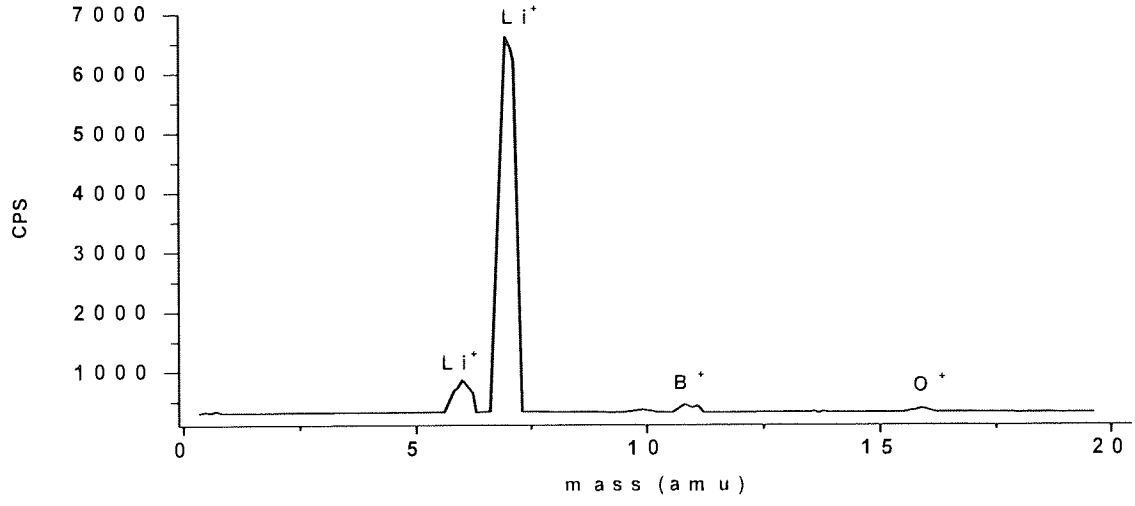

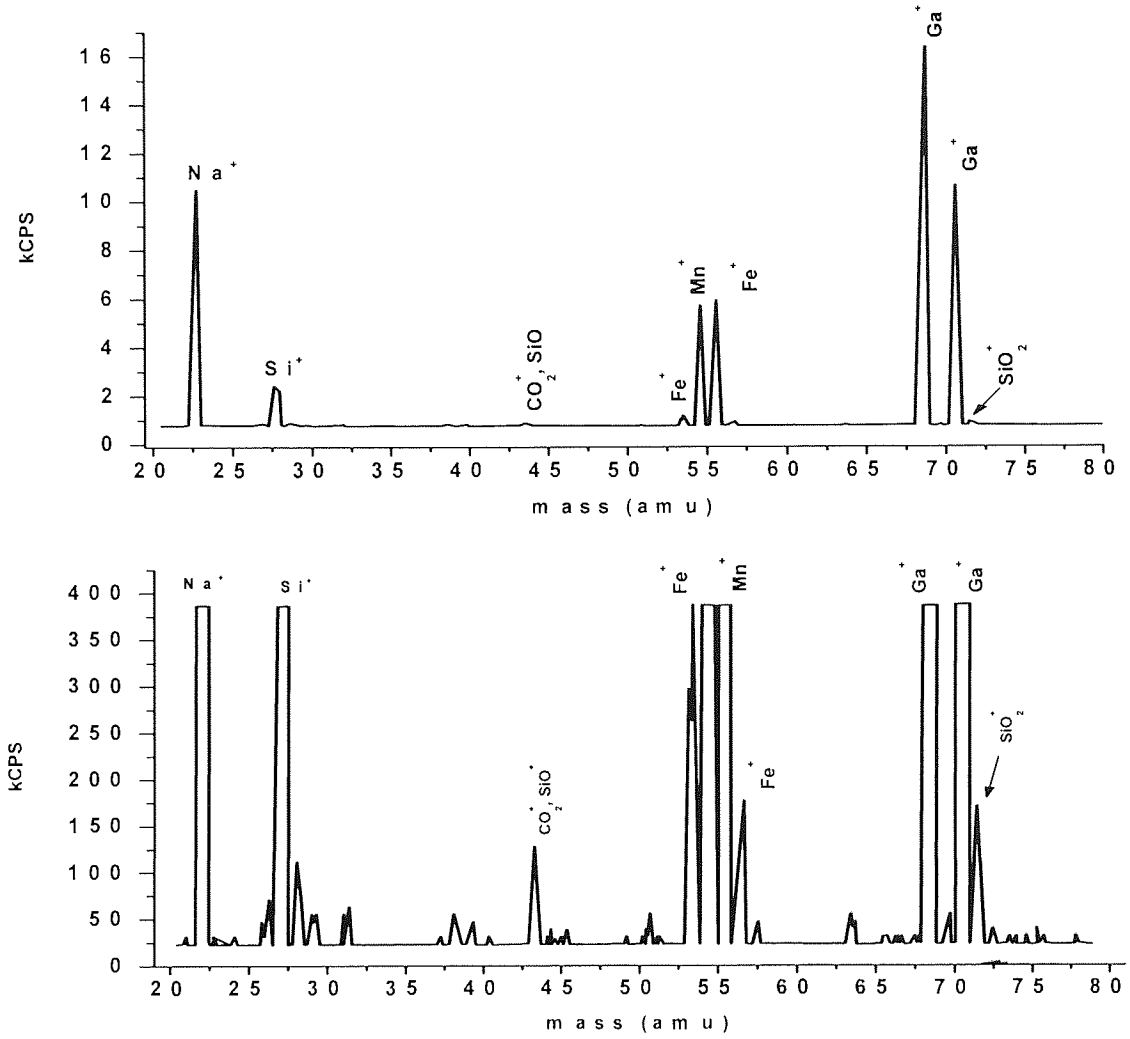

Figure 4-78 SIMS positive spectrum of the head 4

4.7 Experiments with the ferrite samples

4.7.1 Ferrite behaviour at high humidity

In order to assess the changes that occurred in the ferrite's chemical state after exposure to high humidities, the oxygen peak quantification has been used. The graphs below represent the changes, which occurred in oxygen's peak shape. The synthesis was made using three peaks corresponding to the oxygen bonded to the metal (M-O) at 529.5eV, the oxygen forming the iron oxyhydroxide at 531.0 eV and to the oxygen in water at 532.4eV. Under moderate humidity, the amount of iron oxyhydroxide and

physically bonded water was found similar to the sample kept for comparison. The shape of the oxygen peak towards higher binding energies remained the same. However, a dramatic change occurred when the ferrite was exposed to 100%RH due to the physically and chemically adsorbed water as one can see from Figure 4-81. The hump increased in intensity having similar intensity to the main oxygen peak. Taking into account that the relative intensity of the signal coming from the physico-chemical adsorbed water compared with the height of the O 1s peak is increasing at higher take-off angles (Figure 4-82), the conclusion is that the signal is coming from the surface of the ferrite and not from the bulk material.

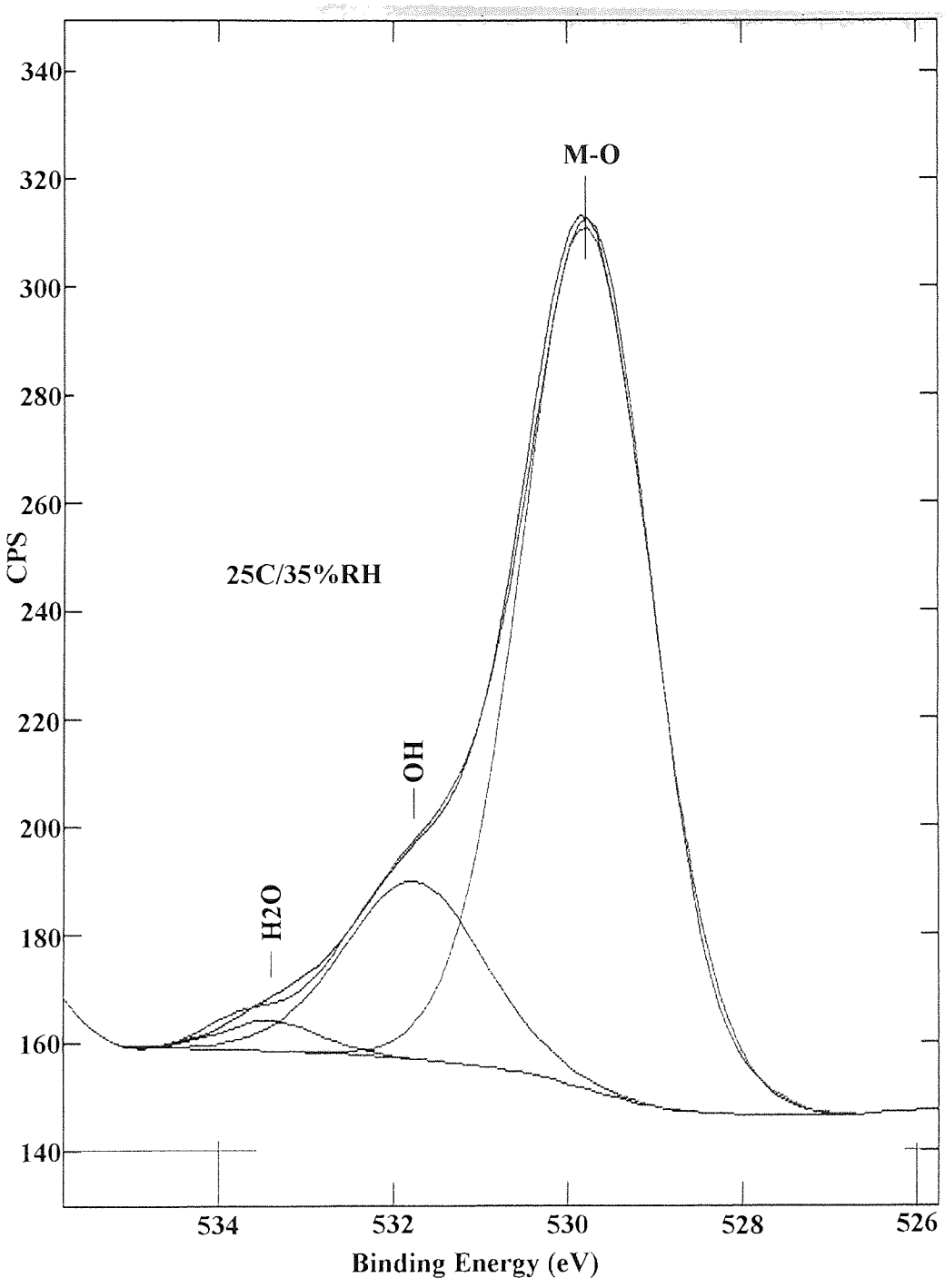

Figure 4-79 The O1s peak of the ferrite under 25°C/35%RH and 0° TOA

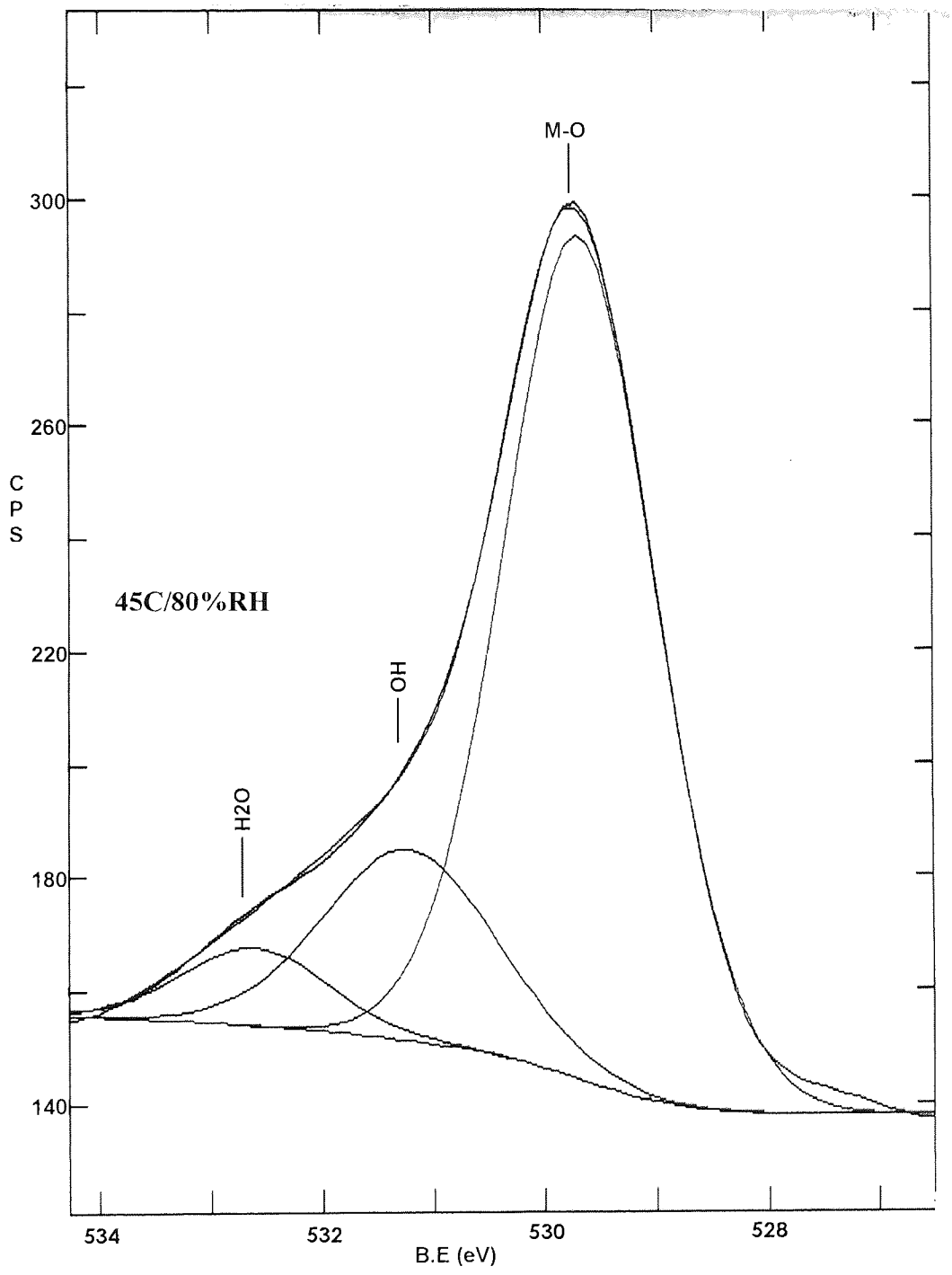

Figure 4-80 The O1s peak of the ferrite under 45°C/80%RH

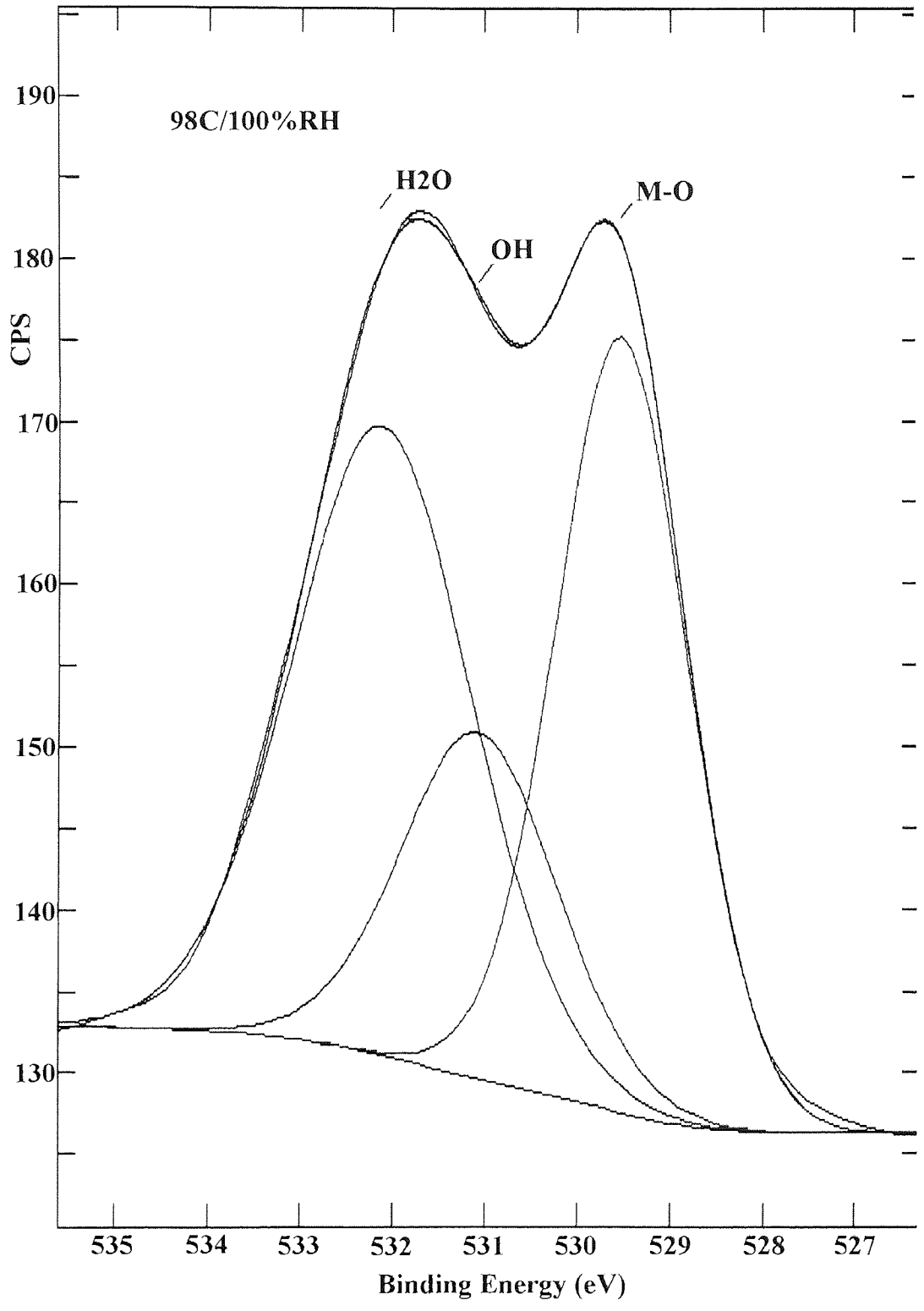

Figure 4-81 The O1s peak of the ferrite under 98°C/100%RH (0°TOA scan)

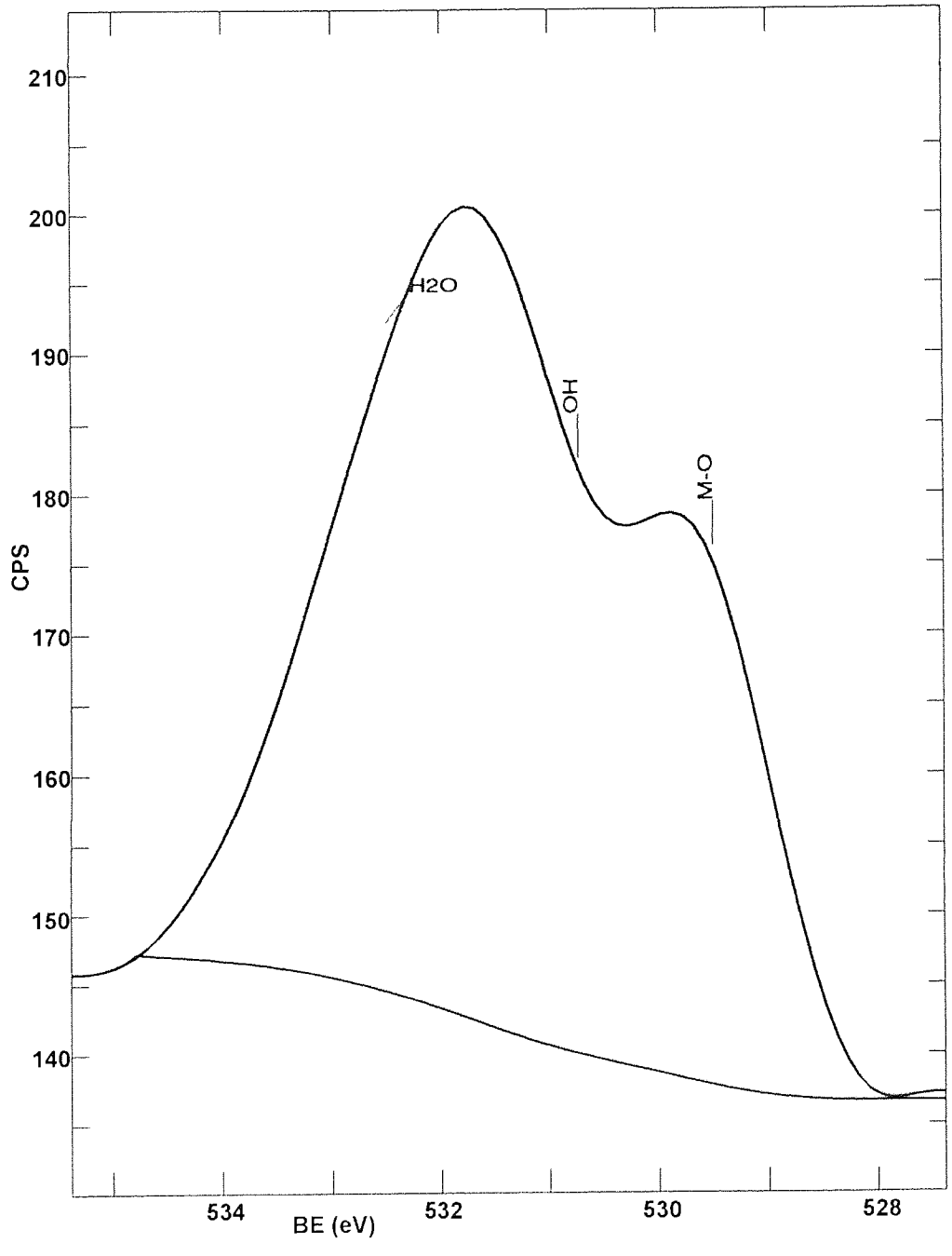

Figure 4-82 The same peak but at 60° TOA

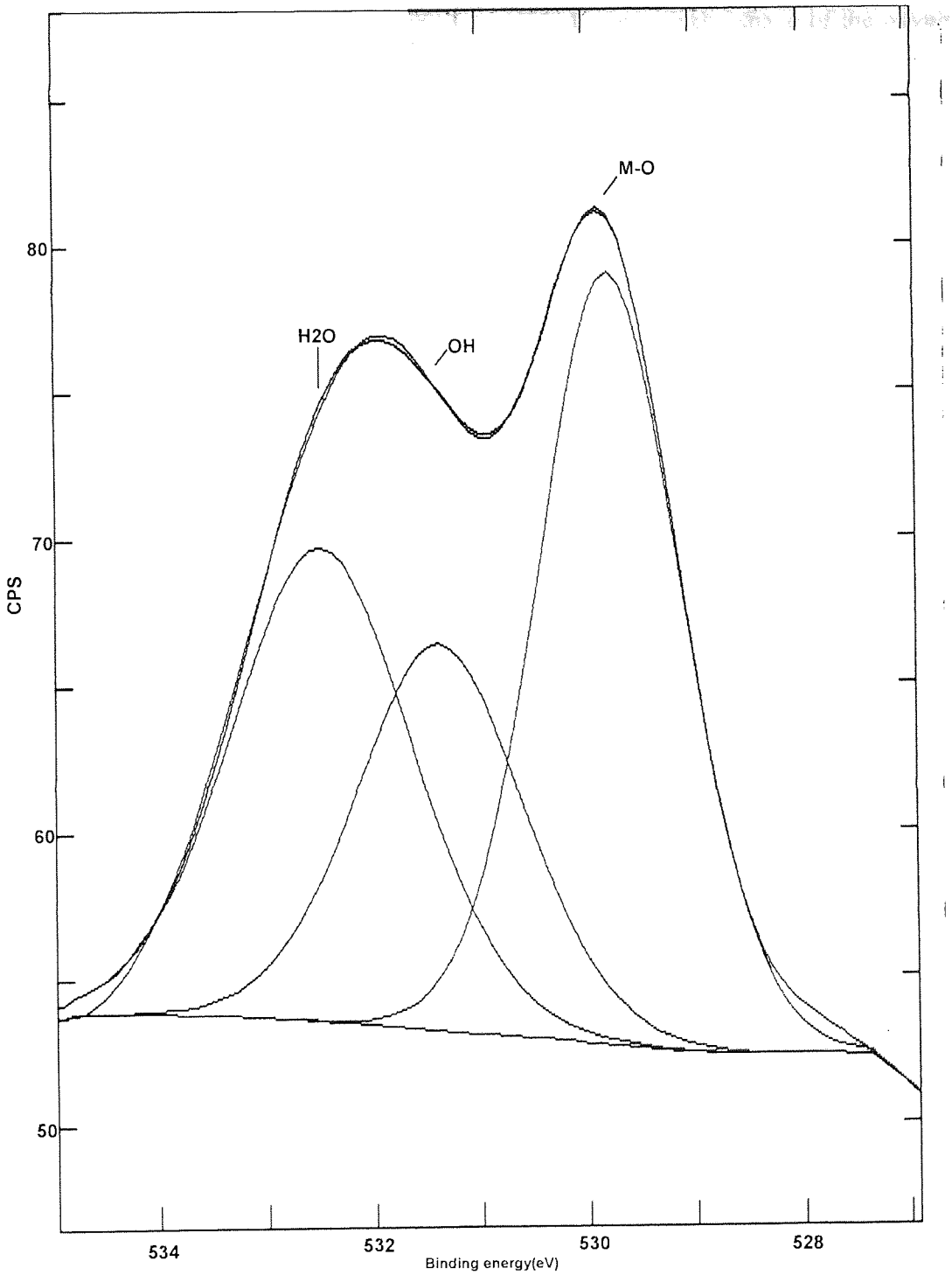

Figure 4-83 The O1s peak after exposing the ferrite to high vacuum

Further series of experiments were designed to see whether the water present at the surface of the ferrite was bonded chemically or physically to the ferrite. Thus, the sample subjected to 98°C/100%RH was left under high vacuum conditions for 12 hours.

Since no change has been observed neither in pressure nor in the shape of the oxygen peak, it was assumed that water has already formed strong bonds with the ferrite surface. Finally, the ferrite was baked at 120°C for about two days and then again subjected to XPS analysis. This temperature was chosen since it is above water's boiling point but below the decomposing temperature of the iron oxyhydroxide. As one can see from the spectra below after the baking process, although the hump of the oxygen peak decreased, it still remained significantly more pronounced compared with that at the beginning of the experiments (see Figure 4-84 and Figure 4-79). Moreover, analysing the sample at higher take-off angles one can see that the newly formed substances are on the surface of the ferrite (Figure 4-84 and Figure 4-85). If water present at the surface had been simply physically bonded, it would have disappeared after prolonged exposure at high vacuum and after baking. Despite a change in the shape of the oxygen peak, the hump corresponding to the oxygen present in water was still present. Given these circumstances, we believe that due to exposure at high humidity the ferrite samples developed a very thin layer of iron oxyhydroxide (FeOOH), a compound, chemically stable up to 135°C. Above this temperature, it decomposes in iron oxide and water.

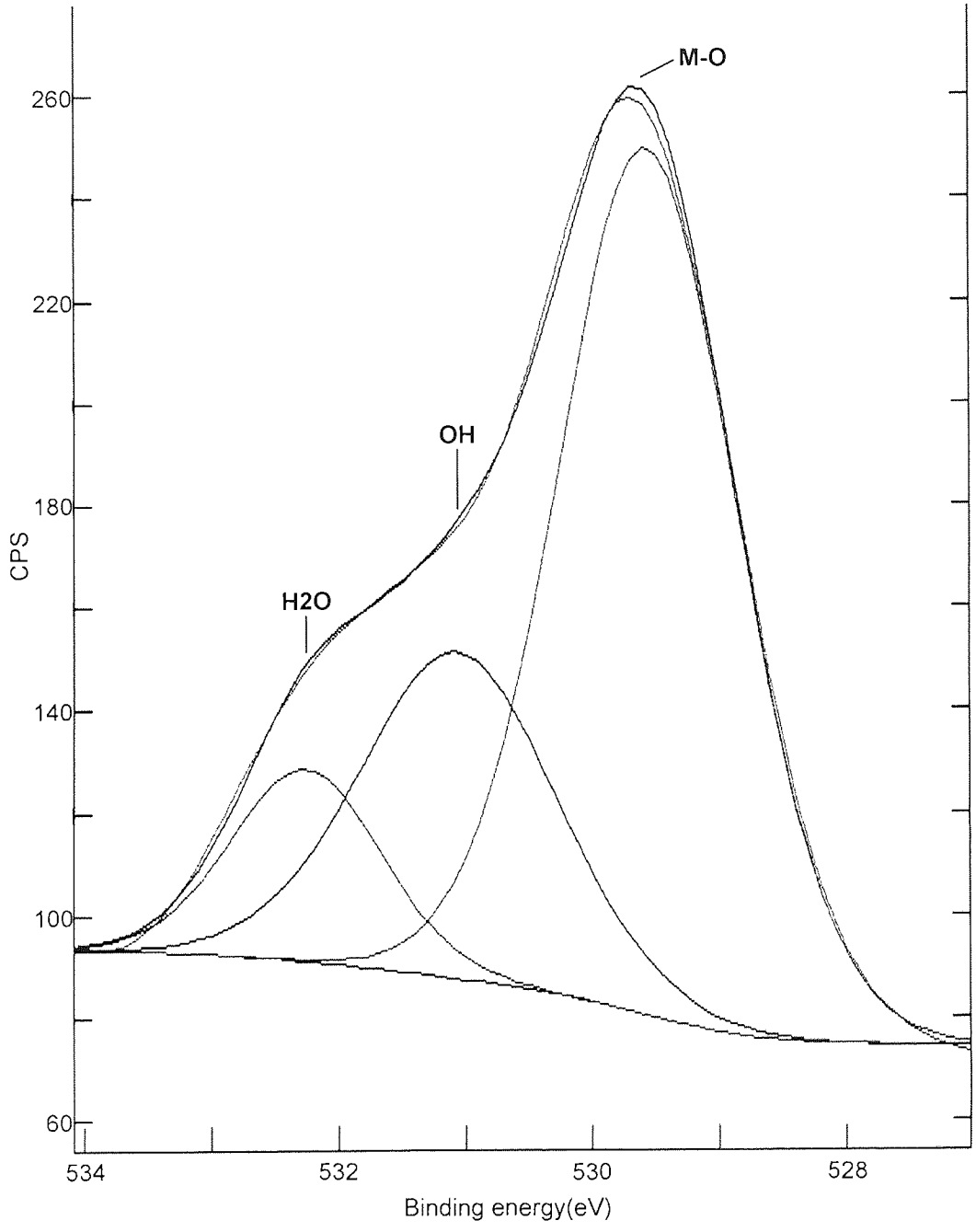

Figure 4-84 XPS scan of the O 1s region at 0° TOA of the baked ferrite sample

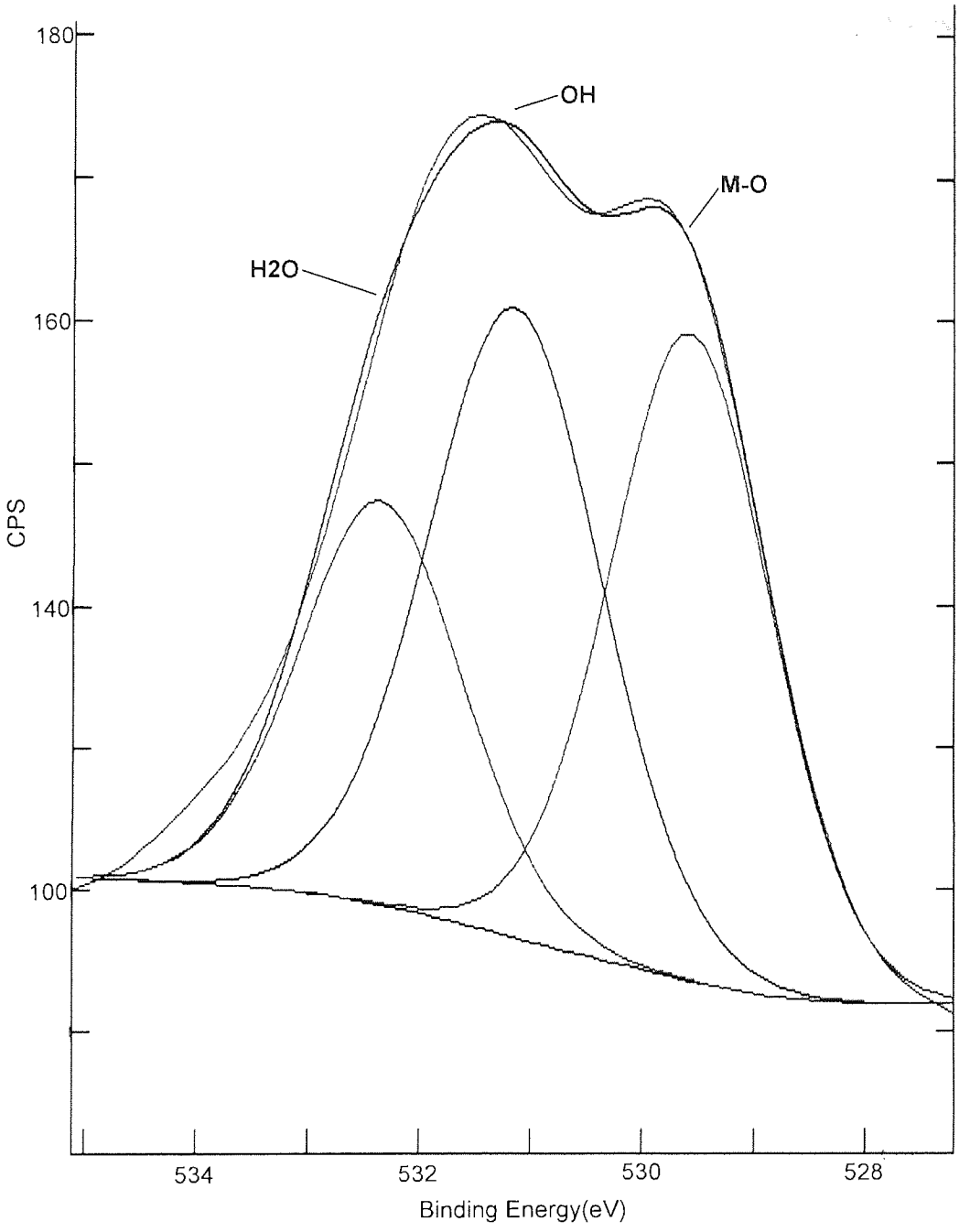

Figure 4-85 XPS scan of the O 1s region at 60° TOA of the baked ferrite sample

The graphs below represent a synthesis of the scans performed on the samples and they show the relative concentration of oxygen at the end of each experiment. It is obvious that after exposure at high humidity, the relative amount of oxygen bonded with hydrogen contained in water or hydroxyl groups increased. Even after baking, when the physically adsorbed water had been practically removed, the concentration of oxygen bonded with iron remained lower than that at 25°C/35%RH which shows that

the remained oxygen is part of chemically bonded water to ferrite as iron oxyhydroxide. The fact that at 60 degrees take off angle the concentration of oxygen bonded with the iron after baking is even lower than that at 0 degrees take off angle emphasises the supposition that the chemically bonded water and the iron oxyhydroxide forms a very thin layer on top of the ferrite surface.

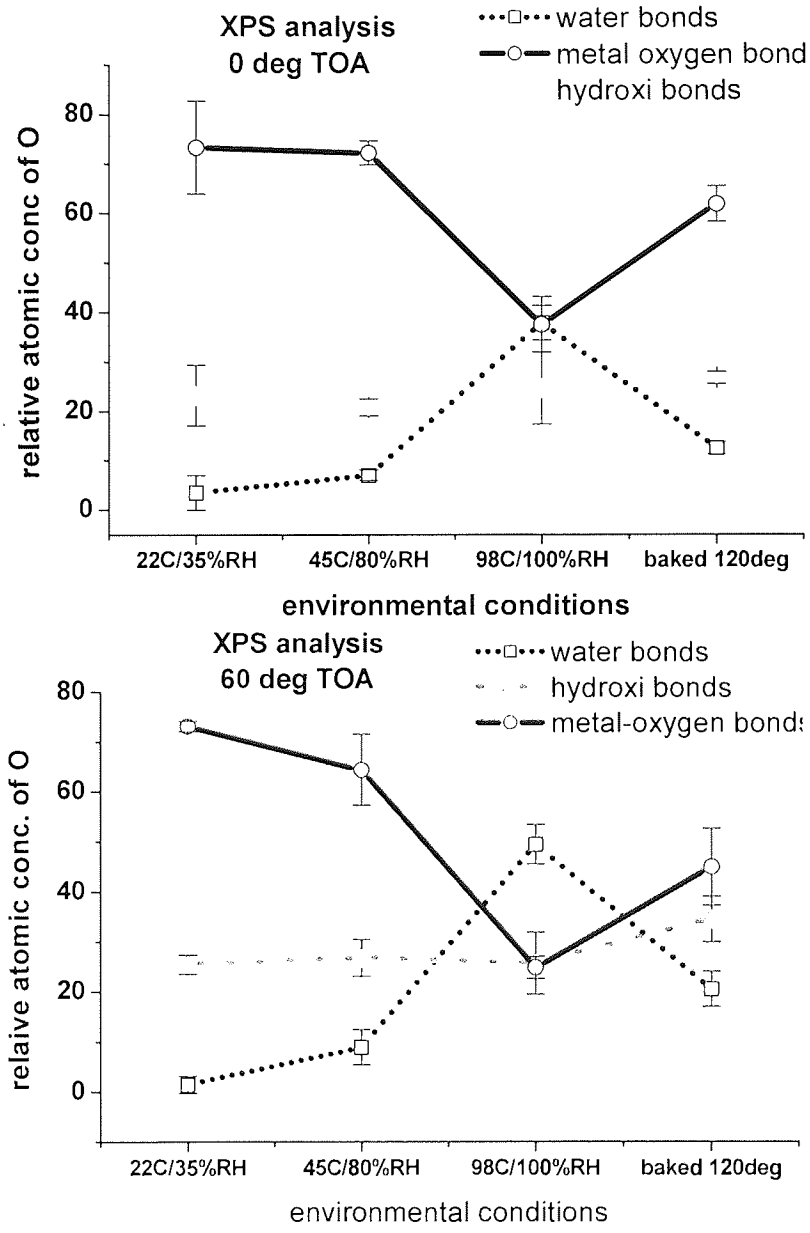

Figure 4-86 The relative concentration of oxygen in O 1s peak after different experiments at 0 and 60 degrees take-off angle

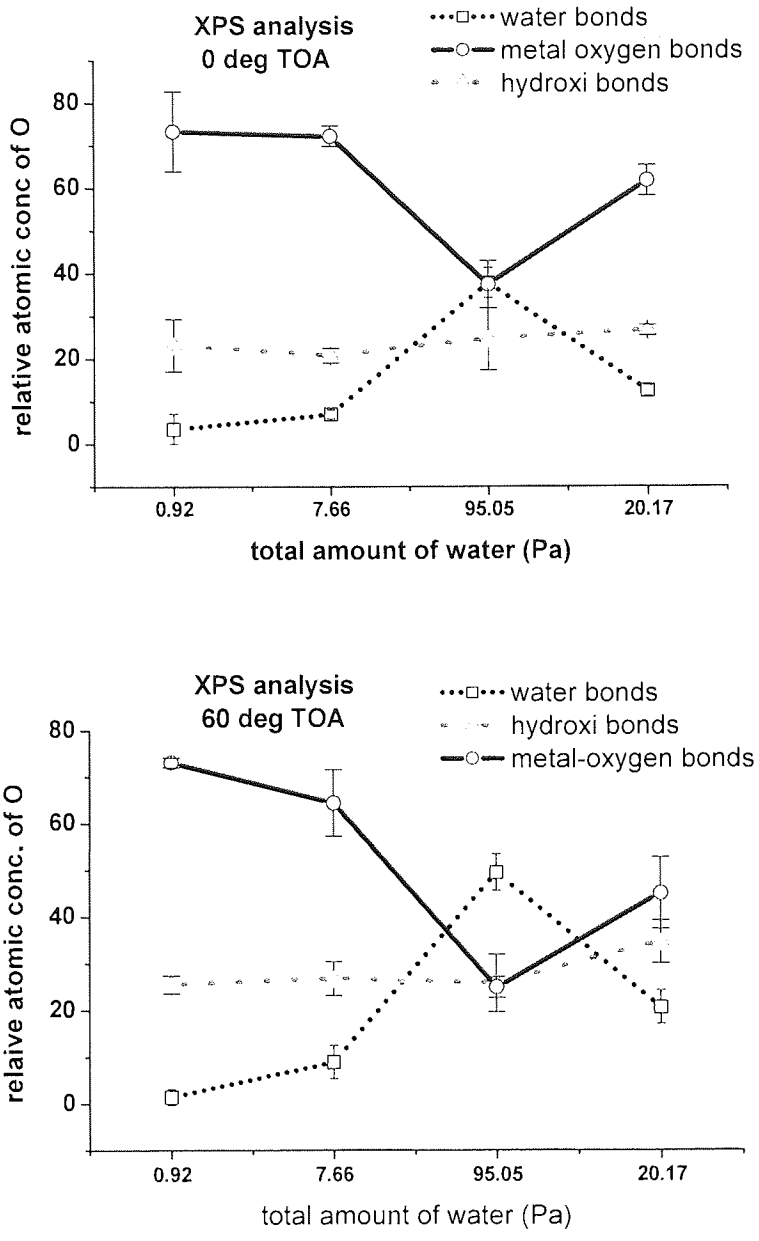

Figure 4-87 The relative concentration of oxygen in O 1s peak after different experiments at 0 and 60 degrees take-off angle upon total amount of water

4.7.2 Ferrite behaviour at low humidity and high temperature (stain simulation)

AFM scans of the ferrite were taken before and after each experiment. An AFM scan of the ferrite surface as received from the manufacturer is shown in Figure 4-88. This shows small ridges of about 2-3 nm in height, randomly oriented, due to the

polishing process. After the experiments AFM scans show a heavily stained surface produced by the slow moving tape (Figure 4-91), and patchy stains on the ferrite on which the tape ran at high speed (Figure 4-90). The stains generated by the slow moving tape on the ferrite form a very thick, continuous layer. This is probably because in this case, the tape ran about 2 days, compared with only half a day for the tape at high speed. The results earlier in this research concerning the DDS-3 heads (Figure 4-52) confirm that these features are wear tracks on a continuous layer of stain and not simply wear tracks on the ferrite. The surface of the ferrite shows wear tracks in the direction of tape motion, generated by the asperities on the tape. Topography measurements revealed that the thickness of the stains generated in both experiments is 14-25 nm, similar to those measured on DDS-3 heads. The AFM scan of the ferrite region of a DDS-3 read head after using DDS2 tapes at 45°C/10%RH reveals similar patchy stains of 14-20 nm peak-to-valley.

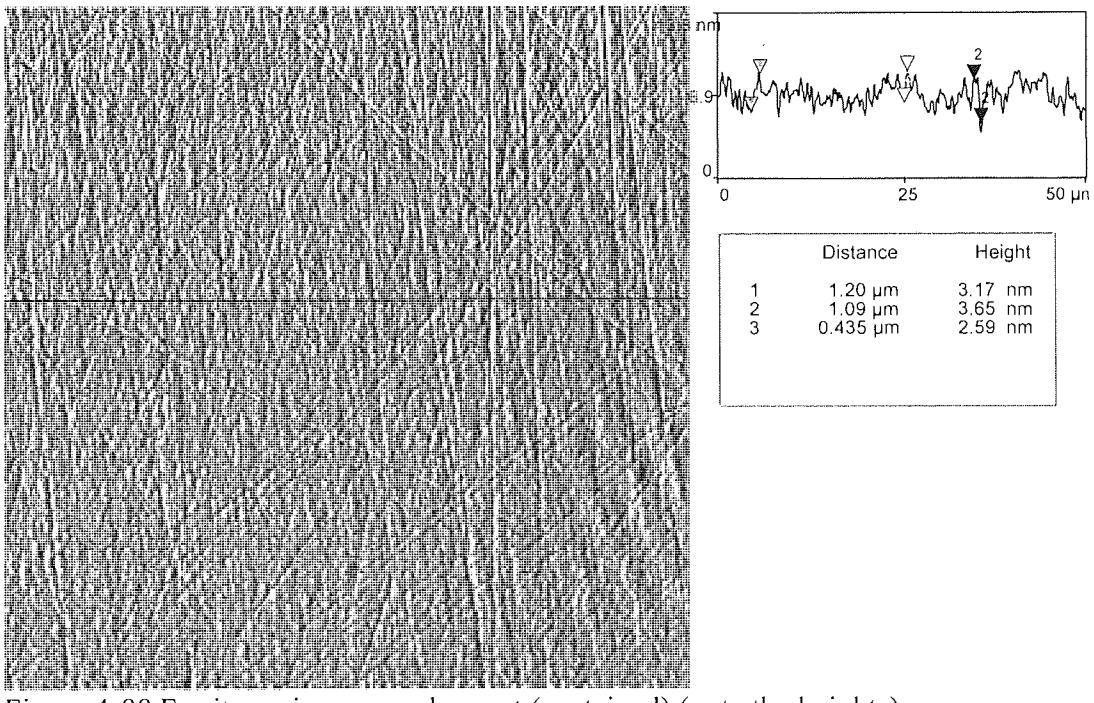

Figure 4-88 Ferrite region; normal aspect (unstained) (note the heights)

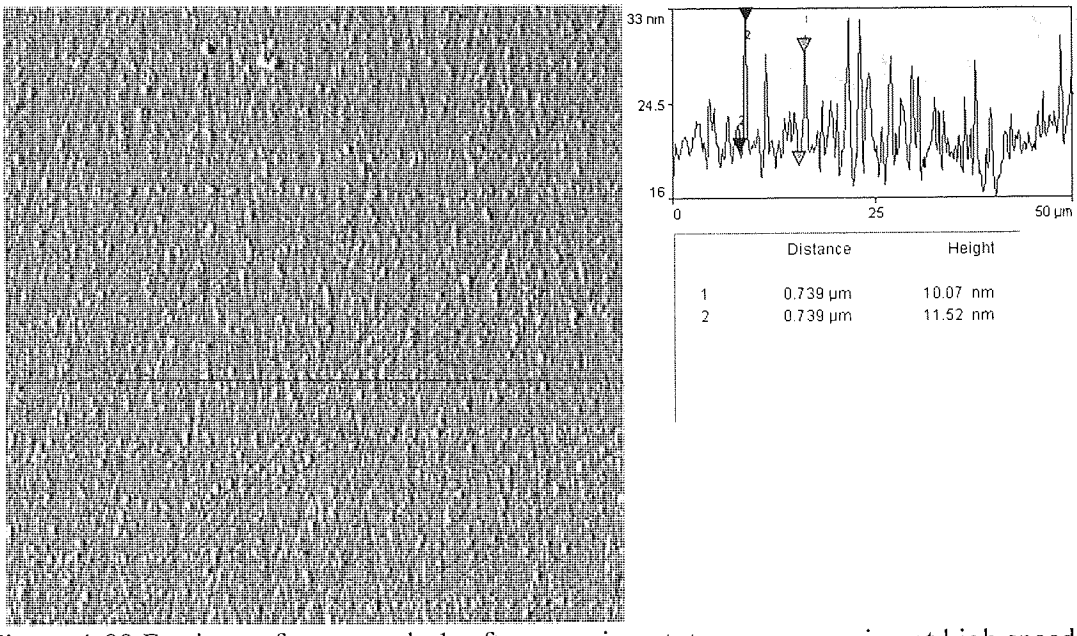

Figure 4-89 Ferrite surface, sample 1, after experiment, tape was running at high speed (50x50µm AFM scan)

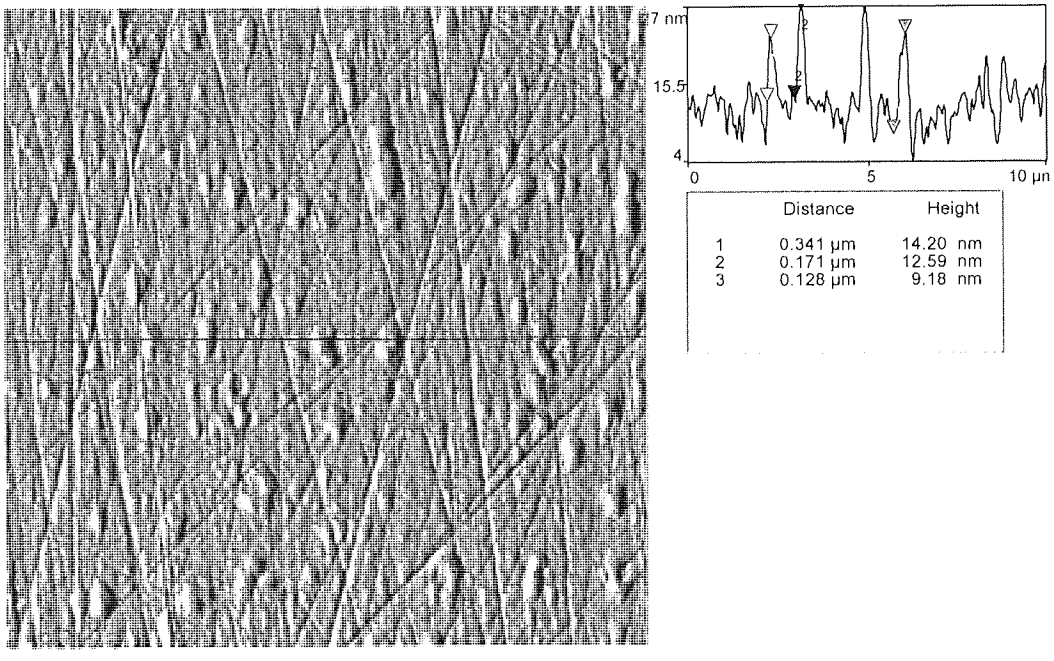

Figure 4-90 Zoom on the ferrite surface, sample 1, after experiment (10x10µm AFM scan)

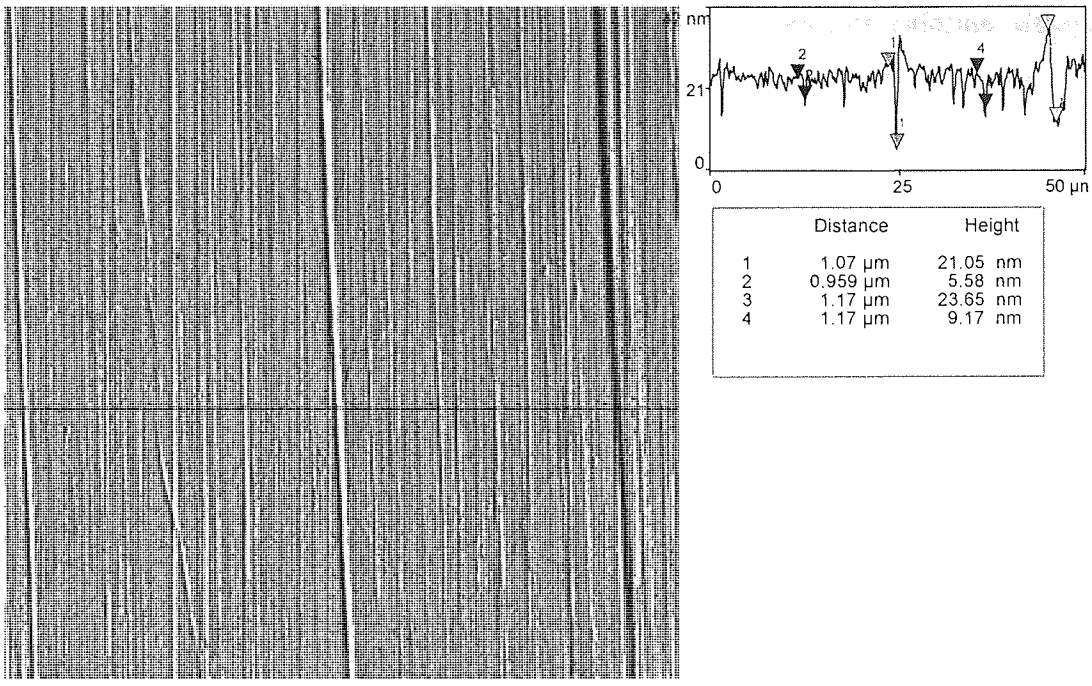

Figure 4-91 Sample 2's stained region at low tape speed

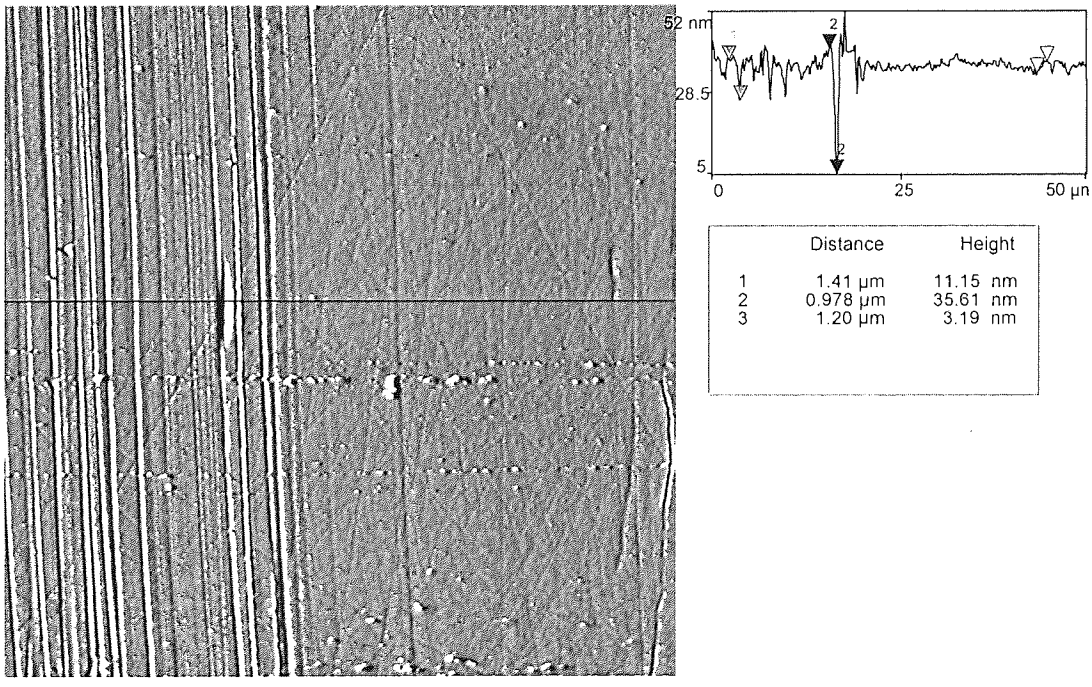

Figure 4-92 Boundary region between stained (left) and clear (right) ferrite areas, sample 2

Chemical analysis of these surfaces using XPS was performed on the virgin sample. On the unstained surface, the results reveal carbon, iron, oxygen and small amounts of Mn and Zn (Figure 4-93). No other elements were seen. However, after staining the

spectra revealed on both samples in addition to the previous elements, chlorine, nitrogen and sodium (Figure 4-94 and Figure 4-95). The amount of the chlorine, nitrogen and sodium varies from sample to sample being higher on the sample where the speed of the tape was lower. This corresponds to the AFM scans that show less stain produced when tape was running at high speeds.

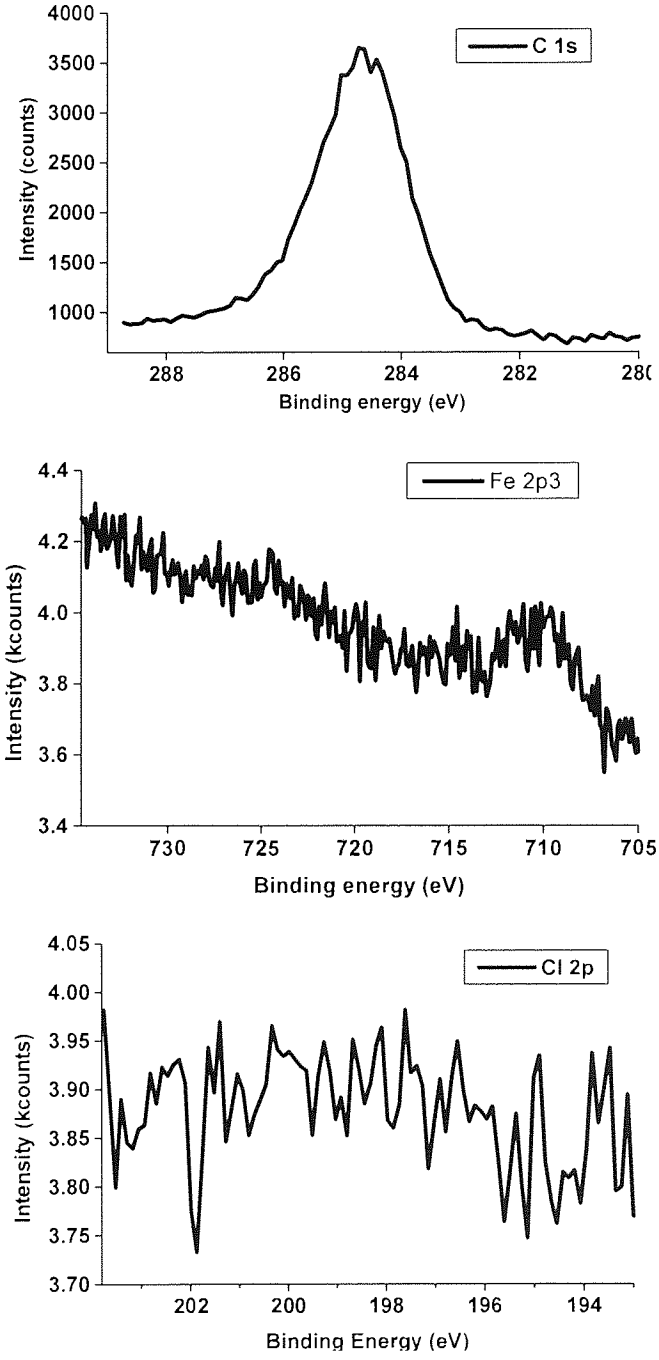

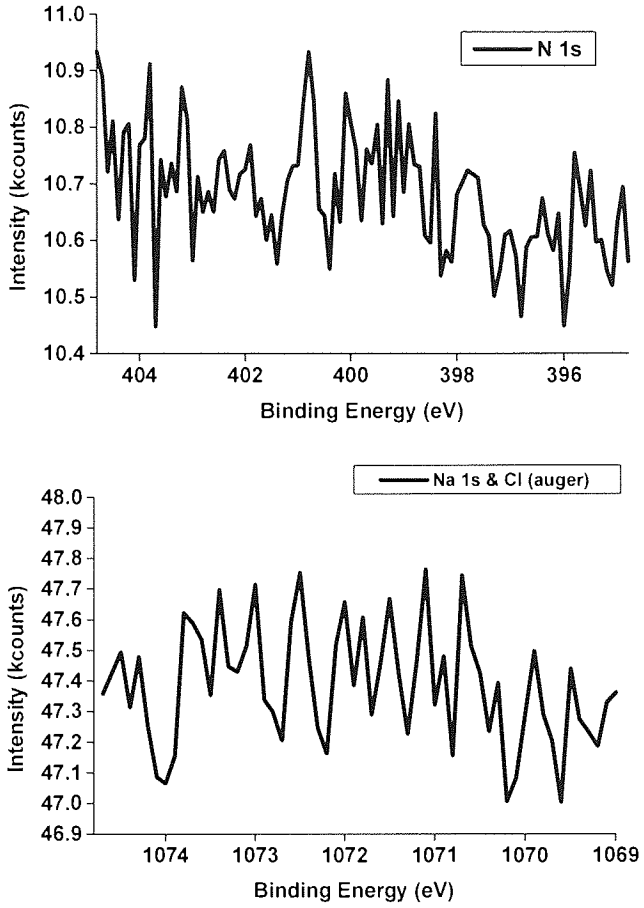

Figure 4-93 XPS spectrum of a virgin ferrite surface showing C 1s, Fe2p3, Cl 2p, N 1s and Na 1s regions

The following are the XPS spectra of the stained ferrite surface under high and low tape speed.

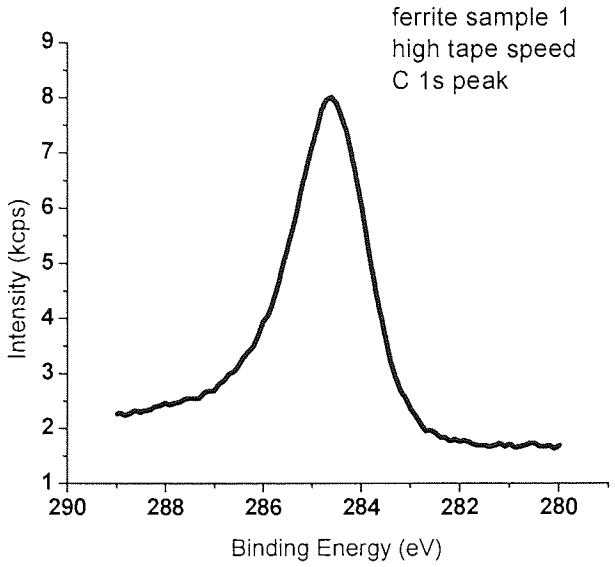
ferrite sample 1
high tape speed
C 1s peak
Intensity (kcps)
9
8
7
6
5
4
3
2
1
290
288
286
284
282
280
Binding Energy (eV)

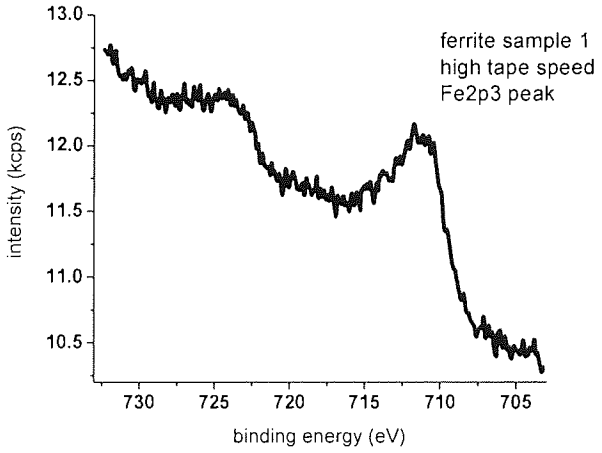
ferrite sample 1
high tape speed
Fe2p3 peak
intensity (kcps)
13.0
12.5
12.0
11.5
11.0
10.5
730
725
720
715
710
705
binding energy (eV)

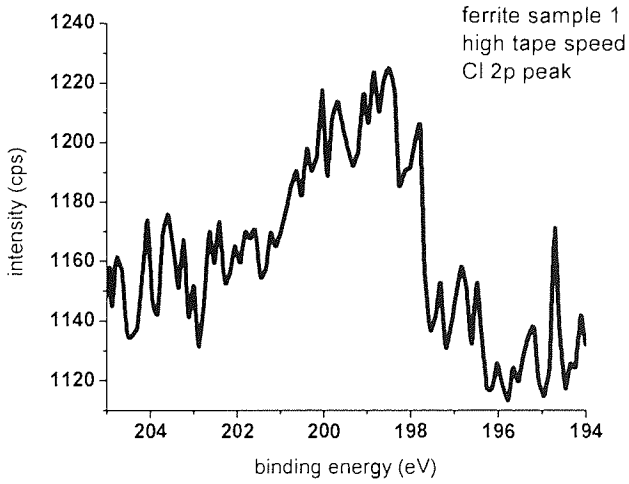
ferrite sample 1
high tape speed
Cl 2p peak
intensity (cps)
1240
1220
1200
1180
1160
1140
1120
204
202
200
198
196
194
binding energy (eV)

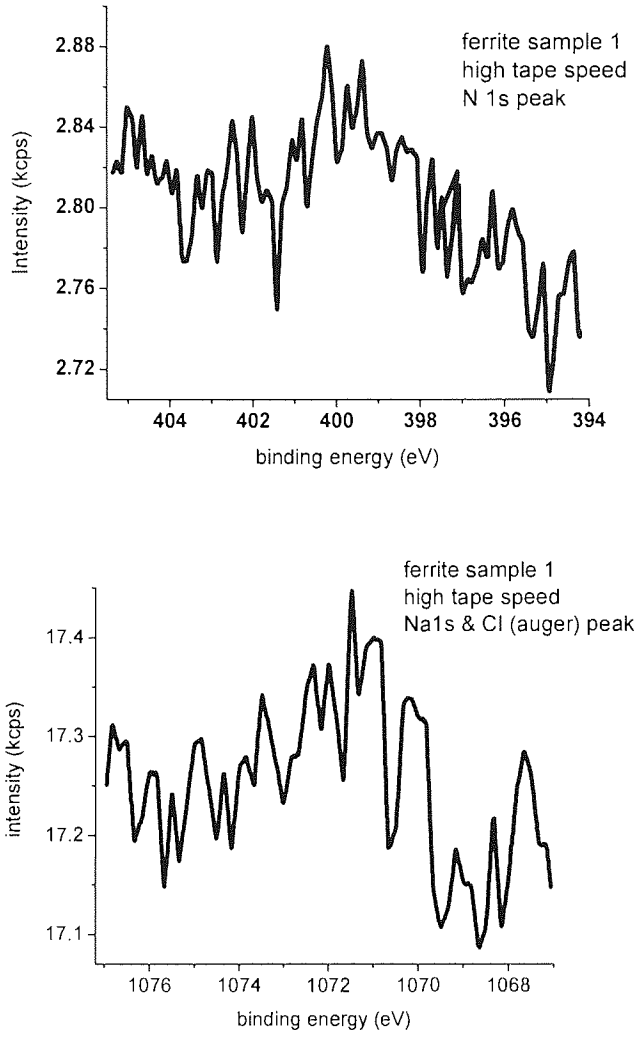

Figure 4-94 XPS spectrum of stained ferrites showing C 1s, Fe2p3, Cl 2p, N 1s and Na 1s regions (high tape speed)

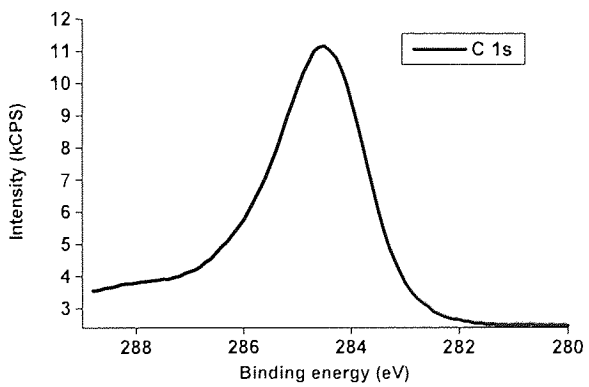

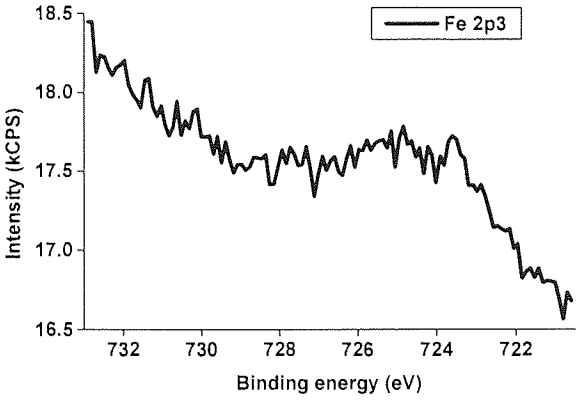
Fe 2p3
Intensity (kCPS)
18.5
18.0
17.5
17.0
16.5
732
730
728
726
724
722
Binding energy (eV)

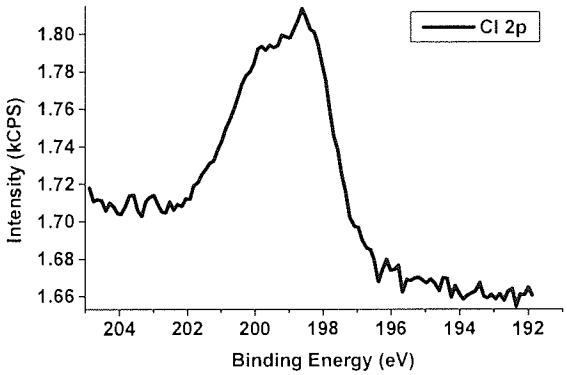
Cl 2p
Intensity (kCPS)
1.80
1.78
1.76
1.74
1.72
1.70
1.68
1.66
204
202
200
198
196
194
192
Binding Energy (eV)

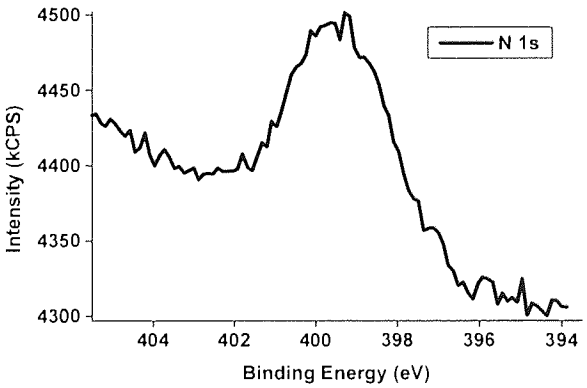
N 1s
Intensity (kCPS)
4500
4450
4400
4350
4300
404
402
400
398
396
394
Binding Energy (eV)

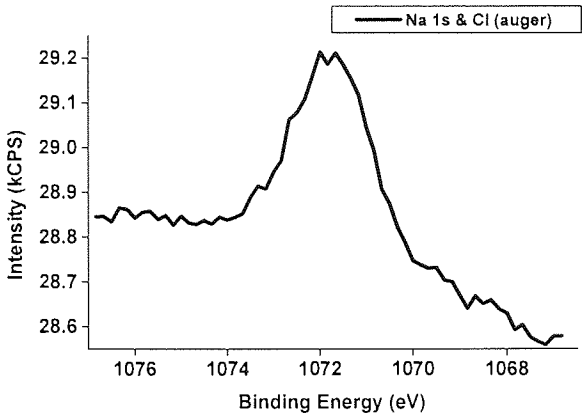

Figure 4-95 XPS spectrum of stained ferrites showing C 1s, Fe2p3, Cl 2p, N 1s and Na 1s regions (low tape speed)

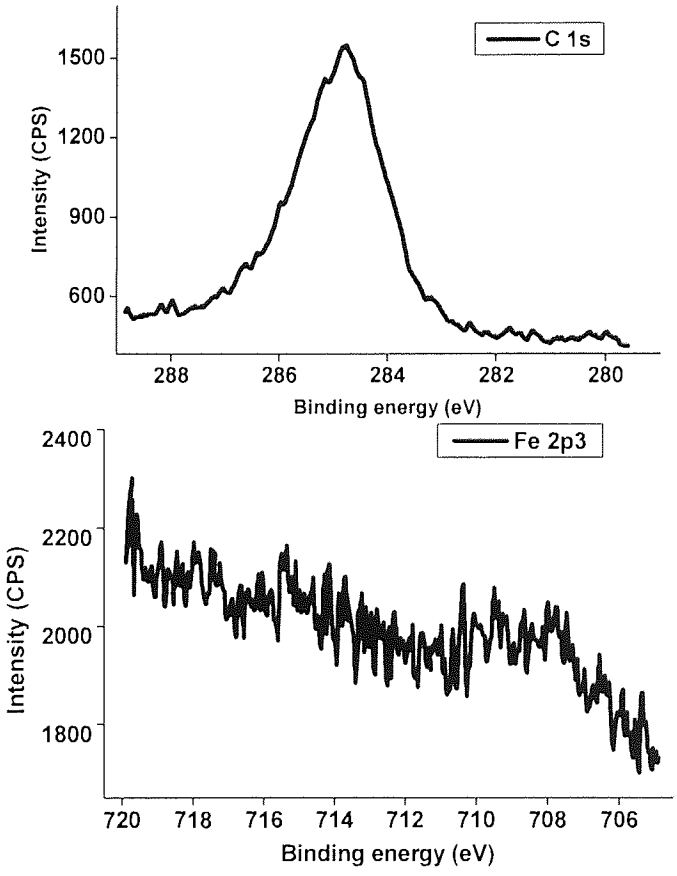

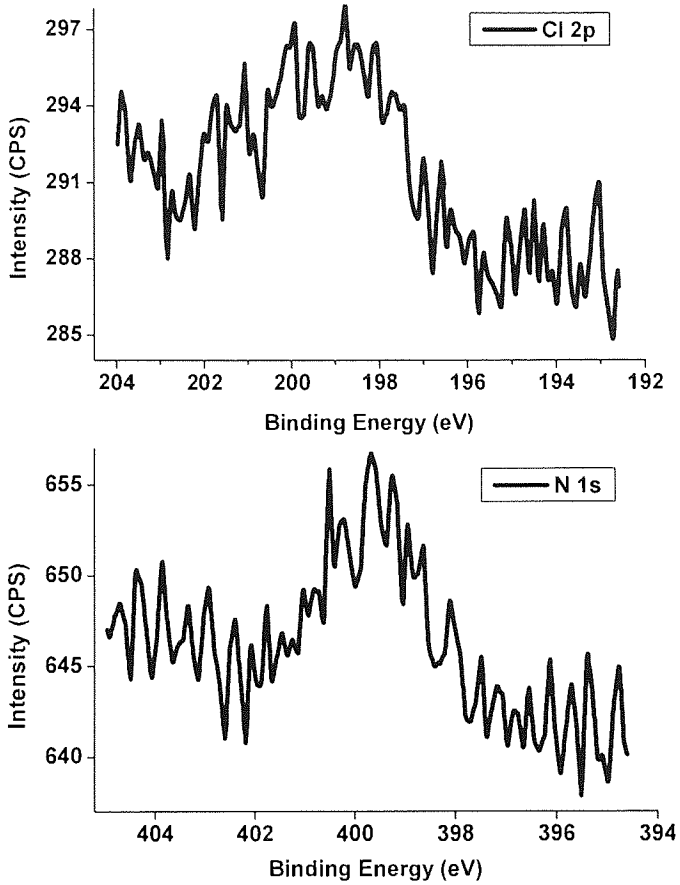

Figure 4-96 XPS spectrum of stained ferrites showing C 1s, Fe2p3, Cl 2p, N 1s and Na 1s regions (low tape speed, sample 2)

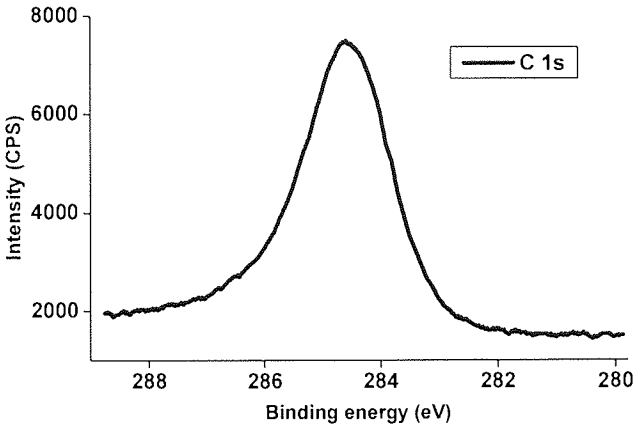
C 1s
Intensity (CPS)
8000
6000
4000
2000
288
286
284
282
280
Binding energy (eV)

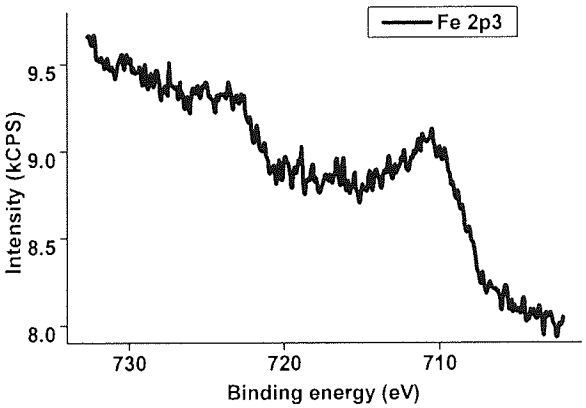
Fe 2p3
Intensity (kCPS)
9.5
9.0
8.5
8.0
730
720
710
Binding energy (eV)

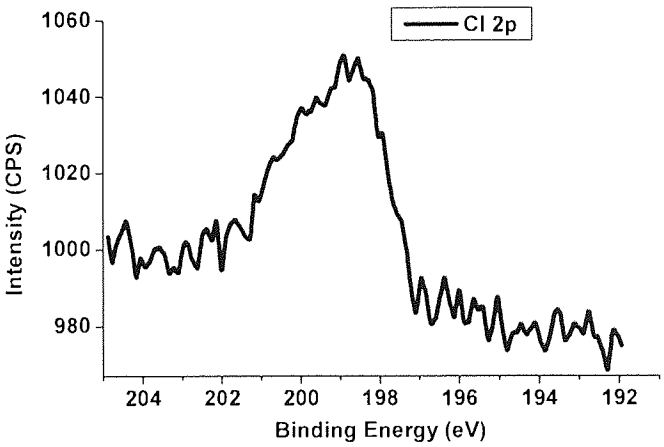
Cl 2p
Intensity (CPS)
1060
1040
1020
1000
980
204
202
200
198
196
194
192
Binding Energy (eV)

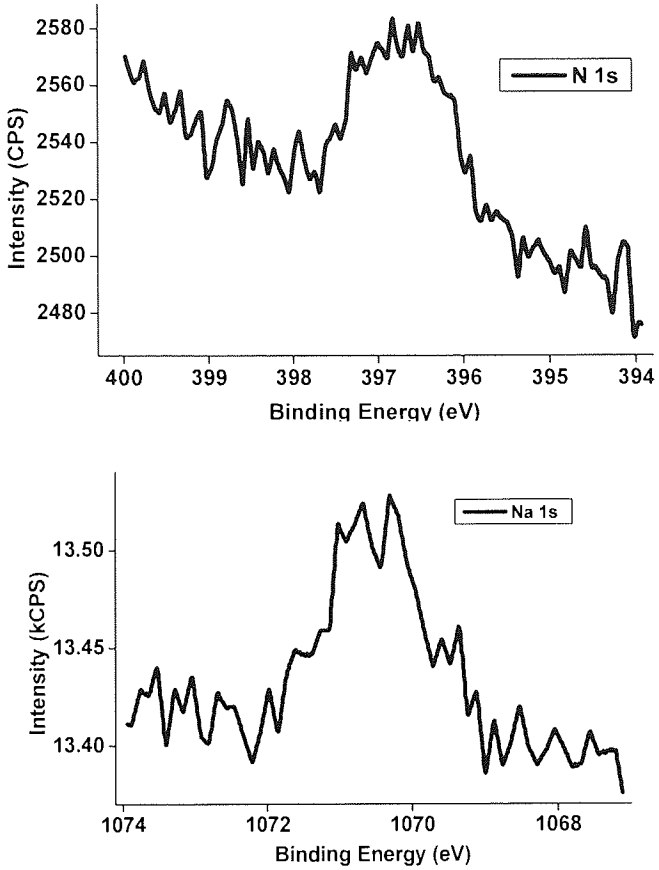

Figure 4-97 XPS spectrum of stained ferrites showing C 1s, Fe2p3, Cl 2p, N 1s and Na 1s regions (low tape speed, sample 3)

Although the presence of chlorine in the spectra can be disputed and can be attributed to NaCl contamination as also can sodium, the presence of nitrogen can be only attributed to the presence of the polymer binder in the stain formulation. However, some tape manufacturers are using sodium salts in the magnetic layer formulation and more precisely in the binder formulation to improve characteristics. Interestingly, the N 1s peak is at 400.1eV, binding energy corresponding to nitrogen bonds in organic compounds.

The quantification table show the following amounts of elements on the surface of the ferrite samples:

element	Binding energy (eV)	Atomic concentration (%)
C 1s	284.6	64.7
O 1s	530.0	22.0
Fe 2p3	711.0	5.1
Mn 2p3	641.0	0.7
Zn 2p3	1021.6	0.3
N 1s	399.9	0.9
Cl 2p3	199.0	0.7
Na 1s	1071.8	5.5

The concentration of chlorine and sodium being different, it is assumed that the presence of chlorine is due to binder presence on the ferrite surface rather than NaCl contamination.

4.7.3 SIMS analysis of the stained ferrite

SIMS spectra have also confirmed the presence of large amounts of chlorine and organic compounds as one can see from the next figures. In the negative range of the spectrum, the interesting peaks were situated at 35 and 37 amu (atomic mass units) corresponding to the two most abundant isotopes of chlorine and at 26 and 61 amu corresponding to CN, CNCl and NH groups, a good evidence of binder presence.

On the other hand, the positive spectrum shows apart from iron peaks large amounts of organic material. Lithium and manganese signals are coming from the ferrite material. The iron peaks are generated both by the ferrite surface and by the acicular magnetic particles that were present in the stain composition.

Together, both spectra have given evidence of binder present on the surface of ferrite samples. The spectra acquired have a similar pattern with the spectra taken of the DDS-2 tapes. (see also Figure 4-69 and Figure 4-70)

Positive and negative spectra of the ferrite surfaces are given below:

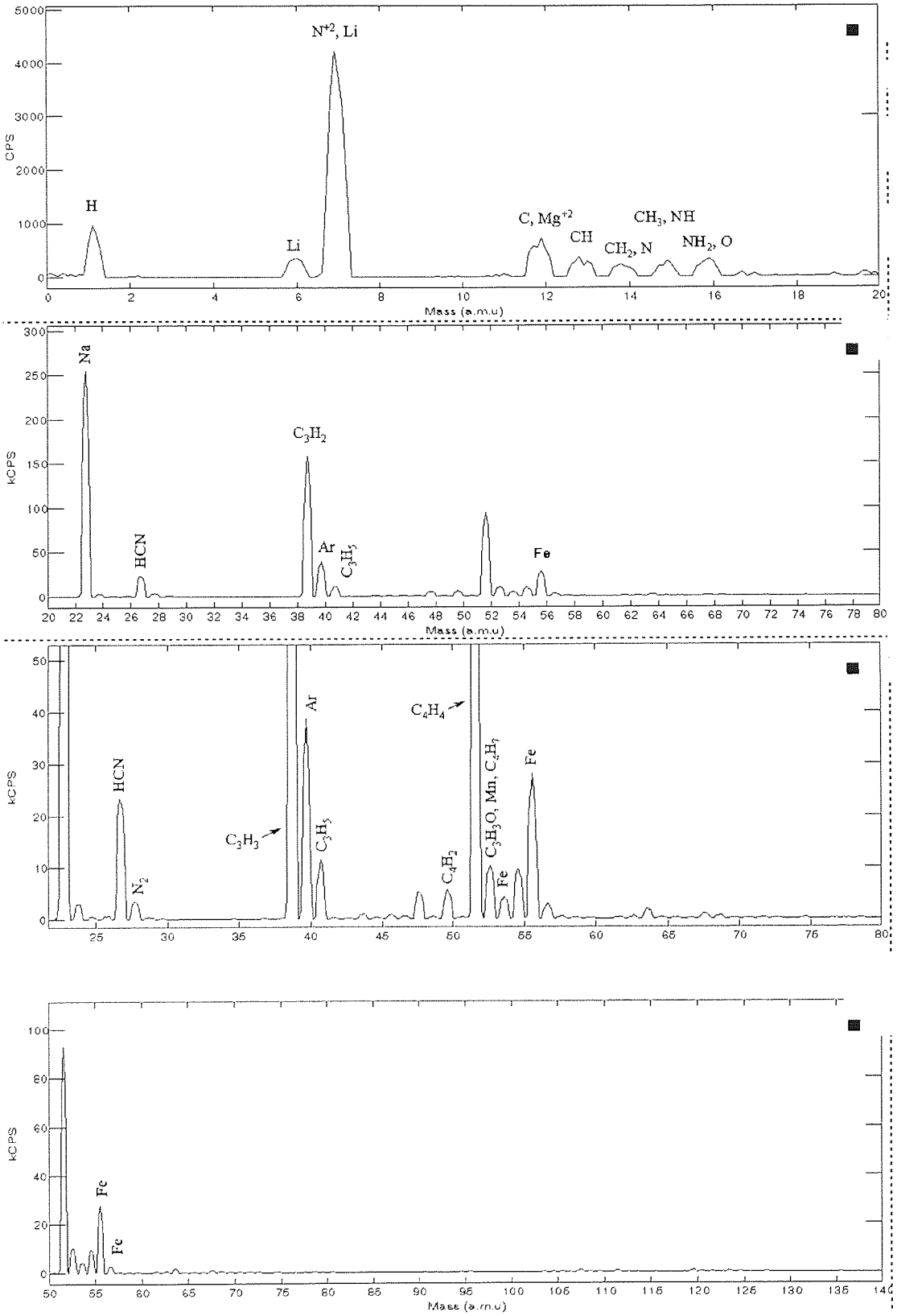

Figure 4-98 Positive spectrum of the stained ferrite surface (sample 1)

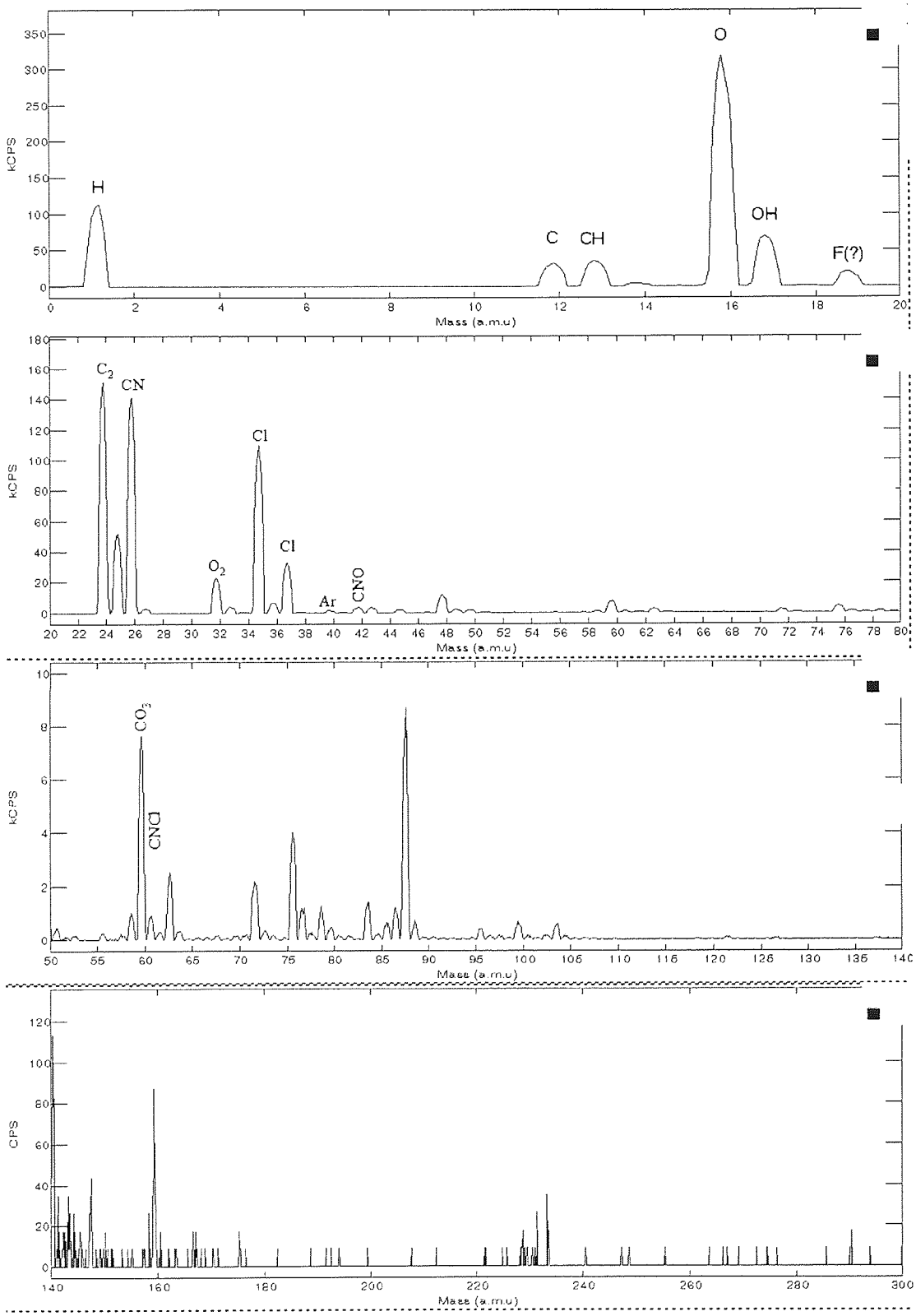

Figure 4-99 SIMS negative spectrum of the stained ferrite surface (sample 1)

The spectra of the ferrite sample 3 showed even larger amounts of organic materials as one can see from figures below.

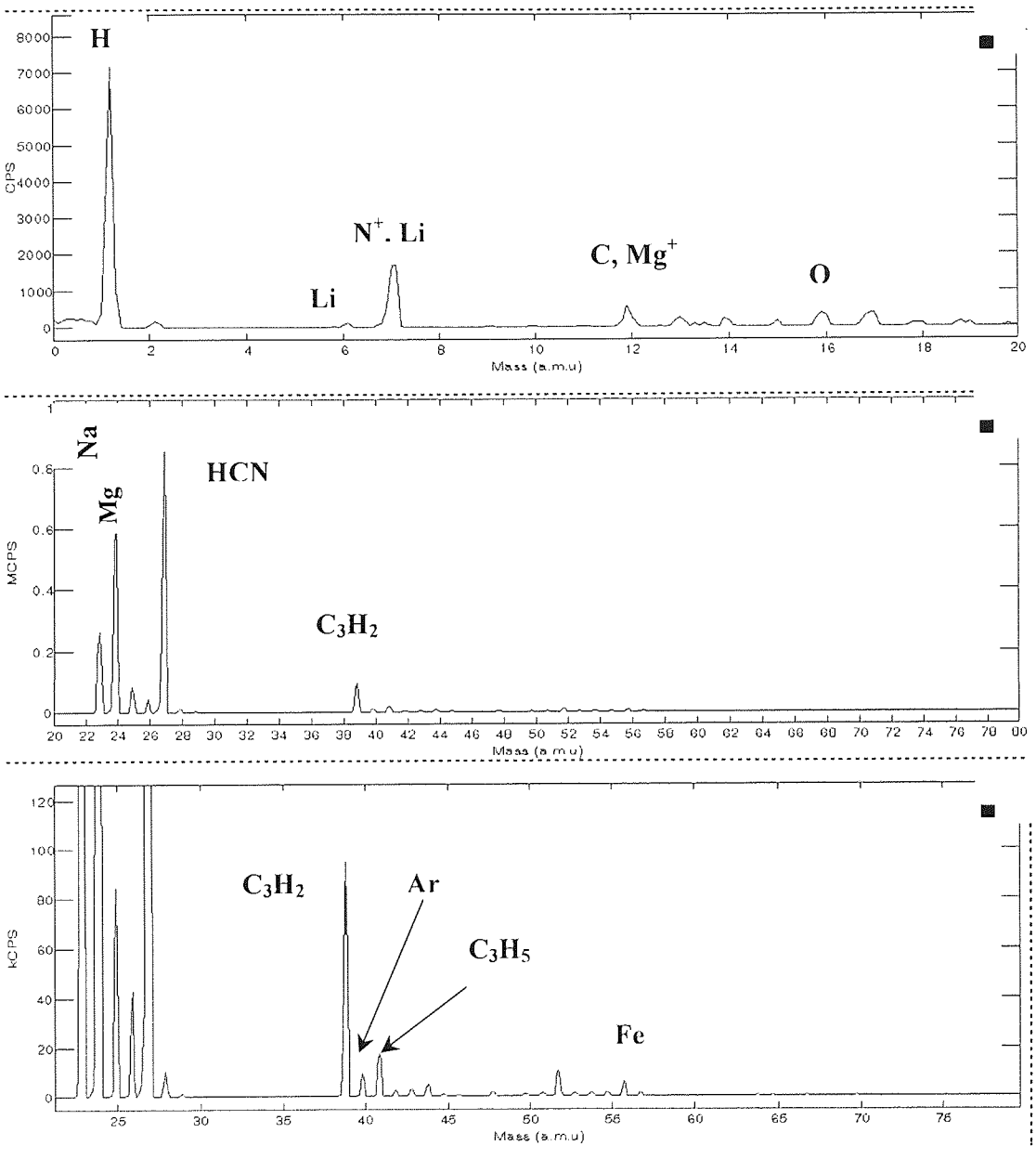

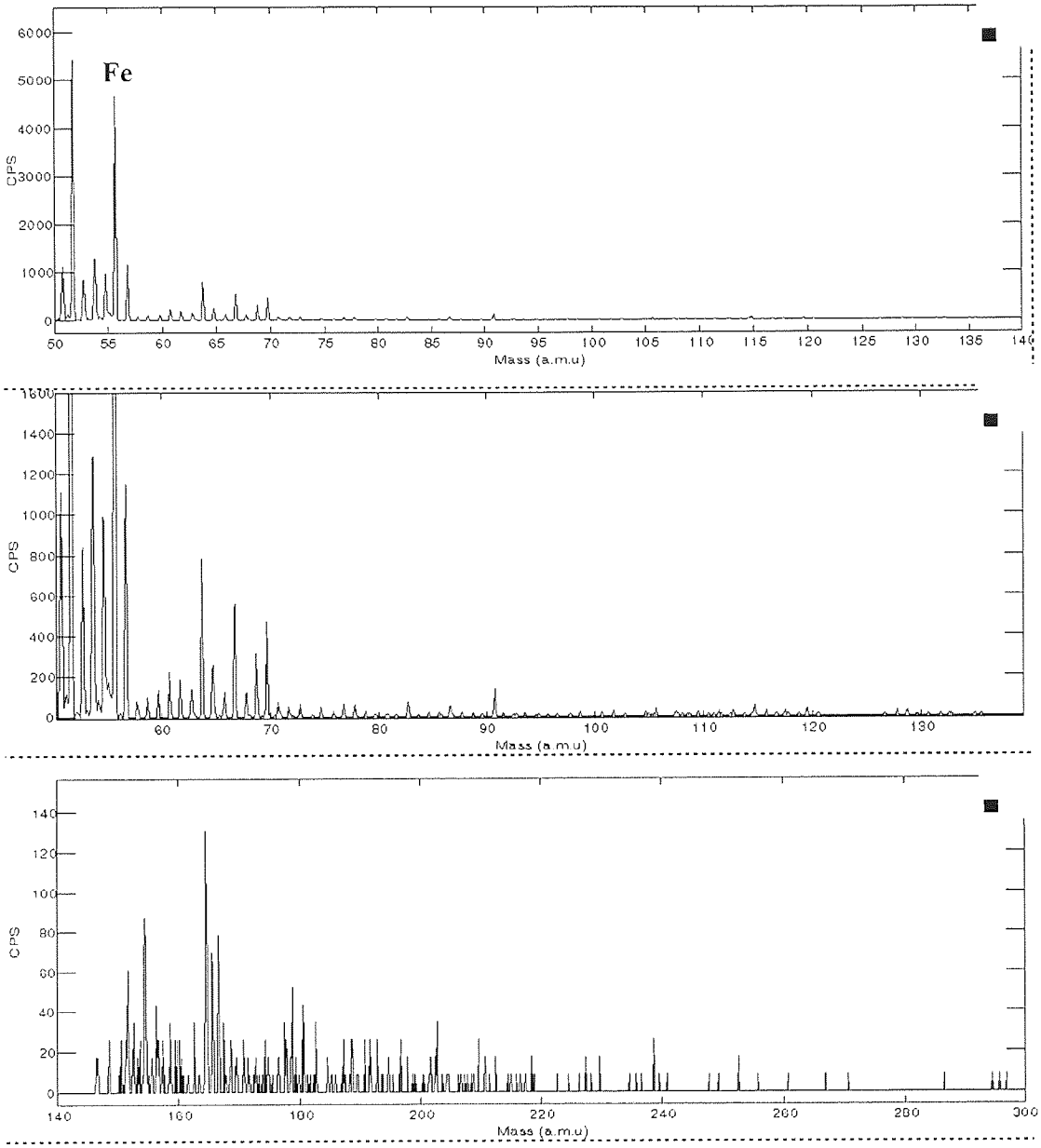

Figure 4-100 The SIMS positive spectrum of the surface of the ferrite sample 3

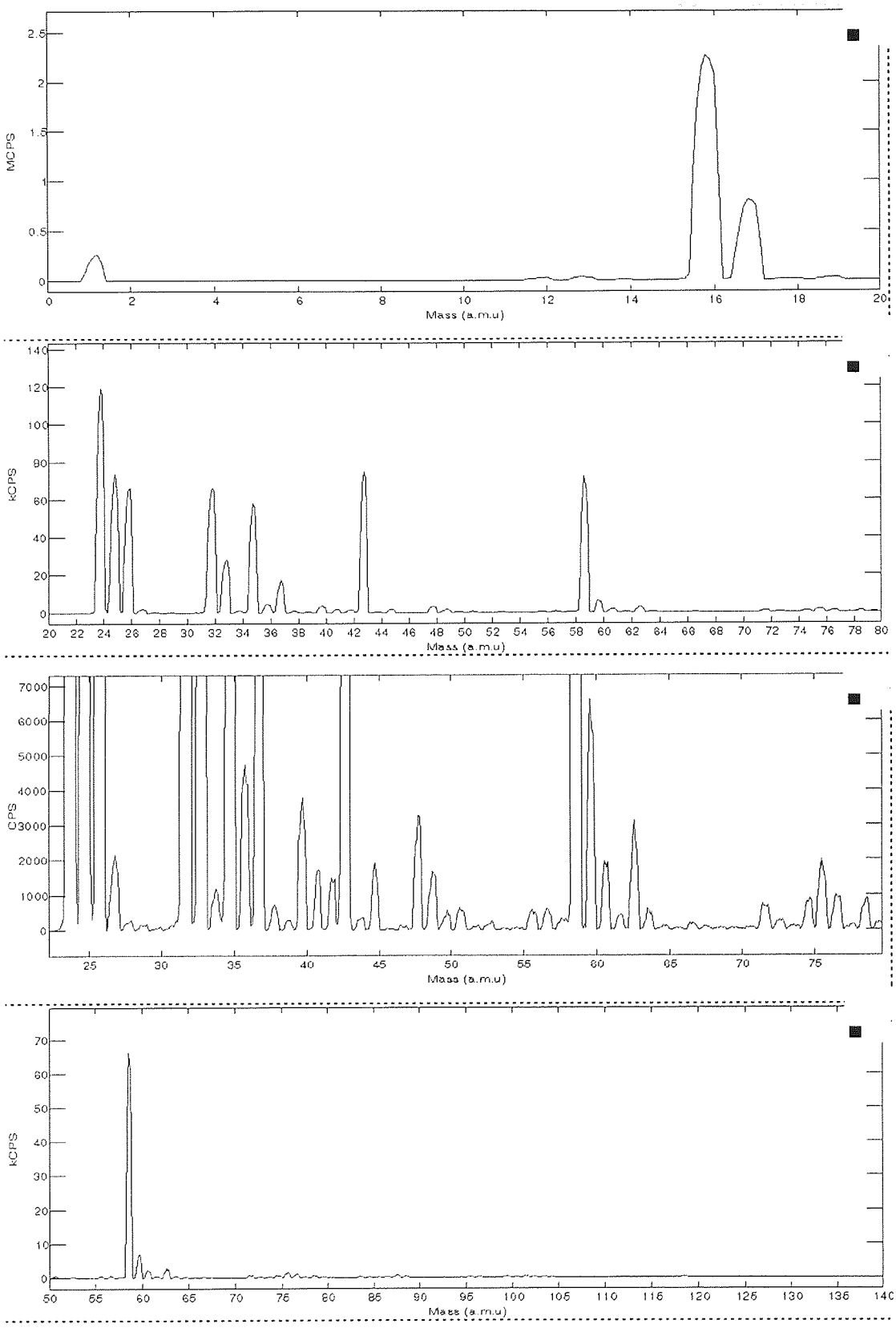
MCPS
Mass (a.m.u)
kCPS
Mass (a.m.u)
CPS
Mass (a.m.u)
kCPS
Mass (a.m.u)

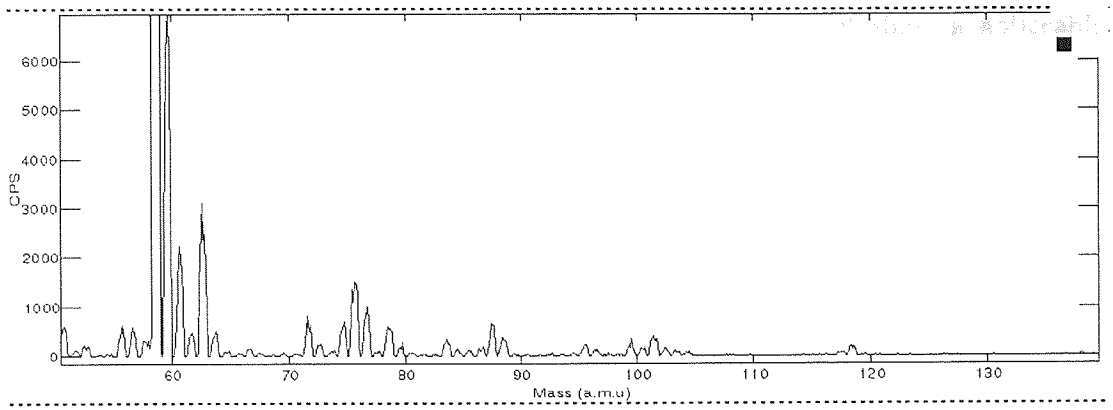

Figure 4-101 The SIMS negative spectrum of the surface of the ferrite sample 3

4.8 Contact angle measurements

Experiments aimed to measure the surface energy variation of both DDS2 tapes and ferrite upon different environmental conditions were made. The pictures below have been taken during contact angle measurements for ferrite using water and diiodomethane.

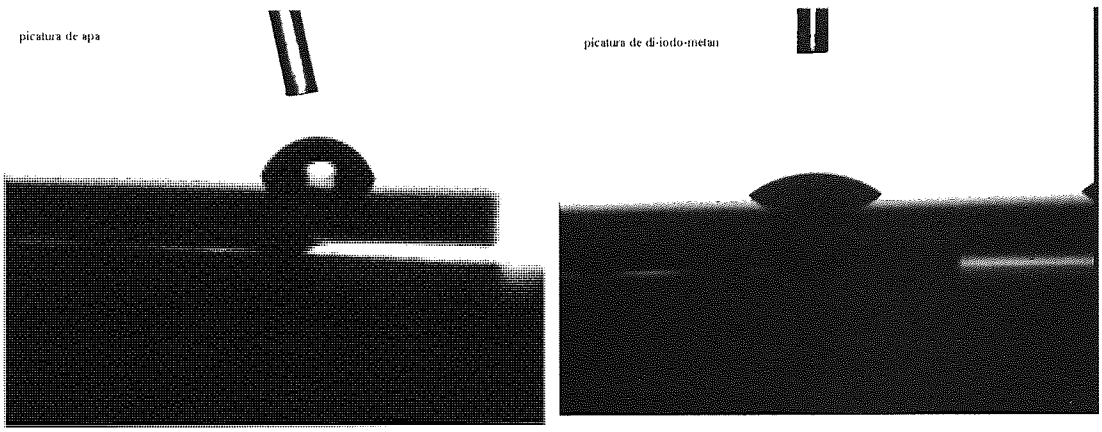

Figure 4-102 Contact angle differences between distilled water (left) and diiodomethane (right) for ferrite surface

Unfortunately, due to device limitations we were unable to perform a full investigation of surface energy behaviour under different environmental conditions. Figure 4-103 shows a preliminary result obtained during these experiments revealing a decrease in contact angle and respectively an increase in surface energy after exposing

the ferrite to 98°C/100%RH. In the same time, the tape did not show a noticeable variation of its surface energy (Figure 4-105). The results are encouraging but further studies are needed in order to draw a conclusion.

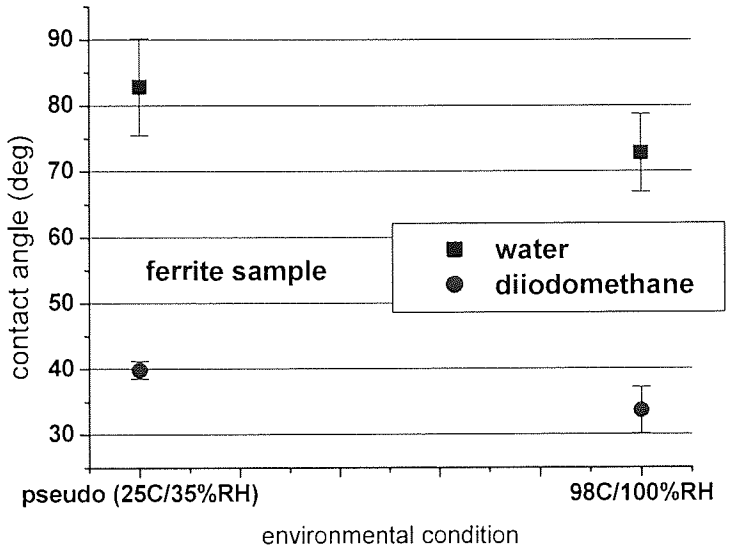

Figure 4-103 Preliminary result of contact angle variation of the ferrite

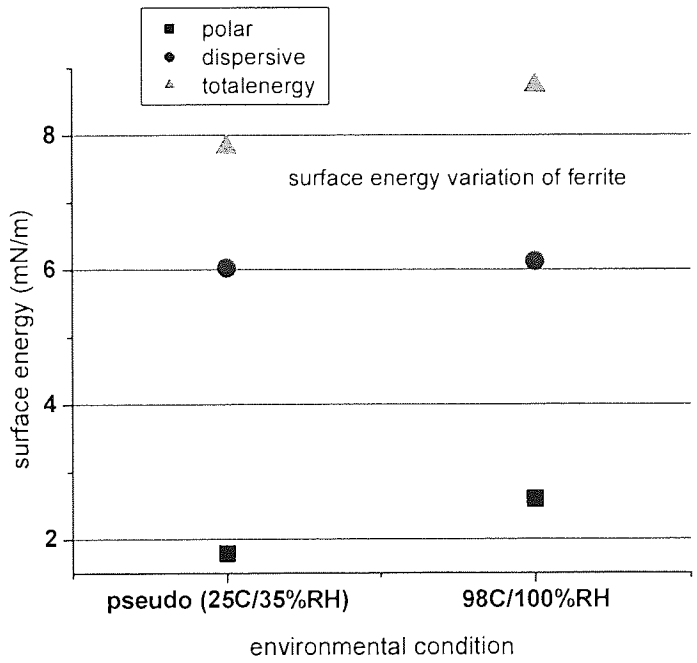

Figure 4-104 Corresponding surface energy variation of the ferrite

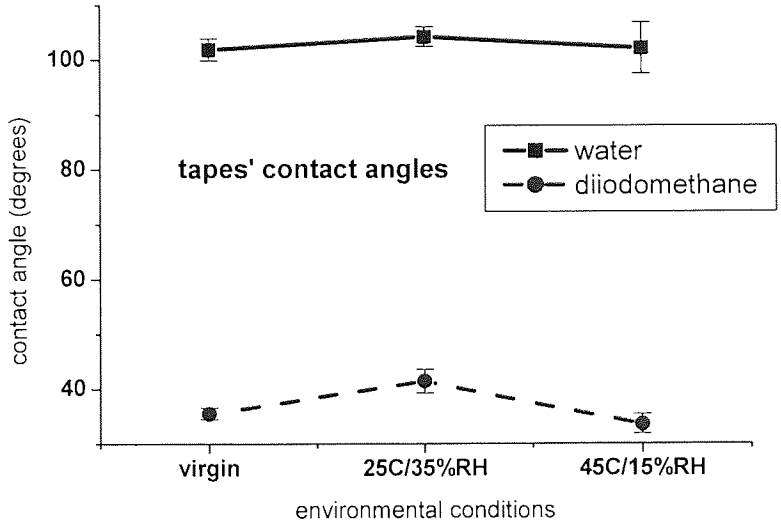

Figure 4-105 Preliminary result of contact angle variation of the DDS2 tape

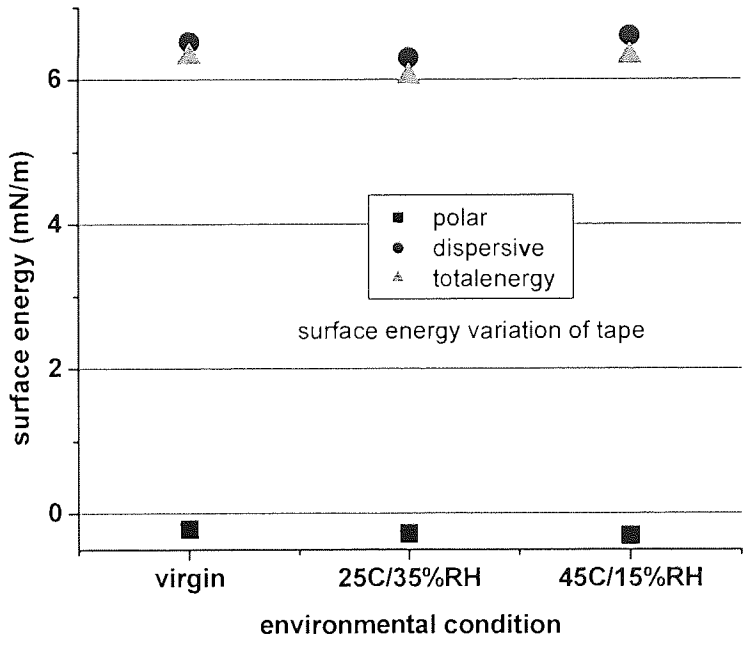

Figure 4-106 Corresponding surface energy variation of the tape

4.9 Study of the DDS4 heads wear rate at the same water pressure

The aim of this section of the research was to determine whether the relative humidity or the amount of water is the critical parameter that influences the wear rate of the heads. The environmental conditions were set in a such way so the amount of water contained in the environmental chamber was the same: 10°C/63%RH, 24°C/25%RH and 41°C/12%RH.

Studying the wear rate of the DDS 4 drives has proven to be difficult. The use of different type of heads compared with the DDS3 drives used before and the DDS4 tapes compared with DDS2 used before, has dramatically reduced the wear rate. Despite the fact that the number of cycles during each experiment has been doubled, the wear rate has proven to be difficult to estimate. Therefore, it is believed that these experiments have to be regarded with the necessary caution and that further experiments are needed. As a general remark, in all cases investigated the wear rate seems to be smaller compared with the rate measured previously on DDS3 drives (see paragraph 4.2).

In this study, the error rate was much smaller so the error in estimating the wear rate is much higher. The calculated value was found to be about ±20%.

The wear rate at 10°C/63%RH was found to be very small on both types of heads investigated. The bulk ferrite heads used for writing and sandwich heads used for reading display an overall wear rate that fluctuate around zero.

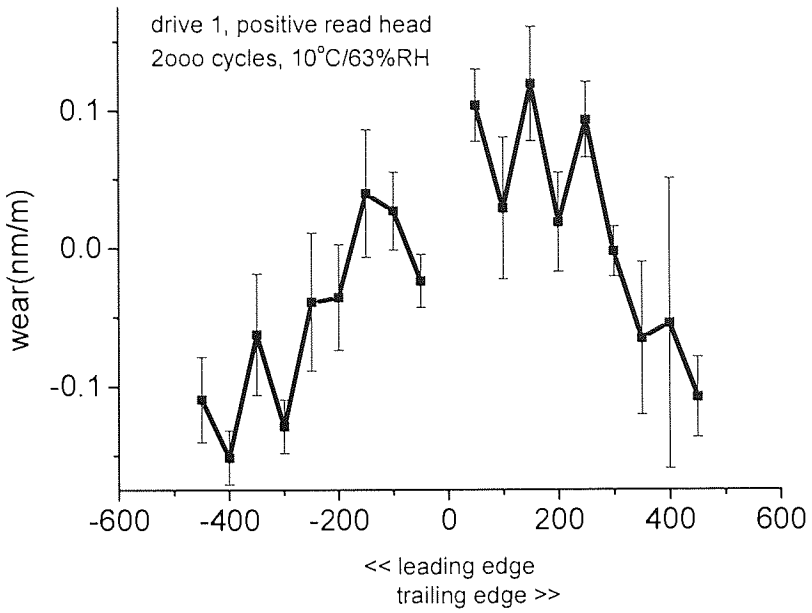

Figure 4-107 Wear of the drive 1 positive read head after 2000 cycles

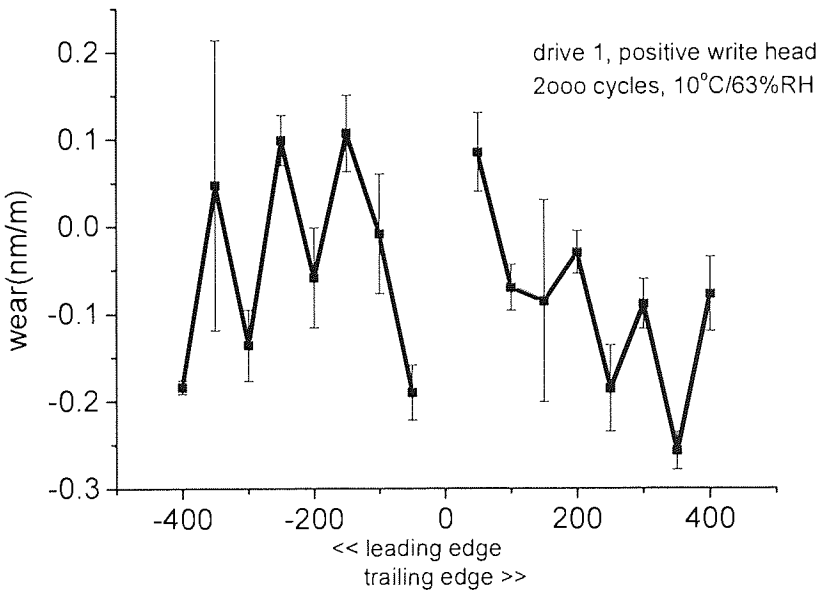

Figure 4-108 Wear of the drive 1 positive write head after 2000 cycles

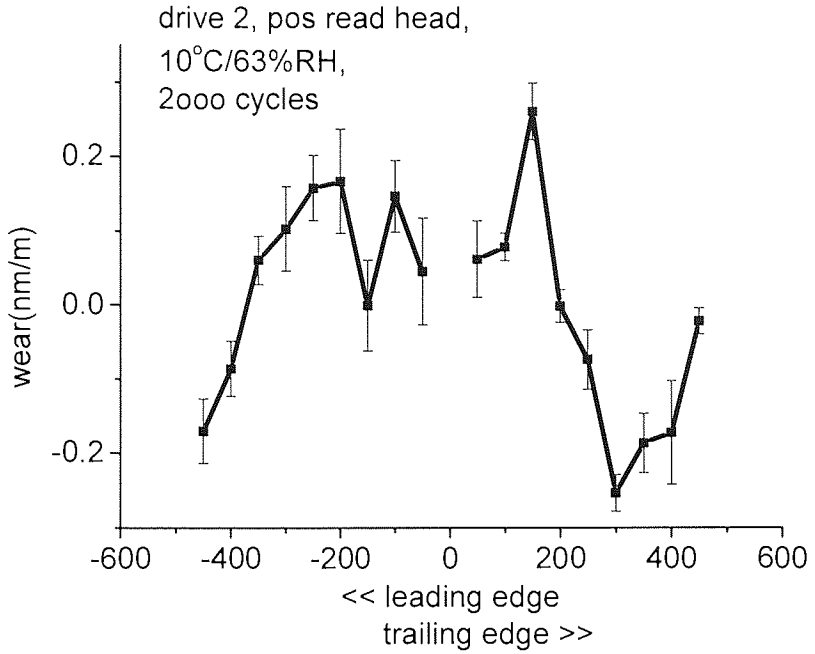

Figure 4-109 Wear of the drive 2 positive read head after 2000 cycles

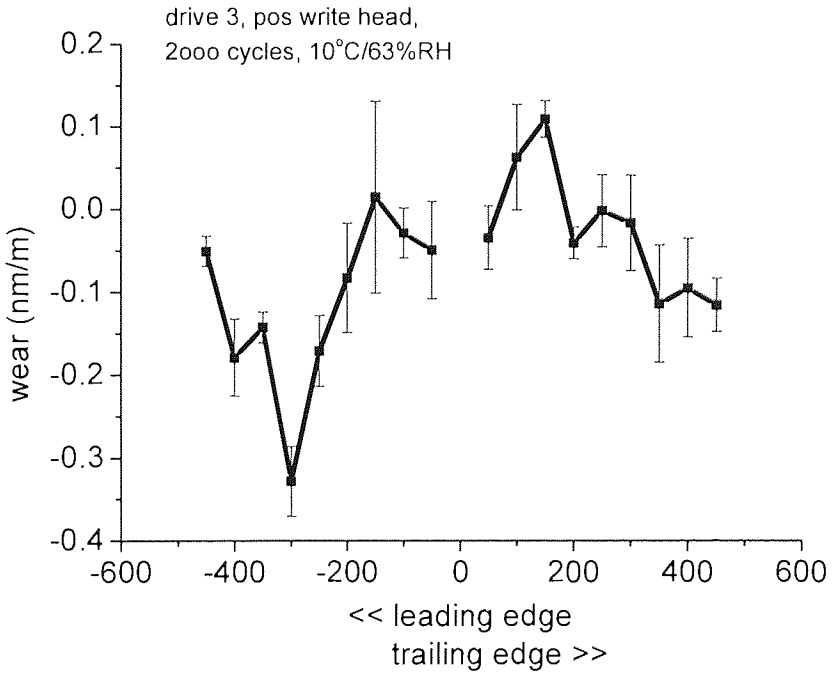

Figure 4-110 Wear of the drive 3 positive write head after 2000 cycles

On the next environmental condition (24°C/25%RH), the wear was found to be greater, on both types of heads. The trailing edge of the heads seems to wear more compared with the leading edge, similar to what was found for DDS-3 heads.

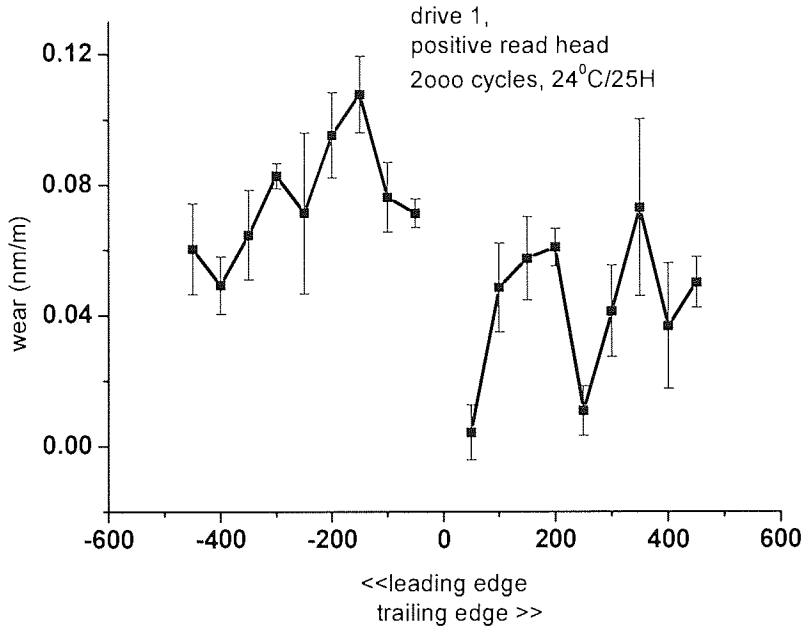

Figure 4-111 Wear of the drive 1 positive read head after 2000 cycles

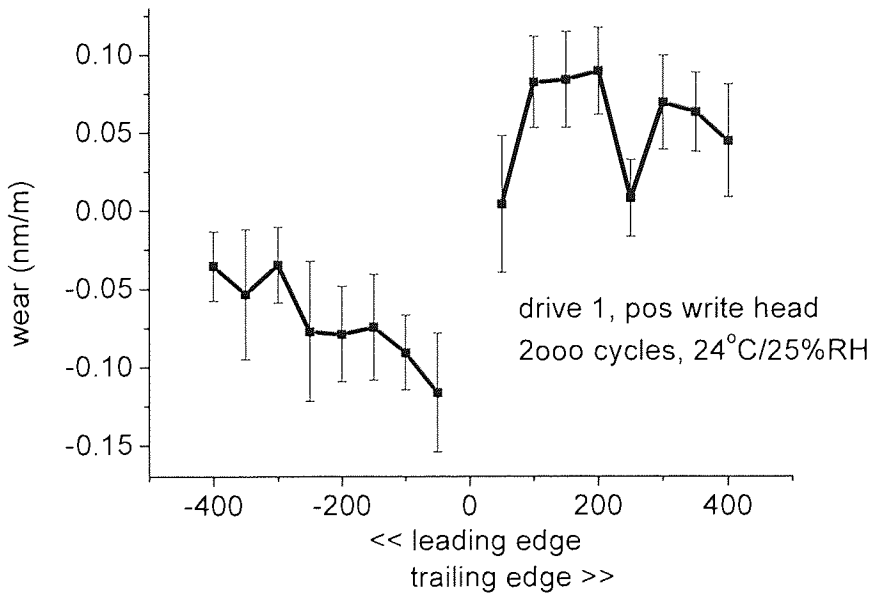

Figure 4-112 Wear of the drive 1 positive write head after 2000 cycles

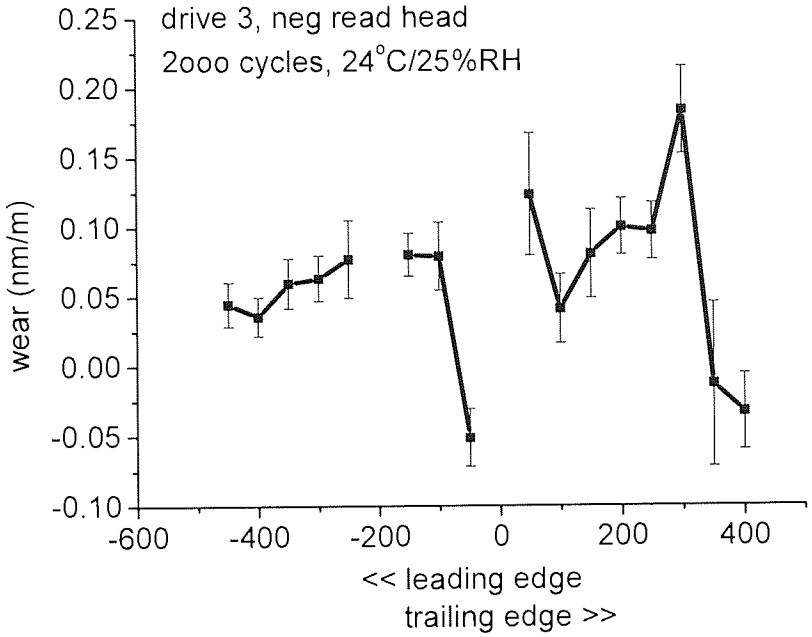

Figure 4-113 Wear of the drive 3 negative read head after 2000 cycles

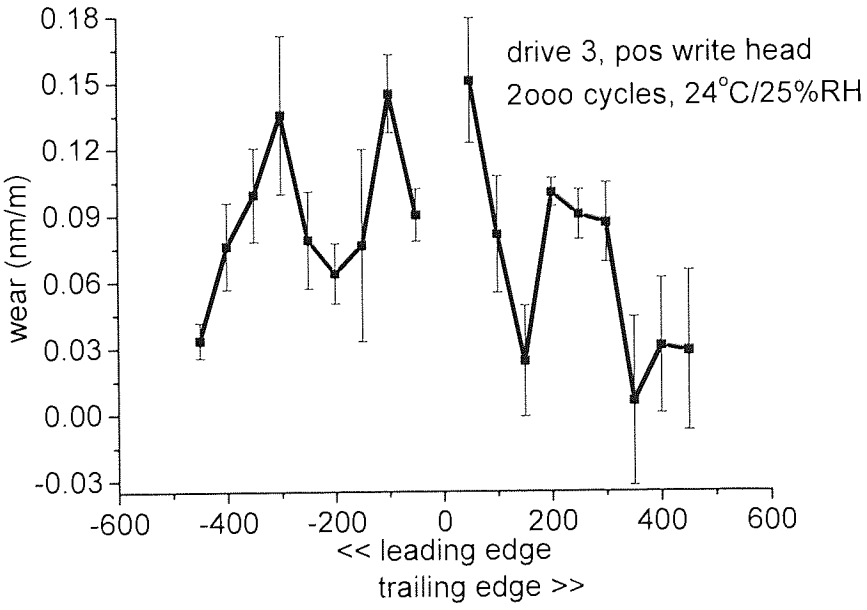

Figure 4-114 Wear of the drive 3 positive write head after 2000 cycles

In the last condition tested (41°C/12%RH), the wear rate was the highest and comparable with the rate of the DDS3 drives. The wear seems to be higher on the trailing edge of the head, except on the drive 3's positive write head.

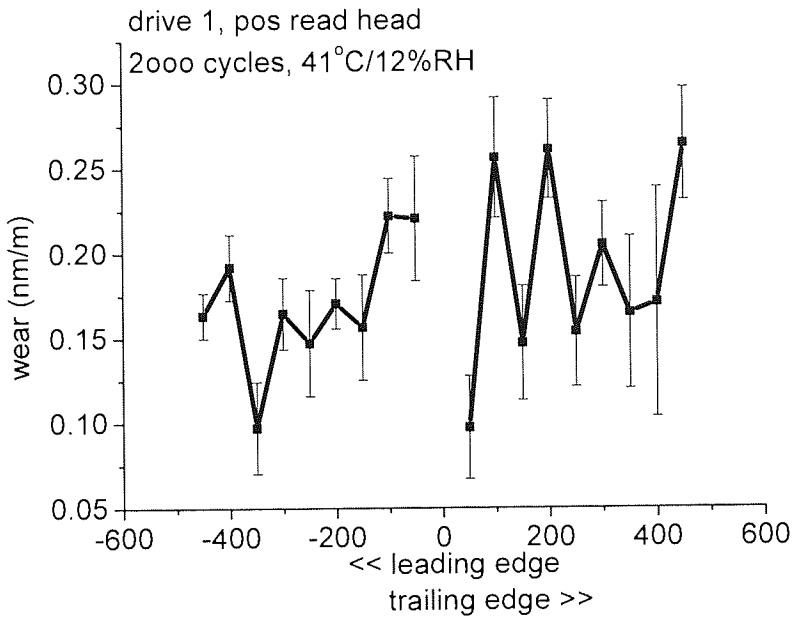

Figure 4-115 Wear of the drive 1 positive read head after 2000 cycles

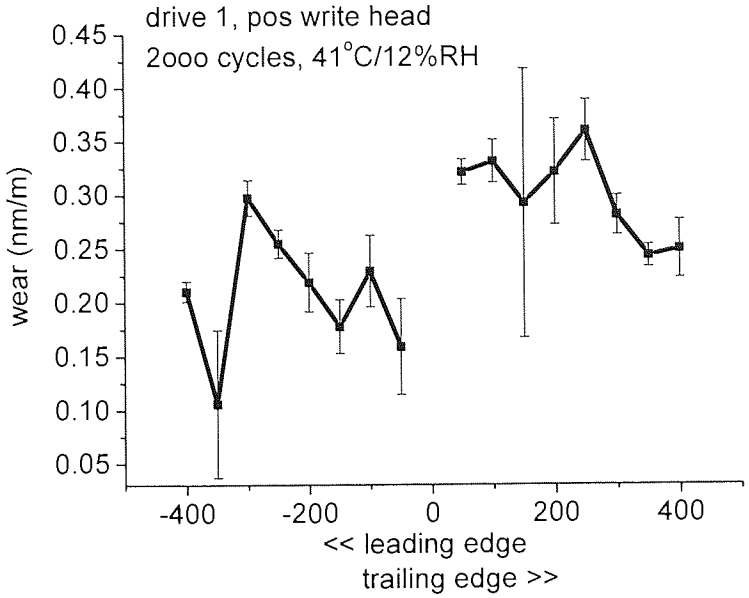

Figure 4-116 Wear of the drive 1 positive write head after 2000 cycles

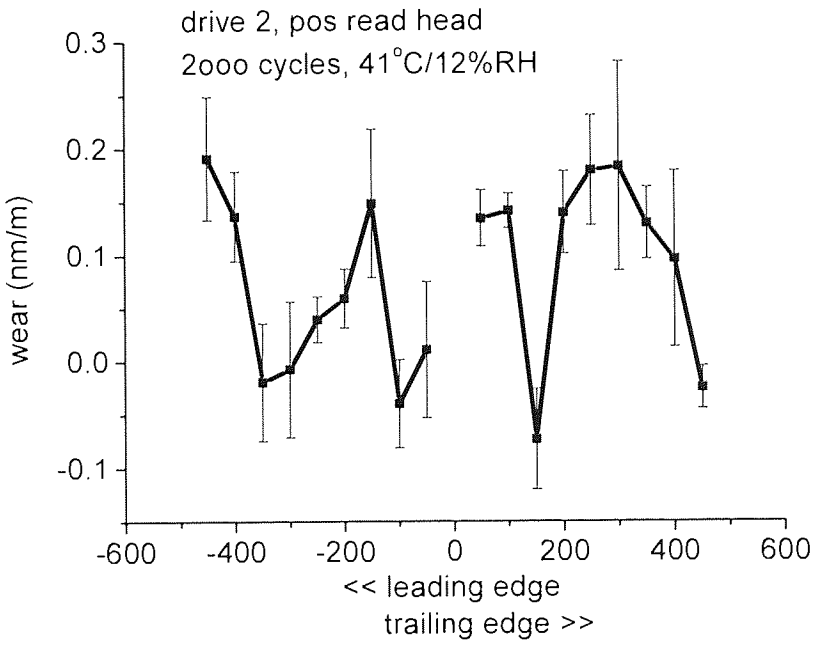

Figure 4-117 Wear of the drive 2 positive read head after 2000 cycles

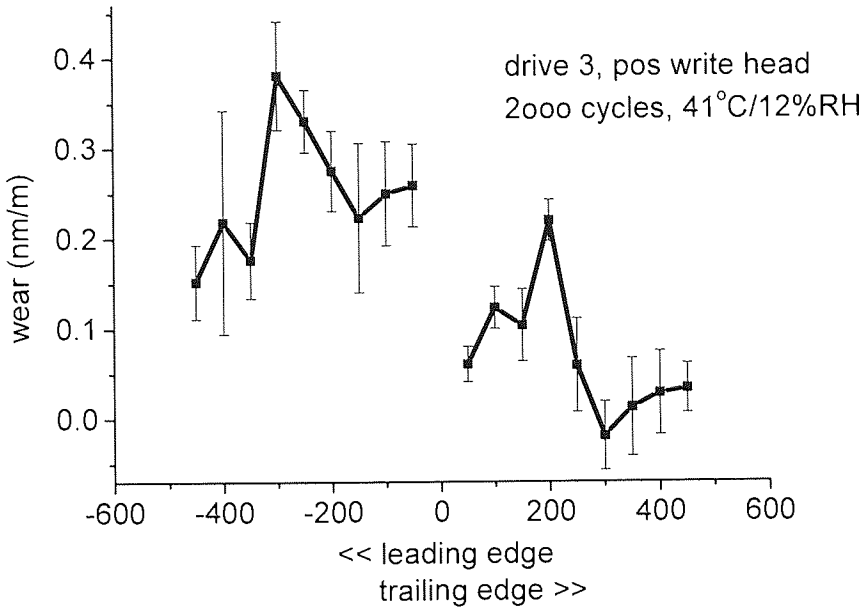

Figure 4-118 Wear of the drive 3 positive write head after 2000 cycles

Based on the preliminary results obtained, no influence on the total amount of water present in the atmosphere was found, and most probably, the wear rate is determined by the relative humidity.

5 A proposed model of stain formation

5.1 Theoretical background of the model

The theory of dispersion and dipole-dipole interaction may describe well several adhesion phenomena such as wetting, adsorption, interdiffusion in the case of interaction of low surface energy liquids or solids. However, in the case of high-energy substrates such as those composed of metals, metal oxides, or silicates and the polymer adhesive, another model - ionic and covalent bonding - describes better the interactions. The vast majority of these models assume that a hydrated oxide surface is covered by a multimolecular layer of physically adsorbed water. These surfaces are hydrophilic and the thickness of adsorbed water depends on temperature and the partial pressure of water in the atmosphere [144]. Most metal surfaces with the exception of Au and fresh surface of Hg show thick layers of oxides of 40 to 80Å at ambient conditions rather than the metal lattice. Although the oxide layer may be dehydrated and dehydrogenated by radical treatments involving high temperature, high vacuum, and ion bombardment, at ambient conditions the oxide layer is hydrated to present a high density of hydroxyl groups. The hydroxylated oxide layer readily adsorbs and strongly retains a multimolecular layer of physically adsorbed water. Common metals, metal oxides or silicates surfaces all display these general surface properties. However, the type of interaction of these surfaces with the polymeric adhesives varies greatly upon the surfaces involved. [144]

On the other hand, polyurethane polymer are susceptible of degradation when exposed to elevated temperatures or high humidities. The reaction by-products can further interact with the ferrite surface and with acicular particles. These phenomena lead to different behaviour of polyurethanes regarding their adherent properties.

5.1.1 Ferrite surface of the magnetic head

As with all iron and iron oxides, ferrites tend to develop a thin layer of iron oxihydroxide (FeOOH) on their surface when the surface is exposed to moisture. In

moist air as well as in water with traces of air, iron is rapidly oxidised to give a hydrous oxide, which gives no protection since it flakes off, exposing fresh surfaces. The process of hydrolysis occurs no matter whether the surface exposed is made of iron or its oxides [95]. Similar corrosion phenomena were seen by others [46, 45, 44] but when investigating the acicular magnetic particles exposed to atmosphere.

Under normal conditions, the iron oxihydroxide is amorphous, resistant to prolonged exposure to vacuum and decomposes at 136°C [42, 43, 44, 45]. Studies made using XPS and infrared techniques showed that the thickness of oxihydroxide layer increases in time at constant humidity due probably to its porous characteristic and with the increase in humidity [46]. This oxihydroxide or other hydrated by-products that result during a tribochemical reaction may also act as a solid lubricant, reducing friction coefficient between head and tape [47, 48].

Since the iron oxihydroxide is a soft material [95], it can be easily removed by the tape during the normal operation of the DDS drive.

Although no other studies of the occurrence of oxihydroxide on ferrite have been made, it is safe to assume that it ferrite will undergo a similar corrosion process since the ferrite is composed mainly from Fe_2O_3.

5.1.2 Adhesion in the case of binder polymer and iron oxides

The interactions between binder polymer and acicular magnetic particles are complex and are dominated by physical and chemical interactions. The binder is mainly an adhesive, its role being to maintain cohesion between the magnetic particles and the substrate. The theory of adhesion suggests that adhesive must be attracted to the adherent by forces like hydrogen bond, van der Waals (dipole moment interaction), although primary chemical bonds may be formed and are desirable [16, 52, 98, 99, 100, 113].

The polyurethane polymers used in tape binder contain atoms and functional groups that may act as electron donors (N, O) and others acting as hydrogen (proton)

donors (NH groups of urethane and urea). In addition, these polymers contain groups having strong dipole moments such as carbonyl groups. As a result, this class of polymers makes a good candidate to bond to a large class of polar adherent materials such as metal, glass, plastics, wood and leather [72]. However the presence of these functional groups is not sufficient and another condition must be fulfilled in order to obtain a good adhesive: the geometric relationship between adhesive and adherent. For example, if the active sites, the potential points of interactions on the solid surface are 10Å apart while the active centres in the polymer are 14Å, only a very small percentage of potential interaction will take place. [72]. This condition is even more important when the adhesive touches only the asperities of the surface rather than having a complete contact with the surface. This is why, in order to obtain good adherent properties between the binder and acicular magnetic particles on one hand and between binder and substrate on the other, the tape manufacturers use various methods to increase the real area of contact and to increase the number of active sites. Such methods were mentioned before and include [16, 52, 98, 99, 100, 101, 102]:

- for tape substrate: corona discharges or plasma treatments to increase real surface area and generate unsaturated bonds;
- In the case of iron acicular particles, surface treatment with aluminium, silicon and phosphorus to increase the number of active sites since these elements behave as electron donors;

The interaction between the binder and the metal particles can be through hydrogen bonding if both polymer and the iron particles have acid sites but in modern tapes, it is an acid-base interaction since the chemical bonds are much stronger thus improving interparticle adhesion and minimising particle shedding [64, 65]. It has been proven that the surface of the passivated iron particles behaves as a base mainly due to the iron oxihydroxide (FeOOH) sites on its surface. In this case, the binder reacts with oxihydroxide on the surface, cleans the surface, and bonds to the surface by primary or secondary valence forces by means of ureas linkages. [66, 72] Additionally, the coupling between the basic sites of the metal particles and acid groups of the binder such as phosphoric acid groups or alcohol groups leads to strong hydrogen bonding between the hydroxyl groups of polymers and particles [59, 67].

The polar groups introduced within polyurethane binder to react as "anchors" (wetting agents) for iron acicular particles are usually -COOM, $-SO_3M$, $-OSO_3M$, $-P{=}O(OM)_2$, $-O-P{=}(OM)_2$ where M could be a hydrogen atom or an alkaline metal salt or group [52]. The phosphates groups reacts better with the active sites of the metal particles or ferrite, however the amount of the functional groups must be optimised since a higher level of functional groups tends to deteriorate the hydrolytic stability of the polymer. [68] On the other hand, the binders containing aromatic isocyanates groups with hydroxyl groups are found to be more reactive than those containing aliphatic isocyanates. [69]

Additionally, the interaction between binder and the substrate is through active sites such as unsaturated bonds or hydrogen bonds, artificially created using various surface treatments methods such as plasma or corona discharges.

5.1.3 Binder stability

One of the main issues of the binder and in the same time with the magnetic tape is the ability of the binder to retain adherent properties when the tape is subjected to various conditions. In particular, it is important that the binder should remain stable and retain its adherent properties at environmental conditions occurring during normal operation of the magnetic tape. Such environmental working conditions include humidity up to 80%RH and temperatures up to 50°C [140]. In fact, the binder must stand even harsher conditions since it is known that flash temperatures may reach up 400°C at contact points between the tape and the magnetic head [10, 51, 88]. From this point of view, the polyurethane based polymers are not the best choice since they can be unstable and degrade. A higher chemical stability can be achieved by increasing the degree of cross-linking between polymer chains but this leads to higher hardness and reduced elasticity of the polymer binder. Increased van der Waals attractive forces results as well in higher hardness, and modulus and a marked increase in permanent elongation as well. [72] However, in the context of the tape binder, a high modulus and high hardness may not desirable, and an optimum must be achieved. Hence, for the magnetic media industry a trade-off solution must be reached

allowing the binder to maintain good mechanical and adherent properties while in the same time chemical stability remains satisfactory.

The chemical alteration of the binder is considered the primary source for the tape breakdown [75]. Degradation of the polymer binder may affect the corrosion of the metal particles, worsening their magnetic properties. [71]

As mentioned before, the main components in the binder systems are polyurethanes and vinyl copolymers. It is agreed that PVC environmental degradation is mainly due to photochemical degradation caused by ultraviolet exposure. The estimated degradation energy is at 75kcal/mol [134]. The stability is greatly enhanced by the lack of branches in the polymer chain structure. On the other hand, polyurethanes being branched polymers are much more prone to interact chemically with other reagents such as water or iron.

It is obvious that these polymers can undergo the same chemical reactions as their monomers, isocyanates. Chemically speaking, an isocyanate is a compound which has in its composition at least one urethane functional group (NCO). The chemistry of the urethanes is complicated but some reactions are emphasised here in particular those with water and those triggered by elevated temperature.

5.1.3.1 Thermal stability of the binder polymer

The thermal stability of isocyanates varies greatly with their structure but it has been pointed out that the most resistant urethanes decompose at 150-200°C whereas some of them decompose as low as 50°C. A polyurethane thermal decomposition reaction would cause rupture of the polymer chains or even de-polymerisation [76]. The most important reaction channels of decomposition are given below:

1. dissociation to isocyanate and alcohol:

$RNHCOOR' \leftrightarrow RNCO + R'OH$

2. formation of primary amine and olefin:

$RNHCOOCH_2CHR' \rightarrow RNH_2 + CO_2 + R'CH{=}CH_2$

and

3. formation of secondary amine:

$$RNHCOOR' \rightarrow RNHR' + CO_2H$$

4. above 100°C the urea and less rapidly urethane groups may react with isocyanate groups to give biuret and allophanate branch points respectively:

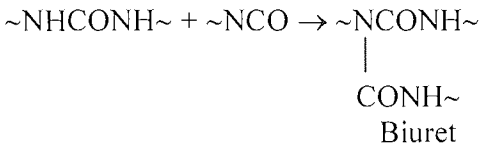

Biuret

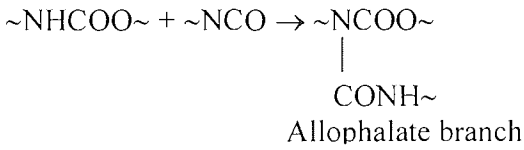

Allophalate branch

The end reaction products have more unsaturated chemical links, and as a result, these resulting by-products have higher adherent properties than the reagents.

A comprehensive study on the degradation channels focused specifically on binder polymers used in tapes upon different environmental conditions was made by Edge and co-workers [63]. If the humidity is low (below 25-30%RH), the thermal degradation is more likely to occur. The polymer chain is splitting off with formation of an amine, carbon mono and dioxide, dissociation into its alcohol and starting components (see above). These molecular components resulted through thermal degradation may react with each other as in eq 4 to give products with yet more unsaturated bonds and hence increased adherent properties. The reactions readily occur above 100°C [72] and such temperatures can be easily surpassed at contact points between tape and head asperities. [10, 47, 51, 57] Direct evidence of chains scission in polyurethane-based polymers as a direct result of the increased temperature was obtained by exposure of unprotected polymer samples in an oxygen bomb at 300 psi (about 20.5 atm) at 80°C for 96 hours. The exposure halved the tensile strength of the polyurethane but did not cause insolubilisation or embrittlement. Furthermore, lose of all mechanical properties was discovered when polymer was exposed to 200°C [72]. Additionally, chemical changes were observed

within the polymer samples by using infrared and ultra-violet spectroscopy. The spectra indicate loss of aromatic structure, urethane group, a loss of C-H structures and indication of formation of a greater variety of "ether" oxygen groups and carbonyl groups. [72] This clearly indicates that in the case of tape binder, degradation occurs during the normal operation of the tape due to heat developed at the head-tape interface.

Below are given representative pathways of the thermal degradation of yet another type of binder polyurethane [63]:

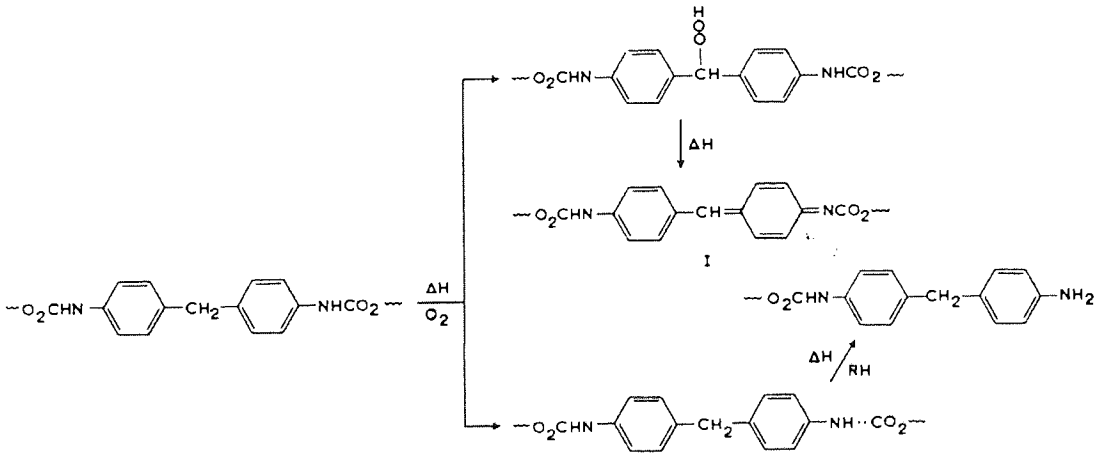

Figure 5-1 Thermal degradation of methylene diphenyl based polyurethane [63]

Apart from chemical interactions between functional groups of the same polymeric chain, hydrogen bonds and van der Waals attractive forces act between polymeric chains. These forces are weaker in their nature than most of the chemical forces hence migration of polymeric chains from the tape to the head is likely to occur.

The influence of the thermal degradation phenomenon of the binder due to chain scission on the magnetic tapes was also investigated among others [63, 66, 75, 76, 126] by Navale who measured that the life expectancy of the tape decreased by three orders of magnitude when the temperature was increased from 20°C to only 40°C. [138]

A quantitative measurement of the degradation through thermal decomposition is given by the reaction constant. The reaction constant measures the variation of the concentration in time of reactants when a certain chemical reaction takes place. In other words, the reaction constant measures the speed at which a certain chemical reaction is occurring. The reaction constant also obeys to the Arhennius law [72], which indicates that the speed of a chemical reaction increases as the temperature increases:

$$K = A \cdot \exp(-E_a/R \cdot T) \qquad \text{Equation 5-1}$$

Where K – reaction constant
A – pre-exponential factor
E_a – activation energy (minimum energy required to produce a chemical reaction)
R- universal constant of gases
T – temperature in Kelvin;

Measurements showed that typical values for polyurethane thermal degradation are [141, 143]:

E_a (kJ/mol)	110 – 191 kJ/mol
A (min^{-1})	$2.2 \cdot 10^6 - 9.7 \cdot 10^{10}$ min^{-1}

Towards elevated temperatures, the reaction constant increases dramatically, which indicates an accelerated process of thermal degradation. A discussion upon different aspects related to this increase is made in the section 6.4.

5.1.1.1 Hydrolytic stability of the binder polymer

A second aspect in the binder stability under environmental conditions is its reactivity with water. It has been shown that water including water from atmospheric moisture plays an important role in the degradation of the main component of the tape binder, the polyurethanes. Cold water does not affect the polymer but prolonged exposure to hot water or steam will affect polyurethanes. Given the fact that flash temperatures between head and tape temperatures can reach up to 400°C [10, 47, 51], it is reasonably to believe that water vapour from atmosphere heated at the head tape

contact points interacts with the binder. Harrington found that boiling polymer for 1000 hours resulted in a loss of 27-100% in the hardness of a variety of polyurethane types, which suggests chemical degradation in particular through hydrolysis. He also indicated that polyether-based elastomers were more resistant to hydrolysis than polyester-based polyurethanes. [72, 135] The degradation process can be represented by the following equation:

$$\underset{\text{isocyanate}}{RNCO} + H_2O \rightarrow \underset{\text{Urea}}{RNHCONHR} + CO_2$$

According to Naegeli et al, the reaction with water follows different routes that will finally lead to the formation of urea:

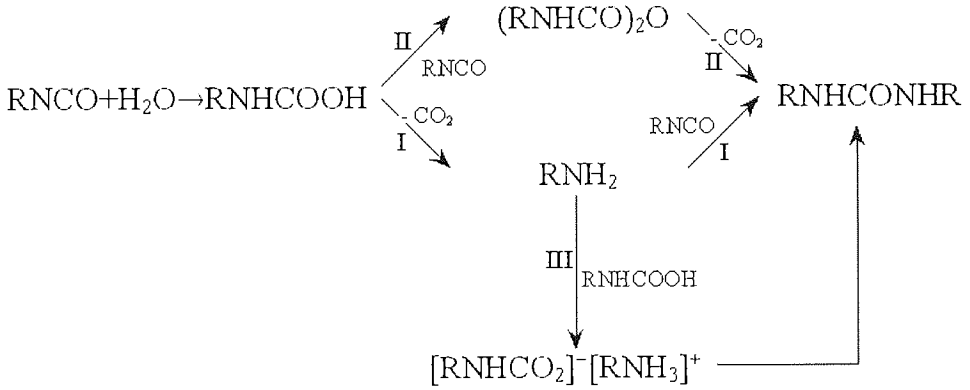

Figure 5-2 Reaction channels between isocyanate and water [21, 72, 73, 74]

In addition, the reaction could be catalysed by tertiary amines many bases and, most important, by some metals or organic compounds of them. The list includes in a roughly descending order of catalytic activity: Bi, Pb, Sn, **Fe**, Cd, Co, Al, Zn, Ni and Cu. [72, 75] More specifically, it was found that Mn, Co and Fe favour thermal degradation of the polyurethane whereas Cr and Cu enhance the thermal stability. In general, it was found that the thermal degradation increases as the amount of the metal ions increases. [136].

Edge and co-workers [63] have been measured that at high humidity, the binder undertakes hydrolysis at polyester compounds according to the reaction below

(Figure 5-3) and any acid produced on hydrolysis of such groups catalyses additional hydrolysis, thus conferring an autocatalytic nature to the degradation reaction.

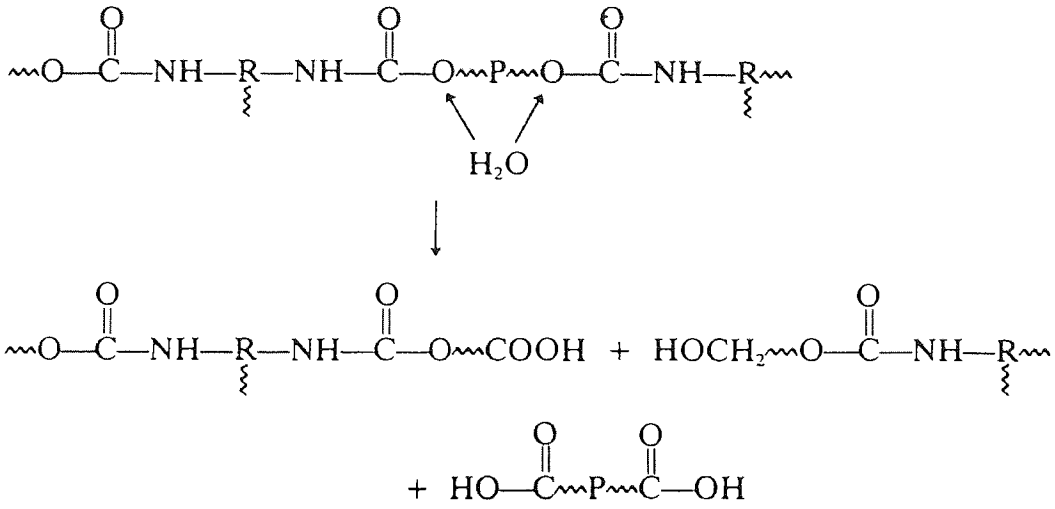

Figure 5-3 Hydrolysis of the tape binder polymer [63]

An increase in chemical stability can be achieved by increasing the number of crosslink sites – by increasing of the so-called degree of cross-linking - between the co-polymers but as said before, the method increases in the same time the hardness and reduces the flexibility of the binder, which is not desirable for use as the magnetic coating. Another method is to use inhibitors that can reduce the rate of binder degradation by trapping and neutralising the reaction products, especially those having an autocatalytic effect.

Several functional groups present in the formulation of the magnetic binder such as biuret, allophanate, urea and urethane groups have bonds that may break as a result of stress. The energy required to break these bonds is situated between 20 and 50 kcal/mol.

Studies on metal particulate tapes under normal ageing conditions, have shown that the reaction constant of hydrolysis for polyurethane, which describes the concentration variation of binder in time when exposed to moisture, is $K=9\cdot10^{-12}min^{-1}$[142] at 30°C/90%RH. A slightly different result, $K=3.5\cdot10^{-12}min^{-1}$, was measured indirectly, through an accelerated aging method, by Yamamoto and Watanabe [143]. At 30°C/60%RH the reaction constant is decreasing to $2.9\cdot10^{-12}s^{-1}$. In

addition, the effect of the temperature on the speed of hydrolytic degradation must be also taken into account given the fact the hydrolytic degradation obeys to Arhennius law as well.

In conclusion, the end result of the hydrolysis effect is the passivation of the chemical "anchors" of the binder used for retaining acicular particles, hence the acicular magnetic particles are becoming loose.

Given the fact that both hydrolysis and thermal degradation may take place in the same time at a given environmental condition, it is crucial to know which type of reaction is dominant in order to explain the behaviour of stains on magnetic heads. In the proposed model, calculations are made to establish the dominant phenomenon.

5.2 A proposed mechanism of stain formation

Based on the experimental findings and on theoretical information available, a model of mechanisms involved stain formation, evolution and destruction is being proposed for the particular case of MP tapes and DDS-3 heads.

According to this mechanism, stain developments on magnetic heads is in a very close relationship with the chemical and mechanical properties and stability of the binder used in tape formulation. The appearance of the stain is also influenced by the head material and by the environmental conditions. Stain does not consist only in metal particles as stated in some previous studies [86] but also in small amounts of binder as the XPS results show (fig 87). The stain structure can be imagined as a brick-and-mortar structure, in which the bricks are the iron particles and the mortar is constituted by the polymer binder. The chemical stability of the binder under different environmental conditions, in particular under high humidity and high temperature dictates whether the stain will form or not, whether it will grow or disappear on the magnetic head.

5.2.1 High humidity

It is well known [63] that the binder polymer is prone to mechanical and chemical degradation. Despite industry's efforts and the use of retardants or stoppers, the process of polymer degradation cannot be entirely stopped, and yet newer polymer binders having better properties are found to be too expensive to be released to the market. It must be noted that big tape manufacturers such as Sony, Maxell or Fuji are using similar mixtures of polymers as tape binders [16, 52, 98, 100, 101, 113]. Polymer chain scission may be triggered by high temperatures but also by mechanical stress. Hydrolysis may occur after exposure to high humidities. Some of the reaction products and some transitional metals and their oxides like iron and its oxides [63, 116, 126, 136] may behave as catalysts and may further increase the speed of reactions. In all these cases, the result is a loss of the binder's ability to retain acicular iron particles to the substrate. If they do not affect the strength of the bonds between iron particles and polymer, they may affect the integrity of the binder polymer itself. The phenomena have been studied intensively by others. [75]

The degradation channels of the tape binder are different upon the humidity and temperature as shown by Edge et al [63], Naegeli et al, and Moroi et al [136]. Hydrolytic reactions are considered as the dominant mode of binder breakdown towards higher humidity and moderate temperature. The ester linkages of the binder are most susceptible of hydrolytic attack from moisture (see also fig. 6-2, 6-3). Although the rate of hydrolytic degradation is relatively low at room temperature, it increases dramatically when hot water or steam is in contact with the binder polyurethane. The reaction by-product, urea, is in turn soluble in water [43], hence it has very low adhesivity to the surfaces. The degradation through hydrolysis is significant at 100°C as shown by Harrington [27] and temperatures of this order of magnitude and well above are encountered frequently at head-tape contact points when tape is sliding against the tape as demonstrated by Sullivan [10] and Bhushan [51, 88]. At the tape head interface temperatures can reach up to 400°C [10, 47, 51] at the contact point asperities, therefore the water vapours will interact with the binder polymer inducing hydrolysis.

In fact, several studies use boiling water to perform accelerated tests in order to investigate life expectancy of the magnetic tapes [75, 137]. By extrapolating the results of these accelerated tests, life expectancy of the tape is found to decrease due to hydrolytic degradation by three orders of magnitude when the humidity is increasing from 30 to 75%RH, from 3.5 to just little more than a half a year even at 20°C [138]. Moreover, any acid produced during hydrolysis catalyses additional hydrolysis, thus conferring an autocatalytic nature to the degradation channel. The by-products of chemical degradation have lower molecular weight and have less or no unsaturated bonds, and are soluble in water [43] therefore in terms of physical properties indicates reduced or no adherent properties. Therefore, through hydrolysis, the binder looses its ability to bond, to adhere to surfaces. Magnetic particles from tape or from the adhesive debris on the magnetic head are shed, hence the removal of previously formed stains from the magnetic head seen at high humidity. Aditionally, water is also responsible for passivating unsaturated bonds on the ferrite surface so making transfer film formation very unlikely. This process may also lead to the production of loose iron/binder particles. These debris particles then become 3rd bodies between head and tape, leading to abrasive wear and increasing the wear of the head [85, 86, 88].

In the same time, as the humidity increases, water vapour chemically interacts with the ferrite of the head and forms a very thin layer of iron hydroxide (FeOOH) (figs 73-80). Since iron hydroxides are soft materials and they tend to flake off, they are easily removed by the tape asperities. A new fresh layer of ferrite being exposed, the process continues. Therefore, no material transferred from the tape can adhere to the ferrite head. The rate of material removal from the heads is higher than the rate of deposition in this case. This phenomenon is also responsible for higher rates of head wear observed by some authors towards higher humidities and confirmed by our experiments (figs 27-28, 114).

According to equation 3-6, the water pressures at the above mentioned environmental conditions are:

Environmental condition	Water vapour pressure (kPa)
20°C/10%RH	0.234
20°C/30%RH	0.702
20°C/75%RH	1.754

For a given volume, considering in a first approximation that the water vapours obey to the law of an ideal gas, the amount of water ratio is:

$$\frac{m_{75}}{m_{30}} = \frac{p_{75}}{p_{30}} \cong 2.5$$

Where:

m_{75} is the mass of water at 75%RH;

m_{30} the mass of water at 30%RH;

p_{75} water vapour pressure at 75%RH;

p_{30} water vapour pressure at 30%RH;

Therefore, the amount of water at 75%RH is more than twice that of 30%RH, hence accelerated hydrolysis of the polymer binder, hence the decrease of the life expectancy of the tapes.

Experimental studies on metal particulate tapes under normal ageing conditions, have shown that the reaction constant of hydrolysis for polyurethane, which describes the concentration variation of binder in time when exposed to moisture, is $K=9\cdot10^{-12}min^{-1}$[142]. A slightly different result, $K=3.5\cdot10^{-12}min^{-1}$, was measured indirectly, through an accelerated aging method, by Yamamoto and Watanabe [143]. Further analysis shows the variation of the reaction constant upon environmental conditions:

Temp (°C)	Humidity(%RH)	Reaction constant $K_H(min^{-1})$
20	65	$5.6 \cdot 10^{-13}$
30	60	$2.9 \cdot 10^{-12}$
30	90	$3.4 \cdot 10^{-12}$
40	60	$1.2 \cdot 10^{-11}$
40	90	$1.4 \cdot 10^{-11}$
50	60	$4.4 \cdot 10^{-11}$
50	90	$5.3 \cdot 10^{-11}$
65	60	$2.7 \cdot 10^{-10}$
65	90	$4.1 \cdot 10^{-10}$
400	60	$5.3 \cdot 10^{-9}$ (*)

Table 5-1 Computed values of the reaction constant for binder hydrolysis (after 143)

(*) –Extrapolated data;

There are several important conclusions that can be drawn from the above table:

- The reaction constant is higher at higher humidities and the same temperature; hence, when the relative humidity increases, the degradation of the binder through hydrolysis is accelerated;
- The reaction constant is higher at the same humidity and higher temperatures; this is a direct result of Arhennius law (Equation 2.1-5-1) which describes the variation of the reaction constant upon the temperature;
- Finally, there is an increase of 3 orders of magnitude of the rate of hydrolysis from 20°C/65%RH to 65°C/90%RH as a result of corroborated effects of increased temperature and humidity on binder hydrolysis;

The high rate of binder hydrolysis and the higher rate of iron oxihydroxide formed on the surface of the head explain the absence of stains on the magnetic heads when experiments were performed at moderate and high humidity as well as the removal of stains from the magnetic heads. The formation of iron oxihydroxide on the

head's surface can explain as well higher rates of wear of the heads observed at high humidities.

5.2.2 Low humidity, increased temperature

Towards lower humidity and high temperatures, another process, chain scission of polymer binder is found to increase at an accelerated rate when polymer is exposed to high temperatures. Direct evidence of polymer chain scission was observed at 80°C [72] and indirect evidence of chain scission has been seen also at 100°C [72, 116] and one has to bear in mind that even higher temperatures of up to 400°C are achieved at the contact points between tape and head due to friction [10, 51, 88]. The degradation of the binder occurs this time by formation of allophalate branches and biuret (eq 4). Having more unsaturated bonds, these by-products give a sticky, gummy property of the degraded binder [63]. In spite the fact that tape manufacturers use inhibitors [16, 101, 113] to reduce the rate of autocatalytic reactions, the phenomena cannot be avoided given the current polymers used as tape binders and the mechanical requirements for the binder. It was found that the rate of degradation through chain scission increased by three orders of magnitude when temperature was raised from 20 to 40°C at 30%RH [138].

It is well known that the reaction constant of polymer degradation obeys Arrhennius law:

$$K = A \cdot \exp(-E_a/R \cdot T) \qquad \text{Equation 5-2}$$

Where K – reaction constant
A – preexponential factor
E_a – activation energy (minimum energy required to produce a chemical reaction)
R- universal constant of gases
T – temperature in Kelvin;

Measurements showed that typical values for polyurethane thermal degradation are [141, 143]:

E_a (kJ/mol)	110 – 191 kJ/mol
A (min^{-1})	$2.2 \cdot 10^6 - 9.7 \cdot 10^{10}$ min^{-1}

If we consider $A=2.5 \cdot 10^6$ min^{-1}, $E_a=133$KJ/mol, then at a temperature of T=300K (27°C) we find the reaction constant:

$$K_{300} = 2.5 \cdot 10^6 \exp\left(-\frac{133 \cdot 10^3 J/mol}{8.31 Jmol^{-1}K^{-1} \cdot 300K}\right) = 16.9 \cdot 10^{-18} \text{ min}^{-1} \qquad \text{Equation 5-3}$$

If we are doing the same calculations for a temperature of 400K (~123°C) and 700K (~423°C), a temperature usually achieved at the contact points between tape and head, we obtain:

$$K_{400} = 2.5 \cdot 10^6 \exp\left(-\frac{133 \cdot 10^3 Jmol^{-1}}{8.31 Jmol^{-1}K^{-1} \cdot 400K}\right) = 10.5 \cdot 10^{-12} \text{ min}^{-1} \qquad \text{Equation 5-4}$$

and

$$K_{700} = 2.5 \cdot 10^6 \exp\left(-\frac{133 \cdot 10^3 Jmol^{-1}}{8.31 Jmol^{-1}K^{-1} \cdot 700K}\right) = 2.94 \cdot 10^{-4} \text{ min}^{-1} \qquad \text{Equation 5-5}$$

The reaction constant at 700K (K_{700}) is much higher than that of 300K (K_{300}), which means that the thermal degradation is much faster.

$$\frac{K_{700}}{K_{300}} = 1.74 \cdot 10^{13}$$

The chain scission of the binder seen by many [63, 66, 75, 76, 126] does not affect the chemical functional groups used as anchors for iron particles (see section 2.5.2). Therefore, in the near surface of the tape, both iron particles and the binder itself will become easily detached by the shear forces developed during motion at the tape-head interface. The adhesion forces (van der Waals, electrostatic forces) will attract the binder and iron particles towards head surface where the binder will interact with the ferrite of the head through these unsaturated bonds re-creating strong

chemical bonds. Friction may supply additional energy required to re-create these chemical bonds. On the head side, after a polishing process at the beginning made by the tape, low humidity will ensure that there is very little FeOOH on the surface, leaving it chemically active towards reaction with the binder polymer. The same chemical forces of adhesion between the iron particles in the binder on the magnetic layer formulation will act between binder polymer and the surface of the head to create strong chemical bonds.

The higher rate of polymer degradation through chains scission towards higher temperatures together with the path followed by the degradation of the binder polymer easily explains the higher amount of stains observed on the magnetic heads at high temperatures during the experiments.

5.2.3 Comparison different phenomena at a given environmental condition

It is very important to compare which phenomenon – hydrolysis or thermal degradation – is dominant at various environmental conditions. If we compare the rate of degradation through hydrolysis with that of thermal degradation, considering the reaction constants found above, at 30°C, one can find:

$$\frac{K_H}{K_{300}} = \frac{2.9 \cdot 10^{-12}\ \text{min}^{-1}}{16.9 \cdot 10^{-18}\ \text{min}^{-1}} \cong 1.72 \cdot 10^{5} \qquad \text{Equation 5-6}$$

which means that hydrolysis (K_H), is the main mechanism of degradation at low temperatures. Taking into account the reaction channels presented and the fact that the reaction by-products have saturated bonds, therefore no adherent properties, one can explain why no stains are seen at these temperatures. Once the binder looses its adhesivity, the iron acicular particles will easily detach from the tape and from the stains, become third bodies entrapped between head and media and accentuating the wear of the magnetic heads.

At elevated temperatures (in this case 400°C) and low humidities the phenomena are reversing:

$$\frac{K_H}{K_{700}} = \frac{5.3 \cdot 10^{-9}\ \text{min}^{-1}}{2.94 \cdot 10^{-4}\ \text{min}^{-1}} \cong 1.8 \cdot 10^{-5} \qquad \text{Equation 5-7}$$

$K_H << K_{700}$ therefore at these temperatures, the chain scission phenomenon is much more important than hydrolysis. Also, taking into account that the reaction by-products of this chemical reaction have unsaturated bonds, it can be easily explained why stains appear and are seen at high temperature.

These calculations confirm many experimental findings [63, 66, 75, 76, 126, 137, 138] that hydrolysis is taking place at lower temperatures and moderate humidities and chain scission is responsible for degradation of the polymer binder towards high temperatures and low humidities.

In the following flow chart is a synthesis of the proposed mechanism is given. The proposed mechanism can explain why large amounts of stain are observed at low humidity whereas at high humidity these stains disappear or they are not forming on the surface of a head. The higher wear rate measured towards higher humidities is, according to the proposed model, a direct consequence of the development of a thin layer of soft material on top of the head surface and higher wear generated by the loose particles through third-body abrasion. In addition, taking into account that certain metals may catalyse the binder degradation, it may explain why some metals (Ni) were seen to inhibit and others (Cu, Fe) to exacerbate the amount of stain generated by the metal particle tape as seen by Liew [87], Lemke [32] and Bhushan [86] when experimenting with heads made from different metal materials. However, it must be pointed out that only iron oxides (ferrite) are used commercially as head material.

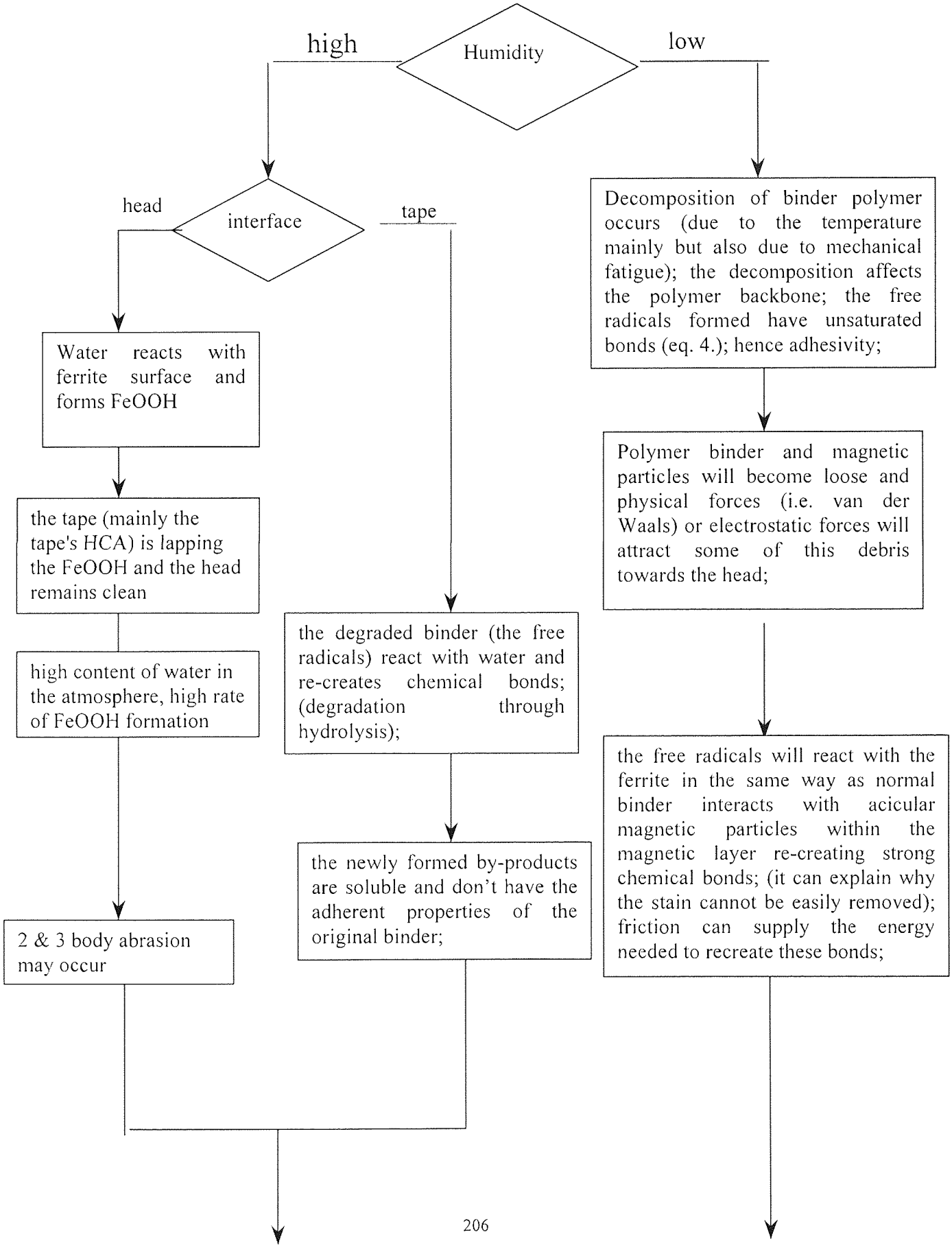
Humidity
high
low
interface
head
tape
Water reacts with ferrite surface and forms FeOOH
the tape (mainly the tape's HCA) is lapping the FeOOH and the head remains clean
high content of water in the atmosphere, high rate of FeOOH formation
2 & 3 body abrasion may occur
the degraded binder (the free radicals) react with water and re-creates chemical bonds; (degradation through hydrolysis);
the newly formed by-products are soluble and don't have the adherent properties of the original binder;
Decomposition of binder polymer occurs (due to the temperature mainly but also due to mechanical fatigue); the decomposition affects the polymer backbone; the free radicals formed have unsaturated bonds (eq. 4.); hence adhesivity;
Polymer binder and magnetic particles will become loose and physical forces (i.e. van der Waals) or electrostatic forces will attract some of this debris towards the head;
the free radicals will react with the ferrite in the same way as normal binder interacts with acicular magnetic particles within the magnetic layer re-creating strong chemical bonds; (it can explain why the stain cannot be easily removed); friction can supply the energy needed to recreate these bonds;

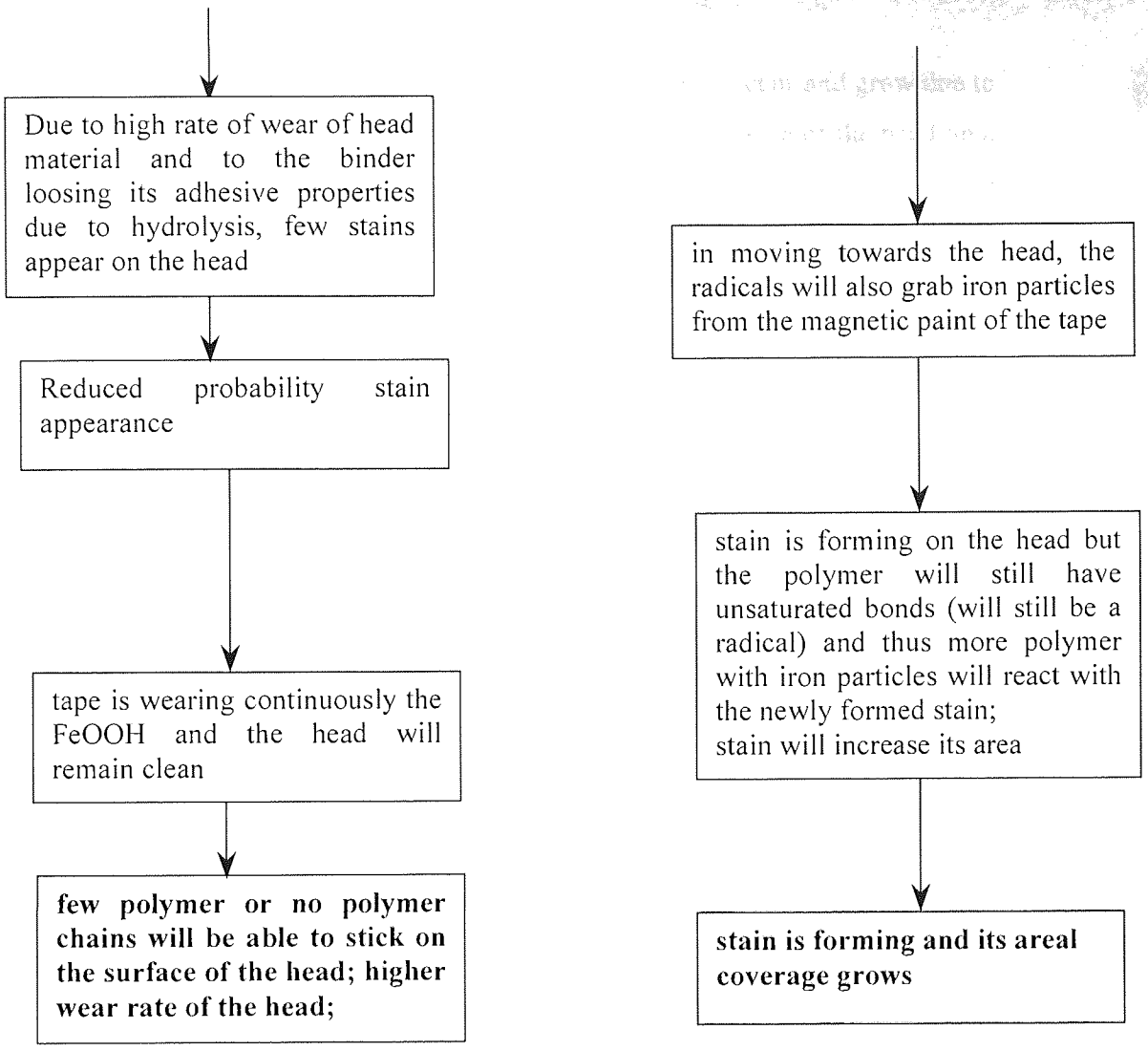
Due to high rate of wear of head material and to the binder loosing its adhesive properties due to hydrolysis, few stains appear on the head
Reduced probability stain appearance
tape is wearing continuously the FeOOH and the head will remain clean
few polymer or no polymer chains will be able to stick on the surface of the head; higher wear rate of the head;
in moving towards the head, the radicals will also grab iron particles from the magnetic paint of the tape
stain is forming on the head but the polymer will still have unsaturated bonds (will still be a radical) and thus more polymer with iron particles will react with the newly formed stain;
stain will increase its area
stain is forming and its areal coverage grows

It has been suggested by some authors [19, 101] that stains occur and grow due to adhesive forces between iron particles of pigment and the iron oxide of the head on a like-on-like basis. The theory cannot explain though the presence of stains on the glass region of the magnetic head nor stains generated by other types of magnetic tapes. However, one should bear in mind that both surfaces of the magnetic particles and head are covered in a thin layer of iron oxyhydroxide that behaves as a base [59, 64, 67, 44, 65]. On the other hand, the type of interaction between the polymer binder and the iron particles or ferrite surface of the head is that of acid base [64]. Being stronger, the second type of interaction is more probable and gives more stability to the newly formed compound.

The stain simulation was able to induce stain on a large area of the ferrite surface thus enabling the use of the very sensitive XPS method to investigate the results. The research was able to show that stains generated by the metal particulate tapes may contain binder polymer in addition to the iron particles. Although in small amounts, the presence of binder polymer in the composition of the adhesive debris is extremely important since the polymer adheres to the head along with iron particles leading to head to tape spacing loss, loss of signal and therefore increased error rate. The chemical stability of the binder polymer under different environmental conditions, especially under high humidity and high temperature, dictates the amount of debris generated by the metal particulate tape and the may influence the delicate balance of the stain dynamic process of formation and removal.

The stain is not an unwanted phenomenon anymore in today's tape drive's, it has been proven that if it forms a continuous thin layer it can reduce dramatically the friction between head [32, 86] and tape therefore understanding its mechanisms can help controlling it and leading furthermore to improvements in tape's storage density. Keeping the amount of stain deposited on the heads under control proved to be however difficult and one key towards higher data densities is to reduce the amount of stains generated by the magnetic tapes.

The proposed mechanism can explain why large amounts of stain are observed at low humidity whereas at high humidity this type of debris disappear or they are not forming on the surface of a head. Strong adhesivity of the stains on the magnetic

heads can also be explain taking into account strong chemical bonds that are forming between surface at the head and binder polymer. The higher wear rate measured towards higher humidities is, according to this model, a direct consequence of the development of a thin layer of soft material on top of the head surface and higher wear generated by the loose particles. In addition, taking into account that certain metals may catalyse the binder degradation, it may explain why some metals were seen to inhibit and others to exacerbate the amount of stain generated by the metal particle tape.

5.3 Mathematical considerations of transfer film formation

The mathemathical model proposed here is based on the model presented by Myshkin in a paper [145] published in 2000. Let us consider two plane-parallel surfaces at a distance z_0 one from the other as in figure below. On the surface situated at z_0 from origin particles appear with their concentration following a given temporal law $\Psi(t)$, which will be described later and are deposited on the other surface situated at origin. Also, the interfaces move tangentially at a certain speed.

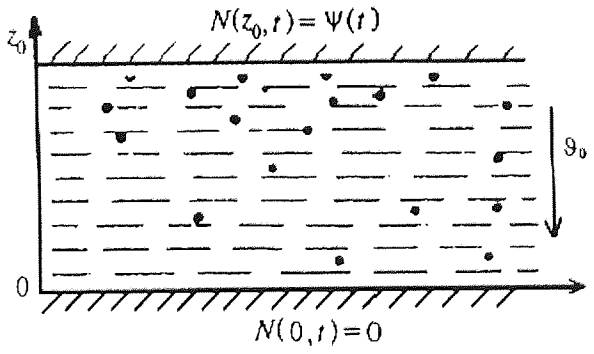

Figure 5-4 Model of mass transfer in a friction contact [145]

This setup aproximates very well the tape surface shedding iron/binder particles and the head surface. Under such circumstances, the law that describes the variation of the particles concentration along z axis is:

$$\frac{\partial N}{\partial T} = D\Delta N + v_0 gradN$$ Equation 5-8

Where N – is the concentration of particles

T – temperature

D –diffusion coefficient

v_0 – velocity of the particle

The equation describes particle movement due to diffusion and convection components respectively. The diffusion component is related to the amount of particles generated at the surface z_0, (the magnitude of wear) and the convection component is related to the movement due to additional fields that may be present at the interface such as electric or magnetic field. In a first approximation we will neglect these fields, although sometimes they can be quite important [145]

The speed of the particles can be evaluated using the Reynolds number:

$$R_e = \frac{v_0 z_0}{\nu}$$ Equation 5-9

R_e – Reynolds number;

ν - kinematic viscosity;

Kinematic viscosity is defined as:

$$\nu = \frac{\eta}{\rho}$$ Equation 5-10

η - dynamic viscosity;

ρ - density

Hence, we find the speed:

$$v = \frac{\eta R_e}{\rho z_0}$$ Equation 5-11

The Reynolds number is below unity for speeds up to 100m/s when z_0 is small (around μm) [145].

Under stationary conditions, the concentration varies upon depth z, and temperature T. Another variable not encountered yet is time t. Hence we can write

N=N(z, t, T) The boundary conditions when resolving an equation such as Equation 5-8 are very important. Another problem is when the concentration at $z=z_0$ is a function ψ dependent of time as in the case of tape-head interaction as we shall see below.

As discussed previously (see section 5.2), there are two main phenomena taking place at the head tape interface at different environmental conditions: polymer chain scission that leads to adherent debris and hydrolysis leading to a loss of binder adhesivity. One can safely suppose that the amount of particle generated is directly proportional with the amount of degraded polymer at a certain environmental condition. Hence, the chain scission will increase the concentration of particles (binder polymer and magnetic particles) at the surface z_0 whereas hydrolysis would decrease it by removing these particles (particles would become loose and will be removed by tape movement). These two phenomena can be quantified, as previously seen, by means of reaction constant: K=dN/dt defined as the variation of the concentration of a given substance in time. Thus, we can estimate theconcentration of particles at the interface z_0:

$$\psi(t)= \int(K_T - K_H)dt \qquad \text{Equation 5-12}$$

with t – time

K_H – reaction constant of polymer hydrolysis;

K_T – reaction constant for binder thermal degradation;

Also, one has to take into account that K_T, K_H obey Arhennius law (see Equation 5-2), hence:

$$\psi(t)= \int\left[A_T \exp\left(-\frac{E_{aT}}{RT}\right) - A_H \exp\left(-\frac{E_{aH}}{RT}\right)\right]dt \qquad \text{Equation 5-13}$$

With:

A_T, A_H – pre-exponential factors for polymer thermal degradation and hydrolysis respectively;

E_{aT}, E_{aH} – activation energy for thermal degradation and hydrolysis;

R – universal constant of gases;

For a given temperature T, the initial (boundary) conditions are:

$$N(0,t) = 0;\ N(z_0, 0)=N;$$

The amount of deposited substance at z=0 (in our case on the head) is:

$$Q=\int_0^t Jdt \qquad \text{Equation 5-14}$$

Where J is the flow at the surface having coordinnate z=0:

$$J = D\left(\frac{\partial N}{\partial z}\right)_{z=0} \qquad \text{Equation 5-15}$$

The diffusion coefficient can be estimated from hydrodynamic theory as being:

$$D=kT/6\pi\eta r_0 \qquad \text{Equation 5-16}$$

k - Boltzmann's constant,

η - dynamic viscosity of polymer

r_0 – radius of particles (in the case of DDS2 magnetic particles, 0.18μm);

Due to the fact that $\Psi(t)$ is linear in time, the solution of the Equation 5-8 can be found using Fourier series. Thus, in our case, the general solution describing the phenomena of deposition and the amount of deposited substance on the surface at z=0 will be:

$$Q=\sum_{i=1}^{n}\left\{A_i t + B_i t^2 + C_i \exp\left[-\frac{\pi^2 D}{4z_0^2}t\right]\right\} \qquad \text{Equation 5-17}$$

with A_i, B_i, C_i being coefficients dependent on D, z_0, and T, and indirectly through $\Psi(t)$ and reaction constants to relative humidity.

Hence, the amount of stains "arriving" on the magnetic head depends largely on the equilibrium that is established between the hydrolysis and thermal degradation. Due to the limited time, we were unable to test this model using the experimental results.

6 Discussion

6.1 *The ERT, AFM and wear experiments*

It has been found that the environmental conditions employed during the experiments influence the error rate. The fluctuation of the error rate seen for all the drives tested at the beginning of the experiments (figs 4-1 to 4-19) was caused by the poor conformity of the tape to the head. These fluctuations cannot be due to adherent or loose debris since AFM scans show for example at 25°C/35%RH that head poles are clean after 100 cycles (figs 4-37b, 4-38b, 4-39b, 4-40b) whereas the error rate graphs display fluctuations of them (see figs 4-1 to 4-4). It is more likely that minute changes of the head curvature, tape tension, wrap angle or other physical properties of the tape such as elastic modulus occur when using different head-tape assemblies thus increasing head to tape spacing and increasing the number of random errors. As the experiments progressed, the conformation of the head improved, the head profile was re-adapting to the new conditions, due to wear and the fluctuations disappeared. Further variations of error rate were caused mainly by loose or adhesive debris. At high humidities (above 35%RH) the error rate decreased and remained at low levels throughout the experiments. At low humidities, after the fluctuations at the beginning, the error rate increased steadily as may be seen in figs 4-5 to 4-8.

AFM scans show at high humidity the ferrite poles of the heads to be clear throughout the experiment, with a few patches of stain of 2-4nm in height present. The height of the stain was too small to induce a significant signal loss, therefore the reduced error rate. The amount of deposit present on the glass region remained below the level of the poles hence had no influence on the signal output. Abrasion marks were visible along the glass region (see 4-37b, 4-38b, 4-40b) caused either by third-body abrasion or by two-body abrasion generated by the head-cleaning agents contained within the magnetic layer of the MP tape. On the other hand, AFM scans of the tape show the presence of the head-cleaning agents after 1000cycles (fig. 4-35) and it is known [52, 98, 99, 100, 101, 112, 113] that these particles are the only

particles with a higher hardness than the Mn-Zn ferrite. These experiments have confirmed a previous finding that stains seldom occurs at high humidity [27, 86, 28].

An interesting feature, similar to those reported by Chandler et al [111] and Harrison et al [114] appeared at 5°C/80%RH. The topography of the heads shows ripples on the poles of one head and what looked to be plastic flow on the other (figures 4-44d and 4-43d respectively). They are different from the usual stains found on heads and they are believed to be generated by a micro stick-slip process, also evident in noise measurements performed by Chandler [27]. There are not very often found on magnetic heads and, as Chandler [27] pointed out, they are generated by a particular configuration (couple) of tape and head. The measurements we performed found their height between 2 nm and 5 nm in good agreement with Chandler's measurements. The glass region shows patches of stain and sometimes scratches generated probably by third bodies entrapped between head and media. The scratches seemed to have been made in a layer of stain. The observation is based on the fact that during the experiments the height between the ferrite poles and the neighbouring glass decreased. It is unlikely that this phenomenon was caused by pole-tip recession but rather by accumulated adhesive debris on the glass region. The measured size of the scratches was between 10 and 16 nm (fig 4-43c, 4-51a, 4-51b). By the end of the experiments, the scratches disappeared being removed by high wear rate as the measurements show (see below).

In terms of wear, high humidity was responsible for the high wear rate measured for the heads. The highest overall wear was measured at 5°C/80%RH and a precise value could not be measured since the indents disappeared after just 1000 cycles. However, it can be said that the rate was at least 1.7 nm/m. A reason for such high wear was the cumulative effect of temperature and humidity. High humidity was responsible for generating the FeOOH at high rates on the surface of the ferrite as discussed later and in the same time lower temperature increased crystallinity of the polymer binder, increasing the elastic modulus of the polymer thus increasing the wear rate. Tape manufacturers choose the glass transition temperature of the polymer binder between –50°C and 100°C [52, 99, 100, 101, 113, 98] but usually it is between 35°C and 90°C [52]. Studies [38, 29] have shown that wear of single crystal ferrite

increases rapidly with the decrease of the temperature due to the increase of the elastic modulus of the tape binder. Hence, the binder polymer became stiffer, increasing the tape abrasivity and ultimately leading to an increase of wear. The wear profile of the heads show the rate was higher towards the trailing edge of the head compared with the leading edge. It was showed that this is the result of the debris accumulating towards the trailing region of the heads and producing third body abrasion [86]. This type of abrasion is more effective in terms of material removal rate compared with the polishing process or two-body abrasion [17, 18].

At low humidity, the behaviour of the drives was different. The error rate increased during the experiments especially when the temperature was elevated. At low temperature, although the rate fluctuated, the error rate had low values (fig 4-9 to 4-12). AFM scans showed that stains tend to accumulate at the beginning on the glass regions of the head since these regions are recessed compared with the ferrite poles and low error rate was recorded (figs 4-43 to 4-49). Stains start as magnetic particles and binder shed from the tape due to binder polymer degradation and then adhere to head surface as physical (i.e van der Waals or hydrogen bonds) and later chemical interactions between head material and binder polymer take place. Frictional heat can provide enough energy to trigger the formation of chemical bonds on the head surface. After filling the glass region, stains grew on the ferrite poles, the spacing between head and media increased and error rate started to increase. However, the amount of adhesive debris deposited on the heads was lower at 10°C compared with 45°C since at the end of the experiments the glass region was more recessed at 10°C (22nm compared with 2-3nm at 45°C). This could be the result of the temperature-induced transition of the tape binder from rubber-like at high temperature to glass-like polymer [22, 20, 77, 62] that resulted in increased tape abrasivity towards lower temperatures. The increased abrasivity resulted in increased rate of stain removal from the ferrite poles. Another phenomenon, the temperature-exacerbated chain scission of the polymer binder within the magnetic layer of the tape resulted in more material and iron acicular particles being shed from the tape, thus more stains. Studies [63] show that at high temperature the binder is prone to chain scission whereas at high humidity the most probable process occurring is polymer hydrolysis.

Although the method used to measure the roughness of the heads is scale and instrument resolution dependent, it gave some indications on the processes occurred during the experiments. At high and moderate humidity, the roughness decreased or reached certain equilibrium. The phenomenon occurred either because the heads were stain free during the experiments or because the layer of the stain was continuous or covered only the depressions. At low humidity and high temperature (45°C/15%RH), the staining process of the heads was accelerated and large amounts of stain were formed on the heads. Under these conditions, the roughness of the heads increased continuously.

In the same time, the wear measured was very low due to stains adhering to the surface of the head and acting as a lubricant of the head-tape interface. The lubricating role of the stain was for the first time seen by Lemke in 1979 [63] and his findings showed that the friction coefficient decreased by as much as 100 times when stains occurred on the heads. Since larger amounts of stain were generated under this environmental condition (45°C/15%RH), the tape was wearing the stains not the head material and hence stains were protecting the head materials. In equilibrium state, even though the rate of stain deposition is higher at 45°C/15%RH, the rate of stain removal can increase as well so that a steady state (equilibrium) is attained but at higher amounts of stain on the heads. On some occasions, (10C/10%RH) the wear rate fluctuated around zero with the leading edge having a slightly higher wear rate (0.05nm/m) towards the trailing edge.

The wear rate of the materials is directly proportional with the normal load which is about 69.85mN for DDS3 drives corresponding to 39.2mN tape tension and a tape wrapping angle of 120°. Taking into account that the glass region is recessed compared with the ferrite region, the normal load hence the wear rate of the glass will be lower. During the experiments the wear rate of the ferrite was measured using the indentation technique and in this particular environmental condition (10°C/10%RH) was low therefore the wear of the glass region will be even lower. On the other hand, the AFM scans showed that height difference between glass and ferrite is decreasing from about 25nm to 15nm as the experiment progressed. Since the wear of ferrite is very low, the decrease of height difference could have come only if the glass regions

were gradually covering with debris. Taking into account that the heads were carefully wiped using cotton applicator and alcohol fact that removed much of the loose debris, the conclusion is that these must have been adhesive deposits (figs 4-32, 4-33, and 4-49) and that they tend to form a uniform and continuous layer.

The wear rate seems not to be related with the amount of water present in the atmosphere, but rather with the relative humidity (figs 4-20 to 4-33) or temperature. It has been showed that the temperature influences the stiffness of the tape [62]. Overall, the wear rate is higher at higher humidities than at low humidity. At high humidity, the ferrite reacts with the moisture [41], so the surface of the ferrite will be covered with a soft, thin layer of FeOOH as XPS studies have shown (figs 4-73 to 4-76). Since the oxyhydroxide is a soft and porous compound [46], this layer is easily removed due to the abrasivity of the tape and new layer of ferrite is exposed. The phenomenon continues, leading to a higher wear rate. At low humidity, the surface of the ferrite will be covered by a layer of adhesive debris that behaves as a lubricant and protect the poles of the head against further wear. Under these conditions, the rate of adhesive debris deposition is slightly higher than the rate of removal and the abrasivity of the tape will ensure a constant level of stains on the heads.

6.2 AFM scans of the tape

Several AFM scans of DDS-2 tapes were taken during the experiments revealing changes in topography as a result of wear. The virgin tape showed small bumps between 10 and 20 nm in height due to probably metal particles being engulfed in the polymeric binder and lubricant. As the tape worn, the top layer of polymeric binder and lubricant is removed revealing crystals of SiO_2 and/or Al_2O_3 that are used in the tape formulation as head cleaning agents (see figs 4-34 to 4-36). At the end of 5000 cycles, the crystals disappeared due to shear forces occurring at the head tape interface and wear of the tape during the operating of the drive revealing a series of depressions on the surface. These depressions are specially designed during the manufacturing process of the tape in order to facilitate the lubricant migration from the bulk magnetic layer towards the surface but also to prevent adhesion of the tape

surface to the recording head [63]. The continuous replenishment with lubricant is necessary since the top layer lubricant is generally removed during the operation of the tape. The phenomenon occurs at all environmental conditions but the speed of migration towards the surface is temperature dependent as Nishida et al have shown [79]. In order to maintain a constant friction force and to reduce the wear of the heads, constant amounts of lubricant must be present on the surface of the tape.

6.3 SIMS analysis of the tape and DDS-3 heads

The SIMS analysis of the tape revealed the presence of the iron from the acicular magnetic particles and a very characteristic pattern of organic compounds that are present in the tape formulation as polymeric binders, lubricants etc. Given the multitude of organic components used in magnetic layer formulation of the MP tape, it was difficult to identify a pattern characteristic to a specific organic polymer. The negative spectrum revealed the presence of chlorine most probably part of vinyl-chloride copolymer that was used in the tape binder formulation. Despite the small number of analysed heads, the spectra have given good indication of the composition of the adhesive debris. The presence of small amounts of organic material is good evidence that the transferred film may contain organic materials. The presence of cyano group (CN) as a result of polyurethane breakdown enhanced the hypothesis that stain may contain binder polymer. The analysis implied destroying the drum and removing the magnetic head from it. Given the very limited amount of heads it was not possible to extend the research to the full range of temperature and humidities that were used during the research therefore heads that were running under two extremes environmental conditions, namely high and low humidity were chosen.

6.4 AES analysis of the DDS-3 heads

The AES analysis has given strong evidences of the presence of the iron within the stain formulation. Due to the fact the this analysis involved dismantling the drum and removing the head, a limited number of heads where investigated and a analysis of the heads running a full range of temperature and humidity was not

possible. The spectrum of a reconditioned head shows no iron presence on the glass region whereas on the stained head, the iron presence is evident. All stained heads analysed had smaller or larger amounts of iron on the glass regions. The results confirm previous researches performed by others [86, 115, 10, 94, 91] showing that stains consist of acicular iron particles from the MP tape. The amount of iron seen on the glass region of the stained heads varied but one has to bear in mind that stains have a patchy feature and some areas of the glass region might have been stain free.

In addition, the results show the high rate at which carbon contamination is taking place even under high vacuum conditions (below 10^{-8}mbar and with liquid nitrogen trap). The carbon peak was removed by etching but after several minutes after starting the experiments, the carbon peak regained its height.

Apart from carbon, oxygen and iron, the AES spectra did not show the presence of other elements in particular nitrogen and chlorine. The negative result was probably caused by several factors:

- Patchy feature of the stains, hence small amount available for investigation;
- relative low sensitivity of the AES method
- the relative small amount of these elements even in the tape formulation. Indeed, the XPS analysis of the tape showed that the relative concentrations of nitrogen and chlorine are only 0.9% and 4.7% respectively.

In addition, the chlorine copolymer is unstable under electron and X-ray bombardment and has a tendency to decompose in high volatile by-products, in particular HCl. [116, 12]

In the case of the reconditioned head, AFM showed no signs of stain and the AES analysis showed no iron presence in the glass region. In the case of the stained heads where high temperature and low humidity was used, all heads investigated showed the presence of iron on the glass region therefore AES experiments proved that the stains consist of iron. Taking into account that AFM showed that stains occur on the ferrite poles as well as on the glass region, it can be concluded that one of the stains main constituents are iron particles.

6.5 Ferrite behaviour at high humidity

Due to the size of the heads, further analysis using a more conclusive method such as XPS was not possible so a way of simulating on a larger surface of the processes that occur at high and low humidity was conceived. On the other hand, despite its sensitivity, SIMS technique does not allow the quantification of an element or the identification of the chemical interactions between elements.

After exposure to high humidity, a fresh layer of FeOOH with adsorbed water was observed. The presence of FeOOH was furthermore confirmed by analysing the ferrite sample after heating them above 100°C but below 136°C, the decomposition temperature of the hydroxide. Similar results were obtained by others [46, 45, 44] but when investigating the acicular magnetic particles. Taking into consideration this observation it is reasonable to assume that a similar phenomenon occurred on the ferrite poles of the magnetic heads when exposed to high humidity.

In moist air as well as in water with traces of air, iron is rapidly oxidised to give a hydrous oxide, which gives no protection since it flakes off, exposing fresh metal surfaces. The process of hydrolysis occurs no matter whether the surface exposed is made of iron or its oxides [95]. Thus, the simulation performed by boiling the ferrite samples accelerated the process of hydroxide formation, increasing the amount of material available for analysis and did not change the nature of interactions. The iron oxyhydroxide being a soft material [95] it can be easily removed by the tape during the normal operation of the DDS drive.

These results allowed to build a model of the phenomena taking place on the head side when exposed to high humidity. When the drives were exposed to these kinds of environmental conditions, the ferrite poles were covered by a thin layer of oxyhydroxide. Since the oxyhydroxide can be easily removed, after starting the experiment tape running on top of these poles was able to remove it. A clean and chemically active layer of ferrite being exposed, the process of formation of oxyhydroxide continued. The phenomenon probably occurred at all humidities, however the amount of oxyhydroxide depends on the relative humidity being higher

towards higher humidities. That means that more ferrite material was transformed into oxyhydroxide hence more material removed and higher wear.

The higher rate of wear observed at higher humidities could explain why the ferrite poles remained stain-free during the experiments under these environmental conditions (see figs 4-37c, 4-38d, 4-40c, 4-45d, 4-47d). This can also account for higher wear rates (see figs 4-27, 4-28) measured for the heads running tapes in high humidity atmospheres.

To conclude, in the case of fresh ferrite surfaces exposed to high humidity a process of corrosive wear (chemical wear) was found to be taking place followed by abrasive wear due to the tape. At lower humidities, the corrosive wear also takes place but at a much slower rate since the amount of water vapours is reduced.

6.6 *Ferrite behaviour at high temperature and low humidity (stain simulation)*

Stain simulation using the ferrite samples and the loop tester was able to induce staining as one can see from figure 4-90 and figure 4-91.

By using computer simulation and interferometry, Muftu and Kaiser [117] showed that that on a flat head the tape might actually form a "tent" and not being in contact with the surface of the flat head. According their model, the distance between head and tape varies between 50 and 100nm on both high and low tape speed used during the simulation. Since the head protrusion of a DDS drive is around 40nm [139, 140], the magnetic tape would not have touched the ferrite without biasing the ferrite. The electrostatic forces developed helped pulling the tape towards the ferrite surface. The amount of stain generated at low tape speed was higher due to higher time the tape ran before snapping (2 days compared to 3 hours at high tape speed).

It is unlikely that the stains generated by biasing the DDS-2 ferrite will differ dramatically from those generated under normal working condition of a DDS drive since the energy of the adhesive bonds of the stains to the surface is very high (up to 10eV) compared with the energy due to electrostatic charging which is about 0.2eV. The latest value was computed for two layers separated by less than 30nm at room temperature and taking into account Novotny calculations [64]. Moreover, studies on the adhesive properties of the polymers on surfaces show that the electrostatic forces arising on the interface between an adhesive layer and the substrate are not significant and they cannot account alone for the strong adhesion properties. Strong adhesion properties are mainly the contribution of the chemical bonds and van der Waals forces. [118, 64]However, electrostatic charging may occur on the ferrite surface taking into account the friction forces between the tape and the magnetic head and that the ferrite is an insulator. Hence, biasing the ferrite bars did not change substantially the working conditions of a magnetic head occurred in a DDS drive.

One type of stain was induced using DDS-2 tape at high speed and its features are very similar to the stains seen earlier on the ferrite poles of the DDS-3 heads. There are small patches of 14nm height and the ferrite substrate with its familiar polishing scratches can still be seen. (figs 4-82 and 4-83)

The second type of stain was induced using a slow moving DDS-2 tape and is a continuous layer probably more than 21 nm thick. These features are probably similar to those seen on the glass region of the heads. Wear tracks in the direction of the tape movement can be clearly seen. Also, there is a clear difference (see Figure 4-85) between the tracks on the clear ferrite surface oriented randomly and that were produced during a polishing process and the wear tracks generated by the tape that are parallel to the direction of tape movement. However, based on the XPS results, it is believed that the later are produced in a thick layer of stain and not on the ferrite surface. The depth of these tracks is 24-30 nm therefore the layer of stain must have been at least 30 nm thick (figure 4-84). In figure 4-85, an AFM scan of the boundary region between clear and stained ferrite is shown. In one occasion, features of 2-5 nm in height were seen (figure 4-43) but they are not stains but more probably plastic flow of polymer binder and tape lubricant. As Chandler pointed out [111] these features occur only at a particular tape-drive assembly and not on a regular basis.

Once the tape or drive is changed, the phenomenon is not occurring anymore. Taking into account that the experiments used different tapes, it is possible that one of these tape had slightly different mechanical properties that triggered the apparition of these ripples. Indeed, after finishing the experiment and changing the tape, the ripples did not appear anymore.

DDS head protrusion is about 40nm as pointed out by various authors [139, 140]. Muftu and Kaiser simulations [117] show that the distance between head and tape is changing according to the tape speed: it is about 50nm at low tape speed and increases to 250-300nm towards high tape speeds. Hence, the probability of a loose particle to be transferred from the tape to the head decreases as the distance between head and tape increases with the increased tape speed. This behaviour can explain the differences seen between the ferrite surface topographies but also higher amounts of chlorine and other tape specific materials measured when tape ran at low speed compared to high speed.

SIMS analysis confirmed the presence of amounts of chlorine and organic compounds for magnetic heads running at 45C°/10%RH. In the negative range of the spectra, radicals such as chlorine, cyano, and CNCl that are specific to the binder polymer were found. Apart from iron coming from the ferrite and acicular magnetic particles, the positive spectrum showed for the heads running at low humidity the typical pattern of polymers.

By using XPS technique, the chemical composition of these deposits on both ferrite samples was investigated even in more detail. In both cases, the presence of chlorine and nitrogen was detected, elements not previously seen on the clear ferrite surface. These elements constitute a clear indication of binder presence, most probably degraded binder polymer. Chlorine and nitrogen were seen on all ferrite samples running at 45°C/10%RH whereas the original and reconditioned (25°C/80%RH) ferrite bars did not display them. The amount of chlorine and nitrogen varied, being larger for the ferrite where the tape ran at low speed and for a longer period of time, which indicates larger amounts of stain generated. The finding was also confirmed by the AFM scans performed on these samples.

These experiments were able to show that the adhesive deposits generated by the MP tapes consist in binder polymer as well, not only acicular iron particles as previously seen. These results were possible by successfully generating stains on a much larger ferrite surface (more than $2mm^2$) than the usual heads (usually less than $200\mu m^2$) and using a powerful technique such as XPS to analyse it. Previously employed techniques were using SIMS or FTIR on magnetic heads hence small surfaces and hence very limited amounts of stains were analysed.

However, the investigations performed by Chandler [115] using ToF-SIMS found iron presence but *no clear evidence of binder* within stain formulation. The research used stained heads and prior to analysis, the heads were sputtered using Ar in order to remove environmental contaminants. In addition, the analysis also revealed presence of materials, other than iron that are generally used by the tape manufacturers in extremely low amounts (less than 0.1%) to improve wettability of iron particles.

There are several outstanding differences between ToF-SIMS and XPS experiments though. Firstly, it has to be pointed out that prior to SIMS experiments the stained surface of the head was cleaned using sputtering. It is well known that in a mixture of elements, preferential sputtering of elements may occur due to difference in sputtering rates of the elements composing the mixture and the phenomenon may change the surface composition. In our case, the stains are a mixture of polymer binder, lubricant and iron oxide acicular particles in a similar way as in Figure 6-1.

However, as one can see from Figure 6-2, due to different sputtering rates, polymer binder might have been removed preferentially during the preparation steps of the surface from the top layer of the stains, leaving mainly iron particles. The assumption is based on the fact that different chemical elements or substances have different sputtering rate than others and, particularly in this case the binder probably had a greater sputtering rate compared with iron particles. Other studies suggest that nitrogen may be preferentially sputtered when using Ar. [119] Indeed, measurements show that the sputtering rate of the polymer when bombarded with a 2keV Ar beam can be as high as 10nm/minute [120] whereas the sputtering rate of the iron much

less: around 1nm/minute [121]. Therefore, this particular way of cleaning would have led to an early depletion of the binder from the surface.

To make things worse, the sensitivity of the SIMS method depends upon the element to be analysed. In the table below the relative sensitivity factor of the SIMS method (RSF) for the common elements found within the tape formulation is given [122]. Smaller numbers mean higher sensibility of the method towards that particular element. As one can see, the method has very low sensibility to nitrogen (it is actually one of the lowest compared with all chemical elements) and relative good sensitivity to chlorine, carbon and iron.

Our SIMS spectra showed indeed traces of chlorine on the stained heads (Fig 4-72).

Element	Relative Sensitivity Factor (atom/cm^3)
Fe	10^{22} (positive spectra)
C	10^{22} (negative spectra)
Cl	10^{21}(negative spectra)
N	10^{25}(positive spectra)
Na	10^{20}(positive spectra)
O	10^{22}(negative spectra)
Cu	10^{22} (positive spectra)
Cr	10^{21}(positive spectra)
Al	10^{21}(positive spectra)
Ti	10^{21}(positive spectra)
W	10^{23}(positive spectra)

Table 6-1 Relative Sensitivity Factors for the common elements found in DDS tape formulation; in parenthesis the type of SIMS spectra where the elements are detected

In the same note, the detection limits numbers (also known as areal density numbers) that show the minimum number of atoms on a given surface in order to be detected using SIMS, follow a similar pattern [123] as in the previous table. Copper, chromium, aluminium, titanium and tungsten are sometimes added in very low amounts to improve wettability of the acicular iron oxide particles, and they have a very good detection limit, which explains why they can be traced even though these elements are in very low concentrations. [16, 52, 98, 99, 100, 101, 124]

Element	Detection limit (10^{10} atoms/cm^2)
Fe	0.08
C	5
Cl	20
N	300
Na	0.01
O	N/A
Cu	0.5
Cr	0.05
Al	0.05
Ti	0.1
W	0.2

Table 6-2 Number of atoms per cm^2 needed in order to be detected using SIMS method

The second table of numbers confirms that iron and sodium can be easily detected even in small amount whereas nitrogen and chlorine that would have been

polymer binder markers are much more difficult to detect. Taking into consideration that the amount of polymer binder is less than that of magnetic particles (volume packing density is 55-60% [16]) it is understandable why so few researchers were able to spot it using this apparently high sensitive technique.

During the experiments, since the polymer was now recessed, the signal came mainly from the iron particles, the signal coming from the binder carbon nitrogen and chlorine was being swamped (drowned) by noise. Moreover, a great deal of information from the binder was possibly lost on high aspect ratio features such as recessed binder in between two iron acicular particles due to shadowing effect (see Figure 6-3 and Figure 6-4). This shadowing affect and poor secondary ion extraction from these deep, jagged features resulted in a greatly reduced signal from the crater bottom, hence very poor information about the binder polymer.

These phenomena had a cumulative effect and one would have found very faint evidences of binder presence and would have probably assumed that the organic traces were due to environmental contamination. In the same time by using sputtering, the iron particles were cleaned off and traces of other metals that were added to the acicular particles to improve cohesion were detected. The model could explain why so little evidence was found about binder presence but in the same time very small amounts of elements added to the iron particles to improve their wettability were still traced. Considering that the polymer binder is only fractions of the magnetic pigment of the tape and the low sensitivity of SIMS towards nitrogen and chlorine – key indicators for binder presence – it is extremely difficult to detect the presence of polymer binder within the stain formulation. Hence, very few references of binder within stains on published papers.

In the case of the XPS experiments, the approach was completely different. The cleaning process employed was different, cotton tipped applicator with alcohol and no sputtering. The stained surface was cleaned of loose debris, but no etching was performed. In addition, XPS is non-destructive method compared with SIMS. Hence the stains retained their original composition, hence the difference in the results coming from these two techniques. The area investigated was also much larger (more

than 2 mm^2) than that investigated using ToF-SIMS (only 50x50 μm^2), thus an improved signal-to-noise ratio.

The figures below graphically show the proposed mechanism of binder depletion during stain analysis using ToF-SIMS techniques. The thickness of the stain is greatly increased for the sake of argument.

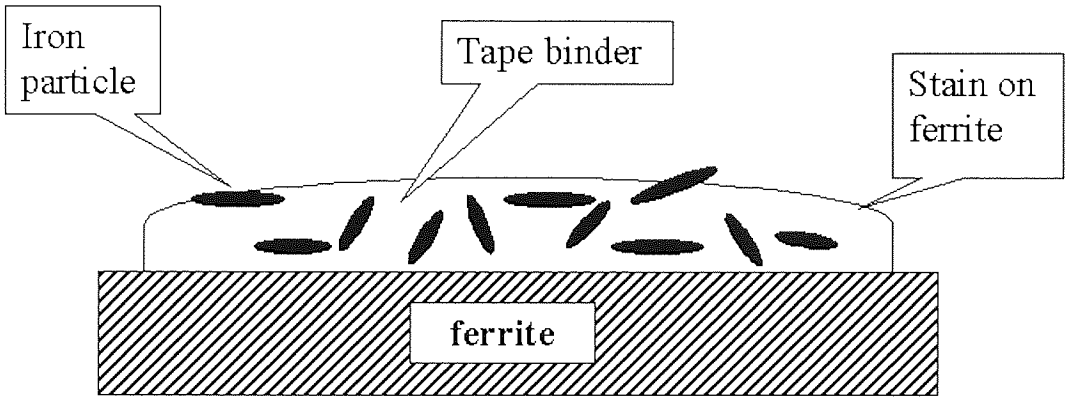

Figure 6-1 Stage 1, the stained surface of the ferrite

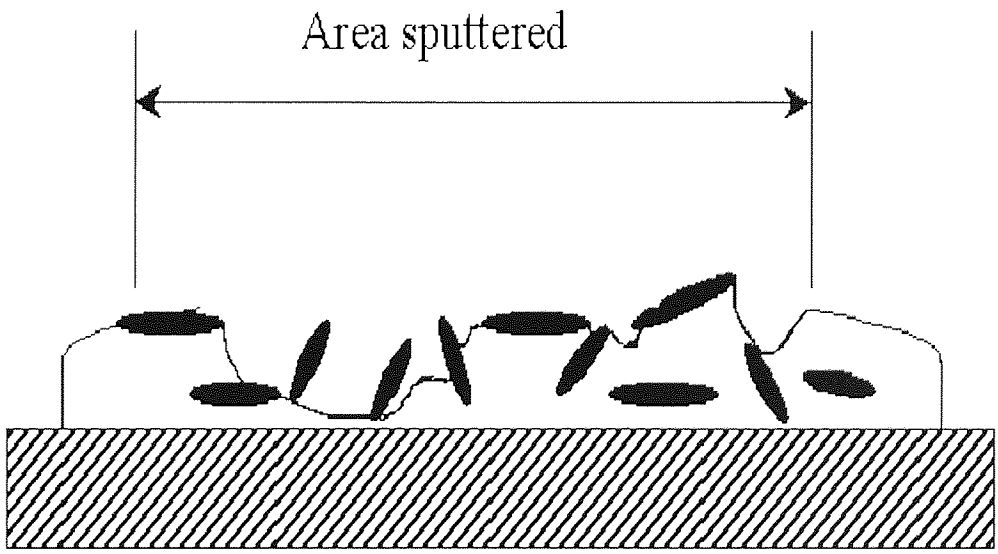

Figure 6-2 Stage 2, after sputtering, due to differences in sputtering rates of iron and polymer, the binder is now recessed and the iron particles are having now a higher profile

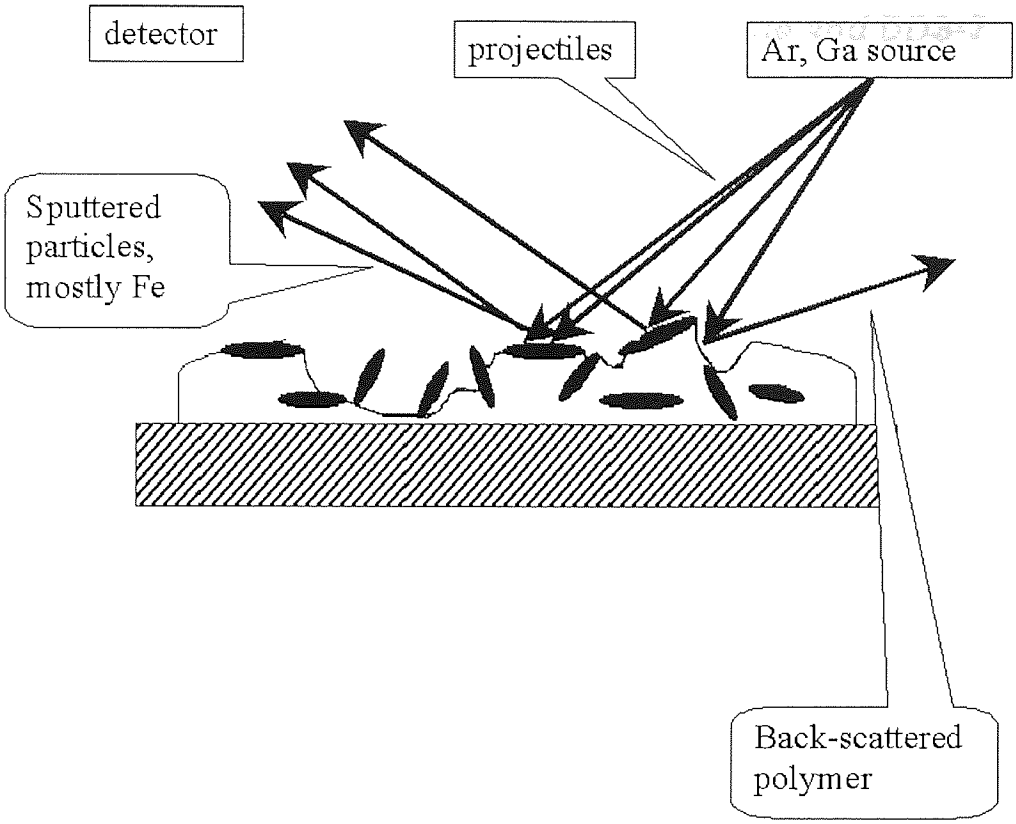

Figure 6-3 Stage 3, before and during SIMS experiment, the signal is mainly coming from the iron particles, that from the binder is either lost due to back scattering or is drowned in noise

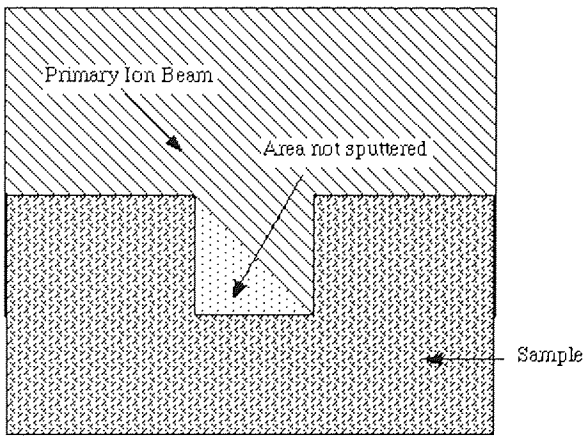

Figure 6-4 SIMS shadowing effect on high aspect ration features [125]

6.7 Surface energy measurements of the ferrite and DDS-2 tape

Although the investigation could not be performed at its full extend due to technical limitations, some remarks can be made from the preliminary results. The surface energy of the ferrite changed after exposure to high humidity. On the other hand, the surface energy of the DDS-2 tape did not change significantly as result of exposure to low humidity.

Surface energy has two components: one is the polar component that basically indicates the hydrogen bonds and van der Waals forces between molecules in the system (mainly adhesive forces) and non-polar (dispersive) component responsible for repulsive forces between molecules. If the contact angle is between the surface and droplet acute, the adhesion (polar) forces are stronger the non-polar forces and there are mainly due to hydrogen bonds as stated by Fowkes [109] The results proved that the surface energy of the ferrite and the tape might vary due to the humidity and temperature changes. The variation may influence the rate of deposition and removal of the adherent debris on the ferrite poles of the magnetic heads. By comparing the adhesion forces of ferrite and tape, one can draw some qualitative conclusions about the probability of a loose particle to migrate towards one surface or to another. If the adhesion forces are higher for ferrites than for tapes surface, then the probability of a particle to stick to ferrite's surface is higher than to tape's surface. On contrary, if the adhesion force is higher in the case of DDS2 tapes, then the probability for a particle to migrate towards the surface of the head will be reduced.

The surface energy can be related with the chemical changes that occur on the surfaces. It can offer information about the probability of a particle to migrate from the tape surface towards ferrite surface. The surface energy measurements were intended to give indications about the trend of the long-range physical forces (van der Waals and hydrogen forces) since one model was supposing that these long- range attraction forces involved in the early stages of stain formation were not van der Waals forces but rather electrostatic ones [115].

The experiments show that the surface energy of the ferrite is different from that of the iron oxyhydroxide. It seems that the surface energy of the tape tends to remain fairly stable with the humidity whereas the surface energy of the ferrite is changing. The surface energy of the ferrite appears to decrease with the increase of the humidity, which may suggest that the adhesion forces were increasing. In particular, the polar component of the ferrite surface is increasing from 1.8mN/m to 2.5mN/m whereas the dispersive components remained constant (about 6mN/m). A theory of stain formation suggests that the stain is forming on the heads due to an increase of the adhesion forces between the head and tape interface as the humidity decreases. However, the preliminary data tend to show the contrary, the adhesion forces seem to increase with the humidity.

Given the amount of data acquired, it was difficult to draw a conclusion and a comprehensive study will be required in order to fully understand the phenomena that are taking place.

6.8 The wear rate at the same water pressure

In the study concerning the influence of the water pressure on the general wear of the DDS-4 heads, no influence on the total amount of water present in the atmosphere was found. The overall wear rate was measured to be smaller compared with the experiments that used DDS-3 drives and DDS-2 tapes even though the number of tape passes was doubled. This is probably due to an increased hardness of the DDS-4 head materials and increased smoothness of the DDS-4 tapes compared with the previous materials. The changes in design of both tape and head led to a very low wear rate hence inconclusive data. Further increase in the number of passes would have led to a dramatic increase of time needed to perform the experiments. Therefore, another way of measuring wear at different environmental conditions needs to be designed.

Most probably, the wear rate is determined by the relative humidity but further studies are needed to determine the mechanisms responsible for this type of wear.

6.9 The model of stain formation

Since a comprehensive presentation of the model was done in the previous chapter, in this sub-chapter we will emphasise here several aspects.

The stain simulation experiments were able to induce stain on a large area of the ferrite surface thus enabling the use of the XPS technique to investigate the results. The research was able to show that stains generated by the metal particulate tapes may contain binder polymer in addition to the iron particles. Although in small amounts, the presence of binder polymer in the composition of the stains is extremely important since the polymer adheres to the head along with iron particles leading to head to tape spacing loss, loss of signal and therefore increased error rate.

The magnetic tape binder plays a crucial role in the formation and dynamic evolution of the stain and its thickness on various environmental conditions. As it has been pointed out, it is very difficult for the tape manufacturers to obtain a chemically inert polymer binder given the nature of polymer and mechanical properties required. Hence, a trade-off between chemical stability and mechanical properties is reached. Hence, the issues with the binder polymer that under harsh environmental conditions will degrade to a certain extend. The main degradation channels are hydrolysis and thermal degradation (chain scission) and the reaction products have completely opposite properties in terms of their adherent properties. As it has been demonstrated in the previous chapter, at high temperature the main degradation process is chain scission and the degradation by-products are sticky given the higher amount of unsaturated bonds. Towards higher humidities the hydrolysis of the polymer occurs and this time the degradated polymer is composed mainly from urea which is in turn soluble. Additionally, the water passivates any remaining unsaturated bonds and as a result the binder loses adhesivity. This leads to the tape shedding both polymer and iron acicular particles that become lose, entrapped between head and tape and increase the wear of the magnetic head due to 3rd body abrasion phenomenon.

The reaction rates of these decomposition processes are also increasing with the temperature according to Arhennius law. Moreover, the degradation rate is also

influenced by the presence of various transitional metals, which explains why several authors [10, 86, 87] have seen variation of the amount of stain generated when the tape was passing on blocks of different metals prior to reaching the head.

On the head interface, a higher amount of iron oxihydroxide (FeOOH) is developing on the ferrite poles when the humidity is elevated. The oxihydroxide is a soft material that can be easily removed from the ferrite poles during the normal operation of the tape. In addition, due to its porosity, the iron oxihydroxide offers no protection against moisture for the underneath layers of ferrite hence apart from abrasive wear taking place at the surface, the corrosive wear takes place in depth. The corroborated effect of two-body abrasion and three-body abrasion and the higher rate of formation of the iron oxihydroxide leads to a higher wear rate of the magnetic heads measured towards higher humidities. Taken also into account the lack of the adherent properties of the degraded polymer binder, it can be explained the absence of stains on magnetic heads seen towards higher humidities due to high rate of removal compared with the rate of deposition.

The model presented here can explain several aspects of stains and environmental-related phenomena, including strong adhesivity of the stains to the substrate, dynamical behaviour on various environmental conditions, variation of the wear rate of the magnetic heads upon environmental condition and the catalytic effect of some metals on stain development. Hence, it is believed that this model is able to cover more aspects and explains more accurately the phenomenology of the stains generated by the MP tapes on the magnetic heads.

7. Conclusions

The error rate measurements show a decrease of the errors at moderate and high humidity and an increase under low humidity with the number of tape cycles. As the AFM scans revealed the trend of the error rate is related to the state of the head's ferrite poles. When the poles remained clear, the errors decreased or remained constantly low whereas when the stain started to cover the poles and form patches, the errors increased. Given the employed data density and taking into account the three-levels error detection algorithms used in the day by day operation of the drive, the corrupted data can be recovered easily. However, the presence of large amount of errors determines an increase in the drive cost due to additional electronic circuitry needed to compensate for such errors and difficulties for further increase of data density.

Wear measurements confirmed early observations that the wear is higher on the leading edge of the head than on the trailing edge. The formation of the stains led to an increase in errors, but also a low wear rate. In these cases, stains covering the ferrite poles behaved like a protective layer, hence reducing the wear rate of the poles. The height of these deposits is usually between 14-20nm, occasionally up to 40 nm. Stains on the glass regions did not influence the errors as long as their heights are below those of ferrite region. Also, the humidity influences the rate of wear of the heads, the rate beeing higher at higher humidities.

Chemical analysis of the stains show the presence of iron acicular particles shed from the metal particulate tape but also constituents of the tape binder polymer. The amount of binder polymer was found to be higher when the tape was cycled at low speed due to a better contact between the tape and the ferrite and extended time the tape ran over the ferrite surface.

Towards higher humidity, the water from atmospheric moisture is responsible of creating iron oxihydroxide on the ferrite poles of the magnetic head. The compound is

then removed from the ferrite's surface by the tape, the phenomenon identified being abrasive wear. Since a fresh surface is exposed the process is repeating, leading to a higher wear of the magnetic poles. Hence, the formation of the FeOOH can explain higher wear rates of the heads seen at higher humidities. Also the increased rate at which the iron oxyhidroxide is forming towards higher humidities can account for the lack of stains at these environmental conditions.

Based on these experiments, and taking into account the possible degradation channels of the polymer binder of the magnetic tapes, a model of stain formation, evolution was developed. The model successfully explains the role and rate of each phenomenon affecting both magnetic media and the magnetic head in formation, evolution and destruction of the stains upon different environmental conditions, as well as variations of the wear rate of the magnetic head upon humidity. Although the model was elaborated for MP tapes and magnetic heads based on ferrite poles, it can be extended and explain similar phenomena encountered on other types of magnetic tapes and heads.

8 Further Work

There are several experiments during the research programme that, due to technical difficulties encountered, could not be performed at full extend.

Further experiments will consist in measuring the variation of the surface energy with the humidity and temperature for both the head and tape. The surface energy experiments may offer valuable hints about the van der Walls forces at the interface ferrite tape under various environmental conditions.

The remaining work will be focussing on studying the wear rate upon different factors such as humidity, amount of water and eventually temperature on DDS-4 heads used in conjunction with DDS-4 tapes. Difficulties have to be overcome since by using different head materials and improved tapes, the manufacturers reduced dramatically the wear rate of the heads. Despite the fact that the experiments performed during the research were done wit an increased number of tape cycles, the extremely low wear rate made the measurements inconclusive and affected by large errors. Therefore, the mtcl scripts and the design of the experiments are to be modified and tested in the future in order to further accelerate the wear of the heads hence reducing the error of measuring it. Equally important, the design of the experiment should take into account that the time period needed for the experiment to finish shouldn't increase too much. The wear experiments will use most probably the indentation technique in order to allow comparison between DDS-3 and DDS-4 drives, between two different technologies of making magnetic heads.

Stain simulation experiments are also to be taken into account but this time, the ferrite samples should be designed with the typical curvatures the usual magnetic heads have, hence eliminating the need of biasing the tape. The XPS analysis should be repeated to see if the polymeric binder is present within the stains.

The theoretical model regarding the amount of stain generated and the height of the stains upon environmental condition needs to be tested to verify the accuracy of the model proposed.

REFERENCES

1. **Nickel J, Gibson G**, Beyond Magnetic Storage: Atoms and Molecules, *NATO Conference, Greece, 2000;*
2. **Speliotis D, Perettie D.J,** Advanced Flexible Recording Media Based on Barium Ferrite and Advanced Polymeric Films, *Datatech –State-of-the art Technology for the Data Storage Professional, ICG Publishing ltd., 2000, pp.81-85;*
3. Hyper CD-ROM, Three Dimensional Optical Memory with Fluorescent Photosensitive Glass, http://www.dntb.ro/users/frdbuc/hyper-cdrom, *december 2000;*
4. C3D Data Storage Technology, FMD ROM Disc and Drive, *http://www.c-3d.net/products.html, december 2000;*
5. Constellation 3D Inc, White Paper, http://www.c-3d.net/, *June 7, 2000;*
6. **Constellation 3D, Inc,** Revolutionary Disruptive Technology for Removable Data Storage Products, http://www.stocksontheweb.com/cddd.htm;
7. Hyper CD-ROM packs Terabytes, *PCWorld.com, http://www.pcworld.com/resource/printable/article.asp?aid=31724, december 2000;*
8. Intel Science Talent Search $100,000 Scholarship Awarded To A 17-Year-Old Female High School Senior From New York, http://www.intel.com/pressroom/archive/releases/ed031300.htm;
9. A Romanian teen-ager revolutes the espionage, http://www.monitorul.ro/arhiva/2000/03/17/news/national_e2.htm
10. **Sullivan J.L,** The Tribology of Flexible Magnetic Recording Media- the Influence of Wear on Signal Performance, *Tribology International vol. 31, no 8, pp. 457-464, 1998;*
11. **Bissell P,** Magnetic Tape for Information Storage – Trends and Developments, *Magnews, summer 1996;*
12. **Hempstock M.S**, An investigation of thin film magnetic recording media, *Ph.D. thesis, September 1997;*

13. **Shoji M, Ohmori H, Yamamoto T et al,** A Multi-Track Magnetic Recording Head for a Helical-Scan Tape System, *IEEE Transactions on Magnetics, vol. 32, no 5, Sept. 1996, pp. 3545-3547;*
14. **Ozue, T, Shirai T, Saito T et al,** High-Density Recording Using MR Heads in Helical-Scan Tape Systems, *IEEE Transactions on Magnetics, vol. 34, no. 4, July 1998, pp. 1492-1494;*
15. **McWilliams A.A,** Tape Recording and Reproduction, *Focal Press, 1964;*
16. **Ejiri et al, Fuji Photo Film Co. Ltd,** Magnetic Recording Medium, US patent 6020022, *February 2000;*
17. **Fisher T.E, Mullins W.M,** Chemical Aspects of Ceramic Tribology, *Journal of Physics Chemistry, 1992, 96, pp. 5690-5701;*
18. Mechanisms of wear, http://www.me.umn.edu/courses/me5209/wear.html;
19. **Tsuchiya T, Bhushan B,** Running Characteristics of MIG Heads Against MP, Barrium Ferrite and ME Tapes, *IEEE Transactions of Magnetics, vol. 30, no 6, Nov. 1994, pp. 4182-4184;*
20. **Seymour R,** Introduction to polymer chemistry, *Mc-Graw-Hill Book Co, 1971;*
21. **Phillips L.N, Parker D.B.V,** Polyurethanes – Chemistry, Technology and Properties, *Iliffe Books Ltd., London, 1964;*
22. **Bely V.A et al,** Friction and Wear in Polymer-Based Materials, *Pergamon Press, 1982;*
23. **Jintang G,** Tribochemical effects in formation of polymer transfer film, *Wear, 245 (2000), pp. 100-106;*
24. **Bahadur S,** The development of transfer layers and their role in polymer tribology, *Wear, 245 (2000), pp. 92-99;*
25. **Tan T, Vermeulen B.,** Digital Audio Tape for Data Storage, *IEEE Spectrum, vol. 26, no 10, Oct. 1989, pp. 34-38;*
26. **DDS Manufacturers Group,** Internal Document, HP Bristol, 1996;
27. **Chandler S, Tucker B, Turner P, Heard P,** Case Study: An Investigation into the Cause of "Error Rate Drift", *Tribology International, Volume 31, Issue8, August 1998, Pages 443-448;*
28. **Ota H, Namura K, Ohmae N,** Brown Stain on VCR Head Surface through Contact with Magnetic Tape, *Adv. Info. Storage Syst., vol. 2, 1991, pp 85-96;*

29. **Mizoh Y.,** Wear of tribo-elements of video tape recorders, *Wear 200(1996), pp. 252-264;*

30. **Aoyagi et al,** Magnetic Head, US Patent 5 856 899, 5 *Jan 1999;*

31. **Kim S, Prabhakaran V, Talke E.F,** Investigation of Head Wear and Contamination in Helical Scan Tape Systems, *IEEE Transactions on Magnetics, vol. 32, no 5, Sept. 1996, pp. 3741-3743;*

32. **Lemke J.U,** Ferrite Transducers, *Annals of the New York Academy of Sciences, 189 (1972), pp. 171-190;*

33. **Inaba H, Ejiri K, Masaki K, Kitahara T,** Development of an Advanced Metal Particulate Tape, *IEEE Transactions on Magnetics, vol. 34, no 4, July 1998, pp. 1666-1668;*

34. **Hung Y.H, Chien Y.T, Ko Y.C,** Influence of quality of water for Fe_2O_3 production on magnetic properties of Mn-Zn ferrite, *Journal of Materials Science Letters* ***14*** *(1995), pp. 422-424;*

35. **Inaba H,** Vaporization and Diffusion of Manganese-Zinc Ferrite, *Journal of Solid State Chemistry 121, 1996, pp. 143-148;*

36. **Kirino F, Ohotomo S, Koiso N,** Electrochemical Characteristics of Single Crystal Mn-Zn Ferrite, *J.Japan Inst..Metals, vol. 61, No. 10 (1997), pp. 1050-1056;*

37. **Koinkar V.N, Bhushan B,** Microtribological studies of Al_2O_3, Al_2O_3-TiC, polycrystalline and single-crystal Mn-Zn ferrite and SiC head slider materials, *Wear 202 (1996), pp. 110-122;*

38. **Kanagawa I, Ogata S, Osaki H,** Effect of temperature, humidity and crystal directions on wear of rotary heads, *Tribology International 2003, in printing;*

39. **Nikolov J, Draghieva I, Georgiev G, Angelov D,** Monocrystal Mn-Zn ferrite and its application in magnetic heads, *Journal of Magnetism and Magnetic Materials 101 (1991), pp.137-139;*

40. **Osaki H,** Flexible media – recent developments from the tribology point of view, *Tribology International 33 (2000), pp. 373-382;*

41. **Ishikawa T et al,** Formation of Magnetite in the presence of ferric oxyhydroxides, *Corrosion Science, vol 40, No 7, pp. 1239-1251, 1998;*

42. **Welsh I.D, Sherwood P.M.A,** Photoemission and electronic structure of FeOOH: Distinguishing between oxide and oxyhydroxyde, *Physical Review B, vol. 40, no. 9, Sept. 1989, pp. 6386-6392;*

43. Handbook of Chemistry and Physics, 54th edition 1973-1974, CRC Press;
44. **Uchikoshi T, Yoshitake M, Sakka Y, Furubayashi T, Yoshihara K,** Characterization of the surface oxide layer of iron ultrafine particles, *Nippon Kagaku Kaishi, 1993, no. 1, pp.92-97;*
45. **Mathur M.C.A, Hudson G.F, Martin R.J,** Kinetic Studies of Iron Metal Particle Degradation at Various Temperature and Humidity Conditions, *IEEE Transactions on Magnetics, vol. 27, no. 6, Nov. 1991, pp.4675-4677;*
46. **Lin T.C, Seshadri G, Kelber J.A,** A consistent method for quantitative XPS peak analysis of thin oxide films on clean polycrystalline iron surfaces, *Applied Surface Science 119 (1997), pp. 83-92;*
47. **Bhushan B, Khatavkar D. V,** Role of water vapor on the wear of Mn-Zn ferrite heads sliding against magnetic tapes, *Wear 202 (1996) pp. 30-34;*
48. **Xu J, Kato K,** The effect of water vapor on the agglomeration of wear particles of ceramics, *Wear 202 (1997), pp. 165-171;*
49. **Van Groenou A.B,** Level differences in hybrid heads after contact with various tapes, , *IEEE Transactions on Magnetics, vol. 26, no 1, Jan. 1994, pp. 153-155;*
50. **Zieren V, de Jongh M,** Ultrathin wear resistant coatings for the tape bearing surface of thin-film magnetic heads for digital compact cassette, *IEEE Transactions on Magnetics, vol. 30, no 2, march 1994, pp. 340-345;*
51. **Bhushan B, Patton S.T,** Tribology in Ultra-High Density Tape Drive Systems: State of the Art and Future Challenges, *IEEE Transactions on Magnetics, vol. 34, no 4, July 1998, pp. 1883-1888;*
52. **Fuji Photo Film Co. Ltd.,** European Patent Application EP 0691 645 A1, *June 1995;*
53. **Okazaki Y, Samoto T,** The Effect of Magnetic Layer Thickness on the Digital Recording Performance of Metal Particulate Tape, *IEEE Transactions on Magnetics, vol. 31, no 6, Nov. 1995, pp.2889-2891;*
54. **Patton S.T, Bhushan B,** Friction, Wear and Magnetic Performance of Metal Evaporated and Particulate Magnetic tapes, *Proc Instn Mech Engrs, vol. 211 part J, pp. 327-348;*
55. **Bhushan B, Lowry J.A,** Friction and Wear Studies of Various Head Materials and Magnetic Tapes in a Linear Mode Accelerated Test Using a New Nano-Scratch Wear Measurement Technique, *Wear 190(1995), pp.1-15;*

56. **Doshita H,** Tribological Characteristics of thin-layer magnetic particulate media, *Tribology International, vol. 31, no. 9, pp. 541-545, 1998;*

57. **Nagai N, Inoue M,** Influence of Magnetic Interaction and Particle Length on MP Tape Noise, *IEEE Transactions on Magnetics, vol. 34, no 4, July 1998, pp. 1669-1671;*

58. **Pear C. B. et all,** Magnetic Recording in Science and Industry, *Reinhold Publishing Corporation, 1967;*

59. **Chen W.J, Wong S.S, Peng W.G, Wu C.D,** Effect of acid-base interaction on magnetic dispersion containing α-Fe metal particles, *IEEE Transactions on Magnetics, vol. 27, no. 6, Nov. 1991, pp. 4648-4650;*

60. **Veitch R.J, Ilmer A, Lenz W, Richter V,** MP technology for a new generation of magnetic tapes, *Journal of Magnetism and Magnetic Materials, 193 (1999), pp. 279-283;*

61. **Warren G.W, Sharma R, Nikles D.E, et al,** Amine quinone polyurethane polymers for improved performance in advanced particulate media, *Journal of Magnetism and Magnetic Materials 193 (1999), pp. 276-278;*

62. **Tsai Y.M, Yu T.L et al,** Physical Properties of Crosslinked Polyurethane, *Polymer International 47 (1998), pp. 445-450;*

63. **Edge M, Allen N.S, Hayes M, Jewitt T.S,** Degradation of Magnetic Tape: Support and Binder Stability, *Polymer Degradation And Stability 39 (1993) pp. 207-214;*

64. **Dasgupta S,** Dispersion characteristics of magnetic particles: surface charge, surface adsorption and acid-base interaction behavior, *Progress in Organic Coatings 28 (1996) pp. 307-311;*

65. **Jeon K, Lane A,** Polymer adsorption on magnetic particles, *Journal of Magnetism and Magnetic Materials, 193 (1999), pp. 300-302;*

66. **Patrick R.L,** Treatise on Adhesion and Adhesives, Volume 2: Materials, *Marcel Dekker Inc, New York, 1969;*

67. **Chen W.J, Wong S.S, Peng W.G, Wu C.D,** Effect of acid-base interaction on magnetic dispersion containing α-Fe metal particles, *IEEE Transactions on Magnetics, vol. 27, no. 6, Nov. 1991, pp. 4648-4650;*

68. **Kim K.J, Glasgow P.D, Kolycheck E.G,** A road to stable dispersions: polymer – particle interactions, *Journal of Magnetism and Magnetic Materials 120 (1993) pp. 87-93;*

69. **Kurihara K, Matsute M, Watanabe H, et al,** Development of highly reactive hardening agents for MP tapes, *Journal of Magnetism and Magnetic Materials, 193 (1999), pp. 296-299;*

70. **Nakamae K, Yamaguchi K, Asaoka S, Karube Y, Sudaryanto,** Lifetime expectancy of polyurethane binder as magnetic recording media, *Int. J. Adhesion and Adhesives 16 (1996) pp. 277-283;*

71. **Arroyo J.C, Saffarian H.M, Warren G.W,** Electrochemical evaluation of the effect of binder additives on iron corrosion, *J.Appl. Phys. 75 (10), 1994, pp. 5568-5570;*

72. **Saunders J.H, Frisch K.C,** Polyurethanes – Chemistry and Technology, part 1, Chemistry, *John Wiley &Sons Inc, 1962;*

73. **Brydson J.A,** Plastics Materials-fourth edition, *Butterworth Scientific, 1982;*

74. **Kim B.K,** Aqueous polyurethane dispersions, *Colloid Polym. Sci. 274 (1996), pp. 599-611;*

75. **Nakamae K, Yamaguchi K, Asaoka S, Karube Y, Sudaryanto,** Lifetime expectancy of polyurethane binder as magnetic recording media, *Int. J. Adhesion and Adhesives 16 (1996) pp. 277-283;*

76. **Grassie N, Scott G,** Polymer Degradation & Stability, *Cambridge University Press, 1985;*

77. **Edge M, Hayes M et al,** Aspects of Poly(ethylene terephthalate) Degradation for Archival Life and Environmental Degradation, *Polymer Degradation and Stability 32 (1991), pp. 131-153;*

78. **Cuddihy E.F,** Hygroscopic Properties of Magnetic Recording Tape, *IEEE Transactions on Magnetics, vol. MAG-12, no. 2, march 1976, pp. 126-135;*

79. **Nishida Y, Nishida Y, Kikkawa M, Kondo H,** Behavior of Lubricant Migration in Particulate Magnetic Recording Media, *IEEE Transactions on Magnetics, vol. 35, no 5, Sept. 1999, pp. 2451-2453;*

80. **Kondo H, Hisamichi Y, Kamei T,** Lubrication of Modified Perfluoropolyether on Magnetic Media, *Journal of Magnetism and Magnetic Materials 155(1996) pp. 332-334;*

81. **Osaki H,** Tribology of videotapes, *Wear 200 (1996), pp. 244-251;*

82. **Nagai N, Kamatani Y et al,** Clear Stains and Their Behaviour in Helical Scan Tape Systems, *IEEE Transactions on Magnetics , vol. 36, no 5, Sept 2000;*

83. **Suzuki T, Tanaka T, Ikemizu K,** High Density recording capability for advanced particulate media, *J. of Magnetism and Magnetic Materials, 235 (2001) pp. 159-164;*

84. **Stahle C.M, Lee T.D,** Characterization of the Deposits on Helical Scan Heads, *Adv. Info. Storage Syst., vol. 4, 1992, pp. 79-86;*

85. **Scott W. W, Bhusan B,** Generation of magnetic tape debris and head stain in a linear tape drive, *Proc Instn Mech Engrs, 1998, 213, part J, pp. 127-138;*

86. **Bhushan B, Hahn F.W jr,** Stains on Magnetic Tape Head, *Wear 184(1995), pp. 193-202;*

87. **Liew Y.F, Lauer J.L, Talke F.E,** Analysis of Deposits from Friction at Head-Tape Interfaces by Raman Spectroscopy, *Tribology Transactions, vol. 38(1995), 3, pp.728-732;*

88. **Scott W, Bhushan B,** Loose Debris and Head-Stain Generation and Pole-Tip Recession in Modern Tape Drives: A Critical Review, *J. Info, Storage Syst, vol 2, 2000, pp. 221-254;*

89. **Kattner K, Bhushan B,** Analysis of Stain Formation and Wear Mechanisms of Magnetoresistive Heads and Magnetic Particle Tape in a Linear Tape Drive, *J. Info. Proc Syst., vol. 2, 2000, pp. 193-205;*

90. **Bhushan B, Lowry J.A**, Friction and Wear of Particulate and ME Magnetic Tapes Sliding against a Mn-Zn Ferrite Head in a Linear Mode, *IEEE Transactions on Magnetics, vol30, no 6, nov. 1994, pp. 4176-4178;*

91. **Gupta B.K et al.,** Chemical Analyses of Stains Formed on Co-Nb-Zr Metal-in-Gap Heads Sliding against Oxide and Metal Particle Magnetic Tape, *J. Mater. Res., vol. 10,no.7, Jul. 1995, pp. 1795-1810;*

92. **Hirofumi K,** Cleaning Liquid for Magnetic Head and Magnetic Head Using the Liquid, *Patent Abstracts of Japan, Application number: 07258656/15.04.97;*

93. **Hirofumi K, Junichi H,** Liquid to Form Protective Coating Film for Magnetic Head, and Magnetic Head using that, *Patent Abstracts of Japan, Application number: 08268448/06.05.98;*

94. **Kamei T, Kishii N, Kurihara K,** Removal of Brown Stain on Magnetic Head by a Chelating Agent on Magnetic Tapes, *Journal of Magnetism and Magnetic Materials 193(1999), pp.291-295;*

95. **Cotton F.A, Wilkinson G,** Advanced Inorganic Chemistry, A Comprehensive Text, *Interscience Publishers, 1962, pp. 707-719;*

96. **Snoeyink L.V, Jenkins D,** Water Chemistry, *John Wiley & Sons, New York, 1980;*

97. **Sullivan J.L,** The Tribology of Flexible Magnetic Recording Media, *Journal of Magnetism and Magnetic Materials 155(1996), pp. 312-317;*

98. **New European Patent Specification,** EP 0 220 580 B2, *25.06.1997, Bulletin 1997/26;*

99. **Yamazaki N, Saito S, Fuji Photo Film Co. Ltd,** Magnetic Recording Medium, US patent 6096406, *August 2000;*

100. **Yamada K, Kojima N, Ide Y et al, Ricoh Company ltd,** Information Recording Medium, US Patent 5080947, *Jan 1992;*

101. **Hirofumi K,** Coating type magnetic recording medium, *Patent Abstracts of Japan, Application number: 05269286/12.05.95;*

102. *http://www.eu.maxell.com/Technical/dds.htm*

103. **Wagner CD, Riggs WM et al,** Handbook of X-Ray Photoelectron Spectroscopy, Perkin-Elmer Co, *1979;*

104. **Briggs D, Brown A, Vickerman J.C,** Handbook of Static SIMS, *John Wiley &Sons, 1989;*

105. **Mott BW,** Micro-indentation hardness testing, *Butterworth's Scientific Publications, 1956;*

106. **TopoMetrix Co–** User's Manual, v. 3.05, *1996;*

107. **TopoMetrix Co–** Software Reference Manual, *1996;*

108. **Bhushan B,** Micro/nanotribology using atomic force microscopy/friction force microscopy: state of the art, *Proceedings of the Institution of Mechanical Engineers Part J- Journal of Engineering Tribology, 1998, Vol.212, No.J1, pp.1-18;*

109. **Adamson AW,** Physical Chemistry of Surfaces – 3rd edition, *John Wiley & sons, 1976;*

110. **Kim S, Kwon H, Kim Y.G, Lee Y.S, Talke E.F** Investigation of wear characteristics of video heads in a helical scan video cassette recorder, *International Conference on Consumer Electronics, 1996, pp. 286-287;*

111. **Chandler S,** Error rate drift caused by rubbing noise in ferrite read heads, *Tribology International 33 (2000), pp. 401-408;*

112. **Scott W, Bhushan B,** Micro/nano-scale differential wear of multiphase materials: pole tip recession in magnetic-tape heads, *Wear (2002) pp. 103-122;*

113. **Hirofumi K,** Lubricant and Magnetic Recording Medium using the same, *Patent Abstracts of Japan, Application number: 08237039/31.03.98;*

114. **Harrison MJK, Sullivan JL, Theunissen GSAM,** Pole tip recession in sandwich heads incorporating a FeTaN soft magnetic track, *Tribology International, 1998; 31(9), pp.491-500;*

115. **Chandler S,** private communication;

116. **Hawkins W.L,** Polymer Stabilization, *John Wiley & Sons Inc., New York, 1972;*

117. **Muftu S, Kaiser J.D,** Measurements and theoretical predictions of head/tape spacing over a flat head, *Tribology International 33 (2000), pp. 415-430;*

118. **Patrick R.L,** Treatise on Adhesion and Adhesives, Volume 1: Theory, *Marcel Dekker Inc, New York, 1969;*

119. **Yu G.Q, Lee S. H, et al,** Synthesis and Characterisation of Carbon Nitride thin films prepared by rf plasma enhanced chemical vapour deposition, *Surface and Coatings Technology, 154 (2002), pp. 68-74;*

120. **Carlsson P, Bexell U, Olsson M,** Tribological Performance of Thin Organic Permanent Coatings deposited on 55% Al-Zn coated steel – influence of coating composition and thickness on friction on friction and wear, *Wear 8878 (2001), pp. 1-10;*

121. **OxleyE, Yang C et al**, Quantitative Depth analysis using microsecond pulsed glow discharge atomic emission spectroscopy, Journal of Analytical Atomic Spectrometry, *DOI: 10.1039/b001969k (July 2000),* *http://pubs.rsc.org/ej/gd/2000/ab001969k.pdf;*

122. **Charles, Evans & Associates**, RSF Factors, *http://www.cea.com/cai/simstheo/rsftable.htm;*

123. **Charles, Evans & Associates,** SIMS Theory, (original reference: R.G. Wilson, Int. J. Mass Spectrometry. Ion Proc., 143, 43, 1995), *http://www.cea.com/literature/AN-SIMS-08_fontchange.pdf;*

124. **Aoyagi et al,** Magnetic Head, US Patent 5 856 899, 5 *Jan 1999;*

125. **Charles G.S, Hunter J.L, et al,** Ion Microprobe Elemental Analyses of Impact Features on Interplanetary Dust Experiment Sensor Surfaces, *http://setas-www.larc.nasa.gov/LDEF/MET_DEB/IDE/REFERENC/CGSLD1CH/CGSLD1CH.HTM*

126. **Jellinek, H.H.G**, Degradation and Stabilization of Polymers, Volume 1, *Elsevier, Amsterdam 1983;*

127. **Nastase C, Sullivan JL,** Analysis of the Stains Produced by Metal Particle Tapes on Helical Scan Heads in Data Recording Applications, *Tribology International 35 (2002), pp. 211-217;*

128. Nebraska Earth Science Education Network, *http://nesen.unl.edu/stedii/humidityc.htm, 2001;*

129. **G. Beamson. D. Briggs** - High Resolution XPS of Organic Polymers, *John Wiley, New York, 1992;*

130. *http://www.sdm.buffalo.edu/scic/auger.html*

131. **Physical Electronics**, Handbook of Auger Spectroscopy 3rd ed., *1995*

132. **BCC Technologies, Advanced Storage Solutions,** White Paper Helical Scan vs. Linear, *Oct. 2001*

133. **Osaki H,** Recent research of tape/drive tribology, Tribology International 36(2003), pp. 349-360;

134. Encyclopaedia of Polymer Science & Technology, *vol. 14, Interscience, John Wiley & Sons, New York, 1971*

135. **Harrington,** - R-Rubber Age (NY) (1959), 85, *pp. 798*

136. **Moroi G,** Influence of ion species on the thermal degradation of polyurethane interaction products with transition metal ions, *J. Anal. Appl. Pyrolysis 71 (2004), pp. 485-500*

137. **Judge J. S.et al**, Media Stability and Life Expectancies of Magnetic Tape for Use with IBM 3590 and Digital Linear Tape Systems, *http://www.storageconference.org/2003/papers/15_Judge-Media.pdf*

138. **Navale V**, Longevity of High Density Magnetic Media, *http://www.thic.org/pdf/Nov02/nara.vnavale.021106.pdf*

139. **Prabhakaran V, Kim S.K, Talke F.E**, Tribology of the helical scan head tape interface, *Wear 215 (1998) pp. 91-97*

140. **Ujvarosy D.R**, Fast DDS-2 digital audio tape drive - HP C1533A 4GB tape drive, *http://www.findarticles.com/p/articles/mi_m0HPJ/is_n6_v45/ai_16314505/pg_1*

141. **Govorcin E.B, Rek V, Agic A,** Thermal degradation of Polyurethane Elastomers: Determination of Kinetic Parameters, *Journal of elastomers and Plastics, vol 35, October 2003;*

142. **Hanai K, Kakuishi Y,** The storage of metal particle media: Chemical analysis and kinetics of lubricant and binder hydrolysis, http://romulus.gsfc.nasa.gov/msst/conf2002/papers/b14ap-kha.pdf, http://citeseer.ist.psu.edu/533839.html, 2002

143. **Yamamoto K, Watanabe H,** A Kinetic Study of Hydrolysis of Polyester Elastomer in Magnetic Tape, http://citeseer.ist.psu.edu/257122.html, http://esdis-it.gsfc.nasa.gov/msst/conf1995/A5_12.PDF, 1995

144. **Kaelble, David H,** Physical Chemistry of Adhesion, Wiley-Interscience, 1971

145. **Myshkin N.K**, Friction transfer film formation in boundary lubrication, *Wear 245 (2000), pp. 116-124*

146. **Jay Kadis**, Introduction to Music 192A, Stanford University, Autumn 2005 http://ccrma.stanford.edu/courses/192a/6-Magnetic_Recording.pdf

Addenda – Published Papers

ELSEVIER

Tribology International 35 (2002) 211–217

TRIBOLOGY INTERNATIONAL

www.elsevier.com/locate/triboint

Analysis of the stains produced by metal particle tapes on helical scan heads in data recording applications

C. Nastasa, J.L. Sullivan *

Electronic Engineering and Applied Science, Aston University, Birmingham B4 7ET, UK

Received 1 June 2001; received in revised form 5 October 2001; accepted 25 October 2001

ELSEVIER

Tribology International 36 (2003) 247–254

TRIBOLOGY INTERNATIONAL

www.elsevier.com/locate/triboint

Transfer film formation on helical scan data recording heads

C. Nastasa *, J.L. Sullivan

Electronic Engineering and Applied Science, Aston University, Birmingham, B4 7ET, UK

8.3 Addenda – resolving eq. 5-8

We need to resolve the equation:

$$\frac{\partial N}{\partial t}(z,t) = D\frac{\partial^2 N}{\partial z^2}(z,t) + v_e \frac{\partial N}{\partial z}(z,t) \qquad \text{Eq 1}$$

with the initial condition: $N(z, 0) = N_0(z)$ and conditions at the limit:

$N(0, t) = 0$
$N(z_0, t) = \Psi(t)$

We can define a new function $\rho(z_0, t)$ so that: $(N-\rho)(0,t) = 0$ and $(N-\rho)(z_0, t) = 0$. One such function can be of the form of: $\rho(z, t) = \frac{z}{z_0}\Psi(t)$

By substituting $w = N-\rho$ the equation becomes:

$$\begin{cases} \frac{\partial w}{\partial t}(z,t) = D\frac{\partial^2 w}{\partial z^2}(z,t) + v_e \frac{\partial w}{\partial z}(z,t) + \frac{v_e}{z_0}\Psi(t) - \frac{z}{z_0}\Psi'(t) \\ w(z,0) = N_0(z) - \frac{z}{z_0}\Psi(0) \\ w(0,t) = w(z_0,t) = 0 \end{cases} \qquad \text{Eq 2}$$

Given the fact that the above equation is linear, the solution w has to be in the the form of:

$w(z, t) = w_0(z, t) + w_p(z, t)$
where $w_0(z, t)$ is the solution of the equation:

$$\begin{cases} \frac{\partial w_0}{\partial t}(z,t) = D\frac{\partial^2 w_0}{\partial z^2}(z,t) + v_e \frac{\partial w_0}{\partial z}(z,t) \\ w_0(z,0) = N_0(z) - \frac{z}{z_0}\Psi(0) \\ w_0(0,t) = w_0(z_0,t) = 0 \end{cases} \qquad \text{Eq 3}$$

and w_p verifies the equation:

$$\begin{cases} \dfrac{\partial w_p}{\partial t}(z,t) = D\dfrac{\partial^2 w_p}{\partial z^2}(z,t) + \nu_e \dfrac{\partial w_p}{\partial z}(z,t) + \dfrac{\nu_e}{z_0}\Psi(t) - \dfrac{z}{z_0}\Psi'(t) \\ w_p(z,0) = 0 \\ w_p(0,t) = w_p(z_0,t) = 0 \end{cases}$$ Eq 4

In order to resolve the equation 3, one has to find solutions of the form of

$\tilde{w}(z,t) = u(z)v(t)$

$u(z)v'(t) = Du''(z)v(t) + \nu_e u'(z)v(t)$ and by dividing by u(z)v(t), we find:

$$\frac{v'(t)}{v(t)} = D\frac{u''(z)}{u(z)} + \nu_e \frac{u'(z)}{u(z)} = \lambda$$ Eq 5

Hence, the above equation can be written:

$$\begin{cases} v'(t) - \lambda v(t) = 0 \\ Du''(z) + \nu_e u'(z) - \lambda u(z) = 0 \end{cases}$$ Eq 6

Based on the limit conditions, we have:

$u(0)v(t) = u(z_0)v(t) = 0$

Since $v \neq 0$ then, $u(0) = u(z_0) = 0$,

$$\begin{cases} Du''(z) + \nu_e u'(z) - \lambda u(z) = 0 \\ u(0) = u(z_0) = 0 \\ u \neq 0 \end{cases}$$ Eq 7

The above equation is linear, therefore the solution can be found by resolving the characteristic equation:

$$D\gamma^2 + \nu_e \gamma - \lambda = 0$$ Eq 8

The only solutions that verify the initial conditions are:

$$\gamma_{1,2} = -\frac{\nu_e}{2D} \pm i\frac{\sqrt{-(\nu_e + 4\lambda D)}}{2D}$$ Eq 9

and the general solution is:

$$u(z) = e^{-\frac{\nu_e}{2D}z}[C_1 \cos(\frac{\sqrt{-(\nu_e^2 + 4\lambda D}}{2D} z) + C_2 \sin(\frac{\sqrt{-(\nu_e^2 + 4\lambda D}}{2D} z)] \quad \text{Eq 10}$$

Since $u(0)=u(z_0)=0$, we can find: $C_1=0$ and $C_2 \sin(\frac{\sqrt{-(\nu_e^2 + 4\lambda D}}{2D} z_0 = 0$. Since $C_2 \neq 0$, then $\sin(\frac{\sqrt{-(\nu_e^2 + 4\lambda D}}{2D} z_0 = 0$, and more, $\lambda = \lambda_0 = -\frac{\nu_e^2}{4D} - \frac{n^2\pi^2 D^2}{z_0^2}$

$u_n(z) = \alpha_n e^{-\frac{\nu_e}{2D}z} \sin(\frac{n\pi z}{z_0})$ and similarly, $v_n(t) = \beta_n e^{\lambda_n t}$

We find:

$$\tilde{w}(z,t) = \alpha_n \beta_n e^{\lambda_n t - \frac{\nu_e}{2D}z} \sin(\frac{n\pi z}{z_0}) \quad \text{Eq 11}$$

and

$$w_0(z,t) = \sum_{n=1}^{\infty} \gamma_n e^{\lambda_n t - \frac{\nu_e}{2D}z} \sin(\frac{n\pi z}{z_0}) \quad \text{Eq 12}$$

Finally, we find:

$$N_0(z) - \frac{z}{z_0}\Psi(0) = \sum_{n=1}^{\infty} \gamma_n e^{-\frac{\nu_e z}{2D}} \sin(\frac{n\pi z}{z_0}) \quad \text{Eq 13}$$

Hence, in eq 12 one must choose:

$$\gamma_n = \frac{2}{z_0} \int_0^{z_0} \left[N_0(z) - \frac{z}{z_0}\Psi(0) \right] e^{\frac{\nu_e z}{2D}} \sin\frac{n\pi z}{z_0} dz \quad \text{Eq 14}$$

The solution of the eq 4 is in the form of:

$$w_p(z,t) = \sum_{n=1}^{\infty} \eta_n(t) e^{-\frac{\nu_e z}{D}} \sin(\frac{n\pi z}{z_0});$$

Taking into account that the solution must verify eq 4, we find the following equation for η:

$$\begin{cases} \eta_n'(t) + (\frac{v_e^2}{4D} + \frac{n^2\pi^2 D}{z_0^2})\eta_n(t) = \frac{2}{z_0}\int_0^{z_0} e^{\frac{v_e z}{2D}}\left[\frac{v_e}{z_0}\Psi(t) - \frac{z}{z_0}\Psi'(t)\right]\sin(\frac{n\pi z}{z_0})dz \\ \eta_n(0) = 0 \end{cases} \quad \text{Eq 15}$$

and since $w_p(0,t) = w_p(z_0,t) = 0$, we calculate:

$$\eta_n(t) = \frac{2}{z_0}\int_0^t\int_0^{z_0} e^{-(\frac{v_e^2}{4D} + \frac{n^2\pi^2 D}{z_0^2})(t-s) + \frac{v_e z}{2D}}\left[\frac{v_e}{z_0}\Psi(s) - \frac{z}{z_0}\Psi'(s)\right]\sin(\frac{n\pi z}{z_0})dzds \quad \text{Eq 16}$$

Putting together all the solutions, we find:

$$N(z,t) = \frac{z}{z_0}\Psi(t) + \left[\sum_{n=1}^{\infty}(\eta_n(t) + \gamma_n e^{\lambda_n t})\sin\frac{n\pi z}{z_0}\right]e^{-\frac{v_e z}{2D}}$$

with:

$$\lambda_n = -\frac{v_e^2}{4D} - \frac{n^2\pi^2 D^2}{z_0^2}$$

$$\eta_n(t) = \frac{2}{z_0}\int_0^t\int_0^{z_0} e^{-(\frac{v_e^2}{4D} + \frac{n^2\pi^2 D}{z_0^2})(t-s) + \frac{v_e z}{2D}}\left[\frac{v_e}{z_0}\Psi(s) - \frac{z}{z_0}\Psi'(s)\right]\sin(\frac{n\pi z}{z_0})dzds \quad \text{Eq 17}$$

$$\gamma_n = \frac{2}{z_0}\int_0^{z_0}\left[N_0(z) - \frac{z}{z_0}\Psi(0)\right]e^{\frac{v_e z}{2D}}\sin\frac{n\pi z}{z_0}dz$$

The above solution is the general solution of the eq. 5-8. However, given the initial conditions, it can be approximated as:

$$N(z,t) = \frac{z}{z_0}\Psi(t) + \left[\sum_{k=1}^{n}(\eta_k(t) + \gamma_k e^{\lambda_k t})\sin\frac{k\pi z}{z_0}\right]e^{-\frac{v_e z}{z_0}} \quad \text{Eq 18}$$

and n can be chosen so the approximation error is below a certain threshold.